Electrochemical Society

GET YOUR FREE COPY OF THIS INFORMATIVE, ILLUSTRATED BROCHURE

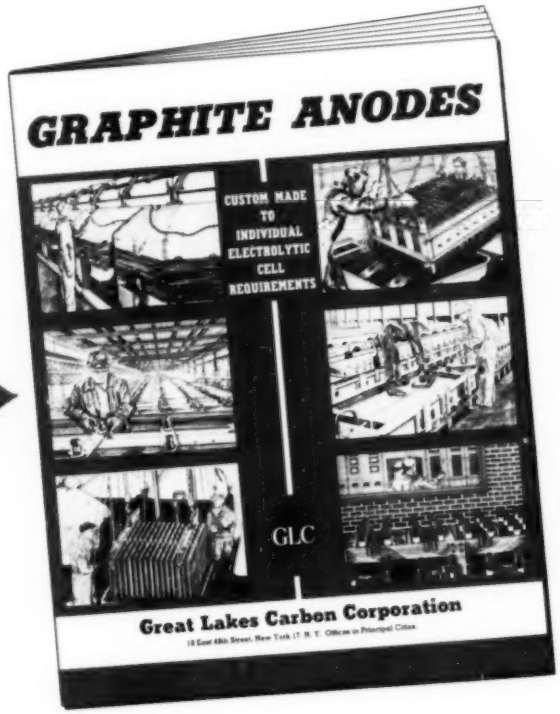

Everyone connected with electrolytic cell operations should have a copy of our new brochure GRAPHITE ANODES. It contains a wealth of useful information.

Here you will find tables of standard sizes and grades of square and rectangular anodes for diaphragm and mercury cells...reasons why anodes custom made to individual cell requirements are more economical and efficient...a brief review of our special anode production and machining facilities...and an explanation of our technical exchange program which has helped our customers lower cell operating costs.

Write us for a copy of GRAPHITE ANODES— it is yours for the asking.

PRODUCTS ELECTRODE GLC DIVISION YOU CAN TRUST ®

GREAT LAKES CARBON CORPORATION

18 EAST 48TH STREET, NEW YORK 17, N. Y.

EDITORIAL STAFF

H. H. Uhlig, Chairman, Publication Committee

Cecil V. King, Editor

Norman Hackerman, Technical Editor

Ruth G. Sterns, Managing Editor

U. B. Thomas, News Editor

H. W. Salzberg, Book Review Editor

Natalie Michalski, Assistant Editor

DIVISIONAL EDITORS

W. C. Vosburgh, Battery

Milton Stern, Corrosion, I

R. T. Foley, Corrosion, II

T. D. Callinan, Electric Insulation

Seymour Senderoff, Electrodeposition

H. C. Froelich, Electronics, I

Ephraim Banks, Electronics, II

Ernest Peskell, Electronics—Semiconductors

Sherlock Swann, Jr., Electro-Organic, I

Stanley Wawzonek, Electro-Organic, II

John M. Blocher, Jr., Electrothermics and Metallurgy, I

A. U. Seybolt, Electrothermics and Metallurgy, II

N. J. Johnson, Industrial Electrolytic

C. W. Tobias, Theoretical Electrochemistry, I

A. J. deBethune, Theoretical Electrochemistry, II

ADVERTISING OFFICE

ECS

1860 Broadway, New York 23, N. Y.

ECS OFFICERS

R. A. Schaefer, President
The Bunting Brass and Bronze Co., Toledo, Ohio

Henry B. Linford, Vice-President
Columbia University, New York, N. Y.

F. L. LaQue, Vice-President
International Nickel Co., Inc., New York, N. Y.

W. J. Hamer, Vice-President
National Bureau of Standards, Washington, D. C.

Lyle I. Gilbertson, Treasurer
Air Reduction Co., Murray Hill, N. J.

I. E. Campbell, Secretary
National Steel Corp., Weirton, W. Va.

Robert K. Shannon, Executive Secretary
National Headquarters, The ECS, 1860 Broadway, New York 23, N. Y.

Manuscripts submitted to the Journal should be sent, in triplicate, to the Editorial Office at 1860 Broadway, New York 23, N. Y. They should conform to the Instructions to Authors, last published in the April 1960 issue, pp. 100C-101C. Manuscripts so submitted become the property of The Electrochemical Society and may not be published elsewhere, in whole or in part, unless permission is requested of and granted by the Editor.

Inquiries re positive microfilm copies for volumes should be addressed to University Microfilms, Inc., 313 N. First St., Ann Arbor, Mich.

Journal of the Electrochemical Society

JUNE 1960 **VOL. 107 • NO. 6**

CONTENTS

Editorial

Planning Our Future. *R. A. Schaefer* 130C

Technical Papers

Conductivity of Silver Iodide Pellets for Solid-Electrolyte Batteries. *J. N. Mrgudich* 475

Sine Wave Pulse Current Tester for Batteries. *K. Kordesch and A. Marko* 480

An Investigation of the Reaction between Aluminum and Water. *W. J. Bernard and J. J. Randall, Jr.* 483

Corrosion Behavior and Passivity of Nickel-Chromium and Cobalt-Chromium Alloys. *A. P. Bond and H. H. Uhlig* 488

Dissolution of Nickel in Acid Ferric and Ceric Solutions. *P. M. Christopher and C. V. King* 493

Oxidation of Niobium in the Temperature Range 350°-750°C. *D. W. Aylmore, S. J. Gregg, and W. B. Jepson* 495

The Difference Effect and Anodic Behavior of Zirconium Dissolving in Hydrofluoric Acid. *M. E. Straumanis, W. J. James, and W. C. Custead* 502

Oxidation of Zirconium and Zirconium Alloys. *H. A. Porte, J. G. Schnizlein, R. C. Vogel, and D. F. Fischer* 506

High-Field Conduction Currents in Liquid n-Hexane under Microsecond Pulse Conditions. *P. K. Watson and A. H. Sharbaugh* 516

On the Physical Characteristics and Chemical Composition of Electroluminescent Phosphors. *P. Goldberg and S. Faria* 521

Preparation and Properties of AlSb-GaSb Solid Solution Alloys. *J. F. Miller, H. L. Goering, and R. C. Himes* 527

The Diffused Shot-Melting Technique for Making Germanium and Silicon p-n Junction Devices. *I. A. Lesk* 534

Polarographic Studies in Acetonitrile and Dimethylformamide, V. Behavior of Aromatic Ketones and Aldehydes. *S. Wawzonek and A. Gundersen* 537

Preparation and Refining of Yttrium Metal by Y-Mg Alloy Process. *O. N. Carlson, J. A. Haefling, F. A. Schmidt, and F. H. Spedding* 540

Exchange Current Measurements in KCl-LiCl Eutectic Melt. *H. A. Laitinen, R. P. Tischer, and D. K. Roe* 546

A Study of the Oxidation of Hydrogen at Platinized Platinum Electrodes. *T. C. Franklin and S. L. Cooke, Jr.* 556

Technical Notes

Charging Curves for Germanium Electrodes. *W. W. Harvey, S. Sheff, and H. C. Gatos* 560

A Comparison of Etching and Fracturing Techniques for Studying Twin Structures in Ge, Si, and III-V Intermetallic Compounds. *J. W. Faust, Jr., and H. F. John* 562

Bonding and Semiconductivity Relationships in Bi_2Te_3 and CdI_2 Type Structures. *C. H. L. Goodman* 564

The Adhesion of Vapor-Deposited Molybdenum Coatings. *S. T. Wlodek and J. Wulff* 565

Brief Communication

Growth of Single Crystal Silicon Overgrowths on Silicon Substrates. *A. Mark* 568

Discussion Section 570

Current Affairs 134C-140C

Published monthly by The Electrochemical Society, Inc., from Manchester, N. H., **Executive Offices, Editorial Office** and **Circulation Dept.,** and **Advertising Office** at 1860 Broadway, New York 23, N. Y., combining the JOURNAL and TRANSACTIONS OF THE ELECTROCHEMICAL SOCIETY. Statements and opinions given in articles and papers in the JOURNAL OF THE ELECTROCHEMICAL SOCIETY are those of the contributors, and The Electrochemical Society assumes no responsibility for them. Nondeductible subscription to members $5.00; subscription to nonmembers $18.00. Single copies $1.25 to members, $1.75 to nonmembers.

Copyright 1960 by The Electrochemical Society, Inc.

Entered as second-class matter at the Post Office at Manchester, N. H., under the act of August 24, 1912.

One of a series

Higher Education for Computers

"Let's put the computer in at the start of a problem, rather than just having it buzz through the computations."

This is the approach being taken by computer specialists at the General Motors Research Laboratories as they explore ways of giving large-scale digital computers a greater role in the solution of problems. The object is to "teach" computers to apply the same rules men use in formulating, analyzing, and solving questions of modern science and engineering.

A recent outgrowth of this work is DYANA, GM Research's new automatic analysis and programming system. DYANA is one of the first computer systems to "understand" declarative statements. For a large class of dynamic problems, the engineer can simply describe his physical system to the computer. The computer figures out how to handle it.

For the solution, DYANA automatically directs the computer to prepare a mathematical model of the system, to write its own program for solving the model, then to execute the program and compute the desired answers.

The higher education of computers currently involves studies in symbol manipulation, problem-oriented languages, character and pattern recognition, and engineering simulation.

Such advanced computer concepts are giving General Motors professional people more time for creative engineering and research—time to explore ideas and to develop "more and better things for more people."

General Motors Research Laboratories

Warren, Michigan

Comparison of program tapes for a vibrational problem expressed in DYANA language, in algebraic-oriented language, and in the basic machine language.

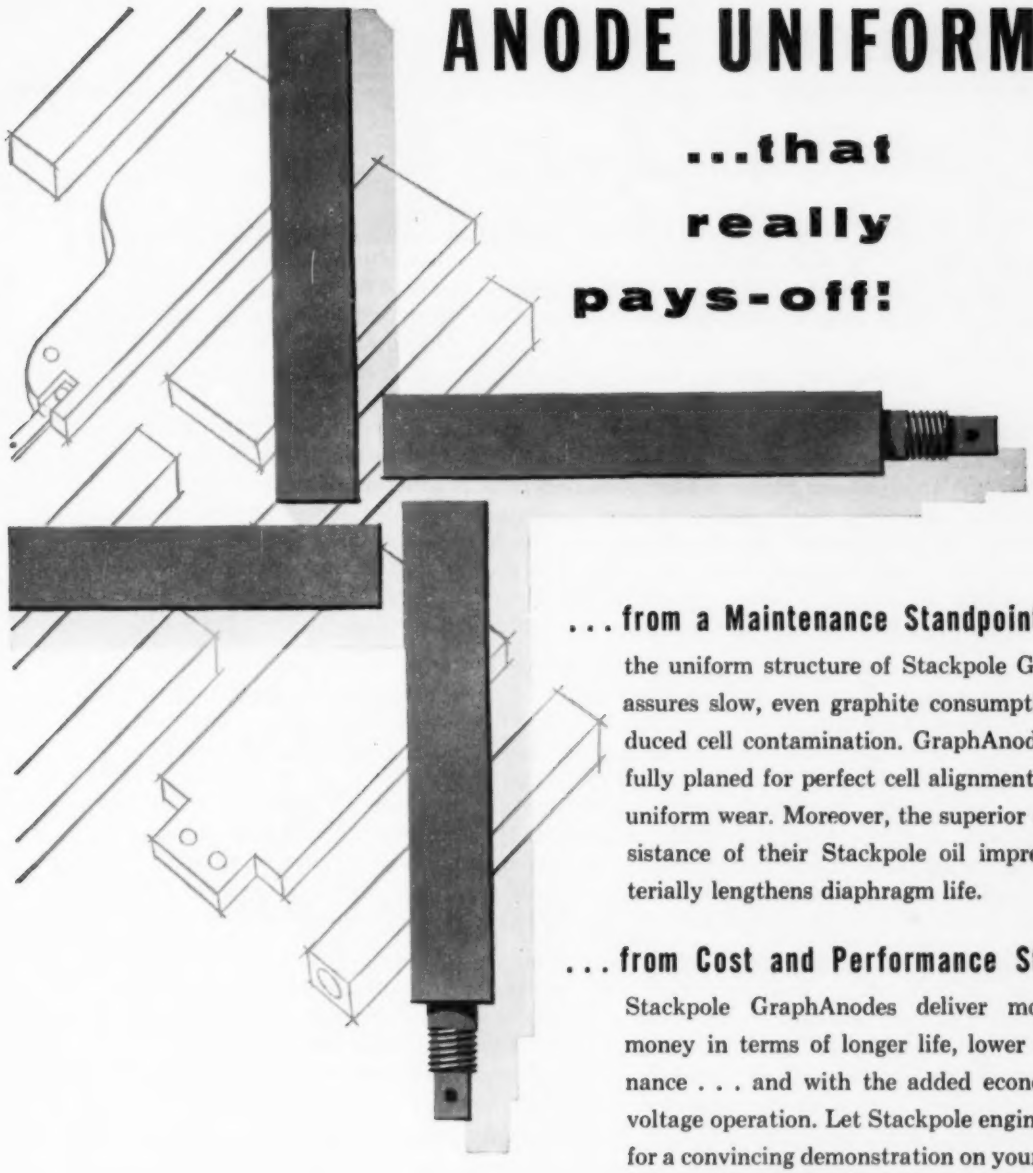

ANODE UNIFORMITY

...that really pays-off!

...from a Maintenance Standpoint

the uniform structure of Stackpole GraphAnodes assures slow, even graphite consumption with reduced cell contamination. GraphAnodes are carefully planed for perfect cell alignment, longer life, uniform wear. Moreover, the superior chemical resistance of their Stackpole oil impregnants materially lengthens diaphragm life.

...from Cost and Performance Standpoints

Stackpole GraphAnodes deliver more for the money in terms of longer life, lower cell maintenance . . . and with the added economy of low-voltage operation. Let Stackpole engineers arrange for a convincing demonstration on your equipment. *Stackpole Carbon Company, St. Marys, Penna.*

STACKPOLE

GRAPHANODES

graphite anodes in grades, sizes and shapes for all electrolytic cells

TUBE ANODES • CATHODIC PROTECTION ANODES • FLUXING & DE-GASSING TUBES • BRUSHES for all rotating electrical equipment • ELECTRICAL CONTACTS • VOLTAGE REGULATOR DISCS • "CERAMAGNET"® CERAMIC MAGNETS • ROCKET NOZZLES • BEARINGS • SALT BATH RECTIFICATION RODS • SEAL RINGS • FRICTION RINGS • ELECTRODES & HEATING ELEMENTS • MOLDS & DIES • WELDING CARBONS • POROUS CARBON • and many other carbon, graphite, and electronic components.

Editorial

Planning Our Future

FROM the dawn of history until recent years, mankind devoted the major portion of his skill and energy to solving the problem of production. Within the past four or five generations, this problem has been answered by the highly industrialized nations. In these countries, mankind enjoys a superabundance of goods and services, compared to the scarcity of products for the past thousands of years. Our age of plenty has been achieved by countless thousands of observations and experimental data on natural phenomena. Over the years, these many scattered bits of information accumulated and ultimately became organized and classified into the various scientific and engineering fields of endeavor. The application of this knowledge has created our present industrial complex system of production, which converts the material and energy of the earth into useful products at rates far exceeding those possible with human toil and animal power. The high degree to which the production problem has been solved is very evident in the large shopping centers within a few miles of our homes, where practically all the articles and services for the necessities and comforts of life are available in several brand names.

Currently, mankind has insufficient knowledge of human behavior to answer the difficult social problem created by the era of production abundance in marketing and distribution of the fruits of applied engineering. This industrial problem of merchandising our ever-increasing productive capacity has initiated and intensified social research studies of man and his habits, desires, and environment as they affect his wants and needs. We are all familiar with the effective use of advertising, style change, market survey, and so forth, to increase the consumption of goods and services; for our industrial complex system can produce more goods and services than mankind can utilize. Hence, no longer can a corporation survive by possessing only manufacturing excellence, but must be equally efficient in distribution techniques.

Today, the principal operating question facing a corporation is: Can we manufacture and distribute present and potential products or services at a profit? It is not sufficient for corporation survival to create new, or improve present, products in its laboratories and leave the marketing of them to chance. Each company in our industrial system must fight for a market position against all other companies manufacturing, or likely to produce, similar products.

The heart and lifeblood of the successful corporation is revolving more and more around the product planner. Many scientists and engineers at both the college and industrial level have failed to recognize this changing pattern of industrial operations. The planner charts technical data, interprets and predicts the social and technical reactions to future products and services before large sums of money are spent in creating products or services which will not sell. Hence, the survival and growth of the corporation, in a free competitive society, rests more and more on the proper blending of our combined natural and social science knowledge to create and market acceptable products competitively. At present, only a few scientifically trained individuals are qualified and are occupying these key product-planning positions in the management of our industrial organizations. The objective thinking of scientifically trained personnel on corporation survival and growth problems can best be summed up by the old adage: "It's how we use tools that count, and it's amazing how different results can be, with the same tools in the hands of different folks."

—RALPH A. SCHAEFER[1]

[1] Electrochemical Society President 1960-1961; The Bunting Brass and Bronze Co., Toledo, Ohio.

Expanding the Frontiers of Space Technology in

ELECTROCHEMISTRY

Lockheed Missiles and Space Division is making significant contributions in electrochemistry in the development of high energy batteries and fuel cells.

Basic research is being conducted in heterogenous catalysis; photochemistry; physical chemistry; solid state chemistry; electrode kinetics; and mass transfer.

Chemical engineering design and development work includes pilot plant operation; fluid flow; heat transfer; and automatic control.

Engineers and Scientists—The advanced nature of Lockheed's projects in electrochemistry provides an excellent opportunity for scientists and engineers to advance their professional status in an ideal working environment. If you are experienced in electrochemistry or in related work, you are invited to share in the future of a company with an outstanding record of achievement and make an important individual contribution to your country's scientific progress. Write: Research and Development Staff, Dept. F-26, 962 W. El Camino Real, Sunnyvale, California. U.S. citizenship or existing Department of Defense industrial security clearance required.

Lockheed / **MISSILES AND SPACE DIVISION**

Systems Manager for the Navy POLARIS FBM; the Air Force AGENA Satellite in the DISCOVERER, MIDAS and SAMOS Programs; Air Force X-7; and Army KINGFISHER

SUNNYVALE, PALO ALTO, VAN NUYS, SANTA CRUZ, SANTA MARIA, CALIFORNIA
CAPE CANAVERAL, FLORIDA • ALAMOGORDO, NEW MEXICO • HAWAII

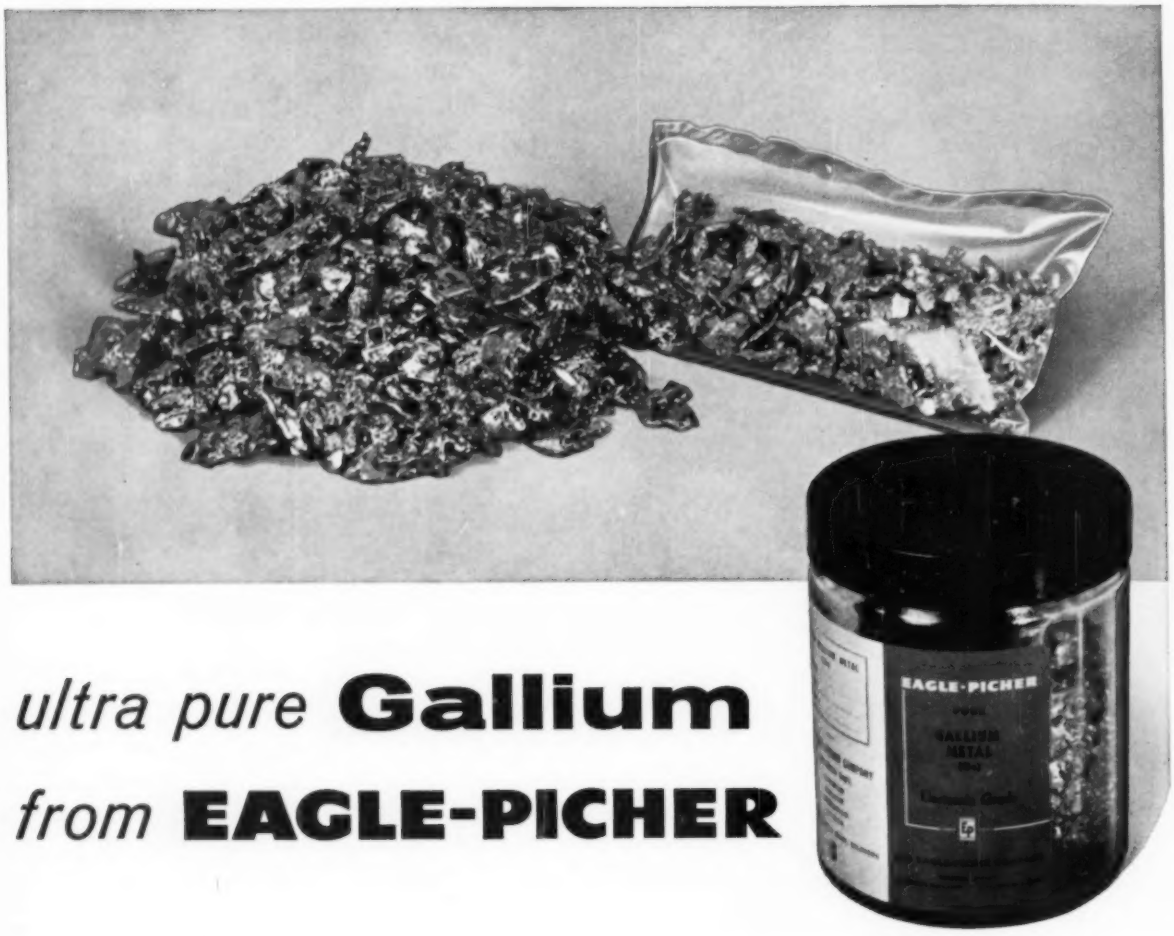

ultra pure **Gallium**
from **EAGLE-PICHER**

New applications for Gallium are being discovered and to meet the growing demand for this rare metal, Eagle-Picher offers painstaking production and dependable supply. We offer, also, a complete line of Germanium products.

Eagle-Picher Rare Metals and Semiconductors

GALLIUM, ultra pure.
Metallic crystals, minimum purity 99.9999%
Metallic crystals, minimum purity 99.999%

GALLIUM SESQUIOXIDE

—also immediately available

CADMIUM SULPHIDE

GERMANIUM DIOXIDE, minimum purity 99.999%

FIRST REDUCTION GERMANIUM METAL, minimum resistivity 5 ohm-cm.

INTRINSIC GERMANIUM METAL, minimum resistivity 40 ohm-cm.

SINGLE CRYSTAL GERMANIUM (undoped) minimum resistivity 30 ohm-cm.

SINGLE CRYSTAL GERMANIUM (doped) to customers' specified resistivity.

SPECIAL SHAPES. Intrinsic Germanium Metal for horizontal or vertical crystal growing. Wide variety in stock, other shapes furnished to customers' specifications.

SCRAP GERMANIUM PLAN. Scrap Germanium may be returned for economical reprocessing under a toll arrangement.

EAGLE EP PICHER

Since 1843
THE EAGLE-PICHER COMPANY
Chemical Division, Dept. JES-660
GENERAL OFFICES: CINCINNATI 1, OHIO

Conductivity of Silver Iodide Pellets for Solid-Electrolyte Batteries

J. N. Mrgudich[1]

Laboratory for Insulation Research, Massachusetts Institute of Technology, Cambridge, Massachusetts

ABSTRACT

Silver amalgam electrodes were found to provide polarization-free contacts for the measurement of the conductivity of compressed AgI powder pellets. Correlation of the conductivity data with x-ray diffraction studies established the presence of a deformed hexagonal phase as an important factor in determining pellet conductivity. Deformation can be induced by compression, but care must be taken to avoid transformation into the face-centered cubic phase with some resultant decrease in conductivity. Preliminary evidence is presented that hexagonal deformation can be induced by suitable thermal or mechanical pretreatment of the AgI powder.

Lehovec and Broder (1) showed that thin sections of certain solid ionic conductors can serve as electrolytes of electrochemical battery systems. Such "solid-electrolyte" batteries, because of inherently easier control and confinement of the electrolyte, promise significant improvement over conventional batteries using liquid electrolytes.

Some of the advantages are illustrated by a cell made by the author in December 1952. Its active components were a sheet of Ag foil as anode, a pellet of compressed AgI powder as electrolyte, and a pellet of 50% AgI and 50% African MnO_2 as cathode. Cross-section diameter was 1.27 cm and overall volume was about 0.15 cc. Despite this small volume the open-circuit voltage, after nearly six years of unsealed storage at ambient room temperature, dropped by only 4% (from 0.56 to 0.54 v) since February 1953. The short-circuit flash current remained substantially constant at 17 μamp. The Ag electrode, except at its periphery where atmospheric oxygen resulted in tarnishing, remained uncorroded.

The most serious shortcoming of such solid-electrolyte systems is their very low flash current, usually measured in μamp/cm^2 of electrode area. This manifestation of high internal resistance follows directly from the fact that the room-temperature conductivity of even the best solid ionic conductors lies six to eight orders of magnitude below that of conventional battery electrolytes. In consequence, unless the room-temperature conductivity of suitable solid ionic conductors can be increased by at least four orders of magnitude, the practical use of the otherwise eminently promising solid-electrolyte batteries will be limited to microwatt power applications.

The purpose of this investigation was to study and develop methods for increasing the room-temperature ionic conductivity of AgI. Silver iodide was chosen because of its reported relatively high room-temperature ionic conductivity, its apparently simple conduction process which involves only Ag^+ ions moving through a fixed I^--ion lattice, and the substantial absence of interfering electronic conduction.

[1] Present address: U.S. Army Signal Research and Development Laboratory, Fort Monmouth, N. J.

Unfortunately AgI is not easily prepared in the form of single crystals stable at room temperature, and there is today little theoretical interest in conductivity measurements on compressed powders. Nevertheless, in view of eventual applications which will of necessity resort to the use of multicrystalline electrolyte in the form of compressed powders, evaporated films, chemical deposits, or painted layers, measurements on such powders and efforts to increase their ionic conductivity are meaningful in a practical sense. Furthermore, multicrystalline electrolytes profit from increased ionic mobility along interfacial surfaces so that, even if single crystals were available, there would be a need for study of the conductivity of compressed powders.

Polarization Phenomena in Measurements of Ionic Conductivity

It is well known that if a d-c voltage is applied across an ionic conductor, the resultant flow of current decreases with time (2, 3). To avoid such polarization effects, a-c voltage (usually 1000 cps), four-probe sample holders, pulse techniques, or combinations thereof are applied. These measures may be adequate when sample temperature is high or when sample conductivity is low. However, blocking layer effects become more pronounced as the temperature drops or as conductivity increases. Brennecke (4), for example, confirming earlier work by Lehfeldt (5), found that d-c conduction through various alkali halides obeys Ohm's law at high temperatures but begins to deviate as temperature decreases. Johnston (6), studying AgBr at room temperature, reported that the a-c conductivity was a function of frequency (even up to 10,000 cps) and that this dependence increased with samples of higher conductivity (about 10^{-7} ohm^{-1} cm^{-1}). There is thus no certainty that conventional methods for minimizing polarization are adequate for a study whose objective is the synthesis of materials exhibiting extraordinarily high ionic conductivities (about 10^{-8} or better) at room temperatures.

Use of Amalgamated Silver Electrodes

In the course of some preliminary studies it was found that application of quite small d-c voltages

across an AgI pellet between identically amalgamated Ag electrodes yielded a remarkably stable current flow. This constancy led to efforts to use such amalgamated electrodes in the development of an apparently polarization-free d-c method for the measurement of the conductivity of AgI pellets.

The amalgamated electrodes were prepared by rubbing Hg onto disks of clean and polished Ag sheet (1.525 cm diameter, approximately 0.15 cm thick). Just before use the electrodes were wiped clean and residual scum removed by rinsing the surface with clean, distilled Hg dropping from a burette.

Pellets of AgI (1.525 cm diameter) were made by compression in a hand-actuated laboratory press (capacity 1120 kg/cm², 16,000 psi). Since the objective was to carry out extensive tests of the reproducibility of a new method, we required ready availability of a relatively large amount of uniform AgI. Most of this work used two different grades of powdered, commercial AgI made homogeneous by thorough mixing after passing through a 35-mesh screen. After compression, the pellets were gently smoothed with 3/0 emery paper to remove peripheral feathering and surface glaze. Then they were placed between identically amalgamated Ag electrodes backed by Pt electrodes to prevent solder contamination of the amalgamated electrodes (Fig. 1).

The voltage across the array could be changed by adjusting the value of the decade-box resistance R_2. Three voltage ranges (0.0001, 0.001, and 0.01 v) sufficed for most of the work. The galvanometer (Leeds and Northrup, D'Arsonval, 0.008 μa/mm deflection at 1 meter) was calibrated for each voltage range by use of a standard calibrated decade resistance replacing the array. Switch S served as an easy means for reversal of current direction to check for the presence of polarization.

Figure 2 compares the results of conductivity measurements on a given pellet of AgI between clean, polished Ag electrodes before and after electrode amalgamation. The slight upward trend of the amalgamated-electrode curve is undoubtedly due to an observed 1°C rise in room temperature during the 64-min run. The lesser fluctuations within each 16-min run fall easily within the errors induced by small random variations of the galvanometer zero. These fluctuations, however, are trivial when viewed in the perspective of Fig. 2 and its very strong evidence of absence of polarization with amalgamated electrodes.

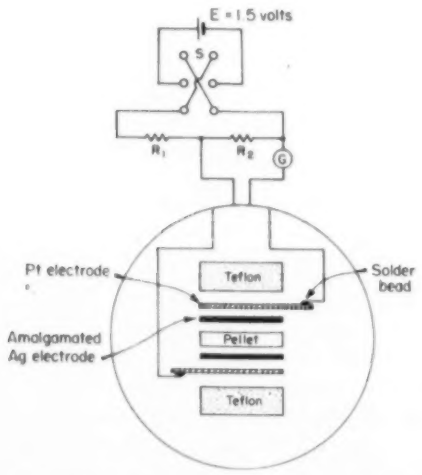

Fig. 1. Exploded view of conducting array, with circuit used to permit easy reversal of applied d-c voltage.

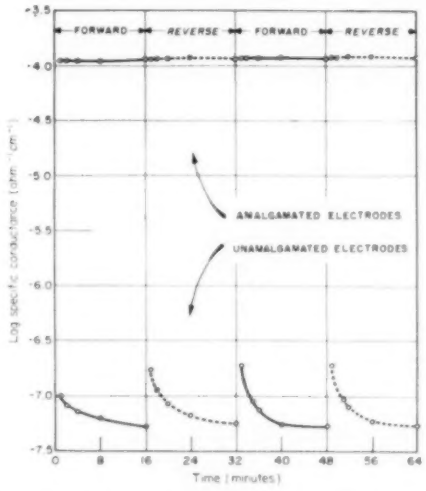

Fig. 2. Elimination of polarization through use of amalgamated silver electrodes.

Considerable time and effort were spent in demonstrating that this method allows for the reproducible determination of the conductivity of AgI at room temperatures. Repeated assembly, measurement, disassembly, electrode reamalgamation, and remeasurement on the same pellet, and variations of pellet dimensions showed that the conductivity is both reproducible and independent of pellet thickness, i.e., that it complies with Ohm's law (Table I).

In a further evaluation of the method, Westphal[2] carried out some a-c measurements of conductivity as a function of frequency. He showed (Table II)

[2] W. B. Westphal, Laboratory for Insulation Research, Massachusetts Institute of Technology, Cambridge, Mass.

Table I. Conductivity of silver iodide—test of reproducibility and compliance with Ohm's law

Material	Pellet No.	Compression pressure (kg/cm²)	Thickness (cm)	Conductivity (ohm⁻¹cm⁻¹) x 10⁴	Average value	Deviation from mean %
AgI*	68	281	0.1068	1.28, 1.31, 1.28 1.27, 1.28	1.28	1.0
AgI*	58	702	0.0986	1.50, 1.48, 1.48	1.51	1.9
	59	702	0.1944	1.47		
	60	702	0.3834	1.54, 1.57		
	61	702	0.7675	1.50		
AgI†	54	702	0.0969	0.98	1.00	1.7
	55	702	0.1894	1.02		
	56	702	0.3813	0.99		
	57	702	0.7692	1.02		

* Mallinckrodt Chemical Works.
† Allied Chemical and Dye Corporation.

Table II. Comparison of conductivities at various frequencies

Electrodes	Ag amalgam		Ag paint		Evap. Ag	
Pellet thickness (cm)	0.384	0.763	0.385	0.762	0.383	0.763
Frequency (cps)						
100	1.54	1.53	1.00	1.29	1.43	1.46
300	—	—	1.35	1.51	1.45	1.52
1,000	1.54	1.53	1.46	1.58	1.44	1.56
3,000	—	—	1.50	1.60	—	1.58
10,000	1.54	1.53	1.52	1.60	1.48	1.59
100,000	1.54	1.54	1.54	1.58	1.48	1.62
300,000	—	—	1.55	1.61	1.49	1.62
1,000,000	1.55	1.52	1.58	1.62	1.50	1.63

All conductivities are given in $(ohm^{-1}cm^{-1}) \times 10^{+4}$. Pellets were made of Mallinckrodt silver iodide powder compressed at 702 kg/cm² and were approximately 16 days old at the time of measurement.

that with Ag paint or evaporated Ag electrodes the a-c conductivities approached constancy only above 10,000 cps and even then yielded values that varied with sample thickness. It will be noted that similar a-c measurements using amalgamated electrodes gave conductivities independent of both frequency and sample thickness.

The major precaution that must be taken with amalgamated electrodes is avoidance of scum. When this is realized, the results are readily reproducible and the pellet, even after week-end contact with the electrodes, shows no discoloration or evidence of reaction with Hg (formation of HgI_2 or Ag_2HgI_4). Addition of weights to the assembled vertical array is of no significant effect up to 100 g. Beyond this point the conductivity decreases by about 6% at 200, 13% at 500, and 19% at 1000 g. This effect seems to be due to squeezing out of a mobile amalgam interface.

When an amalgamated array is first assembled, it exhibits a variable transient voltage that dies away to a fraction of a microvolt within about 10 min. Although this may be due to a slight difference in the temperature of the two electrodes [Reinhold (7) has shown that a difference of 1°C in the relative temperatures of the electrodes of an Ag-AgI-Ag array near room temperature can result in a voltage difference of about 1000 μv], it is more likely that amalgam redistribution is involved since the top electrode is always initially negative with respect to the bottom. Careful conductivity measurements, of course, must await practical disappearance of these transients.

Effect of Compression Pressure on Pellet Conductivity

Although description of a d-c method for measurement of the conductivity of AgI is the major objective of this paper, a few very preliminary applications have been made.

Table III gives the room temperature conductivities of pellets of Mallinckrodt AgI compressed at various pressures and temperatures. The low-temperature compressions were made by quick compression of pre-assembled cavity, plug, sample, and plunger after chilling the pressure chamber and sample overnight at —10°C. Likewise, the high-temperature compressions were made on preheated assemblages.

Table III. Conductivities of pellets as function of compression pressure at different temperatures

Compression pressures		Compression temperatures, °C		
kg/cm²	psi	−10°	27°	95°
140	2,000	0.43	0.65	0.96
281	4,000	1.08	1.23	1.17
421	6,000	1.38	1.36	1.31
562	8,000	1.43	1.37	1.31
702	10,000	1.56	1.48	1.27
843	12,000	1.58	1.55	2.30
983	14,000	1.61	0.89	—
1220	16,000	1.80	0.74	2.66

All conductivities are given in $(ohm^{-1}cm^{-1}) \times 10^{+4}$. Pellets compressed at −10°C and 27°C were 24 days old at the time of measurement; those at 95°C were 4 days old.

The most interesting feature of Table III is the conductivity "break" observed beyond 843 kg/cm² in the room-temperature series. This break was confirmed with a second run of Mallinckrodt AgI and was also observed using the Allied Chemical material.

Suspecting that a phase change was associated with the conductivity break, x-ray diffraction techniques (Norelco diffractometer, filtered Cu radiation, scanning speed of 1°/min, chart speed of 1.27 cm/min) were applied to a study of the second room-temperature pressure series using *unpolished* Mallinckrodt pellets. It is known that there exist at least three modifications of AgI (8). The γ phase, yellow, stable up to about 137°, is face-centered cubic with $a_o = 6.502$Å. The β phase, orange, stable from 137° to about 146°C, but apparently metastable at room temperature, is hexagonal with $a_o = 4.59$ and $c_o = 7.49$Å. The α phase, brown, stable only above 146°C, is body-centered cubic with $a_o = 5.044$Å. It is particularly interesting to note that the axial ratio for the hexagonal phase is very close to the 1.633 value characteristic of ideal close packing. As Manson (9) pointed out, this means that all strong γ-cubic lines will face at nearly the same positions as strong hexagonal lines although there

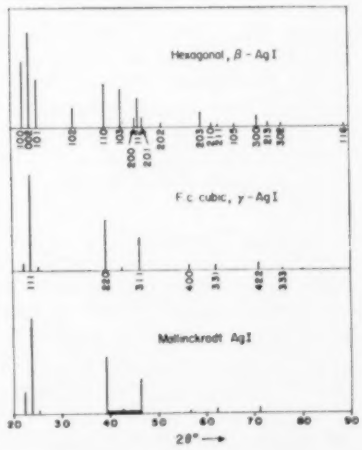

Fig. 3. X-ray diffraction angles and relative intensities of β and γ silver iodide.

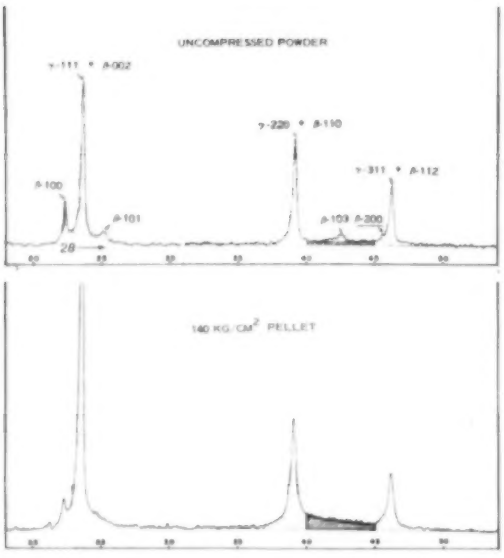

Fig. 4. Structural changes associated with initial compression of AgI powder.

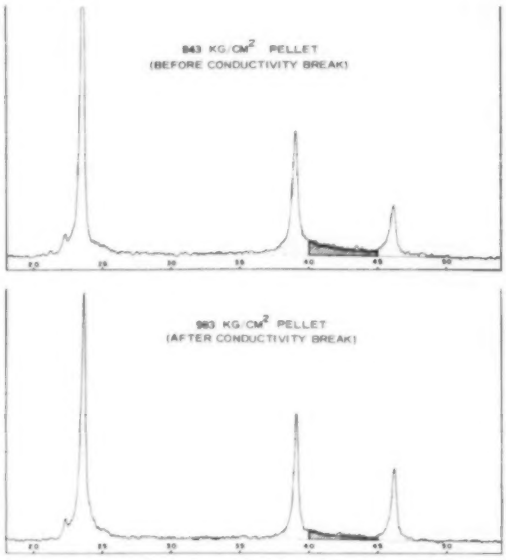

Fig. 5. Diffraction traces of pellets before and after conductivity break.

will be lines in the hexagonal pattern not present in the γ-cubic. The two upper charts of Fig. 3 (practically pure γ and β materials obtained from Mr. Manson[2]) illustrate these line coincidences. The bottom chart shows that the Mallinckrodt material is essentially γ-cubic with easily detectable amounts of β-hexagonal.

Figure 4 illustrates diffraction differences between uncompressed Mallinckrodt powder and a pellet compressed at room temperature at 140 kg/cm² (2000 psi). There is a sharp increase in the $\gamma(111) + \beta(002)$ intensity, all β lines tend to disappear, the entire region between 2θ values of 39-46° becomes abnormally fogged (shaded area), and all cubic lines tend to broaden with asymmetric tailing of the base.

The sharp increase in $\gamma(111) + \beta(002)$ intensity indicates a pressure-induced orientation of grains of one or both phases. The other three effects can be explained on the basis that pressure broadens all hexagonal lines. Such line broadening is indicative of strong deformation of hexagonal crystallites and/or pronounced grain fragmentation. The fact that line broadening occurs at relatively low pressure (even at 35 kg/cm², 500 psi) and the logical assumption that grain deformation precedes grain fragmentation favor acceptance of the lattice-deformation viewpoint.

X-ray traces of pellets compressed at pressures up to 843 kg/cm² (12,000 psi) were essentially the same as for the 140 kg/cm² (2000 psi) pellet. Relatively marked changes took place, however, in the pressure range corresponding to the conductivity break (Fig. 5). There was a decrease in the $\gamma(111) + \beta(002)$ intensity, a decrease in shaded-area fogging, and an increase in line symmetry with some indications of line sharpening. These changes in the diffraction patterns may be due to a pressure-induced tendency for the disappearance of deformed hexagonal phase, probably by conversion to γ-cubic. The associated drop in conductivity is strong evidence of the importance of the deformed hexagonal phase as a conductivity-imparting ionic "solder."

At higher pressure (1,220 kg/cm², 16,000 psi), shaded-area fogging, while still present, diminishes in a manner consistent with the slightly lowered conductivity (cf. Table III).

Some Exploratory Measurements

It has been found that the conductivity of pellets decreases slowly with time. There is a linear relationship between log specific conductance and log time. This is reminiscent of the linear relationship known to exist in metal deformation where per cent recovery of yield stress varies linearly with log time and can be construed as evidence supporting the lattice-deformation concept.

Using a special sample holder (Fig. 6) which employed pools of liquid silver amalgam, it was possible to make a preliminary study of the effect of increasing temperature on the conductivity of a pellet compressed at 702 kg/cm² (10,000 psi) at

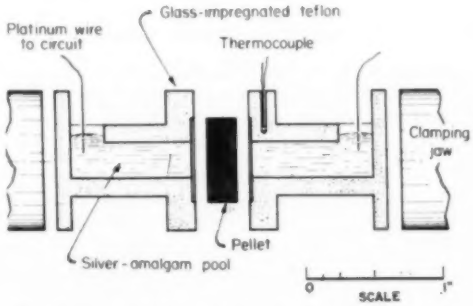

Fig. 6. Conductivity cell using liquid amalgam pools

[2] Air Force Cambridge Research Center, Bedford, Mass.

room temperature. Evidence of a temperature-accelerated relief of hexagonal deformation was noted during an overnight stand at about 75°C. Further temperature increase resulted in a tremendous increase in conductivity, from 7.2×10^{-4} ohm^{-1} cm^{-1} at 132°C to 9 ohm^{-1} cm^{-1} at 138°C. Pellet color changed from greenish yellow to speckled orange with little, if any, change in pellet dimensions. It seems probable that a phase transition from essentially γ-cubic to essentially equally dense β-hexagonal took place. Overnight standby at 138°-139°C resulted in a drop in conductivity to 1.2 ohm^{-1} cm^{-1}. Further increase in temperature resulted in a *drop* to about 1.0×10^{-1} ohm^{-1} cm^{-1} at 146°C beyond which temperature the pellet color changed from speckled orange to solid tan-brown (probably a transformation of β-hexagonal to α-cubic) with no significant increase in conductivity. The pellet underwent sharp expansion. For all practical purposes this expansion concluded the temperature run. Cooling to room temperature gave a canary-yellow pellet (compared to the original greenish-yellow) and a conductivity estimated at 1×10^{-7} ohm^{-1} cm^{-1}. Repeated temperature cycling (room temperature to 180°C) with the expanded pellet showed that pellet-color changes were remarkably consistent; invariably canary yellow below 137°, speckled orange between 137°-146° and tan-brown above 146°C. Furthermore, the conductivity changed sharply only at about 137°C, indicating that the transition from γ-cubic to β-hexagonal is probably more important with respect to conductivity than that from the β-hexagonal to α-cubic.

Time was not available for the preparation of the large quantities of pure γ and β AgI needed for a careful study of the effect of compression temperature and pressure on structurally homogeneous phases. It has been shown, however, that pellets of Manson's purest γ and β materials, at room-temperature compression pressures of 281 kg/cm^2 (4000 psi), gave conductivities of 1.9 and 3.5×10^{-6} ohm^{-1} cm^{-1}, respectively. Both of these are significantly lower than the 281 kg/cm^2 pellet of the Mallinckrodt γ-β mixture at 12.3×10^{-5} ohm^{-1} cm^{-1}. A possible explanation of this anomaly of a mixture having a conductivity higher than either of its two components may lie in the residual deformation present in the uncompressed Mallinckrodt powder (cf. shaded area, top trace of Fig. 4) and absent in the Manson pure-hexagonal material.

X-ray examination of Allied Chemical AgI showed it to be (like the Mallinckrodt material) a mixture of γ and β phases. Grinding in a mechanical mortar for 2 hr resulted in the line tailing, abnormal fogging, and line broadening characteristic of hexagonal deformation. The conductivities of 281 kg/cm^2 pellets of ground and unground materials were 22.4 and 8.0×10^{-6} ohm^{-1} cm^{-1}, respectively, indicating the possibility of inducing hexagonal deformation by mechanical pretreatment of the starting material.

In a quick and incomplete study of the effect of heating and cooling of Allied Chemical AgI it was found that heating the powder in air to 140°, 165°, and 200°C, followed by slow cooling to room temperature, resulted in no significant change in the x-ray traces. However, a sample heated to 200°C for 2 hr and then quenched by sprinkling into a pool of liquid air did show deformation of the hexagonal phase. No conductivity measurements have been made thus far, but thermal shock treatment of powders seems promising.

Prognosis

The work here reported demonstrates that the conductivity of a pellet of compressed AgI can be increased substantially. It does not appear premature to prognosticate conductivities at least one order of magnitude higher (i.e., ca. 10^{-3} ohm^{-1} cm^{-1}) than any yet observed. At this value the conductance of a pellet of 1 cm^2 area and 0.01 cm thickness would correspond to an "electrolyte" resistance of about 10 ohm. Ignoring other resistance sources within the cell, this electrolyte resistance would permit a flash current of about 50 mamp with a cell of 0.5 v open-circuit voltage. Such current outputs would definitely widen the applicability of solid-electrolyte batteries.

However, availability of a highly conductive solid electrolyte, although necessary, is not a sufficient condition for satisfactory battery operation. For example, the conductivity of the cathodic depolarizer must also be high, both from the standpoint of ions entering through the electrolyte from the anode and of electrons entering through the external circuit. Furthermore, volumetric changes associated with discharge (anode consumption and depolarizer expansion) require some compensating physical mobility of the electrolyte or suitable design characteristics. These problems need further study.

Acknowledgment

The author is indebted to Professor A. R. von Hippel and Dr. A. Smakula for many hours of helpful discussion, and to Dr. D. S. Tannhauser and Mr. A. D. Bedrosian for continuing counsel and guidance. Furthermore, he acknowledges the effective co-operation of many members of the Fort Monmouth organization and of the staff and graduate students of Massachusetts Institute of Technology. He is grateful, also, to Professor G. S. Brown, Head, Department of Electrical Engineering, for status as a member of the School for Advanced Study.

Manuscript received Sept. 16, 1959. This work was made possible by a one-year Secretary of the Army Research and Study Fellowship award.

Any discussion of this paper will appear in a Discussion Section to be published in the December 1960 JOURNAL.

REFERENCES

1. K. Lehovec and J. Broder, *This Journal*, **101**, 208 (1954).
2. J. and P. Curie, *Ann. chim. phys.*, **17**, 385 (1889); **18**, 203 (1889).
3. A. R. von Hippel, "Dielectrics and Waves," pp. 228-234, John Wiley & Sons, Inc., New York (1954).
4. C. G. Brennecke, *J. Appl. Phys.*, **11**, 202 (1940).
5. W. Lehfeldt, *Z. Physik*, **85**, 717 (1933).
6. W. G. Johnston, *Phys. Rev.*, **98**, 1777 (1955).
7. H. Reinhold, *Z. anorg. u. allgem. Chem.*, **171**, 181 (1928).
8. J. D. H. Donnay and W. Nowacki, "Crystal Data," p. 497, Geological Society of America, New York (1954).
9. J. E. Manson, *J. Appl. Phys.*, **26**, 423 (1955).

Sine Wave Pulse Current Tester for Batteries

K. Kordesch and A. Marko[1]

Research Laboratory, Union Carbide Consumer Products Company, Division of Union Carbide Corporation, Cleveland, Ohio

ABSTRACT

An instrument has been developed which measures the voltage of a battery during discharge, eliminating its ohmic component. The instrument is portable operated on 60 cycle alternating current and features direct meter readings (instead of an oscilloscope). Its simplicity and ruggedness make it especially suited for development and production control tasks. Results of measurements on different types of cells are presented to illustrate the wide applicability of the instrument.

The intention of the authors was to develop a simple and reliable instrument for the evaluation of battery performance under load conditions. The method of measuring polarization and internal resistance values by means of periodic current interruption was chosen because these parameters are very characteristic for a battery system.

Square wave generators have been used frequently to study the characteristics of electrodes of galvanic systems. The literature reports many of these devices, some of them quite useful in research and development laboratories. However, most of these instruments are complex, use an oscilloscope, and are not suitable for rugged performance conditions. Furthermore, they require highly skilled personnel for interpretation of the measurements (1-3).

The principle of a circuit which enables us to subject a cell to a periodically interrupted discharge (pulse current load) and measure the voltage of the cell between the discharge periods is shown in Fig. 1 (4). In position one, 1, the double pole vibrator switch, S, connects the cell on test to a discharge circuit consisting of a variable resistor, R, and an ammeter, A. In position two, 2, of the switch, the cell is charging a capacitor, C, to the potential existing during the current off-time. A high resistance voltmeter, V_1, indicates this voltage. If the vibrator switch operates at a frequency of at least 50 cycles, the polarization of the cell reaches a steady-state value corresponding to the load current indicated by the ammeter. A booster battery prevents the discharge current from changing too much when the cell voltage changes. The voltmeter, V_2, indicates the terminal voltage of the cell being tested.

[1] Present address: Wright Air Development Center, Dayton, Ohio.

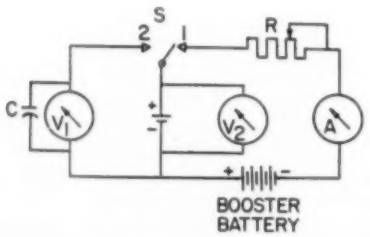

Fig. 1. Vibrator circuit

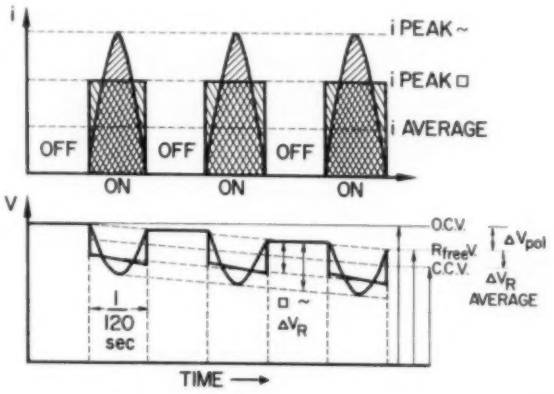

Fig. 2. Effect of square or sine wave pulses on a battery system.

Figure 2 shows in an artist's sketch the oscillographic curves obtained from a battery system subjected to a pulse current. First, only square wave pulses shall be discussed in connection with the just mentioned vibrator switch circuit. The current pulses are pictured in the upper section of the sketch. With an equal "off" and "on" time (1/120 sec) the average current is one half of the peak current. The galvanic cell responds to this average current indicated by a moving coil instrument of the common d-c ammeter-type. In the lower part of the sketch, the effect of the current pulse on the voltage of the cell is shown. Only a few pulses are shown in the drawing, but it should be understood that the system will reach a certain steady state, e.g., after 1 min of closing the circuit, the readings may be taken. The voltage of the cell without the resistance component, R_{free} V, is represented by the top level of the pulse curves. The terminal voltage, CCV, is represented by the average value of the pulses (½ of the square pulse). The difference between the OCV and the R_{free} voltage indicates the sum of all slow polarization effects in the cell system (ΔV_{pol}), the difference between the highest points and the lowest points of the pulse curves represents the resistance

voltage drop caused by the corresponding peak current. The resistance value in ohms is calculated by dividing $\Delta V_{R\square}$ by the current i peak □. It is important to note that the same value is obtained by dividing the difference between the R_{free} voltage and the CCV (ΔV_R average) by the average current. The circuit shown in Fig. 1 provided meter indications of $i_{Average}$, R_{free} Voltage, the initial OCV and the later CCV. From these figures one can calculate the polarization and resistance components of the voltage drop caused by the load condition (ΔV_{Pol} and R). The pulse frequency can be chosen from a range between 30 and 400/sec in which no differences have been found in practical cell testing. Mechanical vibrators operate in the 50-100 cycle range, the later discussed electronic switch circuit uses the line frequency of 60 cycles. A too low pulse frequency causes deviation due to recuperation effects during the "off" time; too high frequencies introduce capacitance errors. However, if we consider that the accuracy of common good meters is not better than one half of a per cent, we do not need a better reproducibility of our measurements than ±5 mv (for a 1-v cell). This is the case with all depolarizers tested (manganese dioxide, nickel oxides, lead dioxide, silver oxides) and with most of the available anodes (zinc, cadmium, lead).

The vibrator circuit of Fig. 1 has been used in battery testing circuits with the main objective of studying the polarization characteristics of cells under heavy load conditions. Powerful depolarizers such as silver or nickel oxides polarize to such a small extent that resistance variations obscured the measurements of polarization effects (5).

Mechanical switching proved to be inadequate for high currents; contact bouncing sometimes caused erroneous meter indications. The production of exact square waves by means of mercury switches or electronic circuits could not be solved with a simple apparatus. The inherent capacitance-rounding of square waves and the "cable ring" effects with longer leads were additional reasons for investigating a circuit employing rectified sine wave pulses for test purposes.

The sine wave pulses needed for the polarization of the cell are conveniently taken from the 60-cycle a-c line. Figure 2 shows the effect of half-wave sine pulses of the same mean current value as the square wave pulses. The actual discharge current is one-third of the peak current in accordance with calculations of the mean values of rectified waves. The factor for the ideal, non-truncated half-sine wave for the period 0-360° is $1/\pi$. In a moving coil instrument with D'Arsonval movement the torque on the coil is proportional to the current; therefore the meter reads the average value, which corresponds to the coulometric value of the current. A hot wire, dynamometer or other square law (RMS) instrument cannot be used in this case because its deflection represents I^2R, in our case about 1.45 times larger than the average current (6).

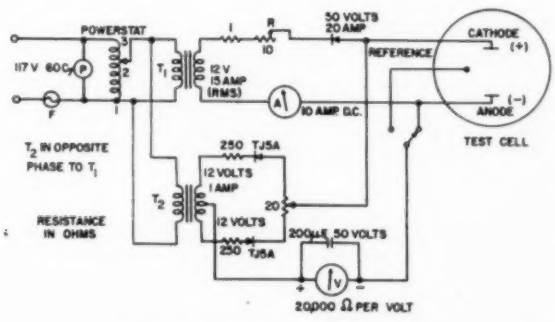

Fig. 3. Sine wave pulse current tester

Figure 3 shows the circuit diagram of one of the most versatile versions of the test instrument. A powerstat transformer circuit, T_1, produces a 12-v alternating current which is rectified and used as a single-phase pulse current to discharge the test cell. The current is regulated at the input of the powerstat and also by means of a variable resistor R. The a-c voltage should be at least six times the cell voltage to assure a clean sine wave shape. The average value of the current is indicated by the ammeter A. In order to connect the voltmeter, V, to the cell between the current pulses (same principle as the vibrator circuit in Fig. 1) a gating circuit is employed represented by a second small transformer T_2 and a double diode bridge. This gating circuit has the purpose of producing alternatingly a very low resistance path and an extremely high resistance connection between the (+) terminal of the voltmeter and the cathode of the test cell. The (−) terminal of the voltmeter is continuously connected to the anode of the cell (or a reference electrode, if desired). The proper timing of the gating circuit is enforced by an alternating current introduced into the bridge by means of transformer T_2. This alternating current does not add or subtract any potential between the center tap of the transformer and the tap of the balancing potentiometer, but it "opens" or "closes" the two diodes in the bridge circuit in opposite phase to the current pulses of the transformer circuit T_1. The voltmeter V indicates the voltage of the capacitor which is charged only during "off current" periods. The proper value of the capacitor is dependent on the resistance of the voltmeter, but not critically. The gating diodes should be of a very high forward/backward current ratio, preferably over 1000:1. Transformer T_2 may be replaced by an additional winding on T_1, but in practice it turned out to be far more convenient to use a separate small transformer for the gating unit, which can be separated completely from the power section in cases where it is desired to subject many cells in series to the pulse current but measure the R_{free} voltages of individual cells.

A reference electrode can be used for the independent measurement of the polarization of cathodes or anodes. The position of the reference electrode is not critical because electrolyte resistance effects are also eliminated.

In some cases where an extension to higher pulse frequencies was desired (e.g., in studies of magnesium electrodes showing passivation effects) we used an audio generator to produce the pulse currents. For work on high resistance batteries (organic depolarizers, solid electrolyte cells) we changed the

silicon diodes of the gating circuit to vacuum tubes and the 20,000 Ω/v meter to a vacuum tube meter (the capacitor across the voltmeter should then be in the range of 1-10 μF).

The principal circuit has been used by the authors for eliminating the disturbing ohmic resistance component in oxygen sensing elements operating on the air-depolarized cell principle, and in connection with fuel cell studies a similar circuit was described at the Electrochemical Society Meeting in October, 1956 (7). Variations of it have been employed for experimental state of charge determination of Ni-Cd batteries (8).

The data obtained with our interrupter have been checked many times against a precision square wave (electronically) switching instrument,[2] and as far as any useful battery system was concerned, no deviation could be detected. With modern rectifier and transistors, the whole instrument can be made small-sized, the largest components being the transformer, the ammeter, and voltmeter. There is no limitation to the current or voltage range of the batteries to be tested; the circuit can be adapted easily to any test requirement.

In order to demonstrate the versatility of the instrument examples of test results with different battery systems are given in the following figures. Differences in depolarizer mix formulation (Fig. 4), influence of geometrical construction (Fig. 5), and system variations (Fig. 6) express themselves in characteristic polarization and resistance curves.

In Fig. 4 (Leclanché cells) Cell A is a regular D-size cell and cell B is a D-size photoflash cell. Both cells have been discharged with a 500 ma pulse current and the R_{free} voltage and the *CCV* are shown as obtained on a simultaneous recording. The ohmic resistance values are calculated from the differences. The cathode of cell A is manufactured mainly from natural ore, the bobbin of cell B contains a large percentage of artificial MnO_2 and more graphite. The gradual loss of depolarizing power or the increase of cell resistance on light intermittent duty or after long storage periods shows up in a similar way if periodic checks (e.g., 1-min tests) are made during the life time of the cells (5, 8).

Figure 5 shows the characteristics of two D-size alkaline MnO_2 cells with powder zinc anodes. Cell

[2] Constructed by Professor E. Yeager, Western Reserve University, for the Research Laboratory of Union Carbide Consumer Products Company.

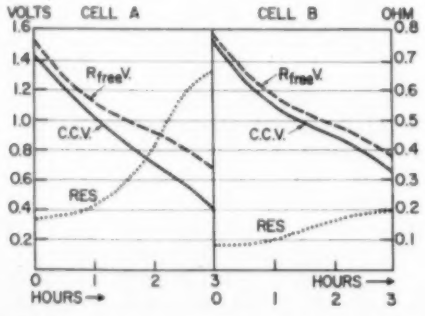

Fig. 4. Discharge characteristics of a standard D-size cell (A) and a photoflash cell (B) 500 ma.

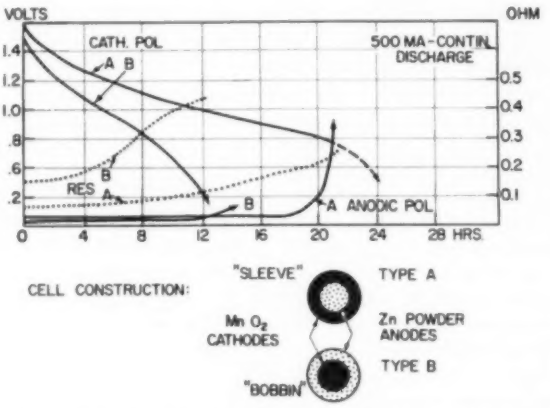

Fig. 5. D-size alkaline MnO_2 cells on 500 ma. Discharge (constr. A and B).

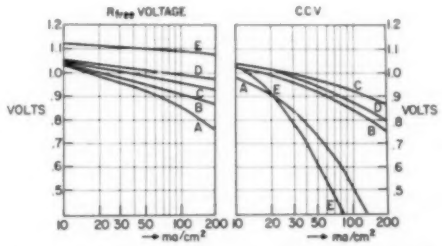

Fig. 6. Terminal voltage and $\Delta V_{R\infty}$ free voltage of hydrogen-oxygen fuel cells. Geometry: A, parallel tube electrodes; B, concentric tube electrodes; C, D, E, parallel plate construction. Electrolytes: A, B, C, 30% KOH at 60°C; D, molten caustic at 200°C; E, fused carbonates, 500°C.

A contains a sleeve type cathode, cell B is made with a bobbin type cathode. In these diagrams only the R_{free} voltages and the resistance values are plotted vs. time. The average discharge current is 500 ma. Here the R_{free} voltage curves are named "polarization curves;" they are measured against a zinc reference electrode positioned between cathode and anode. This gave the possibility to record the anodic polarization curve also.

Figure 6 shows a collection of performance data characteristic for different types of hydrogen-oxygen fuel cells. R_{free} voltage curves are shown on the left side of the figure and *CCV* curves are shown on the right side of the figure. The current density is on a logarithmic scale to cover a wider range. It demonstrates how important it is to know the R_{free} voltage curves to judge performance characteristics. From the terminal voltages (right side) one would say that cell C is the best, cell D the worst; but a look at the corresponding curves on the left side indicates that E has the lowest polarization drop, A the highest. The observed differences are partially due to geometry factors and partially caused by different operating conditions. The R_{free} voltage curves of Fig. 6 agree very well with the values calculated from independent a-c bridge measurement of cell resistances. The advantage of using a pulse current instrument for such studies is the freedom of variation caused by uncontrolled resistance changes during the duration of the test. Lead wire

and contact resistance errors are eliminated. The "true" voltage of the chemical system is directly indicated on the voltmeter.

The pulse current tester described has also been used for charge control purposes. The $R_{t_{max}}$ voltage reading is a better indication of the state of charge than the *CCV* because it is not influenced by conductivity changes in the electrolyte or gas film phenomena in the gassing period of the charging procedure. The use as a sensing circuit for automatic constant voltage charging units has been proposed (5). The gating circuit can be used in connection with thyratrons and magnetic current regulators (8). Adaptation to full wave rectifier circuits is achieved by a C-R phase shift arrangement in the gating bridge, "connecting" the voltmeter only during the very short current off period between the two rectified half-waves (the counter voltage of the cell causes truncated sine pulses).

Manuscript received Nov. 4, 1959. This paper was prepared for delivery before the Columbus Meeting, Oct. 18-22, 1959.

Any discussion of this paper will appear in a Discussion Section to be published in the December 1960 JOURNAL.

REFERENCES

1. D. Staicopoulos, E. Yeager, and F. Hovorka, *This Journal*, **98**, 68 (1951); see also R. R. Witherspoon, H. Urbach, E. Yeager, and F. Hovorka, Tech. Rep. Western Reserve University, ONR, Proj. NR 359-277, No. Nonr 581 (00).
2. E. Newberry, *Trans. Faraday Soc.*, **43**, 127 (1947).
3. A. Hickling and F. W. Salt, *ibid.*, **37**, 450, (1941).
4. A. Marko and K. Kordesch, U.S. Pat. 2,662,211, Dec. 8, 1953.
5. K. Kordesch and F. Kornfeil, U.S. Pat. 2,864,055, Dec. 9, 1958, Rep. of SCEL Proj. No. 3-99-09-021 (1954). K. Kordesch, Technical Memorandum, M-1664, June 9, 1955, U.S. Army Signal Research and Development Laboratory.
6. L. B. W. Jolley, "Alternating Current Rectifications," p. 47, J. Wiley & Sons, Inc., New York (1926).
7. K. Kordesch, Battery Symposium, Electrochemical Society, Oct. 1956, Abstract No. 27.
8. A. W. Speyers, 13th Annual Power Sources Conference, U.S. Army Signal Res. & Dev. Lab., Ft. Monmouth, N. J. Contract rep. by Vitro Laboratories.

An Investigation of the Reaction between Aluminum and Water

Walter J. Bernard and John J. Randall, Jr.

Sprague Electric Company, North Adams, Massachusetts

ABSTRACT

It was found that the film formed on aluminum by the action of water between 80° and 100°C consists of a hydrate of aluminum oxide containing as much as 32% water, rather than stoichiometric $Al_2O_3 \cdot H_2O$, as previously reported in the literature. The reaction is not instantaneous but is delayed by the presence of the natural oxide film on the metal. It was also concluded that hydrated oxide growth does not depend on the movement of aluminum ions through the film.

When pure aluminum is immersed in boiling water, there is an initial period during which no visible reaction occurs, followed by hydrogen evolution and the production of an adherent layer of hydrated oxide. The discharge of gas occurs at first at several widely separated points and then quickly spreads over the entire surface of the metal. The rate of hydrogen evolution soon decreases and is barely perceptible after 10 min or so, although weight measurements show that oxidation of the metal continues beyond this point. Considerable literature exists on the subject of this oxidation, but we are unaware of any previous mention of the existence of the inhibition period. In this paper we are suggesting an explanation for this inhibition period and present some new evidence for the composition of the oxide film which is formed, as well as some observations on the mechanism of film formation.

Experimental

The metal used was 0.003 in. thick high-purity Alcoa aluminum foil, with a guaranteed minimum Al content of 99.986%. Representative samples of this material (Alcoa analysis) gave the following concentration of impurities: 10 ppm Cu, 10 ppm Fe, 10 ppm Si, and 40 ppm Zn. Specimens used had a surface area of 100 cm^2.

Degreased specimens were prepared by soaking in trichloroethylene, rinsing in benzene, and then drying under vacuum.

Foil specimens were electropolished in a bath recommended by Jaquet (1) for a period of 2 min at a current density of 9 ma/cm^2. The solution was cooled in an ice bath and constantly stirred with a magnetically driven stirring bar during polishing. The foil was washed thoroughly with distilled water in order to remove the last traces of the electropolishing solution, since the presence of minute impurities may affect the subsequent reaction with water (2).

Hydrations at 100°C were carried out in Pyrex beakers which were cleaned scrupulously before each run. Specimens were suspended in the water from Pyrex rods. The presence of glass had no noticeable effect on the reaction even after a reaction time of 1 hr, as shown by the fact that a few parallel experiments in Teflon beakers gave essentially the same results. The reaction water had a conductivity of about 1.2×10^{-4} ohm^{-1} cm^{-1} and was preboiled for 15 min before using in order to expel

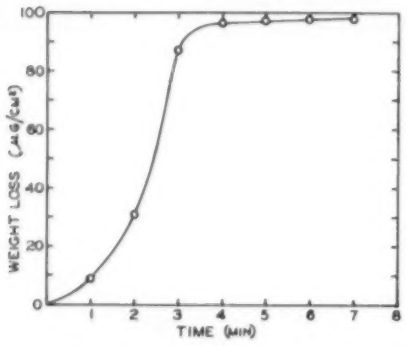

Fig. 1. Rate of removal of hydrated aluminum oxide from the surface of aluminum by CrO_3-H_3PO_4 stripping solution at 85°C. Reaction time with water was 1 hr at 100°C.

dissolved gasses. Reactions at lower temperatures were made in flasks kept in a thermostatted bath. The water was not maintained in an inert atmosphere. For these runs the foil was held in a perforated glass cup which was joined to an extension of a 45/50 $\overline{\$}$ joint. The assembly could be removed easily and quickly at the end of the reaction to be quenched in room-temperature water.

The extent of the reaction was determined by weight changes involving the dissolution of the hydrated oxide film in a solution of 2% CrO_3 and 5% H_3PO_4 at 85°C; the attack of this solution on the underlying metal is reported to be extremely slow (3). The behavior of the stripping solution for a typical hydrated specimen is shown in Fig. 1. After all the oxide is removed the rate of attack on the base metal is only 0.2 $\mu g/cm^2/min$ which is sufficiently slow for our purposes. The method was calibrated by checking the weight loss of anodic films of known weight.

A source of error in this method would result if the hydrated oxide were not completely stable during reaction and if part were lost by dissolution or through mechanical action. However, we were unable to detect the presence of aluminum in the water after a reaction time of 60 min. On the other hand, we observed that, if the water had been used for reaction for a period of some hours, a subsequent oxidation gave slightly higher results than were obtained in freshly prepared water. The reason for this is not clear.

Hydrated oxide was obtained free of metal by dissolving the aluminum in a hot solution of bromine in methanol. It was necessary to wash the oxide thoroughly in order to remove the products of the reaction. This was accomplished by refluxing the oxide in several changes of methanol. The final product was dried at 80°C for 2 hr.

Thermogravimetric analysis was carried out on a Chevenard Recording Balance which was used with a maximum sensitivity of 0.5 mg/mm of chart. The maximum temperature attainable was 1000°C and the heating rate was 2.5°C/min.

Density measurements were made hydrostatically in toluene.

The measurement of the hydrogen evolved in the reaction of the hydrate and the underlying metal was made in an all-glass apparatus. A 10 ml gas burette was connected by capillary tubing to a 12 mm reaction tube containing the sample. The tube was sealed and the entire system was flushed with argon before reaction. The sample was heated quickly to 600°C and held at that temperature for an hour before removing the furnace; Pyrex glass was satisfactory under these conditions. Water from the hydrate was absorbed in a P_2O_5 trap at the exit of the furnace and, therefore, did not contribute to the volume change in the system. This was verified by decomposing $NiSO_4 \cdot 6H_2O$ under the same conditions, whereby the water was absorbed quantitatively. A sample of the isolated hydrate of alumina was also decomposed in this manner and gave no volume increase in the apparatus.

Debye-Scherrer powder patterns were made with samples mounted in a 57.3 mm Phillips powder camera, using CuKα radiation. Exposure times were of the order of 16 hr.

All weighings were made on a Brinkmann-Sartorius Microbalance to the nearest 10 μg.

Results and Discussion

Composition of the film.—It is generally accepted that the product of the reaction above 80°C is boehmite, α-$Al_2O_3 \cdot H_2O$; the characteristic electron diffraction pattern of this compound has been observed by Harrington and Nelson (4), Hart (5), and Kerr (6). Some of the characteristic lines of the boehmite pattern have also been obtained by us by x-ray diffraction. The very diffuse patterns obtained by us and others indicate a poor degree of crystallinity. This evidence is not sufficient to establish the reaction product as pure boehmite, although further support for this composition is given by Bryan (7), whose gravimetric analysis led to the conclusion that the surface product consists of nearly stoichiometric $Al_2O_3 \cdot H_2O$. Bryan's analytical method is subject to criticism, however, on the basis of some of our findings and there is evidence to show that the reaction product contains water considerably in excess of that required for the monohydrate. Bryan reported the water content of the film to be 15.5%, as compared to 15.0% for the theoretical value for the monohydrate. This was determined by heating the metal to 600°C after reaction and measuring the weight loss. However, we have found that this leads to low results because part of the water in the film reacts with the base metal during heating to produce more oxide. If, instead, the hydrated product is separated from the metal by dissolving the aluminum in methanol-bromine solution (8) and then dehydrated, we find that the water content may be as high as 32%. The same results may be obtained by weighing the foil before and after reaction and then removing the reaction products by dissolving in a chromic acid-phosphoric acid solution and reweighing. By the use of the appropriate calculations the three measurements lead to the total weight of hydrated oxide and the amount of water present. This latter procedure is a more convenient method and has been used for the measurements of the rates of reaction discussed below.

We have also shown that the hydrated surface oxide reacts with the base metal during heating by measuring the volume of hydrogen evolved under these conditions. In a typical experiment, a sample of aluminum with an area of 100 cm^2, which had been treated with boiling water for 60 min, produced 1.5 ml of hydrogen when heated to 600°C for 1 hr in an inert atmosphere. This corresponds to 1.2 mg of water, which would not have been detected by Bryan's method, out of a total hydrated oxide weight of 10.9 mg and a water content of 3.0 mg. A more pronounced effect was obtained by the use of etched foil, for which the true surface area is not precisely known but is several times greater than for smooth foil. With this material, volume increases of 5-6 ml were observed under the same conditions.

Finally, the measured density of the oxide was found to be 2.4 ±0.1 g/cm^3, as compared to 3.0 for pure boehmite (9).

The form in which the excess water is combined in the surface product is not known. The composition of the film most frequently approximates that of a dihydrate, but this probably has no significance. It could be postulated that the contribution of an appreciable quantity of trihydrate would give the observed composition but there is no physical evidence to show the presence of either of the two known trihydrates. Thermogravimetric analysis shows that a large fraction of the water is loosely bound and is lost before the expected range of decomposition of boehmite. This is shown by the comparison of the thermograms of the hydrated oxide and pure boehmite[1] in Fig. 2. The thermogram shown here was obtained from the oxide formed at 100°C. Nearly identical traces were observed for the products formed at 80° and 90°C.

Reaction mechanism.—Hart (5) has suggested that the growth of the hydrated oxide occurs by outward migration of aluminum from the metal and offers as evidence the observation that anodic films which have been stripped from the metal and then treated with boiling water do not give the electron diffraction pattern of boehmite. Kerr (6) has modified this experiment so that part of the underlying metal was allowed to remain in contact with the anodic film and then carried out the hydration reaction. Electron diffraction then indicated the presence of boehmite only in the vicinity of the islands of metal. According to these observations, the mechanism of boehmite formation must involve the movement of aluminum to the oxide-water interface, since the anodic oxide itself does not appear to become hydrated.

[1] Obtained from Alcoa Research Laboratories.

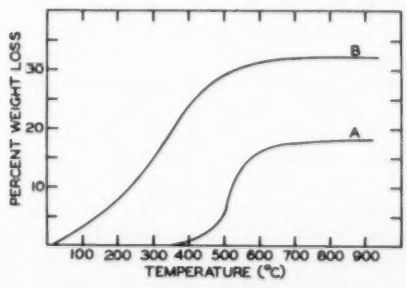

Fig. 2. Thermograms of: A. boehmite; B. reaction product of aluminum and water at 100°C.

Table I. Comparison of x-ray diffraction data of boehmite (ASTM) and hydrated anodic films*

ASTM		Hydrated anodic films	
d	Relative intensity	d	Relative intensity
6.11	100	6.28	Strong (very diffuse)
3.16	65	3.18	Strong (diffuse)
2.35	53	2.35	Strong (diffuse)
1.98	6	1.97	Weak
1.86	32	1.86	Strong (diffuse)
1.77	6		
1.66	13		
1.53	6	1.54	Weak
1.45	16	1.43	Weak
1.43	9	1.40	Weak
1.38	6	1.36	Weak
1.31	15	1.31	Weak

* Only the 12 strongest diffraction lines of boehmite are listed.

On the other hand, Spooner (10) has shown by x-ray diffraction patterns that boiling water transforms isolated oxide to boehmite, and MacLennan (11) has reported that there is no essential difference in the impedance characteristics between isolated and nonisolated oxide films which have been exposed to boiling water. Both of these observations have been made with nonbarrier films (formed in sulfuric acid), but we have also confirmed Spooner's results using barrier films formed to 100 v in ammonium borate solution, taking great care to remove the underlying metal completely, and hydrating for 20 min at 100°. This has also been confirmed by Hinde, Kellet, and Harris (12). A comparison of our x-ray diffraction data for a hydrated anodic film and ASTM data for boehmite is given in Table I. Furthermore, thermogravimetric analysis of this substance gave results which are identical to those obtained from the hydrate in Fig. 2. These observations are in direct contradiction to those of Kerr and Hart, but repeated and careful study leaves no doubt that the presence of metallic aluminum is not necessary for the conversion of anodic oxide to "boehmite."

In the attempt to determine the kinetics of the direct reaction between aluminum and water, we have made the assumption that the formation of oxide occurs at the metal-oxide interface. This is based on the discussion in the preceding paragraph, the physical nature of the final product and the rate at which the consecutive reaction—the hydration of the oxide-occurs.

The final hydrated oxide is completely unlike the coherent film formed by anodic oxidation, consisting of loosely connected particles. This is shown by examination of the oxide after removal of the underlying metal. When in contact with the metal this oxide is probably of a highly porous nature and could be penetrated easily by water, thus making it unnecessary to consider an ionic mechanism for oxide growth.

A further condition which must be met for the reaction to occur at the metal-oxide interface is that

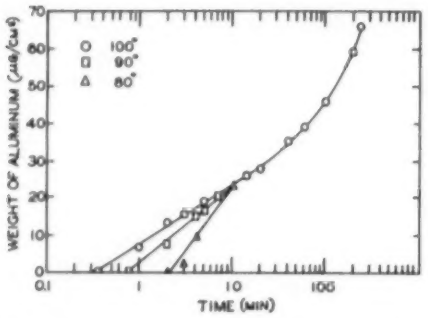

Fig. 3. Weight of aluminum reacted vs. time of immersion in water at 80°, 90°, and 100°C. Data corrected for amount of pre-existing oxide on degreased foil.

the hydration step take place as soon as the oxide is formed. There is some justification for this belief, since, as shown in the following section, anodically formed films are hydrated at a very rapid rate. Calculations show that the rate is greater than the rate of hydrated oxide formation on the metal. There is, of course, no evidence to show that the transitory oxide formed in the water reaction is identical to the anodically formed oxide, but the physical similarities of the final hydrated product of each would lead one to believe that this is the case.

In view of these considerations it would be expected that the rate-determining process would be the diffusion of water through the film, although the kinetics may be complicated to an unknown extent by the rate at which evolved hydrogen is transported from the reaction surface. It should also be recognized that the rate of oxide growth is also strongly influenced by the specific impurities present in the metal; the absolute data presented here, therefore, apply only to aluminum of the composition described earlier.

If the process occurs uniformly over the surface of the metal and if the rate of diffusion of water is dependent on the thickness of the film, a parabolic law would be expected to govern the growth; independence of film thickness would result in a linear rate law. In the cited paper by Hart a constant growth rate is reported, but this is open to question since the change in thickness was followed for only 2 min. The initial rate is extremely rapid and could probably be fitted to a linear plot, but it soon decreases, as shown in Fig. 3. However, a parabolic law also fails to fit the observed data over a reasonable period of time. In Fig. 3 the weight of aluminum reacted at 100°C is plotted as a logarithmic function of time. In this plot the weight of aluminum reacted, rather than the weight of the oxide or the total weight of product formed, is used in order to avoid the assumption of a constant composition of product, since the calculated amount of water in the surface film was found to vary from 23% to 32%.

We have also plotted some of the data obtained from experiments at 80° and 90°C. Results for longer reaction times are not included because of the failure to obtain satisfactorily reproducible results. The observations are anomalous in some respects. There is a marked increase in the inhibition period with decreasing temperature, but about 10 min after reaction starts there is little difference in rates for the first 2 hr. After that time the rate at 100° is significantly greater than at the lower temperatures.

At 100°C an apparent logarithmic rate law is observed for the first 30 min or so, followed by a reasonable fit to a parabolic law up to about 250 min. The nature of the hydration process would not lead us to believe that a true logarithmic law of the type discussed by Uhlig (13) is operating here, but rather that the apparent logarithmic dependence is fortuitous. The fact that a simple parabolic dependence is not observed over the entire time interval studied suggests that a uniform, homogenous reaction layer is not formed, at least in the beginning, or that the evolution of hydrogen complicates the kinetics to a greater extent than was assumed. It is also possible that a form of lateral growth, postulated by Evans (14), may explain this behavior.

The thicknesses of the films are greater than reported by Hart from his electron diffraction measurements. After 1.5 min (on electropolished specimens) he observed a film thickness of 100Å, whereas our calculated thickness under the same conditions, based on the weight of the film and the measured density, is 1500Å.

Inhibition period.—The previously unreported inhibition period is believed to be due to the presence of the existing oxide film on the metal; foil which has been electropolished shows a much smaller inhibition period. The time required for hydrogen to be evolved on degreased foil at 100°C is about 20-22 sec, on foil cleaned in cold H_2SO_4-$K_2Cr_2O_7$ solution it is 15-18 sec, and on electropolished foil 5-11 sec. The fact that the electropolished specimens do not show an inhibition time of zero is a result of the very thin film which is formed on the foil during the washing period after removal from the electropolishing bath. Thin films of aluminum, vacuum-deposited on glass, show an apparent inhibition period of 1-2 sec if transferred rapidly from the vacuum apparatus to boiling water, but it is difficult to observe the effect because the boiling water tends to rupture the thin metal film. However, what appears to be an instantaneous reaction with boiling water is observed with aluminum which has been freshly abraded with a stainless steel point.

The properties of the natural oxide film on aluminum have not yet been elucidated completely. The thickness of the film is dependent on the history of the metal and its environment; a summary of the many investigations of this subject has been given by Hart (15). It is generally agreed that after an initial rapid growth of oxide on the pure metal further growth occurs at a very slow rate at room temperature, and that the thickness of the film probably never exceeds 100Å. In the course of our work we have made direct measurements of the film weight (on acid-cleaned foil) by the stripping method and have found it to be 4.0 $\pm$0.4 $\mu g/cm^2$. If the film were to consist of α-Al_2O_3, the densest form of alumina, the oxide film would be 100Å thick. Since there is little doubt that the film does not consist of α-Al_2O_3, but of some less dense form of alumina, it must be considerably thicker than 100Å.

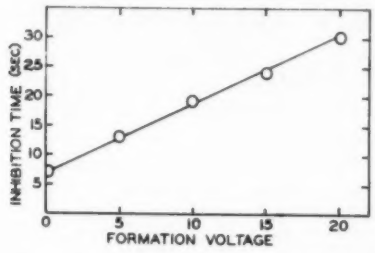

Fig. 4. Inhibition time for the reaction of electropolished aluminum foil with water vs. the thickness of anodic oxide on the foil.

Hunter and Fowle (16) consider the film to consist of a barrier layer about 10Å thick on the metal surface, with a porous layer above the barrier, but it is difficult to reconcile this model with our observations of the inhibition period. If electropolished aluminum foil is anodically oxidized to a specific voltage, up to 25 v, and then subjected to the action of boiling water, the entire oxide film is eventually penetrated and visible hydrogen evolution occurs. The time required to penetrate the film, in addition to the inhibition period characteristic of the foil pretreatment, is approximately proportional to the thickness of the anodically formed layer. This is shown in Fig. 4. At the current density used (0.1 ma/cm^2) the thickness of the anodic oxide is 11.9Å/v (17), and the penetration (or hydration) rate of the oxide is, therefore, about 12A/sec. The pre-existing film on acid-cleaned foil, on the other hand, is penetrated only at the rate of 0.7Å/sec if the barrier portion alone of the film is responsible for the inhibition period. If this is true, then the naturally formed barrier film must be physically quite different from the anodically formed amorphous films. On the other hand, if the porous portion of the film also contributes to the inhibition period, it would be expected to become hydrated during the process. This would result in an easily detectable weight change. No such weight change occurs, and we have concluded that the pre-existing film is probably penetrated without hydration during the inhibition period.

In connection with the hydration of anodically formed aluminum, an interesting observation was made concerning the spatial relationship of the two oxides. Degreased foil shows no weight gain during the first 18-sec immersion in boiling water, but the same foil which has been anodically formed to 25 v before reacting with water shows a weight gain of 1.5 μg/cm^2 during the first 18 sec. Electropolished foil, which has been similarly formed, showed the same weight gain under these conditions. This indicates that anodic formation occurs on the solution side of the pre-existing oxide film, and that anodic growth takes place by aluminum ion movement through the film. This is in agreement with the conclusion of Lewis and Plumb (18) and is analogous to experiments made by Young (19) on tantalum.

Acknowledgment

The authors wish to acknowledge the assistance of Mrs. Concetta Duval and the Analytical Laboratory of this Company.

Manuscript received Nov. 30, 1959.

Any discussion of this paper will appear in a Discussion Section to be published in the December 1960 JOURNAL.

REFERENCES

1. P. A. Jaquet, *Met. Revs.*, **1**, 157 (1956).
2. D. Altenpohl, *Aluminium*, **33**, 78 (1957).
3. J. E. Lewis and R. C. Plumb, *Intern. J. of Appl. Radiation and Isotopes*, **1**, 33 (1956).
4. R. A. Harrington and H. R. Nelson, Am. Inst. Mining Met. Engrs., Inst. Metals Div., Tech. Publ. No. *1158*, 14 pp. (1940).
5. R. K. Hart, *Trans. Faraday Soc.*, **50**, 269 (1954).
6. I. S. Kerr, *Proc. Phys. Soc.*, **69B**, 1055 (1956).
7. J. M. Bryan, *J. Soc. Chem. Ind.*, **69**, 169 (1950).
8. T. J. Nurse and F. Wormwell, *J. Appl. Chem. (London)*, **2**, 550 (1952).
9. R. Fricke and H. Severin, *Z. anorg. u. allgem. Chem.*, **205**, 127 (1932).
10. R. C. Spooner, *Nature*, **178**, 1113 (1956).
11. D. F. MacLennan, *Corrosion*, **15**, 283t (1959).
12. R. M. Hinde, E. A. Kellet, and P. H. Harris, *Nature*, **183**, 39 (1959).
13. H. H. Uhlig, *Acta Met.*, **4**, 541 (1956).
14. U. R. Evans, *Trans. Faraday Soc.*, **41**, 365 (1945).
15. R. K. Hart, *Proc. Roy. Soc. (London)*, **A236**, 68 (1956).
16. M. S. Hunter and P. Fowle, *This Journal*, **103**, 482 (1956).
17. W. J. Bernard and J. W. Cook, *ibid.*, **106**, 643 (1959).
18. J. E. Lewis and R. C. Plumb, *ibid.*, **105**, 496 (1958).
19. L. Young, *Trans. Faraday Soc.*, **53**, 841 (1957).

Corrosion Behavior and Passivity of Nickel-Chromium and Cobalt-Chromium Alloys

A. Paul Bond[1] **and H. H. Uhlig**

Corrosion Laboratory, Department of Metallurgy, Massachusetts Institute of Technology, Cambridge, Massachusetts

ABSTRACT

Pure Ni-Cr alloys containing up to 29% Cr and Co-Cr alloys containing up to 23% Cr were prepared in vacuum. Corrosion rates in sulfuric and nitric acids, corrosion potentials, and critical current densities for passivity were determined at 25°C. It is concluded that specific alloying proportions of passive compositions are better evaluated in relation to electron configuration of the alloy system by critical current densities than by potential or corrosion rate measurements.

Much work on the corrosion behavior of iron-chromium alloys has been published and is useful to an understanding of conditions favoring passivity in alloy systems. Similar data for the cobalt-chromium system have not been reported. For nickel-chromium alloys most of the previous work involved rather impure metals and often ill-defined experimental conditions. Data reported by Rohn (1) and Pilling and Ackerman (2) indicate that as Cr content is increased, corrosion rates of the Ni-Cr alloys in oxidizing media are decreased. Grube (3) showed that in 1*N* HNO_3, the alloys become passive and their corrosion rates reach a minimum at about 10% Cr.

In the present work, relatively pure Ni-Cr and Co-Cr alloys were investigated for the low Cr solid solution range. Particular attention was paid to the quantitative alloying proportions required to achieve passivity.

Experimental Procedure

Alloys were prepared from high-purity Cr purchased from the Electro Metallurgical Company, carbonyl Ni (99.93% Ni) furnished by courtesy of the International Nickel Company, and high-purity Co (99.97% Co) supplied by courtesy of the Cobalt Information Center at Battelle Memorial Institute. Induction melting was carried out under a vacuum of 10^{-4} mm Hg, with the melt contained in a "Morganite" high-purity aluminum oxide crucible. No deoxidizers were added. Samples were cast in a helium atmosphere by drawing the melt into 8 mm diameter "Vycor" tubes and plunging the ingots into water. The helium was purified by passage over Mg chips at 640°C and, in later experiments, over Ti sponge at 800°C. In both cases the helium was passed through a trap surrounded by liquid nitrogen before entering the furnace.

Homogenization of castings was carried out at 1100°C for 12 hr in silica tubes using a helium atmosphere followed by a water quench. The Co-Cr alloys, which were hard and rather brittle, were used in the as-homogenized condition, while the Ni-Cr ingots were cold rolled to a thickness of 2.5 mm, given a 15-min anneal at 1000°C, and water quenched. Composition of each alloy was determined by chemical analysis.

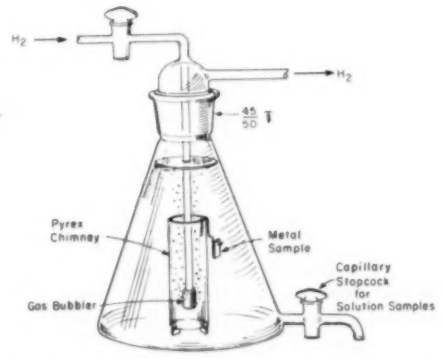

Fig. 1. Cell for measuring corrosion rates by weight loss and solution analysis.

Corrosion rate measurements were carried out in an air thermostat maintained at 25° ±0.5°C, using 2000 ml cells of the type shown in Fig. 1. Laboratory compressed air, filtered by means of glass wool and charcoal, was bubbled through the cells at the rate of 40 ml/min as determined by a flow-meter provided for each cell. Solutions were prepared from laboratory distilled water and reagent grade chemicals.

Specimens of Ni-Cr alloys for corrosion rate determinations were cut as rectangular coupons measuring approximately 3 cm long, 0.5-1 cm wide, and 0.2 cm thick. A hole 0.3-0.4 cm in diameter was drilled near one end so that the sample could be hung from a glass hook. These specimens were abraded smooth, finishing with 600 grit silicon carbide wet polishing paper. After washing with distilled water and wiping dry, specimens were immersed in boiling benzene for 5 min. This was followed by pickling in hot 6*N* H_2SO_4. Pickling was continued until the surface was sufficiently etched to reveal the microstructure of the metal. After pickling, samples were thoroughly washed with distilled water and dried in a desiccator.

[1] Present address: Diamond Fuze Laboratory, Washington, D. C.

Corrosion rates were measured by colorimetric analysis of aliquots of the test solution in which specimens were immersed. By periodic sampling, corresponding weight loss was calculated as a function of time. For Ni the dimethylglyoxime method (4) was used, and for Co the thiocyanate method (4). Conventional gravimetric weight loss measurements were also made and checked with weight losses calculated from analysis of the solution. All runs were continued for sufficient time to reach a constant corrosion rate.

Electrodes for polarization measurements were similar in size and shape to the corrosion rate specimens. Nickel wire was silver soldered to a stem which was machined on the electrode. A Teflon gasket between the electrode and a Pyrex tube was compressed by means of a nut and machine screw silver soldered to the nickel wire, in order to exclude the electrolyte from contact with any metal other than the electrode proper.

Potential measurements were made using a portable potentiometer in series with an electronic pH meter employed as a high resistance galvanometer. An Ag-AgCl, 0.1*N* KCl electrode was the reference electrode. Constant polarization current was supplied by 30 dry cells in series with an adjustable resistance.

Critical current densities for passivity were determined in a cell fitted with two auxiliary Pt electrodes and arranged so that the alloy electrodes could be pickled within the cell with 1:1 H_2SO_4, washed, and the test electrolyte introduced without exposure to air. Test solution and distilled water for washing were contained in 5-gal carboys connected to the cell by glass tubing. Deaeration was accomplished by prepurified grade nitrogen which had been passed over copper turnings at 450°C. The Luggin capillary of the salt bridge filled with the test solution was placed adjacent to the alloy electrode.

Critical current densities for passivity were measured by two methods. For Ni-Cr alloys, the "indirect" method was used. This consisted of applying a series of constant anodic currents slightly above the critical current density and measuring the times required to reach the passive potential. Current density i was then plotted against the reciprocal of time t for passivity in accord with the relation $i - i_c = K/t$, where i_c is the critical current density (5, 6). This relation is linear for currents not exceeding the critical current density by more than a factor of 2 or 3, and can thus be extrapolated to reciprocal time = 0 to obtain i_c. The value K represents the number of coulombs per unit area required to achieve passivity.

For the Co-Cr alloys, the "direct" method was used (7). This consisted of applying a given current and observing the potential. The lowest current which passivated the electrode was taken as the critical current density. At currents below the critical, polarization was continued until the potential changed at a rate less than 2 mv/min. The two methods give comparable values for i_c, as was demonstrated by similar measurements for the Fe-Cr alloys (8).

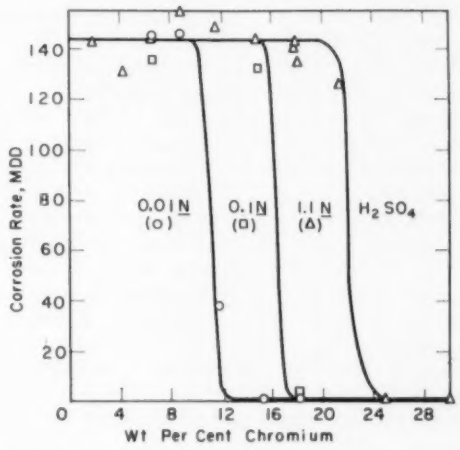

Fig. 2. Corrosion rates of Ni-Cr alloys in aerated H_2SO_4, 25°C, 4-day runs.

Corrosion potentials were also measured in the above cell. The electrodes were prepared in the same way as specimens for the corrosion rate determinations.

Experimental Results

Nickel-chromium.—Corrosion rates were measured in several media. In deaerated 1.1*N* (5%) H_2SO_4, 25°C, 10 day runs, corrosion rates were low, being of the order of 1 mdd, and showed little variation with chromium content.

In Fig. 2 the results of 4-day runs in aerated 1.1, 0.1, and 0.01*N* H_2SO_4 are shown. It can be seen that the corrosion rates of the active alloys are all the same within experimental error, the standard deviation being 6.3 mdd as determined from replicates. However, alloys containing more than a critical amount of Cr show a corrosion rate of practically zero, corresponding to the passive condition. These passive alloys sometimes showed an initial weight

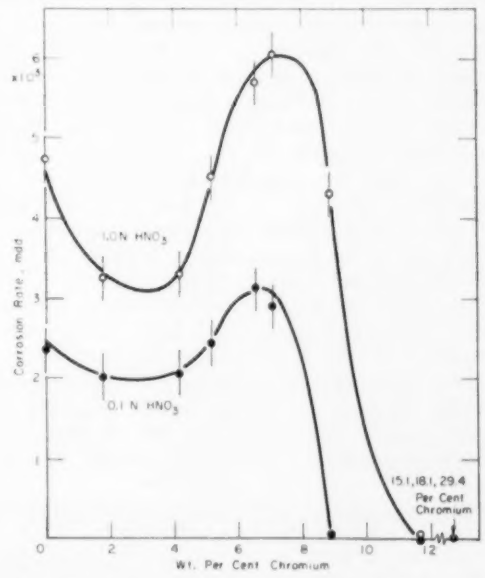

Fig. 3. Corrosion rates of Ni-Cr alloys in HNO_3, 25°C, 1-day runs.

loss as determined by colorimetric analysis, after which any further change was very slight. It should be noted that higher acid concentration shifts the passivity limit to higher chromium contents.

Figure 3 shows corrosion rates of these alloys in 1.0 and 0.1*N* HNO_3 as determined by one-day runs. Confidence limits (95%) were calculated by standard statistical methods (9). It can be seen that the initial Cr additions had little effect on the corrosion rate, causing only a slight decrease. Further additions caused a marked increase, with a peak occurring around 7% Cr. This type of behavior was also observed by Rohn (1) and Pilling and Ackerman (2), while Grube (3) found only a horizontal arrest but not a peak. The transition from activity to passivity is quite abrupt, coming between 7.1 and 8.9% Cr in 0.1*N* HNO_3, and between 8.9 and 11.7% Cr in 1.0*N* HNO_3.

Corrosion rates were also determined in 1*N* H_2SO_4 to which was added 25 g of hydrated ferric sulfate per liter. In this case only one run was made, all samples being placed in the same cell. The data of Table I show that this solution is much more strongly corrosive toward the two alloys which remained active than is 1.0*N* HNO_3. The initial major critical passive composition is shifted to lower Cr content, now lying between 4.2 and 6.6% Cr. These corrosion rates were determined by the conventional weight loss method only, since the high concentration of iron in the solution interferes with the colorimetric determination of nickel. However, since in other oxidizing media studied, these alloys, when in the active condition, exhibited a constant corrosion rate from the beginning of the run, it seems reasonable that this was also true in this case. The active alloys were left in the solution 6 hr, the others for 2 days.

Corrosion potentials of Ni-Cr alloys in deaerated (H_2-saturated) 1.1*N* H_2SO_4 showed no systematic variation with chromium content and, in fact, the potentials of these alloys were not far removed from the potential of the reversible hydrogen electrode. Corrosion potentials in 0.1 and 1.0*N* HNO_3 are shown in Fig. 4. There is a more or less continuous ennobling of the corrosion potential with increasing chromium content with a slight peak being observed in the region of 4-6% Cr.

Critical current densities for passivity were determined for these alloys in N_2-saturated 1.1*N* H_2SO_4 by the indirect method. The results are shown in Fig. 5 and 6. These curves have similar shape, but with the absolute values of critical currents considerably larger in 1.1*N* than in 0.01*N* H_2SO_4. It appears that in both cases the critical current density decreases sharply as Cr is increased to the vicinity of 14%, after which the decrease in critical current density becomes much less steep. Coulombs per square centimeter for passivity in 1.1*N* H_2SO_4 range from 0.3 for high Cr alloys to 2.0 for low Cr alloys.

Table I. Corrosion rates of Ni-Cr alloys in 1.0*N* H_2SO_4 plus 25 g $Fe_2(SO_4)_3 \cdot 9H_2O$/liter, aerated, 25°C

% Cr	1.8	4.2	6.6	8.9	11.7	15.1	18.1
mdd	8259	6950	6	9	0	0	0

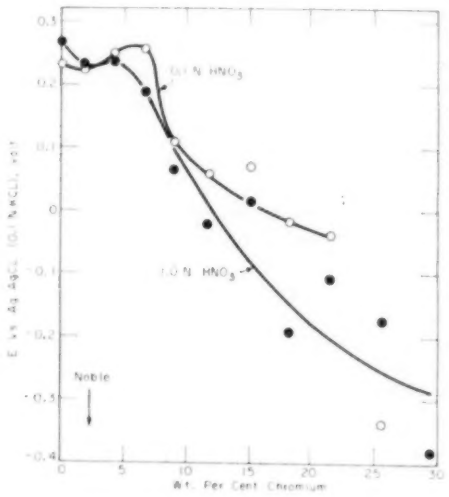

Fig. 4. Corrosion potentials of Ni-Cr alloys in HNO_3, 25°C

Cobalt-chromium.—In contrast to the Ni-Cr system, the Co-Cr alloys do not have a single phase structure. Pure cobalt itself in the annealed condition is a mixture of hexagonal close-packed and face-centered cubic phases, and this behavior is reflected in that of the alloys. There is some disagreement as to the Co-Cr phase diagram (10, 11), but there is agreement that at the annealing temperature of 1100°C all alloys used in this work would be in a single phase field. Also, Wever (10) reported that x-ray data revealed only the face-centered cubic and hexagonal close-packed phases in alloys of 20 and 30% Cr quenched from 1000°C. Since the

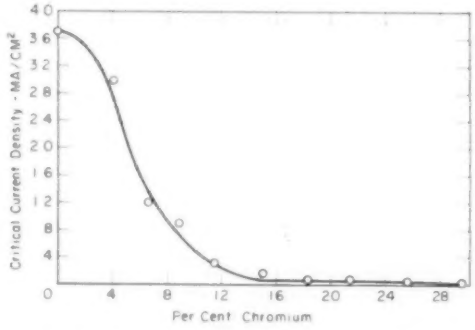

Fig. 5. Critical current densities for passivity of Ni-Cr alloys in N_2-saturated 1.1N H_2SO_4, 25°C.

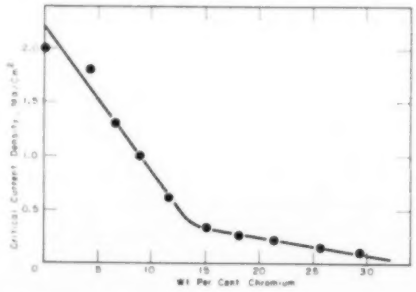

Fig. 6. Critical current densities for passivity of Ni-Cr alloys in N_2-saturated 0.01N H_2SO_4, 25°C.

temperature of the transformation is relatively low (500°-850°C), and the equilibrium two-phase field between the high- and low-temperature modifications is narrow, it appears that very little diffusion would take place during quenching. Therefore, it is probable that the two phases present in the alloys as tested had the same chemical composition.

Kröhnke and Masing (12) studied the corrosion potential and anodic and cathodic polarization behavior of face-centered cubic and hexagonal close-packed Co in 0.1 and 2.0*N* HCl. They found the two crystalline modifications to behave identically. One of us also found that body-centered and face-centered cubic 18-8 stainless steels corrode at essentially the same rates in several media (13). From this it appears reasonable to conclude that the behavior of the Co-Cr alloys was not greatly affected by the presence of two different crystalline forms. Metallographic examination showed that the microstructures of all these alloys are similar and that the observed changes in electrochemical behavior do not correspond to any change in microstructure.

Corrosion rates of the Co-Cr alloys in 0.1 and 1.0*N* HNO_3 are shown in Fig. 7. Time of test ranged from hours to days depending on whether the corrosion rate was high or low. Uniform corrosion was observed in all cases. Pure Co has a corrosion rate about 10 times higher than pure Ni, and the active alloys also show higher rates than do the Ni-Cr alloys. The shapes of the corrosion rate-composition curves also differ for the two alloy systems in that the initial Cr addition causes a marked decrease in corrosion of the Co alloys and no maximum is found. There is, however, a discontinuity in slope in the region from 2 to 4% Cr, similar to the more pronounced change in the Ni-Cr system. The onset of passivity in HNO_3 begins at about 12% Cr, since alloys containing more Cr corroded at a rate of 0 mdd in 0.1 *N* HNO_3 and 0 to 7 mdd in 1.0*N* HNO_3.

Corrosion potentials of these alloys in 1.0*N* HNO_3 are shown in Fig. 8. A pronounced shift toward

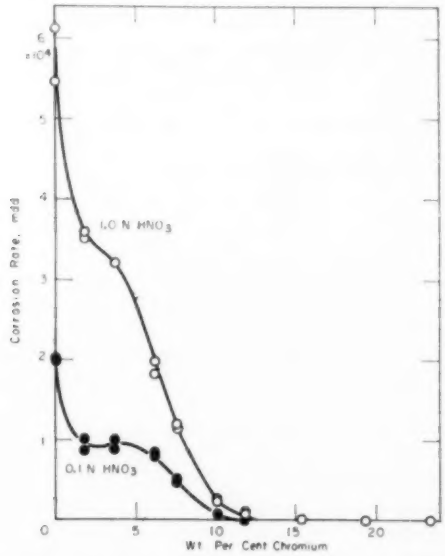

Fig. 7. Corrosion rates of Co-Cr alloys in HNO_3, 25°C.

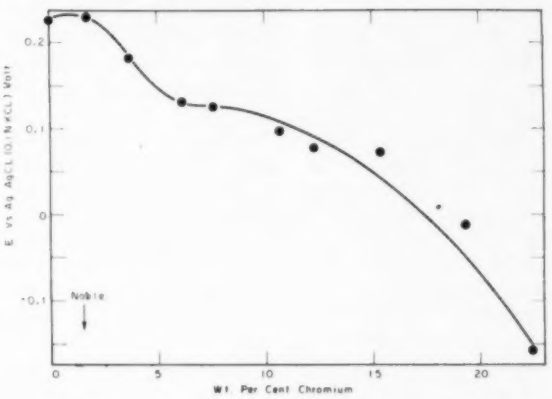

Fig. 8. Corrosion potentials of Co-Cr alloys in 1.0N HNO_3, 25°C.

more noble potentials is observed as Cr content is increased, but it is not possible on the basis of these data alone to draw any conclusions regarding critical composition limits for passivity.

Figure 9 is a plot of critical current densities with composition, obtained by the direct method. Pure Co, as well as alloys containing up to 6.2% Cr, have very high critical currents, while a sharp drop occurs in the vicinity of 8% Cr, followed by a levelling off again. These data give a clear indication of a critical composition in the vicinity of 8% Cr, as well as indicating that for alloys of this or higher Cr content the critical current density (~1 ma/cm²) is low enough for self-passivation of the alloys to be possible in strongly oxidizing media.

Discussion

Nickel-chromium alloys.—In deaerated 1.1*N* H_2SO_4 the corrosion of Ni and Ni-Cr alloys appears

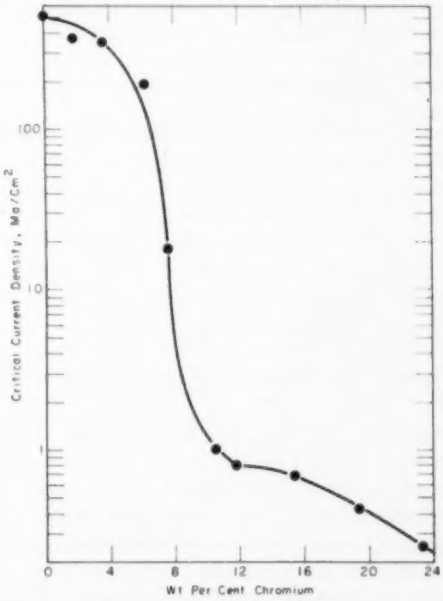

Fig. 9. Critical current densities for passivity of Co-Cr alloys in N_2-saturated 1.0N H_2SO_4, 25°C.

to be largely under anodic control. This is suggested by the fact that the corrosion potentials are not far removed from potentials of the reversible hydrogen electrode. This means that the local cathodes are only slightly polarized.

On the other hand, in aerated sulfuric acid the corrosion rates of the active alloys appear to be controlled by diffusion of dissolved oxygen to the metal surface. This is indicated by the fact that the corrosion rates of the active specimens are essentially independent both of alloy composition and acid concentration. It is also indicated by correspondence of the corrosion rate (140 mdd = 5.3 x 10^{-5} amp/cm^2) to the limiting diffusion current density for oxygen, i.e., in accord with the equation $i = (DnFc/\delta)$, where $D = 2 \times 10^{-5}$ cm^2/sec, $n = 4$, $F =$ 96,500 coulombs/equiv., $c = 2.5 \times 10^{-7}$ moles dissolved O_2/cc, and δ the thickness of the stagnant diffusion layer is assumed equal to 0.035 cm. The latter value of δ is consistent with observed values.

That the corrosion rates of the active alloys should be anodically controlled in deaerated acid and cathodically controlled in aerated acid is in no way self-contradictory. In deaerated acid, the cathodic process is reduction of hydrogen ions to gaseous hydrogen, while in aerated acid the cathodic reaction involves reduction of dissolved oxygen by hydrogen ions to form water. The standard free energy change for the latter reaction is much greater than that of the former, so that in aerated solution the difference between the open circuit anode and cathode potentials is much greater than in deaerated solution. Thus a very large current would be necessary to polarize the local anodes to the open circuit cathode potentials, and long before this happens the limiting diffusion current for oxygen is reached and becomes the rate-determining step.

In all the oxidizing media used in this work the Ni-Cr alloys exhibited a critical composition, that is, alloys containing less than the critical amount of chromium for passivity corroded relatively rapidly compared to those containing more than the critical percent. The term passive, as used in this discussion, is limited to the case of a metal which is polarized to a potential more noble than its Flade potential in the given environment and has an accompanying comparatively low corrosion rate. In the case of those alloys which are passive under a given set of conditions, it can be assumed from previous discussions (7, 14-16) that the local anodic current produced by corrosion of the active alloy exceeded the critical current density for passivity. In this way the low corrosion rate of the passive state follows in sequence the higher corrosion rate of the active state.

It appears to be a general rule that whenever the current density equivalent to the corrosion rate approaches the critical current density passivity is established. The present data bear out this relationship. The corrosion current densities are always less than the critical current densities to an extent dictated by the anode-cathode area ratio, a low ratio accounting for a greater observed difference between the two values than a high ratio.

Based on the fact that the passive film on Fe, Cr, and Cr-Fe alloys is equivalent to about 0.01 coulomb/cm^2 (8) or less, the value of 0.3 to 2 coulomb/cm^2 for Ni-Cr alloys indicates that anodic dissolution of the alloy precedes passivity. The same is true of iron the value for which is about 1 coulomb/cm^2, and as Franck (6) showed, an insulating film of perhaps FeSO$_4$ forms first, favoring high current densities within pores of this film necessary to achieve the passive state. This situation is also borne out by a relatively low initial slope of potential vs. time at constant applied current density for Ni-Cr alloys preceding a rapid fall of potential to the noble passive value, whereas for stainless steels which passivate without initial salt film formation, the potential fall is immediate, and coulombs for passivity are a direct measure of the amount of passive film substance on the surface.

The rather wide variation in the amount of Cr needed to passivate these alloys in different media is a result of the different corrosion rates, anode-cathode area ratios, and critical current densities which prevail in these media. In the case of aerated sulfuric acid, only the critical currents and not the corrosion rates of the active alloys were reduced as the acid concentration was reduced. Decreases in acid concentration correspondingly lowered the critical amount of Cr required for passivity because critical current density decreases with increasing Cr. Since the critical Cr compositions fall in a region where critical current density is changed only slowly with Cr content, small changes in the critical current density for passivity by means of decreasing acid concentration shifted the critical Cr content markedly.

In nitric acid, corrosion rates as well as critical currents were raised as acid concentration was increased. The increase in corrosion rate is probably due to increase in concentration of nitrate ion, which is reduced at the local cathodes, while increase in hydrogen ion concentration increases observed critical current densities. The observed increase in Cr necessary to produce passivity in these alloys on increasing acid concentration indicates that the higher critical current density brought about by increased acid concentration outweighs the effect of increased corrosion current. By adding ferric ions to 1*N* H_2SO_4, a corrosion rate higher than that in 1*N* HNO_3 was obtained at approximately the same hydrogen ion concentration, so that the critical amount of Cr was decreased from about 12 to 6.6% Cr as is seen from data of Table I and Fig. 3.

In retrospect, all the data show that passivity limits for these alloys as obtained from corrosion data reflect not only the basic properties of the alloy system, but also depend strongly on the environment. Important are the nature of the anion, depolarizer concentration, surface *p*H, degree of stirring, etc. This is especially true of a system such as Ni-Cr, because critical current densities do not vary as sharply with composition as they do in the Cr-Fe alloys as shown, for example, by data of King and Uhlig (8).

The variation of critical current density with alloy composition appears to be the important funda-

mental property of alloys capable of becoming passive. The shape of the critical current-composition curve is found to be nearly the same in 1.1 and 0.01*N* H_2SO_4 (Fig. 5 and 6) even though the critical currents are much smaller for the lower acid concentration. In both cases a change in slope occurs or a practical minimum is reached in the vicinity of 14% Cr. This is the figure which it would probably be most profitable to compare with the prediction of a critical composition at 8.2% Cr made by one of us (17) based on electron configuration in the alloy system. Other than the simplified assumptions made in the theoretical calculation, difference between theory and observation may also be a result of experimental factors, such as a possible difference between surface composition from bulk composition of the alloys caused by preferential corrosion of one of the alloy components.

Cobalt-chromium alloys.—The behavior of the Co-Cr system was similar to the Ni-Cr system, as might be expected. Differences in shape of the corrosion-composition curves in nitric acid indicate that Cr alloyed with Co, even in small amounts, decreases the corrosion rate (Fig. 7), while in the Ni-Cr system, Cr markedly increases the corrosion rate just short of the passive composition (Fig. 3). This may be related to the possibility that Co is a better catalyst than Ni for reduction of NO_3^-, which in turn is consistent with a much higher corrosion rate of pure Co than pure Ni in HNO_3. This being the case, if Cr is an intermediate catalyst, an addition of Cr to Co will increase cathodic polarization of Co-Cr alloys while decreasing it for Ni-Cr alloys.

The effect of Cr on the critical current densities of the Co-Cr alloys (Fig. 9) was much more pronounced than in the Ni-Cr system (Fig. 5, 6). In this respect, behavior of Co-Cr alloys is similar to the behavior reported for Fe-Cr alloys (8). The critical current densities for the Co alloys containing more than 10% Cr were about the same or somewhat lower than those of the corresponding Ni-Cr alloys, but the low Co-Cr alloys and pure Co had much higher critical current densities. For this reason, the critical composition is clearly indicated as close to 8% Cr. This is in reasonable agreement with the 6.2% Cr predicted by the electron configuration theory (17).

Acknowledgment

The authors are grateful for support of this research by the Office of Naval Research.

Manuscript received Dec. 3, 1959. This paper was prepared for delivery before the Houston Meeting, Oct. 9-13, 1960.

Any discussion of this paper will appear in a Discussion Section to be published in the December 1960 JOURNAL.

REFERENCES

1. W. Rohn, *Z. Metallkunde*, **18**, 387 (1926).
2. N. B. Pilling and D. E. Ackerman, *Trans. Am. Inst. Mining Met. Engrs.*, **83**, 248 (1929).
3. G. Grube, *Z. Metallkunde*, **19**, 438 (1927).
4. E. B. Sandell, "Colorimetric Determinations of Traces of Metals," Interscience Publishers, Inc., New York (1944).
5. W. Shutt and A. Walton, *Trans. Faraday Soc.*, **30**, 914 (1934).
6. U. F. Franck, *Z. Naturforsch.*, **4A**, 378 (1949).
7. H. H. Uhlig and G. Woodside, *J. Phys. Chem.*, **57**, 280 (1953).
8. P. F. King and H. H. Uhlig, *J. Phys. Chem.*, **63**, 2026 (1959).
9. W. J. Youden, "Statistical Methods for Chemists," John Wiley & Sons, Inc., New York (1951).
10. F. Wever and V. Hashimato, *Mitt. Kaiser Wilhelm Inst., Eisenforsch. Düsseldorf*, **11**, 293 (1929).
11. A. R. Elsea, A. B. Westerman, and G. K. Manning, *Trans. Am. Inst. Mining Met. Engrs.*, **180**, 579 (1949).
12. G. Kröhnke and G. Masing, *Werkstoffe und Korrosion*, **4**, 86 (1953).
13. H. H. Uhlig, *Trans. ASM*, **30**, 947 (1942).
14. H. H. Uhlig and P. F. King, *This Journal*, **106**, 1 (1959).
15. M. Stern, *ibid.*, **105**, 638 (1958).
16. N. Tomashov, *Corrosion*, **14**, 229t (1958).
17. H. H. Uhlig, *Z. Elektrochem.*, **62**, 700 (1958).

Dissolution of Nickel in Acid Ferric and Ceric Solutions

Phoebus M. Christopher and Cecil V. King

Department of Chemistry, New York University, New York, New York

ABSTRACT

Dissolution rates of nickel cylinders rotated in acidified solutions of $FeCl_3$ and $Ce(SO_4)_2$ have been measured. The rates are transport-controlled, but the Ni surface becomes extremely rough, and first-order constants are obtained only if a uniform degree of roughness is maintained during runs. The values of the rate constants then depend on the structure of the metal, e.g., whether it has been annealed, mechanically worked, etc.

The rate of dissolution of nickel in ferric alum solutions was measured by Van Name and his coworkers (1), who found it to be approximately the same as that of several other metals in the same reagent. The authors regarded the dissolution to be controlled by diffusion, or by convective-diffusive transport, of ferric ion to the metal surface.

The present study shows that a polished nickel surface becomes very rough in acidified ferric and ceric solutions, more so in the former than in the latter. This is at least partly due to preferential dissolution at grain boundaries and at flaws in the mechanically worked metal. It indicates that, while the cathodic reaction (reduction of ferric or ceric

ions) probably occurs equally well at any point on the surface, the anodic reaction (formation of aqueous Ni^{++}) is not uniformly distributed. The rough surface of a rotating cylinder increases turbulence in the solution, at least near the interface, which results in larger dissolution rates than are found with smooth cylinders. The effect of roughness has been studied by Makrides and Hackerman in the dissolution of steel (2). These authors decided that roughness may increase the effective surface area at high rotational speeds, where the effective thickness of the boundary layer is small.

Experimental

Cylinders were cut from a nickel anode bar (99.6% Ni, supplied by International Nickel Co.) which had been rolled to an elliptical cross section. They were 2.52 cm long and 1.9-1.7 cm in diameter when in use. They were mounted on a shaft with only the peripheral surfaces exposed to the solutions. Some specimens were annealed by heating at 850°C for 2 hr in argon and cooling over a period of 4-5 hr in the same gas.

The reaction vessel was a square bottle (which has the effect of baffles in the solution), equipped with a tube passing through a hole in one side to admit nitrogen. The solution volume was 400 ml in all cases. Solutions were deaerated since preliminary runs showed that oxygen is reduced freely. All experiments were carried out at 18°-21°C. C.P. $FeCl_3$ was used directly while U.S.P. $Ce(SO_4)_2$ was recrystallized twice. All ferric solutions were made up with 1M HCl and all ceric solutions with 1M H_2SO_4. Dissolution was followed by weighing the cylinders after 2- to 10-min runs.

Results and Discussion

The first experiments were carried out with specimens which were polished with 2/0 emery paper initially, but not repolished when they were removed and weighed. At 3000 rpm the surface very quickly became rough, and the weight loss increased in successive equal time intervals in the same solution; for example in 0.05M $FeCl_3$ (initially) the dissolution rate had doubled after half the ferric ion had been reduced. Figure 1 is a plot of log $(a-x)$ for two unannealed cylinders run in this manner. In 0.02M $Ce(SO_4)_2$ the rate became first-order after 25 min, while in 0.05M $FeCl_3$ a somewhat longer time was required. Values of k (from the slopes, see Eq. [1] below) varied from 0.39 to 1.9 cm/min in the ferric solution, and from 0.34 to 0.71 cm/min in the ceric solution. Examination showed that the surface became rougher in the $FeCl_3$.

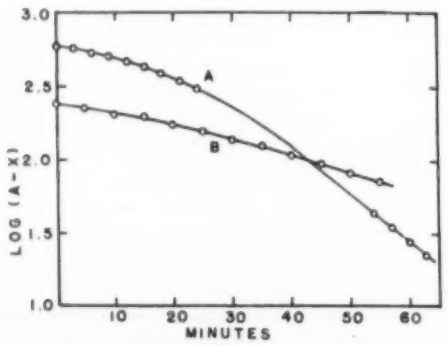

Fig. 1. Unannealed cylinders, polished initially and allowed to roughen with time. A, 0.05M $FeCl_3$ + 1M HCl. B, 0.02M $Ce(SO_4)_2$ + 1M H_2SO_4.

Thereafter runs were made in two ways: (*a*) the cylinder was polished initially and after each short immersion, to keep it as smooth as possible; or (*b*) the specimen was etched before use until there was no further effect on the rate. In both cases consistent rate constants k were obtained with the first-order equation:

$$k = \frac{2.3\,V}{A\,t} \log \frac{a}{a-x} \qquad [1]$$

where V is in cm^3, A in cm^2 (the apparent or projected area), and the other symbols have their usual meanings. Since the metal cylinders dissolved at a steady rate of 0.5 mg/10 min in the 1M HCl solution after all ferric ion had been reduced, a corresponding correction was applied to all weight losses. Dissolution in 1M H_2SO_4 after ceric ion was reduced was negligible.

Table I gives mean values of k for several runs of 60- or 70-min duration with unannealed cylinders. It is evident that the exact values of k obtained with polished samples depend on the time period chosen for immersion between polishings; the value 0.78 for $FeCl_3$ is twice that found from the initial slope of the log $(a-x)$ plot in Fig. 1 This does not, however, apply to the ceric solution.

In addition to the uncertainty of reproducibility with polished cylinders, it became evident that different unannealed cylinders reached different maximum rates after etching. This was probably due to lack of uniformity of structure of the anode bar from which they were cut. Part of the roughness took the form of irregular grooves along the length of the cylinders, in the direction in which the bar had been rolled, and the appearance varied from one cylinder to another. For these reasons some of the cylinders were annealed in order to obtain more uniform structure. On etching, the surface appeared much rougher than that of unannealed specimens, and dissolution rates were higher in most cases. Table II gives some values of k from single short runs designed to test the effect of solution concentration.

The rate constant in $FeCl_3$ apparently can vary from about 1.0 to a maximum of 2.2 cm/min under these conditions, depending on the past history of the metal, but for any one specimen it is reproducible and is independent of reagent concentration. In $Ce(SO_4)_2$ it is possible that the degree of roughness reached depends somewhat on concentration. The dissolution in 0.05M $FeCl_3$ of an annealed specimen,

Table I. Mean values of k in cm/min. Peripheral speed of cylinders, 17,000 cm/min.

	0.05M $FeCl_3$ + 1M HCl	0.02M $Ce(SO_4)_2$ + 1M H_2SO_4
Polished	0.78	0.33
Etched	1.83	0.78

Table II. Values of k in cm/min for etched cylinders in $FeCl_3$ (+HCl) at 17,000 cm/min and $Ce(SO_4)_2$ (+H_2SO_4) at 18,000 cm/min

Conc, M	$FeCl_3$ unannealed	$FeCl_3$ annealed	$Ce(SO_4)_2$ unannealed
0.02	1.08	2.16	0.82
0.04	1.10	2.21	0.87
0.06	1.06	2.22	1.01
0.08	1.14	2.17	1.00
0.10	1.06	2.11	1.05

polished initially, was similar to that shown in Fig. 1, but maximum roughness had not been reached after 55 min in the same solution.

A few runs were made in 0.02M $FeCl_3$ at other rotational speeds, and values of k are plotted in Fig. 2. While the values are consistent among themselves, it will be seen that these cylinders had their own characteristic rates.

The following empirical equation represents dissolution rates for smooth cylinders in a number of cases (3):

$$k = 0.010\ U\ (D/\nu)^{0.6} \qquad [2]$$

where U is peripheral speed, D, diffusion coefficient, and ν, kinematic viscosity. The lower dashed line of Fig. 2 represents this equation, using $D = 7 \times 10^{-6}$ cm²/sec for $FeCl_3$ (4) and $\nu = 9.36$ cm²/sec (the value for 1M HCl). The equation is of course inadequate in this case. At 17,000 cm/min it gives $k = 0.54$; for a smooth copper cylinder in $FeCl_3$ King and Weidenhammer (4) found 0.56 cm/min.

For roughened cylinders Makrides and Hackerman (2) proposed the equation:

$$k = (1.25 + 5.76 \log d/h)^{-2}\ U\ (D/\nu)^{0.644} \qquad [3]$$

where d is the cylinder diameter and h is the average height of surface irregularities. Microscopic examination of annealed Ni cylinders, etched in $FeCl_3$ to maximum dissolution rate, showed a fairly uniform groove depth at grain boundaries of about 0.05 cm. The upper dashed line of Fig. 2 represents Eq. [3] using this value of h and with D and ν as before. It obviously gives a much better prediction of the magnitude of the experimental values. The exponent 0.644 on the inverse of the Prandtl number D/ν has not been verified, and the function is quite sensitive to this exponent; e.g., with a value of 0.8, Eq. [3] gives almost the same slope as the lower dashed line of Fig. 2. Also, Eq. [3] predicts that k should vary with cylinder diameter, but this has not been tested.

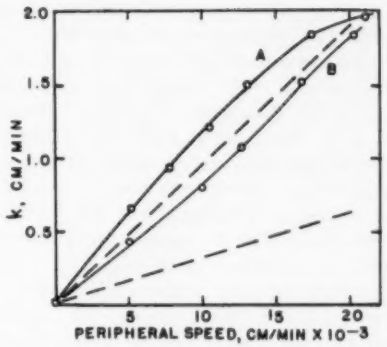

Fig. 2. Rate constant vs peripheral speed in 0.02M $FeCl_3$ + 1M HCl. A, annealed cylinder. B, unannealed. Lower dashed line, Eq. [2]. Upper dashed line, Eq. [3].

Manuscript received Dec. 31, 1959.

Any discussion of this paper will appear in a Discussion Section to be published in the December 1960 JOURNAL.

REFERENCES

1. R. G. Van Name and D. U. Hill, *Am. J. Sci.*, (4) **42**, 301 (1916).
2. A. C. Makrides and N. Hackerman, *This Journal*, **105**, 156 (1958).
3. C. V. King and N. Mayer, *ibid.*, **100**, 473 (1953).
4. C. V. King and L. Weidenhammer, *J. Am. Chem. Soc.*, **58**, 602 (1936).

Oxidation of Niobium in the Temperature Range 350°-750°C

D. W. Aylmore, S. J. Gregg, and W. B. Jepson

Department of Chemistry, University of Exeter, Exeter, England

ABSTRACT

The kinetics of the oxidation of niobium in dry oxygen at 1 atm pressure have been measured at temperatures in the range 350°-750°C with some additional measurements at 0.1 atm. At 350°C, in tests lasting 270 hr, the oxidation is protective, but at 400°C and above the metal oxidizes, apart from an initial period, at a constant rate with a second breakaway reaction (rate transition) at 450° and 500°C but not at higher temperatures. The anomalous temperature coefficient of the linear rate has been confirmed. The specific surface of the oxide scale has been measured and, apart from an anomaly at 400°C, is shown to decrease with increasing temperature of oxidation and this is ascribed to sintering. The oxidation kinetics of a purer batch of niobium were also investigated. The effect of moisture is to decrease the rate at 400° and 450°C, whereas at 600°C the rate is unchanged.

There have been a number of kinetic studies of the oxidation of niobium both in air and in oxygen. Inouye (1) has investigated the oxidation in dry and in moist air at atmospheric pressure at temperatures in the range 400°-1200°C and has found that the effect of moisture was to increase the linear rate

at 400°C and to decrease it at 600°C. Klopp, Sims, and Jaffee (2) have measured the rate of oxidation in both dry oxygen and ordinary air at temperatures in the range 600°-1200°C and have investigated the penetration of oxygen into the metal. The comprehensive study by Bridges and Fassell (3) has dealt with the oxidation in oxygen at pressures from 1 to 41 atm at temperatures over the range 400°-800°C; the linear rate of oxidation was found to be pressure dependent and the temperature coefficient of the reaction was shown to be negative from 550° to 650°C. Gulbransen and Andrew have dealt with the kinetics at 0.1 atm of oxygen in two separate investigations (4, 5) covering the temperature ranges 250°-375°C and 375°-700°C, respectively; at temperatures up to 375°C the metal oxidized according to a parabolic rate law over the first 2 hr, the period of the studies, but at higher temperatures the reaction, after an initial protective stage, underwent a breakaway [Gulbransen and Andrew (5) use "rate transition"] and the rate of oxidation increased up to the constant value, that of the linear rate. The linear rate was found to be almost independent of temperature between 550° and 625°C. More recently, Cathcart, Campbell, and Smith (6) have confirmed the breakaway and shown it to be associated with the development of small, blister-like cracks in the oxide film. Goldschmidt (7), following earlier work by Brauer (8), has re-investigated the polymorphic forms of the oxide product, niobium pentoxide, and shown that there are in fact two, and not three, such forms, viz., the α- or "low-temperature" modification which transforms spontaneously to the β- or "high-temperature" modification even at room temperature.

The present work constitutes an investigation of the oxidation kinetics at temperatures in the range 350°-750°C in oxygen at pressures of 1 atm with some additional measurements at 0.1 atm. The anomalous temperature coefficient of the reaction has been confirmed, and a second breakaway has been found to occur both at 450° and at 500°C but not at higher temperatures; this absence of second breakaway is believed to be due to a sintering of the oxide, which is confirmed to some extent by measurements of the specific surface of the oxide scale. Approximate calculations from these measurements lead to a value for the average crystallite size which is in good agreement with that found by Goldschmidt (7) using x-ray methods. The results for the kinetics in moist oxygen are in disagreement with those of Inouye (1) for moist air; the course of the oxidation differs little from that in dry oxygen.

Experimental

The main kinetic study was carried out by gravimetric determination of the weight gain of the sample on a thermal balance in an oxygen pressure of 1 atm. The niobium sample was contained in a basket of platinum gauze (to hold any fragments of oxide spalling from the metal) which was suspended in the reaction chamber by a length of platinum wire hooked to the underside of the balance pan; at the start of the run the furnace, pre-set to reaction temperature, was raised into position round the reaction chamber and thermal equilibrium was reached within about 10 min. The arrangement was similar to that previously described (9), except that the oxygen was additionally dried by passing it over "Linde" molecular sieves (10).

In addition, several runs were carried out at 0.1 atm using a quartz spring balance of conventional design, while the early stages of the oxidation at two temperatures were examined using a low sensitivity quartz microbalance (11, 12) (precision: 4 μg); with both these techniques, oxygen was admitted to the outgassed sample at reaction temperature.

The bulk of the work was carried out with material (niobium A) obtained from Murex Ltd. in the form of 1/16 in. thick sheet (analysis: C, 0.1%; Al, 0.03%; Si, 0.02%; Fe, 0.03%; Cr < 0.01%; Mn < 0.01%; Cl < 0.01%; Pb < 0.01% and Ta 0.3 to 0.4%). Samples in the form of a rectangle (4 x 1.5 cm) were cut from the sheet and abraded down to Grade 00 emery under petroleum ether and finally degreased in benzene vapor. Some additional runs were also carried out with a purer material (niobium B) in the form of 0.010 in. thick sheet (analysis: C, 0.0162%; Ta, 0.143%; Fe, 0.008%; Zr, 0.65%; Ti, 0.013%; N, 0.028%; O, 0.107%). This latter was kindly donated by Dr. K. F. Andrew and was of the same batch as that used in his study (5) with Dr. E. A. Gulbransen.

Results

Oxidation of Niobium A in Dry Oxygen

At 350°C, the first temperature studied, the weight gain of a sample exposed for 265 hr was only 0.5 mg cm^{-2}, and as far as could be judged, the rate of oxidation decreased with time.

Curves for the increase in weight (mg/cm^2 of geometric surface) against time were obtained for temperatures at 50° intervals in the range 400°-750°C, and the runs were continued at all temperatures, except 400°, until the sample had been oxidized to completion.

The course of the oxidation at 400°C is shown in Fig. 1; the rate increases over the branch OA becoming constant after about 8 hr in agreement with earlier work (3). Runs at this temperature were continued for 230 hr, after which time about 25% of the metal was oxidized, and the rate of oxidation was constant over this period. At 450°, however, the rate increased only for the first 30 min, after which it decreased (AB of Fig. 2), becoming constant after

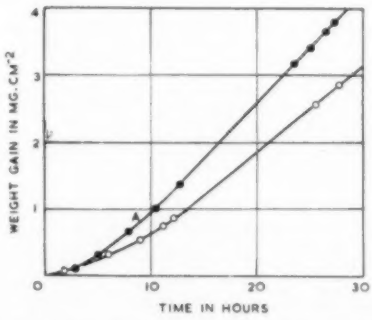

Fig. 1. Oxidation of niobium in dry and in moist oxygen at 400°c. (○, dry oxygen; ●, moist oxygen).

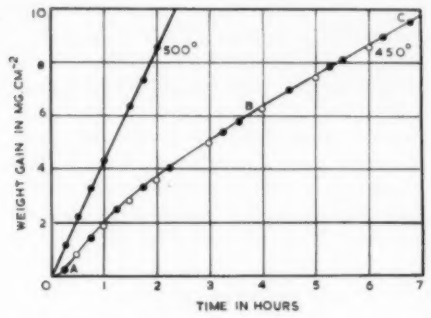

Fig. 2. Oxidation of niobium at 450°C in dry and in moist oxygen and at 500°C in dry oxygen. (●, dry oxygen; ○, moist oxygen).

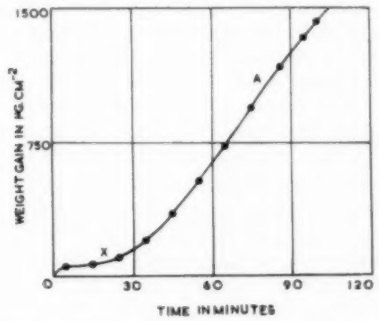

Fig. 3. Oxidation of niobium at 450°C and 0.1 atm oxygen showing the first breakaway at X.

4 hr; the early stages of the oxidation at this temperature were investigated in more detail on the microbalance at 7.6 cm oxygen pressure. From the curve of Fig. 3 which is typical, it is seen that after breakaway at X the rate increases to a maximum value (1.4 mg cm^{-2} hr^{-1}) at A and then decreases. Presumably if the run could have been carried out for a longer period, the rate would ultimately have become constant as in Fig. 2. The weight gain of 70 μg cm^{-2} at which breakaway occurred is in agreement with earlier work (5). The curve corresponding to complete oxidation of the metal is shown in Fig. 4, and it can be seen that the linear branch BC persists for only about 20 hr; at C the rate of oxidation increases, so that a second breakaway can be said to have occurred, and then decreases until at D a further section of the metal undergoes a second breakaway reaction and the metal oxidizes to completion.

At 500°C the material oxidized at a constant rate from the start of the run (Fig. 2) for a period of about 6 hr, after which it began to increase (Fig. 5); toward the end of the run there was a second breakaway reaction and the metal then oxidized to completion at a much higher rate. At 550° and 600°C the kinetics again conformed to the linear rate law from the start of the run; now there was no second breakaway and the linear rate was maintained until about 75% of the metal had been consumed, after which the rate began to fall off (Fig. 5). This was probably due to a decrease in the area of metal undergoing oxidation. The behavior at 650°C was rather similar, except that the decrease in rate occurred after only 25% of the metal had been oxi-

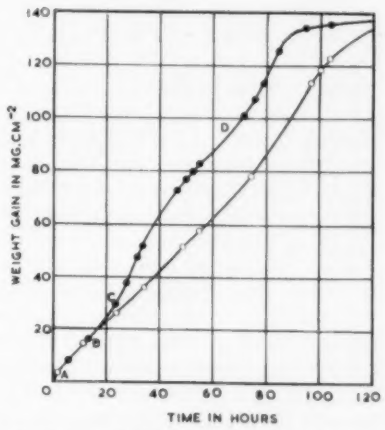

Fig. 4. Oxidation of niobium at 450°C in dry and in moist oxygen. (●, dry oxygen; ○, moist oxygen).

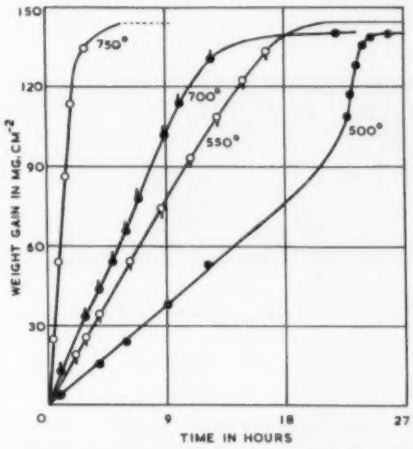

Fig. 5. Oxidation of niobium at 500°, 550°, 700°, and 750°C in dry oxygen.

dized, and cannot therefore be due to a decrease of sample area.

At 700°C the oxidation curve showed no clear linear branch (Fig. 5); after decreasing for the first 5 hr, the rate increased and then slowly decreased again. At temperatures of 550°C and above, no second breakaway was obtained in any of the runs.

At least three runs were carried out at each temperature, and the linear rates at 400°C and at temperatures from 500° to 650°C were in good agreement, often within 2-3% of the mean; at 450°C the spread in values of the rate was wider (about 15%). The times for which second breakaway occurred (450° and 500°C) agreed within about 10% of the mean. The average linear rates for each temperature are given in Table I and are plotted in Fig. 6

Table I. Oxidation rates of niobium in dry oxygen

Temp, °C	Rate, mg $cm^{-2}h.^{-1}$	Temp, °C	Rate, mg $cm^{-2}h.^{-1}$
400	0.163	600	35.7
450	1.31	650	8.72
500	4.0	700	16.9*
550	8.52	750	64*

* Approximate values only.

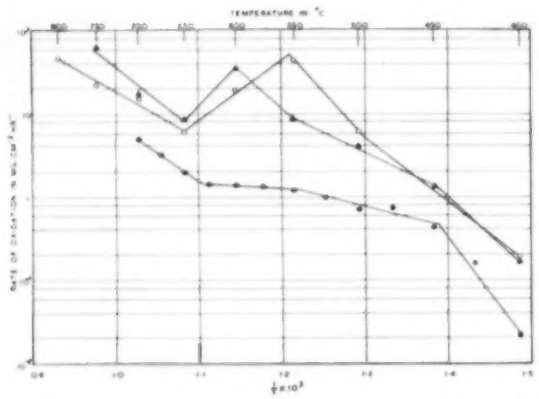

Fig. 6. Summary graph showing the change of linear rate with temperature, the data are plotted in the Arrhenius form [triangles, this work. ○, Bridges and Fassell (3); ●, Gulbransen and Andrew (5)].

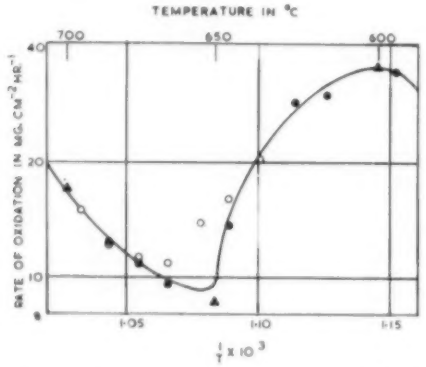

Fig. 7. Negative temperature coefficient of the reaction from 600° to 650°C. ○, ascending temperatures; ●, descending temperatures; ▲, data from Table I.

in the Arrhenius form; values from the literature (1, 5) are included for comparison.

As will be seen, the rate at 650°C is less than that at 600°C, and in order to confirm the apparent negative temperature coefficient of the reaction between these two temperatures, two additional experiments were carried out. In the first, a sample was oxidized for 10 min at 635°C and the linear rate measured, the temperature was then raised in steps of 10° up to 695°C and the linear rate measured at each temperature; in the second, the linear rate was measured at a number of temperatures in the range 685°-595°C, the temperature being lowered stepwise. The results, which are given in Fig. 7, show that over the range 600°-650°C the linear rate does in fact decrease with increasing temperature of oxidation.

The Oxide Product

The weight gain corresponding to complete oxidation of the metal agreed to within 0.01%, after making due allowance for oxidation of the impurity elements, with that calculated for niobium pentoxide (1).

The product obtained on oxidizing the metal to completion at 450°C consisted of a mixture containing approximately equal weights of scale and of fine powder, the latter being composed of particles with diameters up to 50μ, with the majority in the 5-10μ range. Since the product obtained on oxidizing a sample to a weight gain corresponding to a point on branch BC (Fig. 4) was composed only of scale, it may be concluded that the powdered oxide only forms after the second breakaway (point C). Microscopic examination of the metal surface after second breakaway revealed the presence of deep craters which in some cases extended to the opposite face (Fig. 8).

The percentage by weight of scale in the product resulting from complete oxidation of the metal increased with increasing temperature of oxidation, and at 550°C, the lowest temperature at which second breakaway did not take place, the product contained 90% scale. The oxide obtained at each temperature was carefully sieved through platinum gauze (80 mesh/linear in.) to separate the powder from the scale, and the specific surface of the latter was then measured by the method of krypton sorption (13); for the 400°C sample, which was only partially oxidized, a fragment of scale was detached from the metal for the specific surface measurement. Previous work (13) has shown that repeat determinations of the specific surface agree within ±1%. As can be seen from Fig. 9, the specific surface S of the oxide scale varies over a comparatively wide range, from 0.9 $m^2\ g^{-1}$ to 19.8 $m^2\ g^{-1}$ for the oxides formed at 750° and 450°C, respectively.

An approximate estimate of the size of the individual crystallites making up the scale can be obtained by arbitrarily assuming the latter to be made up of equal-sized cubelets of edge-length 1. Using the expression (14)

$$1 = \frac{6}{S\rho}$$

where ρ is the density of the oxide, the 450° and 750°C products then correspond to crystallite sizes of 0.061μ and 0.68μ, respectively. These values are in reasonable agreement with those found by Goldschmidt (7) using x-ray analysis. The decrease of specific surface with increasing temperature of oxidation from 450°C upwards (Fig. 9) points to the scale having sintered after it has been formed. This is substantiated by an experiment where the scale

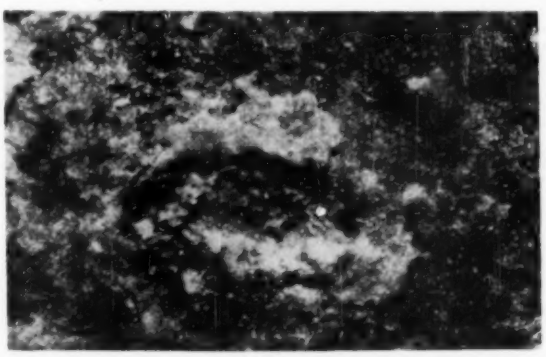

Fig. 8. Characteristic appearance of the metal surface after second breakaway, oxidized at 450°C for 47 hr. Magnification 200X before reduction for publication.

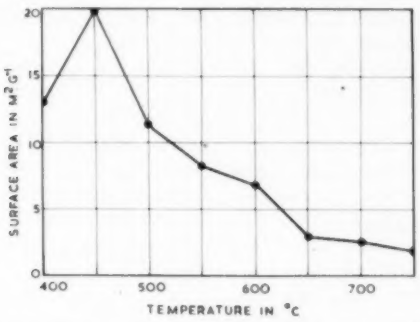

Fig. 9. Specific surface of the oxide scale as a function of oxidation temperature. The times of oxidation were 247 hr (400°), 122 hr (450°), 29 hr (500°), 24 hr (550°), 5 hr (600°), 20 hr (650°), 11 hr (700°), 4.5 hr (750°C).

formed at 500°C was heated for a period of 5 hr in oxygen at 700°C, when the specific surface fell from 11.3 to 5.9 $m^2 g^{-1}$. The rate of sintering of the scale will depend both on the time and temperature of heating, and since the rate of oxidation is not a single-valued function of temperature (see Fig. 6), the fact that a smooth curve cannot be drawn through the experimental points of Fig. 9 is readily understood. Thus, the specific surface of the 600°C product is apparently too large with respect to the 550° and 650°C products, but the oxidation time was only 5 hr for the first, as compared with 24 and 20 hr, respectively, for the last two products.

That sintering should occur is hardly surprising, for the temperature of oxidation expressed as fraction of the melting point (7) of the oxide (1733°K) ranges from 0.39 to 0.59, and, as is well known (15), solid-state processes are greatly accelerated at temperatures above a critical value T_c, characteristic of the solid but lying within the range $0.39T_f$ to $0.53T_f$, where T_f is the melting point of the solid.

Oxidation of Niobium A in Moist Oxygen

Samples of niobium were oxidized in moist oxygen saturated at 25°C (1.8 wt %), at 400°, 450°, and 600°C. At each temperature the course of the oxidation was very similar to that in dry oxygen (Fig. 1 and 2) although at 400°C (Fig. 1) 13 hr elapsed before the rate of oxidation became constant, while at 450°C (Fig. 4) the second breakaway was retarded. The linear rates at 400° and 450°C, viz., 0.133 and 0.97 mg cm^{-2} hr^{-1}, are somewhat less than the corresponding values for dry oxygen (0.163 and 1.31 mg cm^{-2} hr^{-1}, respectively), while at 600°C the linear rate in the moist gas was the same, within experimental error, as that in the dry.

The present results are in marked disagreement with those of Inouye (1) for moist air (1.39 wt %) who found that the rate at 400°C was increased by a factor of about 30 and the rate decreased at 600°C by some 40%.

Oxidation of Niobium B in Dry Oxygen

Samples of the purer material, niobium B, were oxidized at a number of selected temperatures in order to compare both the shape of the oxidation curve and the linear rate with those of niobium A. The oxidation behavior of the two batches of metal differed markedly in that second breakaway and the associated formation of powdery oxide occurred much more readily with niobium B. Thus at 600°C, second breakaway occurred with niobium B after oxidation for 1 hr and the oxide product was largely made up of powder (84%) whereas with niobium A no second breakaway was detected; the two products also differed in appearance (Fig. 10); moreover the linear rate for B (30 mg cm^{-2} hr^{-1}) is significantly less than for niobium A (35.7 mg cm^{-2} hr^{-1}). At 650°C second breakaway occurred (Fig. 11) after about 10 minutes' oxidation and the linear rate could not be measured.

At 550°C and 0.1 atm of oxygen the linear rate of oxidation of niobium B was again less than that of niobium A (1.9 compared with 2.2 mg cm^{-2} hr^{-1}), and second breakaway occurred (Fig. 12) after about 45 minutes' oxidation. A comparison of the linear rate for niobium A at 550°C and 0.1 atm oxygen pressure with that for 1 atm oxygen pressure shows that the rate is pressure dependent.

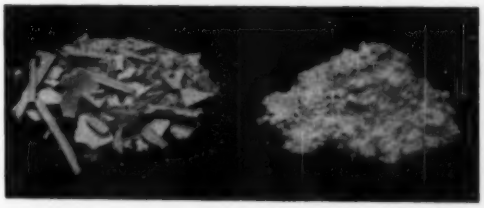

Fig. 10. Comparison of the products obtained on oxidizing niobium to completion at 600°C. left, niobium A; right, niobium B.

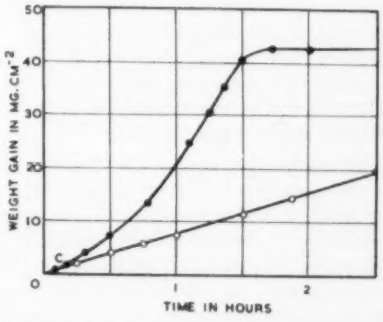

Fig. 11. Comparison of the oxidation of niobium A (○) with that of niobium B (●) at 650°C and 1 atm oxygen. Second breakaway has occurred at C with niobium B.

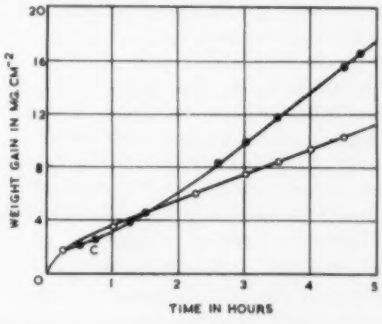

Fig. 12. Comparison of the oxidation of niobium A (○) with that of niobium B (●) at 550°C and 0.1 atm oxygen. Second breakaway has occurred at C with niobium B.

Discussion

It would appear that at 350°C the oxidation of niobium is protective although experiments of much longer duration are needed to settle this point conclusively in view of the fact that the weight gain of the sample after 270 hr (500 μg cm^{-2}) is considerably larger than that for which breakaway occurs at the higher temperatures. At 400°C and above, the oxidation is nonprotective and the metal oxidizes until it is all consumed. Gulbransen and Andrew (5) were unable to detect a first breakaway (cf. Fig. 3) at 525°C and above; similarly in the present work a run on the microbalance at 550°C and 7.6 cm oxygen pressure failed to show a breakaway. This is probably because the rate of oxidation is so large that breakaway occurs before the first reading can be taken on the microbalance; thus after 90 sec the weight gain was 150 μg cm^{-2}, a value which is considerably greater than the 70 μg cm^{-2} for which breakaway occurred at 450°C.

In a recent electron microscope study, Cathcart, Campbell, and Smith (6) have shown that breakaway, and therefore the onset of nonprotective oxidation, is associated with the formation of blister-like cracks in the oxide film. They suggested that the oxide layer thickened by anionic diffusion and that the volume expansion resulting from the build-up of new oxides at the metal/oxide interface produced compressive stresses which ultimately caused the oxide to fracture. Presumably oxygen gas then is able to enter the newly formed crack and allow a new continuous oxide layer to form and to thicken until the compressive stresses reach the fracture strength of the oxide, when a further crack appears. This process will be occurring at points all over the metal surface, and although the thickness of uncracked oxide will never be uniform, it can be regarded as statistically maintaining a constant thickness and so acting as a barrier film.

The specific surface measurements, together with earlier measurements of pore volume (14), show the oxide scale to be porous to oxygen, so that the rate of oxidation must be controlled either by the rate of diffusion of reactant across the barrier film or else by the rate of solution of reactant in the latter. Since the oxidation rate is pressure dependent the barrier film model would (on the basis of the Wagner theory of parabolic oxidation) require the oxidation to proceed either by diffusion of oxygen ions between interstitial positions or by diffusion of Nb^{5+} ions between vacant cation sites. Because of the large positive charge of the Nb^{5+} ion, anionic diffusion seems the more likely. However, either possibility would require a metal-deficient oxide, whereas niobium pentoxide itself is in fact oxygen deficient, although niobium containing comparatively large amounts of tantalum (~1.4%) gives an oxide product which contains greater than the stoichiometric content of oxygen at temperatures near to 450°C (16) (niobium A contains 0.3-0.4% tantalum). It must however be remembered that the structure and composition of the barrier film may differ greatly from that of the scale; the former may in fact be the adherent black substrate found by Klopp, Sims, and Jaffee (2) and shown to contain both NbO and Nb_2O_5.

It is also important to realize that the marker experiment of Cathcart, Campbell, and Smith (6) does not provide evidence for anionic diffusion, in that the conditions (4 hr oxidation at 450°C) were such that breakaway had occurred so that the sample was presumably covered with a layer of porous oxide; and the marker would be expected to remain on the outer surface of the scale irrespective of the type of diffusion through the barrier film. In other words, a marker experiment will not distinguish between the passage of oxygen gas and the diffusion of oxygen ions. Marker experiments on the oxide layer before breakaway would be useful in establishing the type of diffusion, although the experimental difficulties would be considerable (17,18) in view of the small thickness of film involved.

Concerning the shape of the oxidation curves, the initial increase in rate at 400°C (branch OA, Fig. 1) is consistent with the model discussed above, and almost certainly corresponds to a progressive extension of the area of metal undergoing nonprotective oxidation, the point A denoting the completion of this process. Similarly, the increase at 450°C (from X to A of Fig. 3) probably arises from the same cause but the marked decrease along AB (Fig. 2) indicates that the barrier film is increasing in thickness; possibly the development of cracks in the barrier film is influenced by the thickness of scale above it. That the rate of oxidation at temperatures of 500°C and above is constant from the start is clearly because the rate had become constant before the weight gain of the sample was sufficient to be detected on the thermal balance. Certainly the results of Gulbransen and Andrew (5), and also the present results at 550°C and 0.1 atm, clearly show that the rate does in fact decrease to a constant value.

The fact that the linear rates of oxidation, when plotted in the Arrhenius form, do not fall on a straight line (Fig. 6) is probably the most striking feature of the oxidation of niobium. Neither niobium (19) nor niobium pentoxide (7) shows any phase changes in the temperature range of the present investigation, so that any explanation along these lines can be discounted. The reason why the linear rate decreases from 600° to 650°C is not clear, though this effect could come about as the result of a change in the type of diffusion through the barrier film from, say, anionic to cationic. The temperature coefficient of either process will be positive, but from 600° to 650°C the type of diffusion could be mixed, the proportion of the one increasing at the expense of the other with increasing temperature. Simultaneous cationic and anionic diffusion has recently been put forward, for example, to interpret data for the oxidation of zirconium (20).

It is known that the oxidation of niobium is accompanied by diffusion of oxygen into the underlying metal and that the penetration increases with time (2). Second breakaway could thus come about along the lines suggested by Pemsler (21) for zirconium oxidation: namely by detachment of the barrier film from the metal in consequence of the

changing stresses produced in it by the embrittlement of the metal; some evidence for this is provided by the observation that with niobium B the black film is found adhering to the oxide scale after breakaway has taken place. This model is consistent with the absence of second breakaway at 550°C and above; indeed, the ready sintering of the oxide scale at these temperatures points to a high degree of plasticity, which might be expected to be present in the barrier film itself.

The reaction mechanism after the second breakaway is not clear, but the powdery form of the oxide suggests that individual grains of metal have become separated, possibly because of penetration of oxygen down the grain boundaries. Certainly the saturated vapor pressure of niobium at 450°C is so small (22) (an extrapolation from 2000° gives 10^{-48} mm) as to exclude completely any possible reaction between niobium vapor and oxygen, a mechanism which has been suggested (9) to explain the reaction following the second breakaway of magnesium in oxygen.

The fact that the course of the oxidation of niobium in moist oxygen is essentially the same as in the dry gas (except for small changes in the linear rate) is consistent with the fact that niobium pentoxide does not form any hydrates so that only a small fraction of the sites at the oxide/gas interface is likely to be occupied by chemically adsorbed water, and as a consequence the amount of "water" entering the barrier film will be small. With magnesium (9), on the other hand, the effect of water is to increase the linear rate over that in the dry gas by as much as tenfold and to suppress second breakaway, facts consistent with the existence of the hydroxide $Mg(OH)_2$ and the consequent strong adsorption of water on magnesium oxide.

A question, which has already attracted some interest (7), is whether oxidation for a short period at a much higher temperature will anneal out the compressive stresses in the oxide film, and so prevent first breakaway. This point has been tested by Goldschmidt, who found that breakaway still occurred; presumably the rate at which the stressed oxide is formed is greater than the rate at which the stresses are alleviated. This view is supported by the fact that breakaway occurs after a smaller weight gain the higher the oxidation temperature. If the oxide film were annealed in the absence of thickening, that is to say in vacuo, it is conceivable that breakaway could not take place. However, in an experiment where a sample was oxidized at 450°C for 10 min, annealed *in vacuo* for 170 hr at 900°C, and then re-exposed to oxygen at 450°C, breakaway still occurred, the curve of oxidation being the same in shape as that for the un-annealed specimen, with the linear rate actually greater by some 50%.

Acknowledgments

The authors are grateful to Dr. K. F. Andrew for the gift of the niobium sheet, to Mr. E. R. Braithwaite for carrying out the particle size determination of the oxide powder, and to Professor G. K. T. Conn for allowing them the use of the Vickers projection microscope. They are also grateful to the U. K. Atomic Energy Authority for the financial support which they have given to this work.

REFERENCES

1. H. Inouye, U.S. Atomic Energy Commission Publ., 1953 [ORNL-1565].
2. W. D. Klopp, C. T. Sims, and R. L. Jaffee, U. S. Atomic Energy Commission Publ. 1957 [BMI-1170].
3. D. W. Bridges and W. M. Fassell, Jr., *This Journal*, **103**, 326 (1956).
4. E. A. Gulbransen and K. F. Andrew, *Trans. Am. Inst. Mining Met. Engrs.*, **188**, 586 (1950).
5. E. A. Gulbransen and K. F. Andrew, *This Journal*, **105**, 4 (1958).
6. J. V. Cathcart, J. J. Campbell, and G. P. Smith, *ibid.*, **105**, 442 (1958).
7. H. J. Goldschmidt, *J. Inst. Metals*, **87**, 235 (1958-1959).
8. G. Brauer, *Z. anorg. u. allgem. Chem.*, **248**, 1 (1941).
9. S. J. Gregg and W. B. Jepson, *J. Inst. Metals*, **87**, 187 (1958-1959).
10. C. C. Addison, E. Iberson, and J. B. Raynor, *Chem. and Ind.*, **1958**, 96.
11. E. A. Gulbransen, *Rev. Sci. Inst.*, **15**, 201 (1944).
12. D. W. Aylmore, S. J. Gregg, and W. B. Jepson, To be published in J. Inst. Metals.
13. D. G. Smith, Thesis, University of Exeter (1958).
14. D. W. Aylmore, S. J. Gregg, and W. B. Jepson, To be published.
15. G. I. Finch and K. P. Sinha, *Proc. Royal Soc.*, **239A**, 145 (1951).
16. B. B. Argent, Private communication.
17. S. Mrowec and T. Werber, *This Journal*, **6**, 363 (1958).
18. E. A. Gulbransen and K. F. Andrew, *ibid.*, **6**, 363 (1958).
19. C. R. Tottle, *J. Inst. Metals*, **85**, 375 (1956-1957).
20. O. Flint and J. H. O. Varley, *J. Phys. Chem. Solids*, **6**, 213 (1958).
21. J. P. Pemsler, *This Journal*, **105**, 315 (1958).
22. R. Speiser, P. Blackburn, and H. L. Johnston, *ibid.*, **106**, 52 (1959).

The Difference Effect and Anodic Behavior of Zirconium Dissolving in Hydrofluoric Acid

M. E. Straumanis, W. J. James, and W. C. Custead

Departments of Metallurgical and Chemical Engineering, University of Missouri, School of Mines and Metallurgy, Rolla, Missouri

ABSTRACT

Zirconium dissolving in hydrofluoric acid exhibited a positive difference effect of such an efficiency that the hydrogen volume developed by the internal polarization current was completely overbalanced by the effect. As with other metals the effect was independent of the concentration of the acid and was accompanied by a strong shift in potential of the Zr electrode toward noble values (passivation). Similar potential changes were also recorded in presence of salts or more noble metals while they were displaced by the Zr. Simultaneously, the rate of dissolution of Zr dropped (nearly to zero with Pt^{++} additions). In the latter case the black hydride film on the surface disappeared and the Zr turned bright and shiny (passive Zr). A decrease in formation of the hydride film was observed in other cases of anodic polarization. The activity of Zr returned when the anodic current was cut off. As the effect of local currents, due to anodic polarization is reduced to a minimum, the high rate of dissolution of Zr is explained by direct chemical action of Zr with molecular HF.

Only three metals have been investigated in the authors' laboratories for the difference effect exhibited in acids: zinc, titanium, and aluminum. The results obtained with a fourth metal, zirconium, are summarized in the present article.

As discussed previously (1) the difference effect provides information about the polarizability of a metal, without making potential measurements. It reveals the true passivation ability of the metal in a certain solvent being under an anodic current.

Zirconium in HF exhibits a positive effect, meaning that the rate of dissolution V_1 of zirconium, as measured by the rate of hydrogen development, is decreased to V_2, while an anodic current is passing the surface of the zirconium electrode (Eq. [1]):

$$\Delta = V_1 - V_2 \qquad [1]$$

Thus, the difference effect, Δ, expressed in $mm^3\ cm^{-2}\ min^{-1}$, having the dimensions of a rate, is in this case positive. Actually the effect indicates the decrease in rate of dissolution of the metal while under an anodic current.

Procedure and Materials

The measurement of the difference effect was carried out as previously described (2). However, a larger three-necked boiling flask of 500 cm^3 capacity, holding 300 cm^3 of acid, was used instead of the smaller flask, and a stirrer rotating about 200 rpm was added. The stirring rate had little influence on the difference effect itself. A zirconium electrode (3) of 1 cm^2 area exposed to the acid, was always placed 5 mm from a platinized platinum electrode (3). The reactor flask was immersed in a thermo regulated water bath of 25° ±0.1°C. The hydrogen evolved was collected in a gas burette.

The rate of dissolution V_1 in $mm^3\ cm^{-2}\ min^{-1}$ of the zirconium electrode was determined; then the circuit from this electrode to that of platinum was closed (through a milliammeter and a resistance), the current I flowing through the cell was registered, and the rate V_2 was determined from the total rate V_t: $V_2 = V_t - 6.97I$, where 6.97 is the volume of H_2 in mm^3 produced by 1 ma/min. Substituting in Eq. [1] the values for V_2, Δ can be calculated:

$$\Delta = V_1 - (V_t - 6.97I) \qquad [2]$$

High-purity zirconium[1] was used for the anodes. It contained O_2-0.11, N_2-0.05, Fe-0.04, and Hf-0.01% by weight. After rolling the metal the stress was relieved by annealing in vacuum for 30 min at 700°C. From this sheet, approximately 1.6 mm thick, square anodes of 1 and 3.8 cm^2 area were cut. Reagent grade HF (48%) was used for the preparation of solutions of seven normalities. All operations with the acid were performed in polyethylene, polystirole, or wax lined glass vessels.

The Difference Effect

Unlike titanium the reaction of zirconium with HF (neglecting fluoride complexes) proceeds according to Eq. [3] (4):

$$Zr + 4HF \rightarrow ZrF_4 + 2H_2 \qquad [3]$$

This reaction was rechecked several times for Zr/H_2 ratio and was found to be quite accurate (5, 6). One gram Zr develops 491.43 cm^3 of hydrogen at standard conditions, or 1 mm^3 of the gas corresponds to 0.002035 mg Zr.

Although the rates of self-dissolution of Zr in HF are well reproducible (within a few per cent) (5),

[1] Obtained from U. S. Bureau of Mines, Albany, Oregon.

Table I. Positive difference effect on Zr in 0.3*N* HF at 25°C; surface area 3.8 cm². H_2 volumes reduced to STP

Time, min	V_1, mm³/cm² min	I, ma/cm²	6.97I, mm³/cm² min	V_f, mm³/cm² min	Δ, mm³/cm² min	K, mm³/ma min
0	—	—	—	—	—	—
5	410	0	—	—	—	—
10	419	0	—	—	—	—
15	—	16.8 *	118.8	375	158.3	9.28
20	—	17.3		366		
25	401	0	—	—	—	—
30	397	0	—	—	—	—
35	—	5.30	36.9	392	43.9	8.28
40	—	5.30		397		
45	388	0	—	—	—	—
50	375	0	—	—	—	—
55	375	0	—	—	—	—
60	370	0	—	—	—	—
65	—	7.90	55.1	366	72.6	9.19
70	—	7.90		361		
75	392	0	—	—	—	—
80	370	0	—	—	—	—
85	366	0	—	—	—	—
90	—	17.6 *	124	343	146.5	8.23
95	—	17.9		335		
100	357	0	—	—	—	—
105	366	0	—	—	—	—

Average 8.75 ± 0.53†

* Maximum current (no external resistance).
† Largest deviation.

this is not at all essential in determining the difference effect. The independence of the effect from the rate follows from the fact that the same value for the effect is obtained in various concentrations of the acid, in which the rates of self-dissolution vary vastly. However, to obtain conformable results, a constant rate of dissolution is of importance. Therefore, the measurements of the effect were started only then when, after the irregular initial period, the rate of self-dissolution became fairly constant, reaching the maximum. Furthermore, rate determinations were made before and after application of the anodic current; the adjacent rates were taken as an average for the self-dissolution. To show the magnitude of the figures involved and the procedure of calculations, data obtained in 0.3*N* HF are summarized in Table I. The constant K, which shows the reproducibility of Δ-measurements, was calculated from (8)

$$\Delta = KI \qquad [4]$$

by substituting KI for the Δ in Eq. [2]:

$$K = 6.97 + \frac{V_1 - V_f}{I} \qquad [5]$$

As shown in Table I all measurements resulted in a positive Δ-effect, but unlike previous studies V_1 was always larger than V_f (Eq. [5]) resulting in K values appreciably larger than 6.97 mm³/ma min, the differences exceeding the limit of error of the determinations. To eliminate the possibility of a systematic error, additional runs in the same apparatus were made using a Ti electrode instead of Zr. However, the average value of K, which was smaller than 6.97 (V_f was larger than V_1) agreed within 2% with that previously obtained (2). This was an indication that no systematic errors were involved in the determinations, and measurements were continued with Zr in 6 other concentrations of HF. As a result, the Δ-effect, calculated from Eq. [2] and plotted against the anodic current density, gave a straight line (Fig. 1), the inclination of which was independent of the concentration of the acid exactly as observed for Ti (2), Al [in acid (1) and in base (7)] and Zn (8). The variation of the electrode area (3.8 cm² anodes were used for runs in 0.2 and 0.3*N* HF) had no apparent effect on the result. Figure 1 also shows that the Δ-effect is proportional

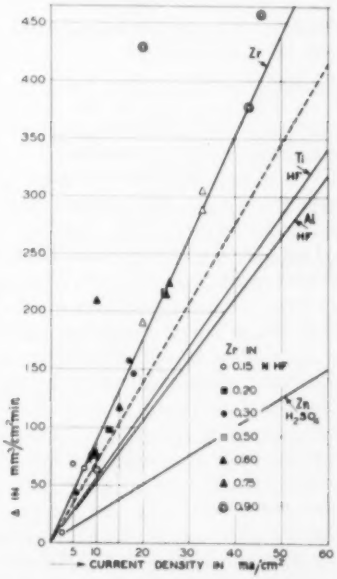

Fig. 1. Difference effect on Zr vs. current density in 7 different concentrations of HF at 25°C. Effects on Zn, Al, and Ti are given for comparison. The dashed line shows the rate of H_2 (= 6.97I) evolution at the cathode by the current.

to current density (Eq. [4]). The K-values calculated were as follows. In 0.15N HF: 8.09, 13.8, 3.56, and 9.17; in 0.2N HF: 7.72 and 8.07; in 0.3N—see Table I; in 0.5N: 8.68 and 6.17; in 0.6N: 8.68, 21.0, 7.73, and 8.65; in 0.75N: 9.21, 9.50, and 8.73; in 0.9N: 9.93, 22.9, and 8.74 $mm^3\ ma^{-1}\ min^{-1}$. Despite the relatively large fluctuations in the K-values, which may be attributed to sudden changes in the rates of self-dissolution while the Zr electrode was under the anodic current, there are only two constants less than 6.97. The mean from all measurements is 9.8; disregarding the less probable values (3.56, 13.8, 21.0, and 22.9), $K = 8.6$ with an average deviation of ± 0.7 is obtained. If the difference from 6.97 had resulted from errors of experimental nature one would expect a random distribution of K values below 6.97.

The average value of $K = 8.6 \pm 0.7\ mm^3\ ma^{-1}\ min^{-1}$ for Zr dissolving in HF means that the rate of self-dissolution of Zr is reduced by 8.6 mm^3 by each milliampere minute flowing anodically through 1 cm^2 of the electrode. As 1 ma min produces (on the cathode) only 6.97 mm^3 H_2, then the current (developed by the Zr electrode itself), not only annihilates this volume, but even decreases the rate of self-dissolution by an additional 1.6 mm^3. This is a behavior not anticipated previously (1). Nevertheless the just mentioned 23% difference is real; it results from a large number of measurements, which in the average were reproducible within 10%, as could be shown by parallel experiments in 0.15N HF. Thus, an anodic current strongly passivates the Zr electrode, and any means (see below) which cause currents should passivate such an electrode.

Potentials and Rates

Potential of zirconium in pure HF.—Before making a study of the influence of an anodic current on the potential of a Zr electrode, the behavior of the electrode in pure HF was explored by measuring the emf of the cell

Zr | HF, salt bridge (sat. KCl sol.), 1N KCl, Hg_2Cl_2 | Hg

and reducing the measured potential of the Zr electrode to the hydrogen scale by adding +0.242 v. The HF solution was always stirred (300 rpm).

The general trend is that the dissolution potential (ϵ') of the Zr electrode is very negative (around −0.90 v in 0.5N HF) right after the immersion, but quickly becomes more positive with time, approaching a steady potential in about 1 hr or more. It becomes more negative with increasing concentration of the acid (5). The potential-acid concentration curve is very similar to that obtained with Ti or Al in HF (1). However, the potential is sensitive to any change occurring on the surface of the electrode, like film formation or breakdown. Thus, the separate measurements made in the same concentration of acid at different times do not agree too well. Nevertheless, the effect of additions of ions of more noble salts to the acid upon the dissolution potential of Zr is so pronounced that there is no doubt about the reality of such measurements.

Potentials in presence of more noble metal salts.—Salt additions of $PtCl_4$, $AgNO_3$, and $AuCl_3$ to the

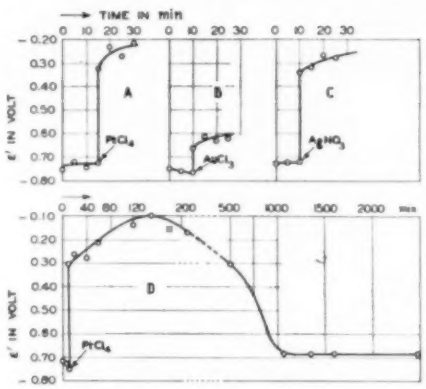

Fig. 2. Effect of salt additions on the potential of Zr dissolving in 0.1N HF, hydrogen scale.

0.1N HF (300 cm^3) were made to give 0.001M solutions for each salt. As shown in Fig. 2 the potential of the Zr electrode shifts considerably toward more noble values immediately after the addition of the salts, as with Al (9). This shift was considerably higher in the case of Pt and Ag (Fig. 2; A, C). Direct observations of the Zr electrode showed that after the addition of noble metal salts the initially black surface (Zr hydride film) (10) turned shiny, the rate of dissolution (H_2-evolution) dropped, and the black (white in the case of $AgNO_3$) loose deposit of the displaced metal started to appear on the zirconium surface. The potential of the metal remained noble as long as there were noble metal ions (Pt^{4+}, Au^{3+}, Ag^+) in the solution. However, the loose deposit did not adhere well to the shiny zirconium surface and gradually broke off. When there was no longer any replacement of the deposit from the solution, the potential of the Zr started to drop (Fig. 2, D) and the rate of dissolution increased again. Thus, the behavior of Zr is just opposite to that of other active metals (Zn, Cd, Fe, Al in HCl): as long as there is a deposit on its surface, the metal is passive; its activity (in HF) returns when the deposit is gone. Aluminum in HF behaves somewhat similarly as its rate of dissolution is retarded by Ag^+, Pt^{4+} and other ions, but is increased by Au^{3+} and Ni^{2+} ions (9).

Dissolution rates in presence of noble metal salts.—The change in rate of dissolution was followed from pressure measurements of the evolved hydrogen. A typical curve is shown in Fig. 3. After start-

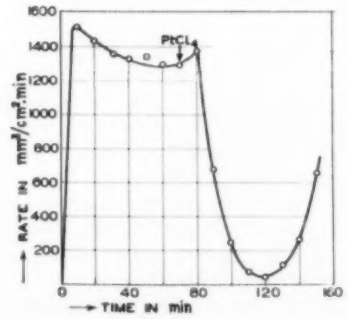

Fig. 3. Effect of $PtCl_4$ addition (0.001M) on the rate of dissolution of Zr in 0.5N HF.

ing the run, the rate of dissolution first increases, (short induction period), then slowly decreases. Upon the addition of the $PtCl_4$ solution the rate increased about 6% in the first 10 min and then decreased in 50 min by 96% resulting in an almost complete passivation of the Zr. However, the Pt deposit adhered loosely, and as before during the potential measurements, began to drop off. Simultaneously the rate of dissolution increased sharply. In the case of $AgNO_3$ and $AuCl_3$ additions, the rate dropped by 18 and 38% respectively and was still decreasing at the termination of the experiments.

In all three cases the zirconium surface under the loose deposit was bright, shiny, and heavily pitted, unlike that observed during the dissolution in pure acid.

The deposits in all three cases were identified by x-rays as the pure respective metals. Thus, there was a definite parallelism between potential and rate measurements.

Anodic Polarization of Zirconium

The anodic polarization of zirconium was investigated by Hackerman and Cecil (12), by van Ysselberghe and associates (13, 14) and others (15). The experiments were made in sodium chloride, carbonate, borate, and other aqueous solutions. In view of the peculiar behavior of zirconium in HF, it seemed worthwhile to make anodic potential measurements of the metal in this acid.

To avoid contamination of the Zr-Pt cell by other than hydrogen gases, no external emf was used at first, but only the current produced by the Zr itself (3). Its potential was measured, as usual, using a capillary touching the dissolving Zr surface. The results obtained are shown in Fig. 4. The strong influence of the anodic current on the dissolution potential of Zr is evident. The increase in potential is stronger the more dilute the acid. This effect is much more pronounced than in the case of Al (1) and already resembles a true anodic passivation. Thus, the internal anodic current (produced by the Zr electrode itself, and used in the Δ-effect measurements) as well as the external strongly shifts the potential of the electrode toward nobler values; simultaneously the rate of self-dissolution of the Zr drops. This is in agreement with the passivation of Zr observed in the presence of ions of more noble salts. However, no shiny surface was observed in absence of these salts.

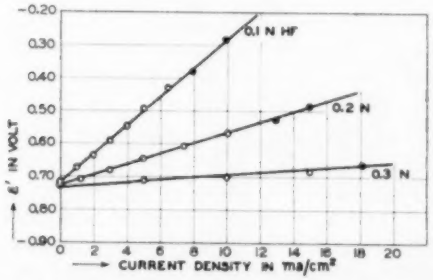

Fig. 4. Potential-current density curves of Zr dissolving anodically in HF (hydrogen scale). Each point is an average of at least two measurements. Solid points are obtained from measurements using an external current.

Discussion

It follows from these experiments that the dissolution of Zr in HF is strongly influenced by the action of local currents. However, this effect is opposite to that of other common metals, where the rate of dissolution is greatly increased by the presence of impurities. When noble metals are deposited on Zr, they cause a slight increase in the rate of dissolution (see Fig. 3) followed by a rapid decrease to nearly total passivation. The explanation is that the current produced by the deposited noble metal after an initial increase in dissolution shifts the anodic potential so far to noble values (see Fig. 2, A,B,C) that the local cathodes on Zr become inactive, i.e., their emf becomes too small to work effectively (1), and the dissolution ceases.

The positive difference effect, the direct potential measurements under anodic polarization, and the dissolution rates with noble metal salt additions testify to the strong passivating action of the anodic current. The difference effect is so strong that the work of the polarizing current is not only completely neutralized, but even overbalanced so that the action of the internal polarization current becomes more than 100% effective (K is 8.6 $mm^3\ ma^{-1}\ min^{-1}$ instead of 6.97– the hydrogen value of the current). Conversely the falling off of noble metal particles from the Zr surface causes the potential to become more negative and causes an increase in rate of dissolution (Fig. 2, D). The reasons for passivation by the anodic current are not yet known. However, it was observed that the initially dark surface (hydride film) of the active metal turned shiny upon passivation (e.g., when noble metal particles were deposited on Zr). Thus, the anodic current prevents hydride film formation by reducing the formation of hydrogen at the anode and apparently promotes the formation of a new film of unknown composition (oxide?). The effect observed by Stern on Ti (16) may be explained similarly. Formation of such passivating layers would reduce the rate of diffusion of molecular HF to the active surface and would account for a higher activation energy, as observed by Vander Wall and Whitener (17), while dissolving Zr in HF-HNO_3 mixtures, rather than in pure HF alone (11).

If now an anodic current passivates the surface of dissolving Zr (and Ti) (2), the fast dissolution rate of Zr in HF (with the anodic current off) can be explained by a chemical reaction of Zr metal with HF, outside the action of local currents, by collision of HF molecules with Zr atoms on the surface of the metal. An anodic current which makes the potential of the metal much more noble then acts as mentioned above. Our own rate measurements (11) as well as those of Smith and Hill (18) and of Vander Wall and Whitener (17) also suggest in the main a chemical action of HF. Some attempts have been made to explain the mechanism and rates of such action by the velocity of dissolution of corrosion products formed on the surface of the metal in the acid; e.g., an attempt was made to show that the dissolution of Fe in HCl is controlled by the rate of hydrolysis of $FeCl_2$ formed on the surface of the metal, or the rate of Al dissolution—by the velocity

of dissolution of $Al(OH)_3$ in the acid (19). However, our experimental and theoretical attempts to explain similarly the process of dissolution of Zr in HF with ZrO_2 as an intermediate product failed.

Acknowledgment

The authors are grateful to the Atomic Energy Commission for its support of this investigation (AT-11-1-73 Project 5).

Manuscript received July 6, 1959.

Any discussion of this paper will appear in a Discussion Section to be published in the December 1960 JOURNAL.

REFERENCES

1. M. E. Straumanis and Y. N. Wang, *This Journal*, **102**, 304 (1955).
2. M. E. Straumanis and P. C. Chen, *ibid.*, **98**, 351 (1951).
3. M. E. Straumanis and P. C. Chen, *Corrosion*, **7**, 229, Fig. 13A and 13B (1951).
4. M. E. Straumanis and J. T. Ballass, *Z. anorg. Chem.*, **278**, 36 (1955).
5. M. E. Straumanis, W. J. James, and A. S. Neiman, *Corrosion*, **15**, 286t (1959).
6. M. E. Straumanis, C. S. Lin, and W. J. James, AEC AT (11-1)-73, Project 5, (1959).
7. M. A. Streicher, *J. (and Trans.) Electrochem. Soc.*, **96**, 170 (1949).
8. A. Thiel and J. Eckell, *Z. Elektrochem.*, **33**, 370 (1927); M. E. Straumanis, *Z. physik. Chem.*, **A148**, 349, 356 (1930).
9. M. E. Straumanis and Y. N. Wang, *This Journal*, **102**, 382 (1955).
10. W. J. James and M. E. Straumanis, *ibid.*, **106**, 631 (1959).
11. W. J. James, W. G. Custead, and M. E. Straumanis, AEC AT (11-1)-73, Project 5, (1959); *J. Phys. Chem.*, **64**, 286 (1960).
12. N. Hackerman and O. B. Cecil, *This Journal*, **101**, 419 (1954).
13. M. Maraghini, G. B. Adams, and P. van Ryssel-berghe, *ibid.*, **101**, 400 (1954); **102**, 502 (1955).
14. H. A. Johansen, G. B. Adams, and P. van Ryssel-berghe, *ibid.*, **104**, 339 (1957).
15. Literature see ref. (13) and (14).
16. M. Stern, *Chem. Eng. News*, April 13, p. 26 (1959); M. Stern and H. Wissenberg, *This Journal*, **106**, 759, 755 (1959).
17. E. M. Vander Wall and E. M. Whitener, *Ind. Eng. Chem.*, **51**, 51 (1959).
18. T. Smith and G. R. Hill, *This Journal*, **105**, 117 (1958).
19. See, e.g., T. G. O. Berg. *J. Chim. Phys.*, **51**, 141 (1954); *Z. anorg. u. allgem. Chem.*, **273**, 96, 101 (1953).

Oxidation of Zirconium and Zirconium Alloys

H. A. Porte, J. G. Schnizlein, R. C. Vogel, and D. F. Fischer

Chemical Engineering Division, Argonne National Laboratory, Lemont, Illinois

ABSTRACT

The rate of oxidation of zirconium followed a cubic rate law in the temperature range 400°-900°C at oxygen pressures of 50, 200, and 800 mm. At 200 mm the activation energy was calculated to be 42.7 ± 0.7 kcal/mole.

The oxidation of zirconium binary alloys containing 1, 2, and 4 atom % of aluminum, beryllium, carbon, chromium, cobalt, copper, hafnium, iron, lead, molybdenum, nickel, niobium, platinum, silicon, tantalum, tin, titanium, tungsten, uranium, and vanadium was studied at 700°C and 200 mm oxygen. For those additives which are soluble in zirconium the initial oxidation rates are explained by a valency effect; the breakaway phenomenon is explained in terms of a 15% deviation of the ionic radius from that of zirconium. X-ray and electron diffraction studies indicate that for some alloys the breakaway coincides with a polymorphic transformation in the zirconium dioxide film.

The reaction of zirconium with oxygen at high temperatures has been studied by several investigators (1-8). A comparison of the results shows discrepancies concerning which rate law, cubic or parabolic, best describes the oxidation kinetics. For example, Gulbransen and Andrew (1) studied the reaction on foil specimens between 200° and 425°C and reported that the parabolic rate law fit their data. But Belle and Mallett (2) showed by replotting the same data in a different fashion that the cubic rate law was obeyed, implying that the interpretation of data can be somewhat arbitrary in some cases.

In another study (3) Gulbransen and Andrew found that between 400° and 600°C the method of surface preparation influenced the reaction kinetics. Mechanically polished foils obeyed the cubic rate law and reacted faster than chemically polished foils which obeyed the parabolic rate law. A later study by Charles, Barnartt, and Gulbransen (8) on the prolonged (up to 500 hr) oxidation of zirconium foils at 350° and 450°C confirmed the cubic rate law for mechanically polished specimens.

There is some reason to suspect that the size and shape of samples may influence the reaction kinetics. Belle and Mallett (2) studied the oxidation reaction on rod specimens between 575° and 950°C and found that the cubic rate law fit the data. On foil specimens in approximately the same temperature range, Cubicciotti (4), Fassell (5), and Garibotti, Green, and Baldwin (6) observed the parabolic rate law.

There is even some evidence that the particular rate law which is followed depends on the temperature range. In a recent study by Kofstad (7), zirconium was oxidized under conditions of linearly increasing temperature. It was shown that between 650° and 950°C the cubic rate law was obeyed and

between 950° and 1100°C the parabolic rate law fit the data.

Some investigators (1, 4, 5) have studied the effect of pressure. The concensus was that pressure has little or no effect on the reaction of zirconium with oxygen.

The reported work on the reaction of zirconium alloys with oxygen has been confined previously to zirconium-tin alloys for which important uses have been found in the field of nuclear reactor engineering. Mallett and Albrecht (9) have studied the oxidation of 1.5 and 2.5 weight % tin alloys at high temperatures. Gulbransen and Andrew (10) studied the reaction of Zircaloy-2 and -3a with oxygen. In both investigations tin was found to increase the rate of oxidation.

Nitrogen also reacts with zirconium, but at a much slower rate than has been found for the reaction with oxygen. Several studies (1, 6, 11-13) have been made, and most investigators agree that the parabolic rate law is obeyed. The product of the reaction at all temperatures has been identified as golden-yellow zirconium nitride. There is some evidence (1) that the presence of small traces of oxygen in the nitrogen noticeably accelerates the rate of the reaction.

Some work has also been done on the reaction of zirconium (11, 14, 15) and zirconium alloys (14, 16-18) with air. In general, the reaction rate is higher in air than in either nitrogen or oxygen alone. Both zirconium dioxide and zirconium nitride have been identified as products of the air reaction. The data on alloy oxidation indicate that in most cases additives to the metal do not improve the resistance of zirconium to oxidation in air.

The purpose of this study was to investigate the fundamental processes involved in the oxidation mechanism. The experimental approach was as follows. First, the influence of such variables as surface preparation and sample form was determined. Next, temperature and pressure dependence studies covering the temperature range 400°-900°C at three pressures, 50, 200, and 800 mm, were made. However, the major effort was devoted to studying the kinetics of the reaction of numerous zirconium alloys with oxygen at 700°C. Simultaneously, an investigation was made of the structure of the oxide films produced.

Experimental

Method.—The reaction of zirconium and zirconium alloys with oxygen was measured by a volumetric method. Essentially, the apparatus consisted of a reaction chamber which was connected through stopcocks to a pressure regulator, a gas buret, and a vacuum system. With the exception of the reaction tube, which was made of quartz, the apparatus was made entirely of Pyrex. The system was evacuated by a two-stage glass mercury-diffusion pump backed by a mechanical pump.

The reaction tube, which was supported in a vertically mounted resistance furnace, consisted of two parts which were joined by a means of a greased ball joint (below the furnace and cooled by a jet of air). Sealed to the lower section was an evacuated inner tube which extended well into the furnace hot zone and filled most of the cross-sectional area of the reactor, thus minimizing the volume of gas exposed to the temperature gradient at the lower end of the furnace. The metal sample rested on top of a long thermocouple well which passed through the center of the inner tube of the reactor.

The reactor was joined by a greased, ground glass joint to a 2-mm capillary line leading to the pressure regulator and the gas buret. The water jacketed gas buret was connected with a flexible tube to a similar buret which served as a mercury reservoir. As the sample consumed oxygen, the pressure in the reactor decreased slightly, causing mercury in the pressure regulator to make contact with a sealed-in tungsten wire. A zero current relay closed the power circuit to a motorized rod runner which raised the mercury reservoir. Mercury flowed into the gas buret, increased the pressure in the system, and the electrical contact in the pressure regulator was opened.

Coupled with the rod runner was a precision helically wound potentiometer (Helipot) which translated the position of the reservoir into an electrical potential. Changes of this potential, recorded on a strip chart potentiometer-recorder, were proportional to the movement of the reservoir and, thus, were proportional to the volume of oxygen consumed by the sample. By application of the gas laws and the measured sample area the consumption could be expressed in micrograms of oxygen per square centimeter of surface. After calibration, sensitivities from 0.05 to 12 $\mu g/cm^2$ were determined, depending on oxygen pressure and the choice of buret diameter.

A hinged-type Hevi-duty combustion tube furnace was used for runs at 700°C and below while a platinum-wound Marshall furnace was used for runs above 700°C. The furnace temperature was controlled to ±3°C by a proportional controller operated by the output from a thermocouple located at sample level outside, but near the reactor.

Before the start of the run the specimen and reaction tube were evacuated at room temperature for 16 hr at pressures of less than 10^{-5} mm to minimize the reaction of zirconium with gases present in the vacuum system during the heat-up period. After establishing thermal equilibrium at the desired temperature, the run was started by closing off the high vacuum line and admitting oxygen to the reaction chamber.

Unless otherwise specifically indicated, all runs were made on specimens which were machined parallelepipeds, 1 x 1½ x 2 cm. Freshly polished specimens were used for each run.

X-ray diffraction investigations of the oxide films were carried out by means of a Norelco X-ray diffraction powder camera (114.59 mm diameter). For electron diffraction investigations, an RCA electron diffraction unit Model EMU-2 was used.

Materials.—Table I shows the principal impurities in the arc-melted Grade I crystal bar zirconium used in the oxidation studies on pure zirconium.

To study the effect of impurities on the oxidation properties of zirconium a series of binary alloys with

Table I. Analysis of zirconium. Chemical analyses for C, H, N, O; all other elements determined by spectrograph analyses

Element	Zirconium used in oxidation studies, amount, ppm	Zirconium used as base metal for alloys, amount, ppm
Ag	<1	1
Al	10	<10
B	<0.1	0.5
C	79	19
Cr	1	5
Cu	5	100
Fe	800	80
H	—	0.6
Hf	<1000	<500
Mg	<1	15
Mn	1	<1
N	23	11
Ni	100	<50
O	185	77
Pb	4	15
Si	50	50

additives at three nominal concentration levels, 1, 2, and 4 atom %, was obtained.[1] The actual analyzed alloy compositions are given in Table IV. Arc-melted Grade I crystal bar zirconium having the analysis also given in Table I was used in the preparation of these alloys.

The oxygen used in these experiments was taken directly from the tank without further purification. Mass spectrographic and dew point analyses showed the following typical impurities (in volume per cent): argon 0.1; carbon dioxide 0.06; nitrogen 0.2; and water 0.005.

Effect of surface preparation.—To determine whether massive parallelepiped samples would show an effect similar to that reported by Gulbransen and Andrew (3) on foils a study was made in the range 400°-700°C. Table II presents a summary of the data. At least two runs were performed for each method of polishing at every temperature and average results are listed.

Mechanically polished specimens reacted somewhat faster at 400° and 500°C than chemically polished specimens, but at 600° and 700°C there was no significant difference in reaction rates. This is essentially the same conclusion reached by Gulbransen and Andrew.

The cubic rate law best expressed the data from all methods of polishing, although in the range 400°-600°C the log-log slopes obtained from chemically polished samples were slightly higher than those obtained from mechanically polished samples. At 700°C the log-log slopes were insensitive to sample pretreatment. Thus, the rate law obeyed by parallelepiped samples was independent of surface preparation.

The reproducibility was good for all methods of polishing. Therefore, since the 600-grit mechanical polish was found to be the quickest and simplest, it was used in all of the pure zirconium and alloy studies.

Effect of sample shape.—In going from massive metal to foil the surface area per unit weight is increased. At the same time several other factors which may possibly influence the rate are affected. Metallurgical condition of the metal, i.e., grain size, crystal orientation, strains, etc., are changed. Also, certain impurities may be introduced during the rolling operations. It would be necessary to separate and study each of these variables to investigate thoroughly the effect of foil samples on reaction rate. Such a study was beyond the scope of this investigation. However, two runs were made on 0.25-mm (10-mil) foils which had been cold rolled from sponge zirconium. The foil samples were polished through 600 grit and run at 700°C and 200 mm oxygen pressure. The slopes of the log-log plots were 0.35 in both cases, in good agreement with the parallelepiped samples. The cubic rate constants were found to be 2.3×10^7 and 2.8×10^7 $(\mu g/cm^2)^3/min$, somewhat larger than values obtained from parallelepiped samples. The more rapid reaction on foil specimens may be explained in part by a higher heat of reaction caused by the increased surface area to mass ratio. Examination of the product immediately after one of the foil runs revealed an adherent black oxide film similar to those formed on the parallelepiped samples.

[1] Zirconium binary alloys were prepared by Oregon Metallurgical Corporation, Albany, Oregon.

Table II. Effect of surface preparation on the reaction of zirconium with oxygen (Oxygen pressure, 200 mm)

Temp, °C	Surface preparation	Slope of log-log plot, $1/n$	Cubic rate constant, k, $(\mu g/cm^2)^3/min$
400	Mechanical polish—600 grit[a]	0.29±0.00	$(11\pm5.2) \times 10^2$
400	Chemical polish[b]	0.36±0.01	$(5.9\pm2.0) \times 10^2$
500	Mechanical polish—600 grit	0.31±0.01	$(3.5\pm0.1) \times 10^4$
500	Chemical polish	0.33±0.01	$(2.1\pm0.3) \times 10^4$
600	Mechanical polish—600 grit	0.33±0.01	$(1.2\pm0.4) \times 10^6$
600	Chemical polish	0.37±0.01	$(1.1\pm0.3) \times 10^6$
700	Mechanical polish—600 grit	0.34±0.02	$(1.6\pm0.2) \times 10^7$
700	Mechanical polish—0.5μ[c]	0.36±0.01	$(1.5\pm0.1) \times 10^7$
700	Attack polish[d]	0.36±0.02	$(1.3\pm0.1) \times 10^7$
700	Chemical polish	0.35±0.01	$(1.5\pm0.2) \times 10^7$

[a] Specimens ground down with successively finer grades of silicon carbide paper to 600-grit paper. Water used as lubricant.
[b] Composition of chemical polish solution: 45 parts H_2O, 45 parts HNO_3 (conc), and 10 parts HF (48%).
[c] Extension of the 600-grit polish with Linde A abrasive on Miracloth lap.
[d] Mechanical polish through 0.5μ in which 1 ml HF (48%) and 0.5 ml HNO_3 (conc) are added to 98.5 ml of Linde A abrasive.

Effect of temperature.—Oxidation rates were measured at various temperatures in the range 400°-900°C at an oxygen pressure of 200 mm. Plots of the log of the weight gain vs. the log of time for typical runs at these temperatures are given in Fig. 1. The straight lines indicate agreement with the general rate expression $W^n = kt$. The values of n can readily be obtained since the slope of the line on this type of plot is $1/n$.

From the values of $1/n$ listed in Table III it is seen that the reaction rate is best expressed by the cubic rate law, $W^3 = kt$. The value of $1/n$ increased slightly from 400° to 800°C and then dropped a

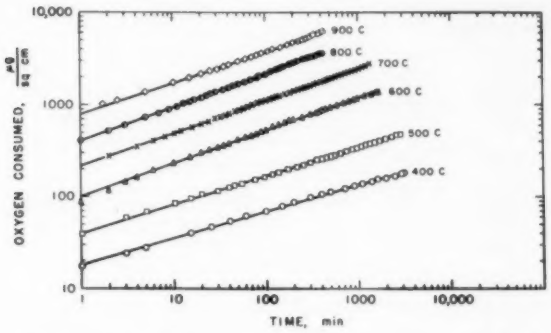

Fig. 1. Effect of temperature on the reaction of zirconium with oxygen.

bit at 900°C. There is no apparent reason for the increasing trend in the value of $1/n$; however, the drop from 800° to 900°C may be attributed to the transformation from α to β zirconium which occurs at 862°C. The cubic rate law constants listed in Table III were obtained from plots of W vs. $t^{1/3}$.

A plot was made of the log of the cubic rate constants vs. $1/T$ for the temperature range 400°-900°C. The equation of the best straight line through the points was determined by the method of least squares and the activation energy was calculated to be 42, 700 ± 700 cal/mole by the Arrhenius-type equation, $k = Ae^{-E/RT}$. The corresponding rate constant for the reaction in $(\mu g/cm^2)^3/min$ was

$$k = (5.94 \times 10^{15})e^{-42,700/RT}$$

In comparison, Belle and Mallet (2) obtained an activation energy of 47.2 kcal/mole and Charles, Barnartt, and Gulbransen (8) calculated a value of 38 kcal/mole.

The length of the runs, as indicated in Table III, varied from a minimum of 400 min to several thousand minutes in some cases; however, the run length had no effect on either the log-log slopes or the cubic rate constants. No breakaway phenomena were observed in any of the runs, even at the higher temperatures. One run at 800°C was carried out for longer than 5600 min without giving any sign of a breakaway.

Table III. Cubic rate constants for the reaction of zirconium with oxygen

(Oxygen pressure, 200 mm)

Temp, °C	Length of run, min	Slope of log-log plot, $1/n$	Cubic rate constant, k, $(\mu g/cm^2)^3/min$
400	3235	0.29	1.6×10^9
400	4275	0.29	5.6×10^9
500	4238	0.30	3.5×10^{11}
500	2860	0.32	3.6×10^{11}
600	1660	0.33	1.6×10^{13}
600	4250	0.34	8.9×10^{12}
700	1415	0.29	1.5×10^{15}
700	1400	0.31	1.8×10^{15}
700	1400	0.33	1.5×10^{15}
700	1400	0.33	2.0×10^{15}
700	1323	0.35	1.7×10^{15}
700	400	0.36	1.6×10^{15}
700	1345	0.36	1.3×10^{15}
700	1408	0.36	1.4×10^{15}
800	5645	0.36	1.3×10^{16}
800	400	0.37	1.3×10^{16}
800	413	0.38	1.3×10^{16}
800	415	0.39	1.3×10^{16}
900	400	0.32	5.3×10^{16}
900	418	0.34	5.3×10^{16}

The reaction produced a shiny blue-black oxide at all temperatures. A few white specks were observed on the surface of the oxide at 900°C.

Because of the high solubility of oxygen in zirconium (29 atom %), the reaction is somewhat complicated. A sample which had been run at 900°C was mounted in Bakelite, polished, and then a photomicrograph was taken. The thickness of zirconium dioxide, as measured from the photomicrograph, was found to be 22 μ; the thickness calculated from the amount of oxygen consumed was 41 μ, based on the assumptions that (*a*) the ratio of the real to measured surface area was one and (*b*) the only product formed was zirconium dioxide having a density of 5.73 g/cc. Evidently, an appreciable solution of zirconium dioxide in zirconium takes place at 900°C.

Effect of pressure.—The effect of variation in pressure on the reaction rate kinetics was determined. Runs were made at oxygen pressures of 50, 200, and 800 mm in the temperature range from 400° to 900°C. The data showed that the oxidation rate was relatively insensitive to pressure. The values of the log-log slopes indicated the cubic rate law at all pressures. The cubic rate constants agreed very well at the different pressures, and no apparent trend could be seen at any temperature. These results confirm the work of other investigators who found no pressure effect.

Effect of additives to zirconium.—The study of the effect of small amounts of impurities on the oxidation kinetics of zirconium was carried out using a series of binary zirconium alloys. These were alloys of zirconium with aluminum, beryllium, carbon, chromium, cobalt, copper, hafnium, iron, lead, molybdenum, nickel, niobium, platinum, silicon, tantalum, tin, titanium, tungsten, uranium, and vanadium. Each binary system included three nominal compositions, 1, 2, and 4 atom %, except that the 4 atom % tungsten alloy was impossible to fabricate.

The experimental conditions used were 700°C and 200 mm of oxygen. The choice of a particular temperature and pressure was somewhat arbitrary, but was dictated by certain important considerations. It was desirable to work at some high temperature in the alpha zirconium region, so that the oxidation would take place at a conveniently measurable rate at reasonable pressures. This limited the temperature range from approximately 600°C to the alpha to beta transformation temperature, 862°C. Certain metals, e.g., cobalt, copper, chromium, iron, molybdenum, nickel, niobium, platinum, tantalum, titanium, tungsten, uranium, and vanadium, could be expected to lower the transformation temperature (19). Therefore, it was decided to work at 700°C, which was far enough below 862 to be sure that beta zirconium was not present in any of the alloys. Another factor in favor of choosing 700°C as the

Table IV. Oxidation of zirconium alloys (700°C and 200 mm oxygen)

Alloy composition, atom %	Slope of log-log plot[a] $1/n$		Rate constant[b]	Break-away time, min	Break-away weight, $\mu g/cm^2$	Break-away rate, $\mu g/(cm^2)$ (min)	Length of run, min	Total weight gain, $\mu g/cm^2$	Color and character of oxide film
Pure Zr	0.33		1.6	No breakaway			1400	2845	Blue-gray; adherent
1.42 Al	0.36		14.0	25	1467	58.9	280	14100	Ivory with raised edges; adherent
2.15 Al	0.33		12.0	24	1401	49.3	280	13683	Ivory with raised edges; adherent
3.62 Al	0.29		8.0	7	948	84.2	198	16232	Black; adherent
0.90 Be	0.29		1.2	No breakaway			1400	2513	Blue (gold tinge); adherent
2.09 Be	0.34		1.3	No breakaway			1400	2542	Black (blue tinge); adherent
4.23 Be	0.30		1.1	No breakaway			1400	2400	Black with white raised edges; adherent
0.65 C	0.36		2.5	No breakaway			1400	3256	Silver-gold with white edges and spots; adherent
1.64 C	0.41	p	2.7	48	1225	15.3	600	7400	Gold with rough surface; flakes off
3.72 C	0.46	p	4.8	23	1076	25.4	600	17500	Gray cinder-like oxide; some flakes off
0.86 Co	0.34		1.6	No breakaway			1285	2725	Gray-black; adherent
2.49 Co	0.34		1.7	No breakaway			1400	2884	Gray; adherent
3.72 Co	0.33		2.2	No breakaway			1400	3118	Gray (gold tinge); adherent
0.77 Cr	0.33		1.7	No breakaway			1400	2850	Black; adherent
1.63 Cr	0.34		1.9	No breakaway			1400	2987	Blue-gray; adherent
3.61 Cr	0.33		1.7	No breakaway			1400	2923	Black; adherent
1.08 Cu	0.34		1.1	No breakaway			1400	2458	Black; adherent
1.84 Cu	0.33		0.90	No breakaway			1400	2347	Black; adherent
3.60 Cu	0.33		0.78	No breakaway			1400	2385	Black; adherent
1.09 Fe	0.34		3.0	No breakaway			1300	3400	Gold-gray; adherent
1.98 Fe	0.35		2.7	No breakaway			1400	3335	Blue-gray; adherent
3.95 Fe	0.33		2.4	No breakaway			1400	3200	Gray; adherent
1.03 Hf	0.34		1.4	No breakaway			1400	2673	Black with raised edges; adherent
2.22 Hf	0.34		1.4	No breakaway			1400	2648	Gray-black with raised edges; adherent
4.08 Hf	0.35		1.4	No breakaway			1400	2529	Black with raised edges; adherent
1.03 Mo	0.36		2.5	No breakaway			1400	3492	Black with raised edges and white spots; adherent
2.34 Mo	0.35		7.0	40	1368	13.1	850	10300	Silver-gray with raised edges; adherent
3.65 Mo	0.36		7.5	64	1248	11.9	850	10200	Silver-gray with raised edges; adherent
0.91 Ni	0.35		1.5	No breakaway			1400	2715	Black; adherent
2.48 Ni	0.34		1.1	No breakaway			1400	2484	Black; adherent
4.22 Ni	0.32		1.0	No breakaway			1400	2436	Gray (gold tinge); adherent
0.60 Nb	0.36		5.9	365	2680	5.0	875	5717	Black with raised edges; adherent
1.82 Nb	0.46	p	6.2	500	5625	7.7	875	8500	Silver with raised edges; adherent
3.82 Nb	0.35		6.7	49	1550	16.3	680	10519	Silver-black with raised edges; adherent
0.58 Pb	0.28		1.1	273	1465	9.7	890	5938	Black with raised edges; adherent
1.62 Pb	0.30		1.6	34	835	15.9	580	9123	Black with raised edges; adherent
4.00 Pb	0.28		0.85	7	460	9.7	895	11165	Silver-gray with raised edges; adherent
1.08 Pt	0.34		1.5	No breakaway			1400	2684	Black; adherent
2.04 Pt	0.32		0.91	630	1815	2.9	1400	3225	Black with blisters; adherent
4.22 Pt	0.31		0.81	655	1763	1.8	1400	2980	Black with raised edges; adherent
0.80 Si	0.40		3.4	No breakaway			1400	3396	Gray with white specks on faces; adherent
1.94 Si	0.43	p	2.2	115	1650	12.7	600	5921	Tan with rough surface; flakes off
3.60 Si	0.39		1.7	6	439	97.0	165	12046	Tan with rough surface; flakes off
0.96 Sn	0.28		0.92	235	1345	12.8	650	4450	Tan with black spots; adherent
1.68 Sn	0.32		1.1	111	1098	12.9	650	7100	Coral; adherent
3.60 Sn	0.31		2.2	20	521	292.0	117	13071	White; flakes off

Table IV. Oxidation of zirconium alloys (cont'd)

Alloy composition, atom %	Slope of log-log plot[a] 1/n	Rate constant[b]	Break-away time, min	Break-away weight, μg/cm²	Break-away rate, μg/(cm²)(min)	Length of run, min	Total weight gain, μg/cm²	Color and character of oxide film
1.04 Ta	0.60	p 39.5	No breakaway			500	13200	Blue-black with raised edges; adherent
1.78 Ta	0.66	p 30.5	No breakaway			500	11600	Black with raised edges; adherent
3.54 Ta	0.60	p 26.9	270	7830	26.1	500	13000	Silver-white with raised edges; adherent
1.08 Ti	0.37	69.7	370	6215	9.3	930	11134	Black with raised edges and blisters; adherent
2.12 Ti	0.39	251	385	9468	13.0	790	14770	Black with raised edges and blisters; adherent
4.16 Ti	0.43	p 90.8	275	15975	33.1	590	24917	Black (gold tinge) with raised edges; edges flake off; faces adherent
0.89 U	0.36	3.2	No breakaway			1400	3535	Black with raised edges; 2 faces gold flaky oxide
1.76 U	0.36	4.1	No breakaway			1400	3938	Black with raised yellow edges; adherent
3.52 U	0.35	3.5	530	2645	1.7	1400	4078	Black with raised yellow edges; adherent
1.01 V	0.35	4.5	530	2810	3.9	1285	5292	1 face black and 5 faces yellow and black; adherent
1.84 V	0.41	p 4.3	120	2363	6.8	1175	9195	Black with raised edges and yellow-green spots; adherent
3.88 V	0.42	p 29.0	No breakaway			615	14272	Dark yellow with raised edges; flakes off
0.68 W	0.35	1.9	No breakaway			1400	2980	Black; adherent
1.96 W	0.32	3.5	No breakaway			1400	3700	Black with yellow adherent oxide at flaws in metal; adherent

[a] The log-log slope applies only to the portion of the run before breakaway.
[b] Cubic rate law constants [10^7 (μg/cm²)³/min] unless preceded by p which signifies parabolic rate law constant [10^4 (μg/cm²)²/min]. Both apply only to the portion before breakaway.

temperature at which to make the study was that in a recent study (9) on the high-temperature oxidation of two zirconium-tin alloys it was reported that the minimum times for breakdown of the protective properties of the films occurred at 700°C.

The kinetic data for the oxidation of the alloys are presented in Table IV. In most cases duplicate 1400-min runs were made with each alloy composition and the results averaged.

A number of alloys oxidized similar to pure zirconium. Many others, however, exhibited the oxidation phenomenon usually referred to as "breakaway." In these cases the oxidation kinetics changed from an initially cubic or parabolic rate to a faster essentially linear rate of oxidation. When the data were plotted in the usual fashion, log oxygen consumed vs. log time, it was found that, after the initial straight line portion of the plot, an upward curvature took place which eventually leveled off into another straight line portion. The "breakaway time" and "breakaway weight" were defined as the time and oxygen consumed at the last point on the initial straight line portion of the oxidation curve. Within a given system the breakaway weights and breakaway times usually decreased with increasing additive concentration as illustrated in Fig. 2 for the tin alloys.

An examination of the results revealed that the alloys could be grouped conveniently according to four types of reaction behavior as indicated in Fig. 3.

Many of the alloys and pure zirconium (Group I, Fig. 3) oxidized according to the cubic rate law and did not exhibit breakaway phenomena. Slopes of log weight gain vs. log time plots were in the range 0.28 to 0.40. The cubic rate constants ranged from 0.78 x 10^7 to 3.5 x 10^7 (μg/cm²)³/min.

The 1 and 2 atom % tantalum and the 4 atom % vanadium alloys (Group II, Fig. 3) oxidized according to the parabolic rate law and did not exhibit

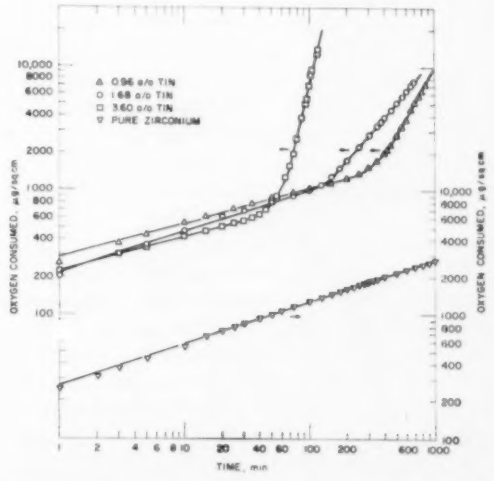

Fig. 2. Reaction of zirconium-tin alloys with oxygen at 700°C and 200 mm oxygen pressure.

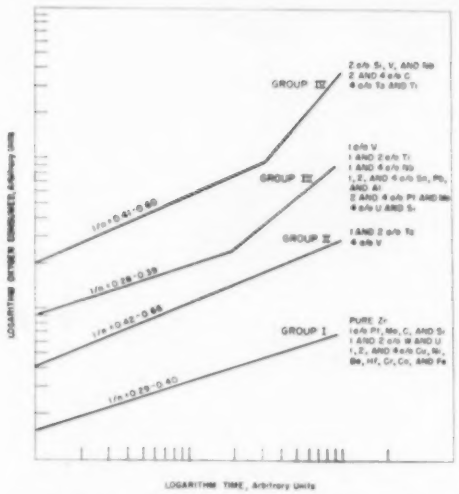

Fig. 3. Oxidation of various zirconium alloys at 700°C and 200 mm oxygen pressure, general oxidation characteristics.

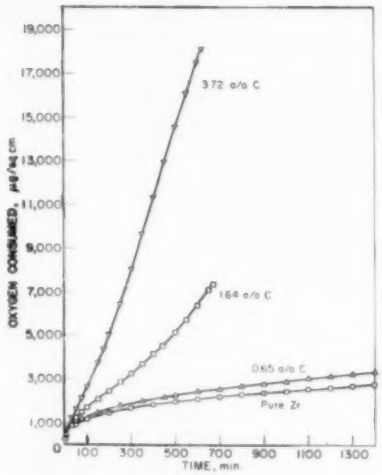

Fig. 5. Oxidation of zirconium-carbon alloys at 700°C in 200 mm oxygen.

breakaway phenomena. They had log-log slopes in the range 0.41-0.66. The parabolic rate constants were 39.5 x 10^4, 30.5 x 10^4, and 29.0 x 10^4 $(\mu g/cm^2)^2$/min, respectively.

Another large group of alloys (Group III, Fig. 3) oxidized initially according to the cubic rate law but later exhibited breakaway phenomena. The cubic rate constants ranged from 0.81 x 10^7 to 251 x 10^7 $(\mu g/cm^2)^3$/min. Breakaway times ranged from 6 to 655 min, and breakaway weights ranged from 439 to 9468 $\mu g/cm^2$. After the breakaways, faster linear rates, ranging from 1.7 to 292 $\mu g/cm^2$/min, were followed for the duration of the runs.

The last group of alloys (Group IV, Fig. 3) oxidized initially according to the parabolic rate law but later exhibited breakaway phenomena. The parabolic rate constants ranged from 2.2 x 10^4 to 90.8 x 10^4 $(\mu g/cm^2)^2$/min. Breakaway times ranged from 23 to 500 min, and breakaway weights varied from 1076 to 15,975 $\mu g/cm^2$. The faster linear rates after breakaways ranged from 6.8 to 33.1 $\mu g/cm^2$/min.

Of the 20 binary alloy systems investigated only the copper, nickel, beryllium, and hafnium alloys showed any increased resistance to oxidation as compared with pure zirconium. The oxidation behavior of the copper alloys is illustrated in Fig. 4.

In some alloy systems, as typified by the carbon system (Fig. 5), the lower concentration alloys oxidized at slow initial rates without a breakaway while the high concentration alloys oxidized at faster initial rates (sometimes even following a different rate law) and then exhibited breakaway.

Widely different types of breakaway phenomena were observed. For instance, in the tin system (Fig. 2) the breakaways were distinct and obvious, while in the titanium system (Fig. 6) the breakaways represent little more than a gradual increase of an already fast rate.

A description of the films formed during the oxidations has been included in Table IV. For the alloys where no breakaway occurred, the oxide films were

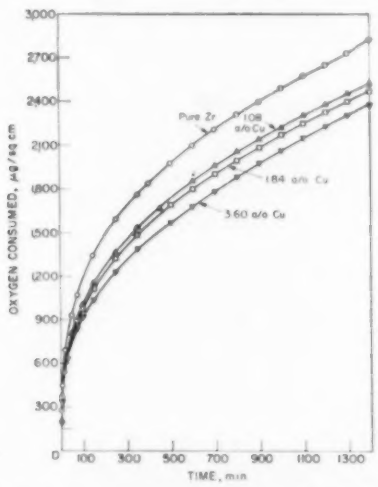

Fig. 4. Oxidation of zirconium-copper alloys at 700°C in 200 mm oxygen.

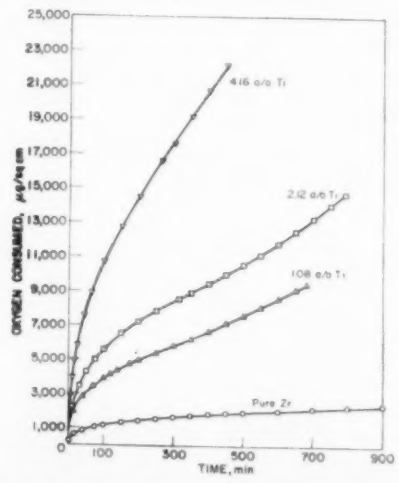

Fig. 6. Oxidation of zirconium-titanium alloys at 700°C in 200 mm oxygen.

usually black or gray and very adherent. In contrast, the films observed after the breakaway occurred still may have been adherent but were generally light-colored and cracked or porous.

Discussion

Mechanisms.—Several studies have been made to determine the mechanism of formation of the oxide film on zirconium. By employing inert markers it has been observed (9, 21) that the oxidation proceeds by oxygen (anion) migration through the oxide film toward the metal-metal oxide boundary. In another study (22) it was reported that anodic oxidation of zirconium at room temperature under low electric fields also proceeds by anion migration through the zirconium dioxide.

Consideration of the size of oxygen ions shows that they are too large to occupy interstitial positions in the zirconium oxide lattice. Therefore, it may be concluded, at least in thin films without cracks, that anion diffusion takes place by lattice defects or holes.

Measurements of thermoelectric power[2] on films of pure zirconium and zirconium-tin alloys gave negative values (9). Thus, it may further be concluded that these films were anion deficit semiconductors (n-type).

A few attempts have been made to provide a theoretical basis for the cubic rate equation. Mott (23, 24) derived a cubic rate equation based on the premise that diffusion of cation vacancies is rate controlling, where the number of vacancies is proportional to the number of negative ions per unit surface area and to a linear field set up by the ions. Engell, Hauffe, and Ilschner (25) derived a similar equation based on migration of positive holes and diffusion of lattice vacancies. Both of these derivations were based on p-type oxide films. A different approach has been taken by Uhlig (26) who recently derived a cubic rate equation based on electron flow from the metal as the controlling step in the oxidation process. This equation would be applicable for films of thickness up to several thousand angstrom units in which case the space charge in the oxide is important.

An attempt to explain the cubic oxidation of titanium has been made by Kofstad and Hauffe (27). They suggested that, in view of the high solubility of oxygen in titanium, the cubic rate law could be interpreted in terms of diffusion of oxygen through the outer layer of oxygen-enriched titanium. Since zirconium also has a high oxygen solubility, it is probable that the cubic oxidations of zirconium and titanium follow a similar mechanism.

Thus, it is not altogether surprising that the oxidation of zirconium, which ostensibly proceeds by inward oxygen diffusion, does not obey the simple parabolic rate law because the oxidation kinetics are complicated by oxygen dissolution in the outer layer of zirconium metal.

Correlation of isothermal rate data with Wagner-Hauffe theory.—According to the Wagner-Hauffe (28) semiconductor approach to alloy oxidation, foreign ions of lower valency than zirconium should increase the rate of oxidation, since they create more lattice defects. Conversely, ions of valency higher than zirconium should reduce the concentration of oxygen ion defects and thus decrease the oxidation rate. Although this theory was derived for oxidation obeying the parabolic rate law, it is not necessarily limited to this, since it has been found to apply to the case of zinc, which followed a logarithmic rate law (29).

A condition which must be met for the Wagner-Hauffe theory to apply is that the metal which is added to zirconium must share in the film formation but must not give rise to the formation of a new phase. Examination of the oxide films formed on several alloys was attempted by x-ray and electron diffraction, but because the alloys were so dilute it was impossible to determine whether or not a new phase was formed since neither additive metal oxides nor unoxidized additive metals could be detected. Thus, it is necessary to predict the composition of the films from available solubility data.

Since solubility equilibrium does not have an opportunity to be established in the oxide phase in experiments with the conditions of this study, it is believed that solubility data for the oxide systems are not germane. A more appropriate way of predicting the composition of the oxide film is in terms of the solubility of added metal in zirconium before oxidation. Thus, if the added metal is in true solution in the metallic state, it is assumed that segregation into two distinct oxide phases will not occur on oxidation, even if the oxide of the added metal is insoluble in zirconium dioxide. This statement should be true for reasonably dilute alloys and for temperatures sufficiently low that the mobilities of the metal ions in the oxide phase are low. For the problem under immediate consideration both of these conditions are true.

In the case of a metal insoluble in zirconium, the alloy probably consists of agglomerates of the second metal randomly situated throughout the zirconium. Then, when oxidation occurs, these islands of additive metal produce additive metal oxide which remains as a separate oxide phase.

In Table V data are presented for the alloy systems which were studied in this program and which are in the category of the additive metal being reasonably soluble (greater than 1 atom %). The Wagner-Hauffe theory should be applicable to these systems. Only for the case of lead does the prediction of the theory disagree with the experimental data. Lead is an exceptional additive in that its Goldschmidt ionic radius is 52% greater than that of zirconium. All of the other additives considered in this table have ionic radii less than that of zirconium. The oxide of lead most likely formed, PbO, is also thermodynamically the least stable additive oxide of the series by many kilocalories. Therefore, for these two reasons lead can be considered unique. As predicted by theory, none of the additives which were soluble in zirconium increased the oxidation

[2] To determine the type of conduction (electrical) in a semiconductor it is necessary to make measurements of thermoelectric power. If the current is carried exclusively by electrons then the thermoelectric power will be negative, whereas the thermoelectric power must be positive if the current is carried by the positive holes.

Table V. Prediction of initial oxidation behavior and breakaway phenomena of some zirconium alloys

Initial oxidation rate predicted to increase if oxidation number of additive is less than 4. Breakaway predicted to occur if ionic radius of additive differs from Zr^{4+} by 15% or more.
Consideration restricted to zirconium alloys whose additive solubility in alpha zirconium is greater than 1 atom % (a/o).

Alloy additive	Solubility in Zr at 700°C,[a] a/o	Most likely oxidation No. in oxide[b]	% Difference of additive ionic radius from Zr^{4+} radius[c]	Observed breakaway phenomena[d] and ratio[e] of initial rate constants 1 a/o[f]	2 a/o[f]	4 a/o[f]
Al	1.6	3	−34	8.8 B	7.5 B	5.0 B
Hf	Miscible	4	−3.5	0.88	0.88	0.88
Nb	3	2	−21	3.7 B	P B	4.3 B
Pb	3	2	+52	0.69B	1.0 B	0.50B
Sn	2	4	−15	0.58B	0.69B	0.75B
Ta	5	2[g]	−22	P	P	P B
Ti	Miscible	2	−21	4.4 B	157 B	P B

[a] From data compiled by G. L. Miller, "Zirconium," Academic Press, Inc., New York (1957), Chap. 13.
[b] Predicted from free energy of formation at 973°K/g atom of oxygen from data compiled by A. Glassner, ANL-5750 (1957).
[c] Goldschmidt ionic radii used. Ionic radius of zirconium as 0.87A.
[d] Breakaway phenomenon indicated by letter "B".
[e] Ratio of cubic rate constant of alloy to that for pure zirconium at 700°C; rate considered to be increased if ratio greater than 1.5. Symbol "P" indicates oxidation followed parabolic rate law in which case the oxygen consumed per unit time was greater than that for pure zirconium.
[f] Nominal concentrations. For exact concentrations see Table IV.
[g] Experimentally demonstrated that TaO formed when Ta reacts with ZrO_2 at 1700°C [W. A. Chupka, J. Berkowitz, and M. G. Ingram, *J. Phys. Chem.*, 26, 207 (1957)].

resistance because none had oxidation numbers greater than four.

The agreement of experimental results with predicted results is actually better than indicated by six metals out of seven. The phase diagrams in the literature indicate that beryllium, carbon, chromium, cobalt, copper, iron, molybdenum, nickel, platinum, silicon, tungsten, uranium, and vanadium are relatively insoluble in zirconium at 700°C. These additives, therefore, should not follow the predictions of the valence effect of Wagner-Hauffe theory. In the 13 cases cited, 11 do not follow the prediction and only 2 (vanadium and iron) follow the prediction. However, the oxide of vanadium, V_2O_5, has a low melting point (675°C) and thus is not typical. The other additive (iron) shows a slightly increased rate of oxidation which follows the prediction despite the very low solubility in zirconium. It is felt that no single theory is adequate to explain the oxidation rate effects of additives which are not soluble in zirconium, for which the Wagner-Hauffe theory does not apply . In these cases it is necessary to consider the properties of the individual oxides concerned such as preferential oxidation relative to zirconium, protective nature of the oxides, diffusion rates of ions in the oxides, and electrical conductivities of the oxides.

Breakaway phenomenon and ionic radius.—The breakaway phenomenon is a general characteristic of high-temperature zirconium corrosion and oxidation. It has been observed to occur in high-temperature water (20), in air (6, 14, 15, 30) and in oxygen (6, 9, 10). The interpretation given to the breakaway has been that, since the volume ratio of zirconium dioxide to zirconium is 1.5, the oxide grows under compressive strain and, at a certain film thickness, cracks to release the compression, thus leading to the breakaway. According to the assumed model, when zirconium alloys containing soluble additives are oxidized the film produced consists of additive metal dispersed in zirconium dioxide. If the ionic radius of the additive ion is sufficiently different from the ionic radius of zirconium, it is reasonable to expect that the lattice of zirconium dioxide will become distorted and breakaway will occur at a lower film thickness than is the case with pure zirconium.

As an extension of this reasoning a general rule, which appears useful in predicting the occurrence of the breakaway phenomenon, was formulated. This rule is that a breakaway will occur when the Goldschmidt ionic radius of the soluble additive element differs by 15% or more from the ionic radius of zirconium.

Reference to Table V shows that all 7 soluble additives (aluminum, hafnium, lead, niobium, tantalum, tin, and titanium) follow the rule. Actually, 19 out of 21 alloy compositions obeyed the rule, the only exceptions being the lower concentration tantalum alloys.

For insoluble additives the oxide film consists of zirconium dioxide and separate agglomerates of additive metal oxide. In the low concentrations encountered in this study these additives should not have any effect on the breakaway. This was borne out experimentally since out of 38 alloys containing insoluble metals, 27 did not show breakaways during the period of observation. In the 11 cases where breakaway did occur the additive metal oxide may have interfered with the adherency of zirconium dioxide to zirconium, but there are probably several causes for this effect, and any relationship between breakaway and ionic radius of insoluble metals is undoubtedly coincidental.

Structure of zirconium dioxide film.—In one study (31) concerned with the growth of oxide films on zirconium in high-temperature water, it was reported that an initial film of tetragonal zirconium dioxide transformed to the monoclinic oxide after which the corrosion proceeded at an accelerated rate.

In a recent electron-diffraction and kinetic study (30) of the oxidation of zirconium and some of its alloys with aluminum, tin, and titanium in air it was proposed that the breakaway is associated with a phase transformation in the film of zirconium dioxide. According to the theory advanced, the initial film formed on zirconium is the cubic polymorph of zirconium dioxide. As the oxidation progresses the film transforms to the tetragonal and finally to the monoclinic (stable) form of zirconium dioxide. The breakaway, it was reported, coincides with the last transformation.

To test this hypothesis and to obtain a better understanding of the mechanism of oxide film growth on zirconium alloys, electron and x-ray diffraction analyses have been obtained on oxidized zirconium alloy samples.

The oxide structures observed on 16 different alloys after oxidation to selected extents are presented with the oxidation data in Table VI.

Of the 13 samples (pure zirconium and 12 alloys) examined after less oxidation than the breakaway

Table VI. Oxide phases on oxidized zirconium alloys (Oxidized at 700°C in 200 mm oxygen; evacuated cooled and examined)

Alloy, a/o	Breakaway weight,[a] μg/cm²	Observed oxide phase[b]	
		Before breakaway	After breakaway
Pure Zr	(None)	fcc	—
1.42 Al	1467	fcc	Monoclinic[c]
1.64 C	1225		Monoclinic[c]
3.72 C	1076 p	fcc	
3.60 Cu	(None)	fcc plus unknown	—
4.08 Hf	(None)	Monoclinic	—
1.82 Nb	5625 p	Unknown bcc plus unknown	
4.22 Pt	1763	fcc	fcc
3.60 Sn	521		Monoclinic[c]
1.94 Si	1650 p		Monoclinic[c]
1.78 Ta	(None) p	fcc plus unknown	—
3.54 Ta	7830		Monoclinic[c]
2.12 Ti	9468	fcc	fcc plus unknown
4.16 Ti	15975 p	fcc plus unknown	fcc plus unknown
3.52 U	2645	Unknown bcc	Monoclinic[c]
3.88 V	(None) p	Monoclinic	—
1.96 W	None	fcc	—

[a] Initial oxidation follows cubic rate law unless indicated as parabolic by letter p.
[b] Electron diffraction by glancing from oxidized parallelepiped surface; interpretation by H. Knott and M. Mueller, Metallurgy Division. It was not possible to distinguish the cubic from the tetragonal modification of ZrO_2.
[c] Determined by x-ray diffraction of powder removed from surface. Interpretation by D. S. Flikkema, Chemical Engineering Division.

weight, 9 showed the face-centered cubic structure (3 of which had another unknown phase), 2 showed an unknown body-centered cubic structure, and 2 showed the monoclinic structure.

Of the 9 alloys oxidized beyond breakaway, 3 showed the face-centered cubic structure (2 of which had another unknown phase), and 6 showed the monoclinic structure.

Some of the unidentified phases found may be binary or ternary compounds with the alloying element. To identify the unknown phases would involve an extended research program beyond the scope of this investigation.

Although a majority of the alloys showed a relationship between the oxidation kinetics and the change of structure of the oxide film, careful consideration of the data show enough exceptions to the predicted sequence of polymorphic transformations to make it clear that there is no rule which is applicable *a priori* to all zirconium alloy systems.

The predicted sequence of phase transformations in the zirconium dioxide film and the relationship to the oxidation kinetics as outlined above is probably an oversimplified explanation which may be applicable for pure zirconium and some zirconium alloys but cannot be extended to include all zirconium alloys.

In order to understand better the mechanism of oxide film growth on zirconium, more information concerning the nature of the film must be obtained. The most promising way of accomplishing this appears to be through further electron diffraction studies of oxide films.

Acknowledgment

The assistance in the laboratory of A. Porter and of student aides, V. Sidhu and P. Tonne, is gratefully acknowledged. The authors are indebted to V. H. Munnecke for assistance in procurement of the alloys, D. S. Flikkema for x-ray diffraction analyses, and H. Knott and M. Mueller for electron diffraction studies.

Manuscript received Sept. 8, 1959. Work on this paper was performed under Contract No. W-31-109-Eng-38, U. S. Atomic Energy Commission.

Any discussion of this paper will appear in a Discussion Section to be published in the December 1960 JOURNAL.

REFERENCES

1. E. A. Gulbransen and K. F. Andrew, *J. Metals*, **1**, 515 (1949).
2. J. Belle and M. W. Mallett, *This Journal*, **101**, 229 (1954).
3. E. A. Gulbransen and K. F. Andrew, *J. Metals*, **9**, 394 (1957).
4. D. Cubicciotti, *J. Am. Chem. Soc.*, **72**, 4138 (1950).
5. M. W. Fassell, NP-4246 (1952).
6. D. J. Garibotti, H. M. Green, and W. M. Baldwin, Jr., AECU-3013 (1955).
7. P. Kofstad, *Acta Chem. Scand.*, **12**, 701 (1958).
8. R. G. Charles, S. Barnartt, and E. A. Gulbransen, *Trans. Am. Inst. Mining Met. Engrs.*, **212**, 101 (1958).
9. M. W. Mallett and W. M. Albrecht, *This Journal*, **102**, 407 (1955).
10. E. A. Gulbransen and K. F. Andrew, *Trans. Am. Inst. Mining Met. Engrs.*, **212**, 281 (1958).
11. E. T. Hayes and A. H. Roberson, *J. (and Trans.) Electrochem. Soc.*, **96**, 142 (1949).
12. A. Dravnieks, *J. Am. Chem. Soc.*, **72**, 3568 (1950).
13. M. W. Mallett, J. Belle, and B. B. Cleland, *This Journal*, **101**, 1 (1954).
14. L. F. Kendall, R. B. Wheeler, and S. H. Bush, *Nucl. Sci. Eng.*, **3**, 171 (1958).
15. C. A. Phalnikar and W. M. Baldwin, Jr., *Proc. Am. Soc. Testing Materials*, **51**, 1038 (1951).
16. F. B. Litton and S. L. Ogburn, AF-TR-5943 (1959).
17. C. T. Anderson, E. T. Hayes, A. H. Roberson, and W. T. Kroll, BM-RI-4568 (1950).
18. J. A. Burka, C. S. Crouse, and R. E. Swift, AECU-3661 (1957).
19. ASM Symposium, "Zirconium and Zirconium Alloys," Cleveland (1953).
20. B. Lustman and F. Kerze, Jr., "Metallurgy of Zirconium," pp. 610, 625, McGraw-Hill Book Co., Inc., New York (1955).
21. J. Chirigos and D. E. Thomas, WAPD-53 (1952).
22. O. Flint and J. H. O. Varley, *Nature Lond.*, **179**, 145 (1957).
23. N. Mott, *Trans. Faraday Soc.*, **36**, 472 (1940).
24. N. Cabrera and N. F. Mott, *Rept. Prog. Phys.*, **12**, 162 (1949).
25. H. Engell, K. Hauffe, and B. Ilschner, *Z. Electrochem.*, **58**, 478 (1954).
26. H. H. Uhlig, *Acta Met.*, **4**, 541 (1956).
27. P. Kofstad and K. Hauffe, *Werkstoffe und Korrosion*, **7**, 642 (1956).
28. O. Kubaschewski and B. E. Hopkins, "Oxidation of Metals and Alloys," pp. 120-130, Butterworths Scientific Publications, London (1953).
29. W. H. J. Vernon, E. I. Akeroyd, and E. G. Stroud, *J. Inst. Met.*, **65**, 301 (1939).
30. I. I. Korobkov, D. V. Ignatov, A. I. Yevstyukhin, and V. S. Yemelyanov, A/Conf. 15/P/2054, Proceedings of the Second International Conference on Peaceful Uses of Atomic Energy, Geneva (1958).
31. C. M. Schwartz, D. A. Vaughan, and G. C. Cocks, BMI-793 (1952).

High-Field Conduction Currents in Liquid n-Hexane under Microsecond Pulse Conditions

P. Keith Watson and A. Harry Sharbaugh

Research Laboratory, General Electric Company, Schenectady, New York

ABSTRACT

A novel pulse technique has been developed for measuring conduction currents due to millisecond, microsecond, and submicrosecond pulses of voltage. Using this method, a study has been made of conduction currents in liquid n-hexane at fields from 0.1 to 1.4 Mv/cm and at gap spacings from 2.5 to 25 mils. No evidence for electron multiplication was obtained at fields below 1.25 mv/cm, but there are marginal indications of the beginning of an α-process above 1.3 Mv/cm.

At fields near breakdown extremely large values of current have been measured; the authors' calculations indicate that these currents originate at microscopic points on the cathode surface. Because of the large current density and the high local field, the energy input to the liquid at the tips of these asperities is possibly as large as 10^7 watts/cm^3. This could lead to local vaporization of the liquid to form a bubble even in times as short as a few microseconds. If a bubble is so formed, then breakdown of the liquid could readily proceed by subsequent growth of the bubble across the gap to form a spark channel.

Considerable progress has been made in the measurement of electric breakdown strength in the liquid phase through the use of rectangular pulse techniques (1-3), and such methods of measurement are now widely used. On the other hand, measurements of conduction currents in insulating liquids have continued to rely on d.c. (2, 4, 5), presumably because of the experimental difficulties inherent in making reliable measurements of currents under short pulse conditions.

With the advances that have taken place in electrometer design and in pulse techniques during the past few years, it has become possible to surmount these difficulties, and we have developed a method for measuring conduction currents at high fields due to millisecond, microsecond, and submicrosecond pulses of voltage.

In a series of preliminary experiments, a comparison was made between the d-c and pulse methods (6). The measurements were made under virtually identical chemical and physical conditions, the only differences being in the methods used for applying the voltage and for measuring the resulting conduction currents in the liquid.

The present paper describes the extension of the pulse measurements to the high-field region, stresses of the order of 1.5 Mv/cm having been attained in some of the experiments. Thus the current measurements have been extended to include field strengths which approach the highest breakdown fields reported for hexane.

Experimental Technique

Equipment.—The hexane used in the experiments was first purified, using previously described techniques (7). It was then passed through silica gel, refluxed over sodium, and distilled into an electrolyzer, in which it was subject to a field of 10 kv/cm for 24 hr to remove the last traces of polar impurities. Finally, it was allowed to pass into the test cell via an ultra-fine fritted glass filter (average pore size, 1 μ). From the test cell, the hexane could be returned to the still for recycling.

The test cell was an integral part of the purification system; it was made of glass, with optical windows to allow microscopic examination of the test gap. A number of electrode sizes were used, ranging from 3/16 to 1 in. diameter across the flat portions; these surfaces were flat to within 0.05 mils, and their edges were provided with Rogowski profiles. The electrode material was stainless steel. An electrical contact method was used for determining the gap zero, and a micrometer was used for setting the gap length. A capacitance test was developed for determining the degree of parallelism of the electrodes.

D-C measurements.—Our d-c measurements were carried out over a range of gap lengths from 2.5 to 25 mils and up to field strengths of 300 kv/cm. When voltage was applied to the liquid, there was a pronounced initial current decay, which lasted some minutes, until the current settled down to its steady-state value, which was often several orders of magnitude smaller than the initial value. These findings are in agreement with those of Whitehead (8), Nikuradse (9), and others, but little attention appears to have been paid to this disturbing phenomenon by recent workers (2, 4, 5).

This fall in current is probably due to the build up of polarization charges in the vicinity of the electrodes, thus resulting in a distortion of the field in the liquid as a whole. On the basis of these and other results there seems to be good evidence for

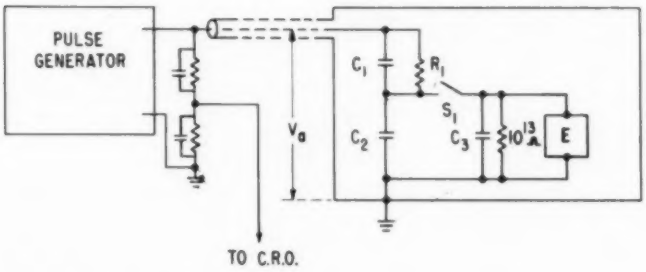

Fig. 1. Circuit used for pulse measurements of conduction currents. V_a is the applied voltage; C_1, capacitance of conduction cell; C_2, storage capacitor; C_3, input capacitance of the electrometer circuit; R_1, resistance of the liquid; S_1, switch; E, electrometer.

suspecting that d-c conduction current measurements in liquids are of an extremely complex nature and are unreliable as a guide to pre-breakdown phenomena.

Pulse measurements.—The pulse measurement technique which we have developed is to be described in detail elsewhere; briefly it is based on the fact that a voltage pulse, V_a, applied to a series circuit consisting of a resistance, R, and capacitance, C, leaves behind on the capacitor a charge proportional to $(V_a/R)\tau$. Here τ is the pulse duration, which must be short compared to the time constant CR.

In the present circuit, shown schematically in Fig. 1, a rectangular voltage pulse is applied to the series combination C_1R_1 and C_2, where C_1 is the capacitance of the conduction cell, R_1 is the resistance of the liquid, and C_2 is the capacitance of the high quality storage capacitor.

After the voltage pulse has passed, the charge remaining on C_2 is measured by closing the switch, S_1, and reading the voltage V_2 on the electrometer. The resistance R_1 is then given by,

$$R_1 = \frac{V_a C_2 \tau}{V_2(C_1 + C_2)(C_2 + C_3)}$$

The limit of sensitivity of the method is governed by background noise. A charge of 10^{-12} coulombs on C_2 can be measured with an accuracy of about 5%, and this error decreases with increasing charge magnitude. This charge sensitivity corresponds to a current of 1 μa for a pulse of 1 μsec duration; obviously, the current sensitivity increases linearly with pulse width. Moreover, by integrating the charge over a train of pulses, the sensitivity may be increased.

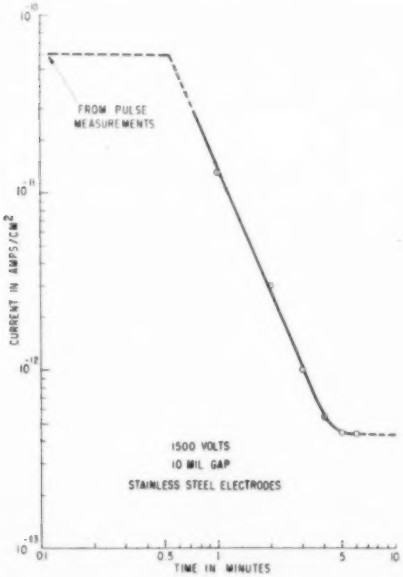

Fig. 2. Time dependence of typical d-c current measurements in n-hexane.

Experimental Results

Comparison between d-c and pulse measurements.—The results obtained using the pulse method are quite different from d-c results. The main differences are as follows: first, the absolute magnitudes of the currents obtained are orders of magnitude greater than for d.c.; and second, in the range 10 msec to 1 μsec the magnitudes of the pulse currents are independent of the duration of the applied field, whereas, in the d-c case, the currents decrease with time.

The d-c decay has been analyzed in the light of the pulse measurements, and a typical series of d-c measurements is shown in Fig. 2. These currents were measured at 1-min intervals during the first six minutes after the application of voltage to the liquid. It will be seen that the initial value of the d-c sequence is, in fact, of the same order as the corresponding pulse measurement, whereas the final d-c value is a factor of 10^{-2} smaller.

Pulse measurements at high fields.—We have used the techniques described above to make current measurements in hexane as a function of magnitude and duration of applied voltage, and also of gap width.

The results obtained fall naturally into two ranges of field strengths: the first covers the sub-breakdown range, from 100 v/mil (40 kv/cm) up to 1200 v/mil (500 kv/cm), and the second includes the range from 1500 v/mil up to fields in excess of 3700 v/mil (1.5 mv/cm). Breakdown of hexane can occur throughout the latter range, although the actual value of breakdown voltage depends on a number of other variables such as pulse width, gap width, and electrode surface.

Our results in the sub-breakdown range are plotted in Fig. 3, which shows the current density as a function of applied voltage for gap widths of 5 through 20 mils. These results were obtained using 10 msec pulses of voltage, but virtually identical results were obtained with pulse widths as short as 100 μsec. The dashed lines in the figure are curves of constant field strength. These are virtually horizontal throughout the range, that is, the currents

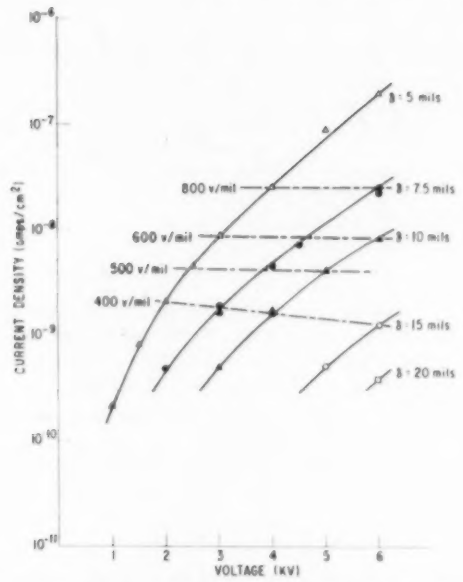

Fig. 3. Dependence of current density on voltage, n-hexane, stainless steel electrodes, 10 msec pulse width.

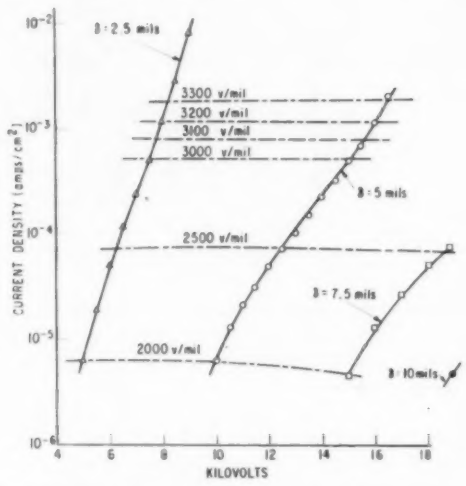

Fig. 4. Dependence of current density on voltage, n-hexane, stainless steel electrodes, 5, 3, 1.5 μsec pulse widths.

are essentially independent of gap width at all field strengths shown in the figure.

At field strengths of the order of 1200 v/mil (0.5 Mv/cm) breakdown occasionally occurred; after only one such breakdown, the current magnitude increased very markedly. This effect was attributed to decomposition products arising from breakdown in the liquid. These spuriously high currents continued to be obtained even after changing the sample, and in order to restore the former low value of conductivity, it was necessary to remove the electrodes and clean them. In order to make current measurements at higher values of field, it was necessary to use single pulses of voltage rather than trains of pulses. It was also necessary to resort to shorter pulse widths and so make use of the well-known increase of breakdown strength with decrease in pulse width.

Despite the use of short pulses, occasional breakdowns still occurred. Fortunately, at fields above about 1 Mv/cm, the electronic conduction currents are usually so much larger than the ionic currents that one can continue to use a sample, even after several breakdowns have taken place. After each breakdown, the sample conductivity was checked at a lower field in order to determine if any increase in current had occurred as a result of the breakdown. If a measurable increase was found, it was compensated for in the subsequent analysis.

The test then proceeded at a shorter pulse width until breakdown occurred again, at which point the pulse was shortened further. This procedure was followed, down to a pulse width of 0.5 μsec (the shortest pulse which the generator would deliver).

By means of this technique we have been able to make current measurements at fields as large as 1.4 Mv/cm; the results obtained are shown in Fig. 4.

Wherever possible, the measurements have been made at a number of gap spacings, and from this data we have plotted the constant field lines shown in Fig. 4.

As in the lower field region, we see that the constant field lines are essentially horizontal up to fields of 3100 v/mil (1.2 Mv/cm); this indicates that the measured currents are independent of gap width up to this field. At fields of 3200 and 3300 v/mil there may be evidence of a slight increase of current with gap width.

In concluding this description of the results we may summarize as follows: The currents are independent of pulse width, within the limits of experimental accuracy over the range from 10 msec to 1 μsec. The currents are proportional to electrode area and are independent of gap width up to fields of 3100 v/mil (1.2 Mv/cm).

Finally, it may be noted that the accuracy of the method of measurement is well indicated by the constant field lines; errors in the setting of voltage, gap width, and pulse width would lead to erratic constant field lines. However, as may be seen in Fig. 3 and 4, even a fourfold change in gap width does not appear to incur any appreciable deviation from a smooth curve.

Discussion of Results

Evidence for Electron Multiplication

One of the most controversial points in the interpretation of conduction and breakdown measurements in liquids concerns the presence (or absence) of an electron multiplication process in the liquid. Those who interpret behavior at high fields by means of a Townsend model are prone to favor the existence of an electron multiplication, or "α-process," and some have published d-c conduction data which are consistent with this model (2, 5, 9).

On the other hand, there are others who doubt the existence of an α-process in liquids and have d-c measurements to support their point of view (4, 10). The possibility of resolving this problem is regarded as one of the most important aspects of the present work.

The only satisfactory method for detecting and measuring a multiplication process involves the determination of the gap width dependence of conduction currents at constant field strength. In the presence of multiplication, currents will increase with gap width in accordance with the equation $I = I_0 \exp \alpha\delta$; that is, at constant field, the current should increase exponentially with gap width. I_0 is the current emitted at the cathode and will be field dependent. In the present work we have measured the current over a wide range of fields and at a limited number of gap widths in an attempt to determine whether or not such a multiplication process exists in liquid hexane.

The current obtained at fields up to 1 Mv/cm show no sign of increasing with gap width, indeed, at the lowest fields there is some evidence of a decrease of current with increasing gap, although this effect may not be real.

On the other hand, the currents at the very highest fields do show a slight increase with gap width, which might be indicative of an incipient α-process. We have therefore carried out a statistical analysis of the data at fields above 1 Mv/cm in order to determine whether this rise is significant.

The ratio of currents at gaps of 5 mil and 2.5 mil was taken as our statistic. The mean of these ratios at the eleven highest field strengths was 0.993, with a standard deviation of 0.075. Applying Bessel's correction to obtain the best estimate of the standard deviation, σ, of the parent population, we obtain $\sigma = 0.079$. Obviously, the mean ratio does not differ significantly from unity, so that there is no evidence for an α-process in the bulk of the data above 1 Mv/cm.

The ratios of the currents at the two highest fields were then examined: Their mean is 1.08, and the standard error of the mean for a sample of two is $S_2 = 0.079/\sqrt{2} = 0.056$, so that the mean ratio differs from unity by $1.43 \times S_2$. Now, the probability that a normally distributed statistic will differ from the mean by $+1.43$ standard deviations by chance alone is 7.6%, so that the observed results are possibly significant, but further evidence is required before the existence of a multiplication process can be established.

Thus we conclude that there is no evidence for an α-process at fields up to 1.2 Mv/cm, but that there are marginal indications of the beginning of such a process at 1.3 Mv/cm.

Electron Emission Processes at the Cathode

We have presented, above, the observations that lead us to conclude that electron multiplication in the gap is relatively unimportant. Therefore it is assumed that the observed field dependence of the current is explicable in terms of electron emission from the cathode, and the various possible emission mechanisms are examined below.

One possible source of current is field emission as described by the Fowler-Nordheim equation

$$I = 6.2 \times 10^{-6} \frac{\mu^{1/2} S}{(\mu + \phi)\, \phi^{1/2}} E^2 \exp (-6.8 \times 10^7 \phi^{3/2}/E)$$

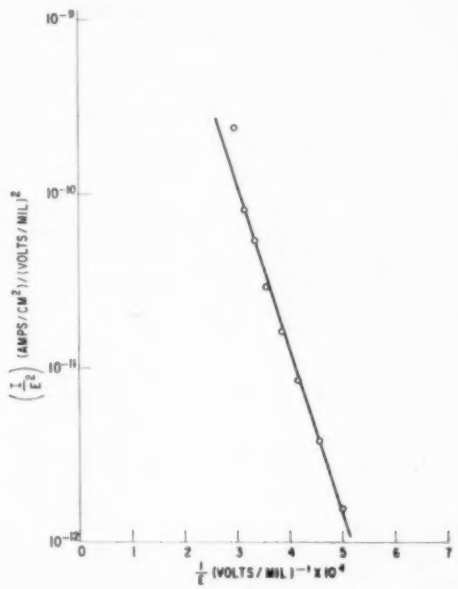

Fig. 5. Field emission plot, n-hexane, stainless steel electrodes.

Here μ is the Fermi level of electrons in the metal, and is usually taken as 5 e.v., ϕ is the work function in e.v., S is the emitting area in cm^2, and I is the current in amps. Figure 5 shows that our data give a good fit to this equation although this in itself does not constitute sufficient evidence for its validity. From the slope and intercept of the straight line in the figure, we calculate a value of $\phi = 0.25$ e.v. and an emitting area $S = 8 \times 10^{-8}$ cm. These values are lower than one might expect.

More realistic values for the work function ϕ are obtained if one takes into account the roughness of the metallic surface. As is well known, although a surface may be highly polished, it is still microscopically rough and local fields at the tips of asperities may exceed the applied field by orders of magnitude. We have taken this into account by introducing a field multiplication factor M and have recalculated ϕ and S as a function of M. The results are given in Table I. The work function becomes more reasonable at a field multiplication of ten, but our largest observed currents (greater than 10^{-8} amp) would then lead to local current densities of 10^6 amp/cm^2 for an emitting area of 10^{-8} cm^2; this is obviously unreasonable.

However, it has been shown by Jones and Morgan (11) and Goodwin (12) that the difficulties with the Fowler-Nordheim equation can be resolved by invoking the presence of an oxide layer on the cathode; this is obviously present in the case of our stainless steel electrodes.

Table I. Dependence of field emission parameters on M

M	ϕ (e.v.)	S (cm^2)
1	0.25	8×10^{-8}
10	1.2	2×10^{-9}
100	5.4	8×10^{-11}

Table II. Dependence of field emission parameters upon M for surface with oxide layer

M	ϕ_1	S
1	0.25	8×10^{-2}
10	1.2	2×10^{-3}
100	5.4	8×10^{-5}

The emission of electrons through such a barrier has been examined by Jones and Morgan on the basis of an analysis by Stern, Gossling, and Fowler (13). The equation derived by the latter shows that the theoretical current is given by

$$I = 6.2 \times 10^{-6} \frac{\mu^{1/2} S}{(\mu + \phi_1)\, \phi_1^{1/2}} E^2 \times \left[\exp\left(-6.8 \times 10^7\, \phi_2^{3/2}/E\right) \frac{\phi_1}{\phi_2} \right] B$$

where ϕ_1 is the work function of the metal, ϕ_2 is the work function of the oxide layer, and B is the barrier term

$$B = \exp\left\{ -6.8 \times 10^7 \left[\frac{\phi_1 + \phi_2 + (\phi_1 \phi_2)^{1/2}}{\phi_1^{1/2} + \phi_2^{1/2}} \right] a \right\}$$

where a is the film thickness. It will be seen that the only major difference between the Stern-Gossling-Fowler equation and the Fowler-Nordheim equation lies in the barrier term.

Inserting typical values for ϕ_1 and ϕ_2, and assuming an oxide film thickness of 10^{-7} cm, we obtain $B = 10^{-6}$. Using this factor we have recalculated Table I to yield the values shown in Table II. As before, S is the total emitting area per unit of electrode surface; it arises from the combined effects of many individual surface irregularities. These values for the emitting area are much more reasonable than those calculated on the basis of the Fowler-Nordheim equation. Taking $M = 10$ as representative, we obtain current densities of the order of 1 amp/cm^2 at the tips of the asperities.

We note, however, that a current density of this magnitude may lead to appreciable space charge distortion of the applied field. This results in a decrease of the field at the cathode and ultimately to space charge limitation of the current.

A calculation of this effect is complicated by the nonuniformity of emission from the cathode. Nevertheless, we may make a rough estimate as follows: assume that the local current density at the points is 1 amp/cm^2, and that this current density decreases with the square of the distance from the center of the asperity, tending toward the measured current density of 10 ma/cm^2 at the anode. For a hemispherical boss of radius 10^{-4} cm and an electron velocity of 10^7-10^8 cm/sec (14), we obtain a reduction of 10-100 kv/cm in the cathode field. This suggests that some space charge limitation of the cathode currents may occur at slightly higher fields. For the moment, however, we have chosen to ignore the effect, and to assume that the field in the gap is determined solely by the applied voltage and the electrode geometry.

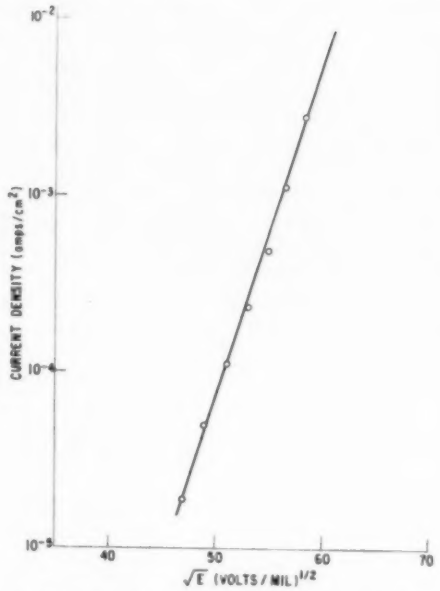

Fig. 6. Schottky plot, n-hexane, stainless steel electrodes

Another possible source of current which should be considered is field-enhanced thermionic emission of electrons, as described by the Schottky equation:

$$I = I_0 \exp\left[4.4\sqrt{E}/\sqrt{\epsilon}T\right]$$

Here I_0 is the thermionic current density at an absolute temperature T, and ϵ is the dielectric constant of the medium adjacent to the emitting surface. Figure 6 shows that our data from 0.2 Mv/cm to 1.4 Mv/cm give a good fit to this equation although, as observed in the case of the Fowler-Nordheim equation, this in itself does not prove that the equation is applicable. From the slope of the straight line in Fig. 6 and a knowledge of T and ϵ, we compute a value of five for the field enhancement factor M. From the zero field intercept of this line we obtain a value of 10^{-14} amp/cm^2 for I_0; in order to account for a thermionic emission current of this order at room temperature, one needs to postulate a work function of the order of 1.25 e.v.

It should be pointed out that the computed value of ϕ is very insensitive to the value of I_0; a change of 10^5 in I_0 changes the work function by 25% in the opposite direction. However, taking into account the uncertainty with which we know the value of the work function for emission into a liquid, we conclude that the magnitude of the observed current is consistent with that to be expected from field-enhanced thermionic emission.

In order to distinguish between Schottky emission and field emission, it is proposed to repeat our conduction measurements as a function of temperature.

Conclusions

On the basis of our measurements we arrive at the following conclusions:

1. An electron multiplication process does not play a significant role in conduction and, therefore, in breakdown in hexane.

2. Currents originate either by Schottky emission, or by field emission, from asperities on the cathode; in the latter case, their magnitude would be influenced strongly by an oxide layer on the cathode.

3. The average energy input to the liquid near breakdown is unexpectedly large (about 10^4 watts/cm^2). At the tips of the asperities the energy input may be as large as 10^7 watts/cm^2, and this could lead to local vaporization of the liquid in times as short as a few microseconds.

4. Thus we conclude that liquid breakdown involves the formation of a vapor bubble at the cathode and its subsequent growth toward the anode, bridging the gap with a vapor channel of low electric strength.

It has long been recognized that cavitation may play a role in the breakdown of liquid dielectrics, bubbles being formed either from dissolved gas (15, 16) or by the local vaporization of the liquid itself (17). Indeed, the fact that the breakdown strength of a liquid is pressure dependent is direct evidence that a change of phase is involved in the breakdown mechanism (18-20).

We believe, however, that until the present work was carried out, the mechanism of formation of these bubbles was unknown; we anticipate that this knowledge will enable us to extend our understanding of the breakdown mechanism.

Manuscript received Nov. 2, 1959. This paper was prepared for delivery before the Philadelphia Meeting, May 3-7, 1959.

Any discussion of this paper will appear in a Discussion Section to be published in the December 1960 JOURNAL.

REFERENCES

1. K. A. Macfadyen and W. D. Edwards, *Nature*, **163**, 171 (1949).
2. D. W. Goodwin and K. A. Macfadyen, *Proc. Phys. Soc.*, **66**, 85 (1953).
3. A. H. Sharbaugh, J. K. Bragg, and R. W. Crowe, *J. Appl. Phys.*, **24**, 814 (1953).
4. W. B. Green, *ibid.*, **26**, 1257 (1955).
5. H. House, *Proc. Phys. Soc.*, **70**, 913 (1957).
6. P. K. Watson and A. H. Sharbaugh, Ann. Rep., 1957 Conf. on Elec. Ins., p. 1.
7. A. H. Sharbaugh, R. W. Crowe, and E. B. Cox, *J. Appl. Phys.*, **27**, 806 (1956).
8. J. B. Whitehead and R. Marvin, *Trans. AIEE*, **45**, 299 (1929).
9. A. Nikuradse, "Das flussige Dielektrikum," pp. 83 and 133, Springer, Berlin (1934).
10. L. Inge and A. Walther, *Tech. Phys. U.S.S.R.*, **1**, 539 (1935).
11. F. Llewellyn Jones and C. G. Morgan, *Proc. Roy. Soc.*, **A218**, 88 (1953).
12. D. W. Goodwin, *Proc. Phys. Soc.*, **B69**, 61 (1956).
13. Stern, Gossling, and Fowler, *Proc. Roy. Soc.*, **A124**, 699 (1929).
14. O. H. LeBlanc, *J. Chem. Phys.*, **30**, 1443 (1959).
15. F. Koppelmann, *ETZ*, **46**, 1413 (1931).
16. F. M. Clark, *J. Franklin Inst.*, **215**, 39 (1933).
17. A. Gunther-Schulze, *J. Radioaktivität u. Elektrotechnik*, **19**, 92 (1922).
18. W. D. Edwards, *Can. J. Phys.*, **29**, 310 (1951).
19. P. K. Watson and J. B. Higham, *Proc. I.E.E.*, Pt. IIA, **100**, 168 (1953).
20. K. C. Kao and J. B. Higham, *This Journal*, being reviewed.

On the Physical Characteristics and Chemical Composition of Electroluminescent Phosphors

Paul Goldberg and S. Faria

General Telephone and Electronics Laboratories Inc., Bayside, New York

ABSTRACT

Through controlled removal of surface layers, it was found that surface chemical barriers are not responsible for electroluminescence in zinc sulfide phosphors. Polycrystalline phosphors are shown to be almost uniform with respect to chemical, physical, and electroluminescent properties as one passes from the surface into the crystallite bulk. Electron micrographs show the character of the particles as successive layers of phosphor surfaces are removed by acid etching. The experimental results at progressive stages of etching are interpreted in terms of an inefficient surface layer and of decreased particle size after etching. Regions capable of serving as the site of field intensification are held to exist throughout the volume of the particles.

If a phosphor is to emit visible light on exposure to an electric field, the phosphor must first accept energy from that field. The mechanism by which this is done is a major problem of electroluminescence research. Only a few phosphor types are known to absorb electrical energy and emit light. It is important to elucidate the nature of the physical and chemical differences between these phosphors and similar but nonelectroluminescent materials. At least one difference in zinc sulfide phosphors is held to be the presence of a barrier region in the electroluminescent particles which leads to impact ionization of luminescent centers (1, 2). Throughout the literature one finds emphasis placed on a chemical inhomogeneity in the crystal which is held to serve as the barrier site (3-6). Presumably no electroluminescence would be found were this inhomogeneity removed. It is the aim of the present work to explore the surface and volume of electroluminescent zinc sulfide to ascertain the degree of physical and chemical uniformity and to relate the results to current concepts.

It has been stated that the barriers responsible for electroluminescent excitation reside on the phosphor surface. Supporting this view are the following two experiments: (i) Zalm has deposited copper sulfide on a nonelectroluminescent zinc sulfide phosphor, and, by this simple process, converted a nonelectroluminescent phosphor into one which is electroluminescent. Cyanide washing removed the copper sulfide and destroyed the phosphor's ability to be field-excited (5); (ii) Destriau performed etching experiments to remove phosphor surfaces and found that this caused an initial improvement followed by ever diminishing sensitivity of the electroluminescent materials (7). In contrast, barriers inside powder particles have been proposed from observations on the spatial distribution of emission from individual grains (8). In single crystals both surface and volume barriers were reported, again from observations on location of light emission (5, 9-12).

Regarding the barrier composition some qualitative ideas have been formulated by various workers (4-6). The preparation of electroluminescent phosphors usually involves copper concentrations above that which yields maximum photoluminescent intensity. The barrier may thus be related to this copper excess. Zalm associates the barriers with conducting particles of copper sulfide on the phosphor surface (5).

In the work reported here, the principal experimental approach was the step-by-step removal of portions of the phosphor mass by chemical etching. At each successive etching stage the properties of the phosphor were studied. These properties include the phosphor cell emittance and electrical loss as functions of voltage. Electron microscopy and x-ray diffraction of the powders were employed as auxiliary analytical tools. Chemical analyses for copper were also performed. To the extent that phosphor material is removed uniformly from the surfaces, these measurements reflect properties of the phosphor as a function of depth into the crystal. In etching experiments of this type it is clear that account must be taken of changes in particle size and possibly in particle shape.

Experimental Technique

Phosphors and analytical methods.—The phosphors studied were mainly of the ZnS:Cu,Cl type. They contained 0.08% Cu by weight and were green-emitting below 1 kc. In most of the work the electroluminescent phosphor was first fractionated by elutriation to yield specimens with improved uniformity of particle size distribution. A potassium silicate solution was employed as a dispersing agent for the settling from aqueous solution. The phosphors were etched with solutions of 6*N* HCl by agitation of the mixtures at 60°-80°C. The progress of the etching was monitored by weight loss due to H_2S evolution. Specimens etched to various extents were obtained by either of two methods: (i) etching of a large mass of phosphor with periodic sampling, and (ii) etching of individual samples to the desired mass reduction. The two methods led to roughly comparable results. The electron micrographs were recorded of representative samples with a minimum of nine photographs per sample. Direct platinum-shadowed carbon replicas were employed throughout.

X-ray diffraction patterns were obtained with a recording diffractometer. Quantitative spectrographic analyses for copper for each stage of etching were also tabulated. In a few instances, particle size distribution data were obtained with a Coulter particle size apparatus (13).

Optical and electrical measurements.—The brightness data were taken with a demountable electroluminescent cell 25 x 25 x 0.150 mm in size with a castor oil dielectric at a phosphor volume fraction of 0.33. Brass and conductive glass (500 ohms per square) served as electrode materials. The detector was an RCA 1P21 photomultiplier corrected by a Wratten No. 106 filter to yield an approximate eye response. The brightness was recorded with a Photovolt Model 520 photometer calibrated with a Spectra 100 ft-L standard brightness source.

The measurement of electrical losses was achieved with a bridge circuit which measured the capacitance and the equivalent parallel resistance of the test cell.

Experimental Results

Electroluminescent properties of etched phosphors.—The brightness L and electrical loss of the etched phosphors were measured as a function of voltage V. In Fig. 1 the brightness data are shown plotted as log L vs. $V^{-1/2}$ for a constant frequency of 1 kc. Two effects should be noted: (i) after initial etching the brightness is improved at all voltages, and (ii) subsequent stages of etching give increased slopes as would be expected from decreases in particle size (14, 15).

The efficiency, η, of this group changes with extreme etching according to the trend established by Lehmann for efficiency variation with particle size

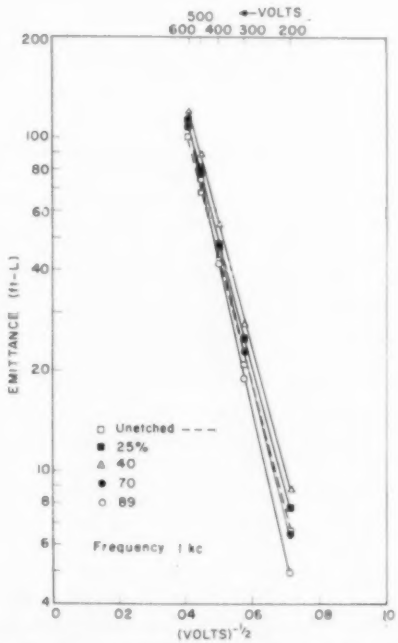

Fig. 1. Log L vs. $V^{-1/2}$ plots at 1 kc for a family of phosphors subjected to various amounts of etching.

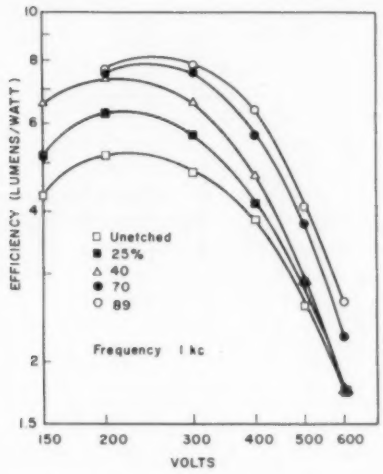

Fig. 2. Log η vs. Log V for phosphors in Fig. 1, frequency is 1 kc.

(14). Figure 2 contains data of log η vs. log V at a constant frequency of 1 kc with the degree of etching as a parameter. The voltage at which maximum efficiency occurs remains fixed for the initial stages of etching. Heavy etching occasions a shift in this voltage which is probably a consequence of smaller particle size. The maximum efficiency depends only slightly on frequency with the optimum range falling near 300 to 400 cps.

The improved brightness and higher efficiency resulting from extensive etching of these phosphors do not appear to be a consequence of the particular phosphor synthesis employed. Thus in addition to the ZnS:Cu, Cl already mentioned, the following phosphors, etched to remove between 60% and 90% of the phosphor mass, all show as high or higher levels of brightness and efficiency as before etching: ZnS:Cu,Cl-Pb (16); ZnS:Cu,Al (4); Zn(S,Se):Cu,Br (17); and ZnS:Cu,Cl-Mn.

Chemical analyses for activator inhomogeneity.—The aim of these chemical analyses was to probe the chemical homogeneity of the phosphor on the assumption that the particle mass was removed uniformly.[1] Table Ia gives results of spectrographic analyses for copper in the remaining solids as a function of degree of etching. The relative particle size is specified in Table I with the diameter of the unetched material designated as unity. The mean diameter of the unetched phosphor is 8.3μ as measured by the gas adsorption (BET) method and 22μ as determined with the Fisher Sub-Sieve Sizer. Table Ib gives similar data for another phosphor of different average copper content. Before analyzing for copper, the powders were washed with 1% potassium cyanide solution to remove any loosely bound Cu_2S which forms by precipitation on exposed surfaces subsequent to destructive etching.

The values in Table Ia show that the samples possess gradients in Cu concentration of less than 5×10^{-6} g at Cu/mole per micron of crystal. This value is determined by the precision of the analyses.

[1] The absence of specific etch geometry in most of the etched phosphors suggests that all surfaces experience about the same degree of dissolution.

Table Ia

Wt. % removed by etching	Fraction of initial size (calculated) [a]	Wt % Cu found (±a.d.)	No. of samples analyzed
0	1.00	0.065 ± 0.002	4
25	0.91	0.066 ± 0.002	3
33[b]	0.87	0.065 ± 0.002	2
70	0.67	0.067 ± 0.003	3
89	0.48	0.069 ± 0.002	4

Table Ib

Wt. % removed by etching	Fraction of initial size (calculated)	Wt % Cu found (±a.d.)	No. of samples analyzed
0	1.00	0.15 ± 0.015	2
50	0.79	0.16 ± 0.015	2
90	0.46	0.15 ± 0.015	2

[a] Calculated from weight loss assuming spherical geometry.
[b] This sample is not included in the measurements shown in Fig. 1 and 2.

The results do not rule out the existence of an inhomogeneous impurity distribution. Significant activator concentration gradients may be too small to be detectible by methods described above. It appears, however, that there is no bulk activator phase residing on the surface of these phosphors which is of critical importance to electroluminescence.

Electron Microscope Studies

Unetched electroluminescent phosphors.—The appearance of the grains is mainly globoid. The surfaces are on the whole mottled by tiny protuberances or crater-like depressions with dimensions of a half micron or less. Terracing, characterizing the original crystal growth, is found in localized regions. Striations are also evident in restricted parts of most grains. The terracing and striations are the only surface features indicating a high degree of crystallinity. Prismatic faces are conspicuously absent. A typical particle is shown in Fig. 3.

Etched electroluminescent phosphors.—Materials at the initial stages of etching show little of the

Fig. 3. Electron micrograph of a representative unetched electroluminescent particle showing a mottled surface.

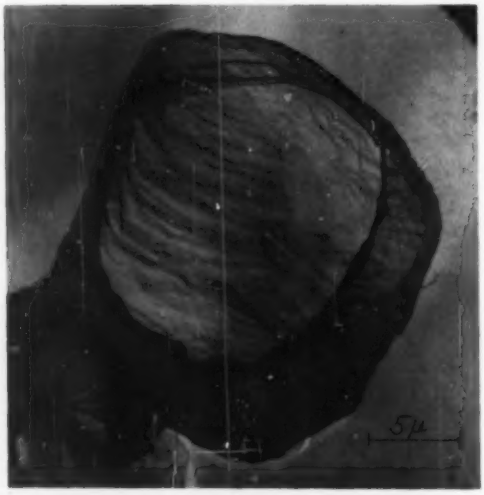

Fig. 4. Electron micrograph of an etched electroluminescent particle, about 40% mass removed. This general appearance is preserved at higher degrees of acid etching.

mottled surface character and are apparently chemically polished. Here the geometry is more characteristic of a crystalline substance. Crystal faces can be discerned in a representative particle shown in Fig. 4. These are disturbed by small bumps, regions of striae, and irregular depressions. Only rarely is an etch pit of regular geometry found. This character persists through all stages of etching. From this information (and the x-ray data) a picture of fragmented crystal order emerges for the electroluminescent particles.

After about 90% of the phosphor mass is removed, the photographs show a distinct reduction in particle size. If a spherical geometry is assumed, a reduction in mass by 90% is equal to a reduction in diameter of about 50% which is on the average the order of the observed decrease in size. Some particle size distribution measurements were made which show that mass removal was achieved by attacking particles of all sizes rather than the fine ones preferentially. Figure 5 shows the histogram of size distribution by volume (or weight) of an unetched phosphor. Figure 6 is the distribution of this phosphor after etching away 80% of the mass. The significant feature is the shift in the apparent mean size from approximately 35-40μ to about 25-30μ showing extensive etching of the larger grains. The electroluminescent properties of these two phosphors are related in the same way as already described in Fig. 1 and 2 for the unetched and the heavily etched phosphors.

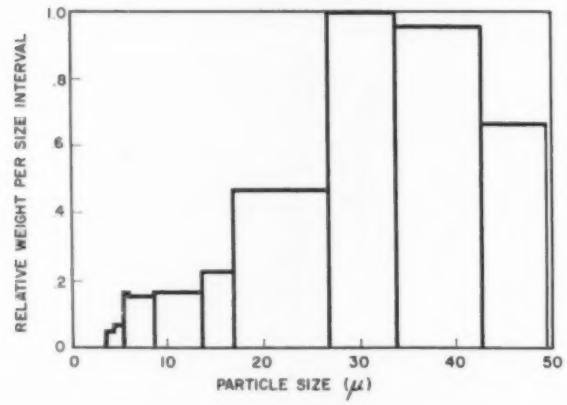

Fig. 5. Distribution of particle size by volume (or weight) of a representative unetched electroluminescent phosphor; measurement range is 3.4-49 μ.

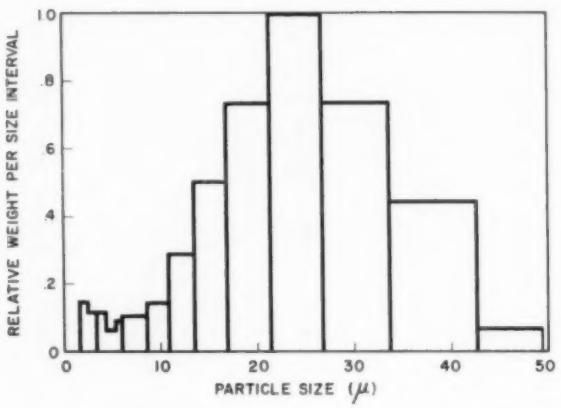

Fig. 6. Distribution of particle size by volume (or weight) of the phosphor shown in Fig. 5 after etching away 80% of the mass; measurement range is 1.7-49 μ.

Nonelectroluminescent phosphor particles of the ZnS:Cu,Cl type show qualitatively about the same degree of structural discontinuity as do their electroluminescent counterparts. There are, however, in these materials none of the striations seen in the electroluminescent phosphors.

Specific etch patterns.—In one specimen an etch geometry of an unusual character was found. The specimen was etched to 93% mass removed.[2] Two representative particles are shown in Fig. 7. The char-

[2] The etching procedure was different here. First 80% of the mass was etched away; the phosphor was dried and etched again with fresh acid.

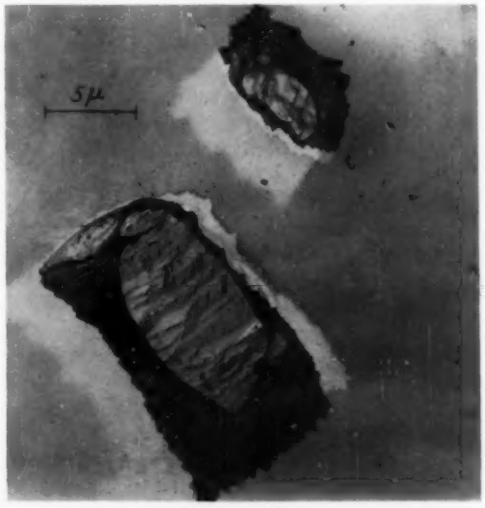

Fig. 7. Uncommon geometry in a highly etched electroluminescent specimen (93% mass removed) showing pyramids on one end. The crystal structure of the powder, of which this particle is representative, is cubic with little or no hexagonal content.

acteristic shape is oblong with one end showing well-defined pyramidal peaks. The peaks fall mainly into two groups whose average angles are 62° 51′ (±1° 40′) and 70° 45′ (±2° 10′), respectively. These particles show cubic structure in the x-ray diffraction pattern with a small hexagonal content and some birefringence. They possess ridges running normal to the direction in which the peaks point. Peaks within one particle are found which point in directions which are out of parallel with others by about 5° of arc. Also, the lateral ridges are, in some particles, out of parallel by as much as 13°. These facts point to structural units whose boundary divides the particle parallel to the direction of the pyramids.

It is possible that the occurrence of peaks only on one side of each particle is a consequence of the absence in the sphalerite lattice of a structural center of symmetry. Recently White and Roth (18) have shown how asymmetric etch patterns in GaAs wafers (sphalerite structure) etched in (111) planes correlate with the noncentrosymmetric structure. We may thus postulate that the peaks in Fig. 7 point in the <111> direction. This contention is supported by x-ray diffraction patterns obtained from individual particles in the etched specimen. Wolff has reported that in ZnS crystals the rates of dissolution by HCl of (111) faces and ($\bar{1}\bar{1}\bar{1}$) faces are different. He suggests that this is a consequence of structural asymmetry along the <111> direction and that the face made up primarily of sulfur atoms is attacked at the greatest rate (19). Thus we postulate that the pyramids in Fig. 7 appear on the "sulfur" face.

The light output from a sampling of fifteen particles from this material was followed visually with a microscope arrangement similar to that of Waymouth and Bitter (20). In all but one case the particles were distinctly more luminous with the elongated axis parallel to the applied field rather than perpendicular.

Crystal structure.—The structure of the family of phosphors which have undergone successive etching is, to a first approximation, uniform throughout the lattice. The dominant form is cubic in most of the electroluminescent materials reported upon here. The nature of the phosphor synthesis is such that the cubic structure may have occurred as a consequence of either low-temperature annealing or of milling the hexagonal form at a stage following crystallization. The diffraction patterns show some subtle qualitative changes at various stages of etching. A small residual hexagonal component existing in the unetched phosphor is reduced in the more heavily etched phosphors. Also, from observations on line breadth in the back reflection region, the highly etched grains are found to have a greater degree of order than the unetched phosphor. Assuming that strong etching exposes the particle cores, the ordering effect may arise from a slower cooling rate in the inner layers after the synthesis. In support of this the interiors are found to have a stronger blue component in the photoluminescence than the unetched parent phosphor. Leverenz states that the shorter wave lengths are favored by slower cooling (21).

Discussion

The results show that the polycrystalline phosphors are nearly homogeneous in chemical, physical, and electroluminescent properties as one passes from the surface and penetrates deeply into the crystallite bulk. One exception to this is the existence of a thin inefficient surface layer much like that found in cathode ray phosphors (22).[3] Following the removal of this layer, the electroluminescent properties vary with the extent of etching in a fashion like that previously described for particle size reduction (14, 15). The results are at odds with the concept that a surface chemical phase is responsible for the potential barrier and thus for the source of electroluminescence excitation, since strong electroluminescence persists following the removal of substantial amounts of surface material. It would appear that the phosphor particle's surface modifies its electroluminescent capability, but does not serve as a site of intrinsic electroluminescent properties. Such modification of a solid's bulk properties by its surface is often encountered in other areas of semiconductor studies.

The most acceptable physical description of electroluminescent particles is one in which regions capable of serving as the location of field intensification are to be found throughout the electroluminescent particle. The location within the particle of the site which finally serves as the active barrier is not certain. The following, however, does appear well founded on the basis of the above experiments: if the site of field intensification exists on or near the particle surface, removal of this surface brings new barrier sites into play with equal capabilities for the generation of electroluminescence. The particular site which serves as a barrier may depend on particle orientation, shape, and contact with other particles. It appears likely as a consequence of arguments based on particle size effects that only one or two barriers are operative in a particle at any one time (15).

The concepts proposed here are in disagreement with Zalm's model (5) of a conducting surface phase. The source of the disagreement lies in the fact that electroluminescence which is produced by impurity activation at high temperatures and that arising from the deposition of conducting phases on nonelectroluminescent phosphors are different in two important ways. First, the field-excited emission from an otherwise nonelectroluminescent phosphor with a copper sulfide surface phase is orders of magnitude below that of products synthesized by conventional methods. Second, conventional electroluminescent phosphors cannot be deactivated by washing with a cyanide solution. Thus, we find that a phosphor which was refluxed with a 50% KCN solution loses little if any of its sensitivity.

The experiments of Larach and Shrader (6) do not offer convincing evidence for a region near the

[3] Kremheller proposes that etching, and therefore roughening, of the surface of some phosphors improves light output owing to decreases in multiple internal reflections (23).

particle surface which is richly interdiffused with copper, as they maintain. They have performed no chemical analyses as a function of penetration into the crystal volume. It would be of interest to know if their phosphors experience the same type of changes described in this report or if the materials lose sensitivity following destructive etching.

Destriau's work on etching of electroluminescent phosphors (7) may, on the basis of this report, be thrown into different perspective. His measurements were of the minimum voltage required for visibility as a function of the extent of etching. The course of his curve shows an initial decrease (sensitivity increase) followed by a monotonic increase (sensitivity decrease). This is the same pattern followed by the data in Fig. 1 in the low voltage region. Initial etching increases sensitivity; heavier etching produces an apparent sensitivity decrease which is more precisely a consequence of particle size change.

One finds subtle effects on penetrating the grains which, in the second approximation, show the grains to be inhomogeneous. These are the bluer photoluminescence and more ordered structure of the internal regions. The relation, if any exists, of these effects to electroluminescence cannot be made on the basis of the above experiments.

Acknowledgments

It is a pleasure to acknowledge many helpful discussions with Drs. D. H. Baird, A. K. Levine, R. N. Summergrad, and Mr. C. F. Tufts. Also thanks are due J. T. Ragusin for aid in phosphor preparation, S. Weisberger for chemical analyses, Mr. Tufts for the electron micrographs and the Crystallography Staff for x-ray work.

Manuscript received Feb. 1, 1960. This paper was prepared for delivery before the Chicago Meeting, May 1-5, 1960.

Any discussion of this paper will appear in a Discussion Section to be published in the December 1960 JOURNAL.

REFERENCES

1. D. Curie, *J. Phys. Rad.*, **13**, 317 (1952).
2. W. W. Piper and F. E. Williams, *Phys. Rev.*, **87**, 151 (1952).
3. G. Destriau and H. F. Ivey, *Proc. IRE*, **43**, 1911 (1955).
4. H. C. Froelich, *This Journal*, **100**, 496 (1953).
5. P. Zalm, *Philips Res. Repts.*, **11**, 353, 417 (1956).
6. S. Larach and R. E. Shrader, *J. Phys. Chem. Solids*, **3**, 159 (1957).
7. G. Destriau, Symp. Brooklyn Polytech. Inst., Brooklyn, N. Y. (Sept. 1955).
8. A. H. McKeag and E. G. Steward, *This Journal*, **104**, 41 (1957).
9. E. E. Loebner, Symp. Brooklyn Polytech. Inst., Brooklyn, N. Y. (Sept. 1955).
10. E. E. Loebner and H. Freund, *Phys. Rev.*, **98**, 1545 (1955).
11. G. Diemer, *Philips Res. Repts.*, **10**, 194 (1955).
12. D. R. Frankl, *Phys. Rev.*, **100**, 1105 (1955); *ibid.*, **3**, 1540 (1958).
13. The particle size measurement is an electrical one in which pulses are counted the heights of which are proportional to particle volume; R. H. Berg, ASTM Special Technical Publication *No. 234*, 245 (1958).
14. W. Lehmann, *This Journal*, **105**, 585 (1958).
15. P. Goldberg, *ibid.*, **106**, 34 (1959).
16. H. H. Homer, R. W. Reulon, and K. H. Butler, *ibid.*, **100**, 566 (1953).
17. I. J. Hegyi, S. Larach, and R. E. Shrader, *ibid.*, **104**, 717 (1957).
18. J. G. White and W. C. Roth, *J. Appl. Phys.*, **30**, 946 (1959).
19. G. A. Wolff, Information presented at the 1959, Fall Meeting of the Electrochemical Society, Columbus, Ohio.
20. J. F. Waymouth and F. Bitter, *Phys. Rev.*, **95**, 941 (1954).
21. H. W. Leverenz, "An Introduction to Luminescence of Solids," p. 217, J. Wiley & Sons, Inc., New York (1950).
22. G. F. J. Garlick, *Handb. der Physik* (Light and Matter II), **26**, 1 (1958).
23. A. Kremheller, *This Journal*, **107**, 8 (1960).

December 1960 Discussion Section

A Discussion Section, covering papers published in the January-June 1960 JOURNALS, is scheduled for publication in the December 1960 issue. Any discussion which did not reach the Editor in time for the June 1960 Discussion Section will be included in the December 1960 issue.

Those who plan to contribute remarks for this Discussion Section should submit their comments or questions in triplicate to the Managing Editor of the JOURNAL, 1860 Broadway, New York 23, N. Y., *not later than September 1, 1960*. All discussion will be forwarded to the author(s) for reply before being printed in the JOURNAL.

Preparation and Properties of AlSb-GaSb Solid Solution Alloys

J. F. Miller, H. L. Goering, and R. C. Himes

Battelle Memorial Institute, Columbus, Ohio

ABSTRACT

Ingots of the quasi-binary GaSb-AlSb alloy were prepared by progressive casting and zone casting at various rates of crystallization. Results of x-ray diffraction studies, metallographic studies, hardness determinations, and chemical analyses indicate that, with the possible exception of a narrow composition range between 10 and 30 mole % AlSb which was not investigated, solid solution prevails in the system. Bulk specimens of single phase, solid solution alloy were obtained by use of low linear rates of crystallization (0.05 in./hr), while at higher rates of crystallization (¼ to 1¼ in./hr) two intermingled solid phases were characteristically obtained.

Vegard's law was found to be at least roughly applicable; with lattice constants for the alloys ranging between values of 6.0963Å for pure GaSb and 6.1361Å for pure AlSb. Optical energy gaps determined for alloy specimens increased regularly with cell size from a value of 0.68 ev for GaSb to a value of 1.74 ev for AlSb. Values of electrical resistivity and hole mobility for the relatively impure alloy specimens were also intermediate between those for the compounds in a like state of purity.

Liquidus data are also presented for the system.

In recent years, there has been considerable interest in systems composed of two intermetallic compounds of the A^{III} B^{V} type (e.g., GaSb-InSb, InAs-InSb, etc.). This interest arises because of the possibility of obtaining semiconducting materials, the properties of which can be varied over a continuous range of values. Since regular variation of the structure-sensitive properties with composition can be expected only for those systems or composition ranges in which solid solution occurs, the majority of previous investigations (1-8) in this area have been concerned chiefly with the existence of such ranges in the various systems.

In a number of instances, however, apparently conflicting results have been reported. In the case of the system GaSb-InSb, for example, Koster and Thoma (1) report a degenerate eutectic diagram with no appreciable terminal solid solution, while Kolm, Kulin, and Averbach (2) report approximately 10% solid solution at each end of the diagram. On the other hand, results reported by Goryunova and Fedorova (3), Woolley, Smith, and Lees (4), Woolley and Smith (5) indicate that a complete range of solid solution exists in this system. Similarly conflicting conclusions have been reached regarding the systems InAs-InSb (3, 5, 6), AlSb-InSb (1, 5), and AlSb-GaSb (1, 5). Woolley and Smith (5) suggest that the discrepancies exist because, in some instances, the samples were in a metastable state. Results of those investigations for which adequate information is given regarding thermal history of the materials (e.g., cooling rate during crystallization, or time and temperature used for heat treatment) appear to be consistent with this observation. Satisfactory evaluation of all previous work is not possible, however, since in some cases no details are given concerning heat treatment of specimens. Firm conclusions regarding the precise nature of these systems therefore must be based to a large extent on the results of additional investigations.

This investigation was concerned with temperature-composition relationships for the system AlSb-GaSb and with pertinent physical properties of the alloys obtained. The study is incomplete in the sense that full characterization of the system and full development of certain of the analytical and preparative techniques have not yet been realized. Data presented do, however, furnish much new or confirmatory evidence regarding the nature of this particular system, and it is believed that certain of the techniques which are discussed may be applicable to other alloy systems of this type.

Experimental Procedures

All samples studied were prepared by direct reaction at elevated temperatures, of proper proportions of highly purified elements[1] sealed in quartz or Vycor under an atmosphere of pure argon. Atmospheres of hydrogen, used in some early experiments to suppress oxidation, were not considered to be satisfactory. Numerous small voids, which apparently were formed by precipitation of the gas from solution on freezing, were always present in alloy specimens solidified under hydrogen. In work with compositions other than pure GaSb, temperature of each sample was initially held in the range 1060°-1080°C (just above the melting point of AlSb) for a period of one-quarter hour to react the elements and homogenize the melt before proceeding with the experiment. Since the glasses (quartz, Vycor, etc.) are attacked rapidly by molten samples containing Al or AlSb, internal crucibles or boats of pure graphite[2] were used for such compositions.

[1] Gallium, 99.995 + %; aluminum, 99.992 + %; antimony, 99.996 + %.

[2] National Carbon Co., AUC grade.

Differential thermal analysis was employed in making the phase-diagram study. Samples were contained in graphite cells which had a graphite thermocouple well extending into the center of the sample chamber. Graphite was used as a reference material. Both temperatures and temperature differential were recorded continuously by means of a dual-unit Brown Electronik Potentiometer-Recorder. At cooling rates of 3°C/min, well-defined thermal arrest points were obtained. Thermometry of the apparatus was calibrated by measuring the freezing points of high-purity lead, antimony, and germanium. The measured freezing point of GaSb, 702°C, which is in good agreement with values of 703°C and 706°C reported by others (1, 6), served as a check on the calibration.

Alloy ingots were prepared by two techniques: progressive casting and zone casting. Progressive casting, in which crystallization is caused to progress at a controlled rate along an initially wholly molten ingot, maintained in a horizontal position, was used for exploratory purpose. [This method of crystallization has been termed normal freezing by Pfann (10).] Because of the variation of composition with distance along a progressively cast ingot (except at an invariant point or in the case of an ideal solution), a number of specimens having different compositions usually can be obtained from a single ingot.

Relatively large specimens of uniform composition are, however, required for certain physical studies (e.g., solidus determinations, chemical analyses, etc.). Zone casting, which is essentially single-pass zone melting, was investigated as a potential means of obtaining such specimens. Theoretically, for a system or composition range in which the components form solid solutions, this method of casting should yield ingots which are of uniform composition over a considerable portion of their length. If a macroscopically homogeneous charge is used, composition of the recrystallized ingot should change appreciably in only the first several and the final zone lengths. When material of a given composition (representing some point on the solidus of the system) is used as the main charge, and material of the corresponding liquidus composition is used as a charge in the first zone length, then composition of the recrystallized ingot should vary only in the final zone length. Solid charges consisting of either air-quenched ingots or thoroughly blended lots of the alloy material in powder form were recrystallized in this way. Induction heating was employed for all casting experiments, and the rate of movement of the ingot through the induction coil was considered to be rate of crystallization. Molten zone-length to ingot-length ratios of 0.2 to 0.25 were used for the zone casting. Alloy ingots were cast progressively under a number of conditions, and specimens from selected locations in these ingots were examined by use of x-ray diffraction, metallographic techniques, and hardness tests.

In preparing specimens for metallographic examination, a staining etch of 10 g $FeCl_3$, 1000 ml H_2O, and 100 ml concentrated HCl was used. In Knoop hardness determinations, 100 and 500 g indenter loads were used. Except for Sample PC-1-4, which spanned a range of progressions, all samples taken for x-ray, optical, electrical, and chemical analyses were from thin slab-like sections which were cut along planes normal to the longitudinal axes of the ingots so as to minimize the effect of variations in composition.

X-ray diffraction studies were made on powder samples prepared by grinding the bulk specimens under anhydrous benzene. The diffraction patterns were obtained by use of Ni K radiation and a 114.6 mm diameter Debye-Scherrer camera. In determining precision lattice constants, results were corrected for film shrinkage and other errors (11) by extrapolating the plots of apparent lattice parameters against the function $\frac{1}{2}[(\cos^2\theta/\theta) + (\cos^2\theta/\sin\theta)]$, where θ is the Bragg angle.

Infrared transmission spectra were obtained at room temperature for polished platelets of the compounds and alloys ranging in thickness from 0.003 to 0.010 in. The Beckman D U, Beckman Model IR-2, and Perkin-Elmer Model 21 spectrometers were used for the wave-length ranges, 0.4 to 1.5, 0.65 to 2.0, and 2.0 to 15 μ, respectively, as was required. In determining optical energy gap, cutoff wave length was taken as that wave-length at which value of the Beer-Lambert absorption coefficient reached a value of 200 cm^{-1}. Use of this convention has yielded values for a number of other semiconducting compounds (12) which are generally in good agreement with other published values (e.g., room temperature values of 0.16 ev for pure InSb, 0.35 ev for InAs, 1.32 ev for InP, and 1.39 ev for GaAs).

In making the electrical measurements, both antimony films and solder contacts were used to eliminate the very high contact resistance exhibited by the alloys, especially by those rich in AlSb. The antimony films were formed *in situ* by use of hot concentrated KOH as a reducing agent. Tungsten probes then were held in contact with the films by spring tension. The solder contacts, made with Sn-Pb solder and aluminum solder flux, appeared to be more reliable for low temperature measurements. All Hall data were taken at a field strength of 5000 gauss.

For chemical analyses, the samples were dissolved in alkali. The total amount of antimony present was determined by titration with potassium bromate. Aluminum and gallium were converted to the mixed oxides and the total amount present was determined gravimetrically. The fraction of each present in the mixture was calculated then by the classical method.

Experimental Results and Discussion

Physical properties of GaSb *and* AlSb.—As a first step toward characterization of the system, pertinent physical properties of the compounds GaSb and AlSb were measured. The values obtained, which are summarized in Table I, were determined for specimens prepared from high-purity elements as has been described. Purity of the specimens studied, as deduced from electrical measurements, was about 2×10^{17} impurity atoms/cm^3.

The lattice constants, 6.0963Å for GaSb and 6.1361Å for AlSb, are roughly equal in magnitude to those reported by Blunt, *et al.* (13, 14), but are

Table I. Physical constants of GaSb and AlSb

	Melting point, °C	Lattice constant (a_0), Å	Optical energy gap (ΔE at 300°K), ev	Knoop hardness
GaSb	702	6.0963 ± 0.0003	0.68	309
AlSb	1050 (25)	6.1361 ± 0.0003	1.74	304

reversed in order of assignment, i.e., Blunt assigns the larger value to GaSb. The cell size for GaSb is slightly higher than that obtained by Kolm, *et al.* (2). However, values reported here, which represent the results of a number of determinations, are in good agreement with other reported values (5, 15), are consistent with expected interatomic distances for these compounds calculated according to Pauling (16), and are consistent with the cell size-composition relationship observed in our studies of the alloys.

The optical energy gap for GaSb, 0.68 ev, agrees reasonably well with other published values (17-20), which all fall in the narrow range between 0.67 and 0.71 ev. On the other hand, published values for the optically determined band-gap width of AlSb at 300°K (18, 20-22) range from 1.52 to 1.7 ev, while that obtained in this work is 1.74 ev. Some disagreement is to be expected because of the different methods used to select the cutoff wave length, but the wide divergence of reported values indicates that other factors such as sample purity and surface condition probably are involved also. For example, AlSb is slowly attacked by atmospheric water vapor. As is indicated in Fig. 1, presence of the products of this reaction on the surface of the specimen drastically alters the spectrum, and may be responsible for some of the low gap values reported.

The difference between Knoop hardness values, 309 for GaSb and 304 for AlSb, is insignificant. However, for systems in which the components form solid solutions, hardness passes through a maximum at some intermediate composition because of the effects of lattice distortion (23, 24). It is possible, therefore, to use hardness measurements as an analytical tool.

Temperature-composition data. — Differential thermal analysis of selected alloy compositions

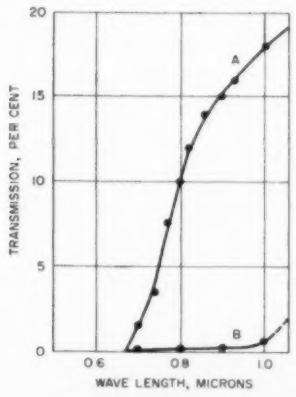

Fig. 1. Transmission for Specimen of AlSb. A, Protected from atmosphere; B, after 20-hr exposure to atmosphere.

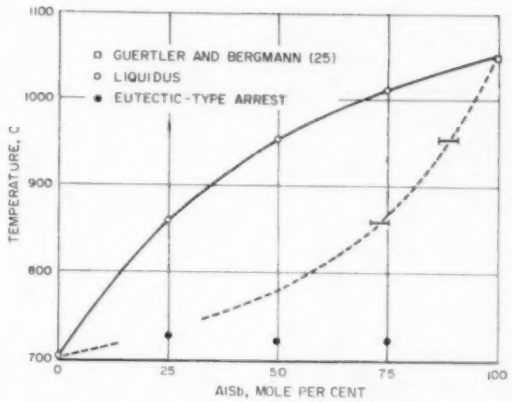

Fig. 2. Thermal data for GaSb-AlSb system

yielded accurately reproducible data on the liquidus of the system. These data are plotted in Fig. 2. Cooling curves were obtained for four compositions, at 0, 25, 50, and 75 mole % AlSb. Each liquidus point plotted represents the average of three determinations for which precision and accuracy were within the range indicated by the circle about the point. The AlSb point is that of Guertler and Bergmann (25). In each of the alloy samples, freezing took place over a wide temperature range, and near the end of freezing a "eutectic-type" arrest was noted which consistently occurred slightly above the freezing point of GaSb. The shaded circles on the plot show these latter halts.

The data are consistent with those to be expected for a system with a miscibility gap in the solid, but could also result from nonequilibrium conditions. Stohr and Klemm (26), for example, initially obtained similar data for the Si-Ge system but were able, after annealing samples for extremely long periods at temperatures slightly below the expected solidus, to demonstrate the existence of an uninterrupted range of solid solutions in that system.

Since sizeable, homogeneous alloy specimens were not available, solidus studies were not undertaken on the AlSb-GaSb system. Results of other types of studies to be discussed, however, show that wide ranges of solid solution exist in this system also and, further, strongly suggest that complete solid solution can be obtained as has been reported (27). Location of the dotted solidus curve was approximated from the results of x-ray diffraction studies (Table II) on recrystallized alloy ingots, PC-1, PC-2, ZC-1, ZC-2. As is indicated in the Fig. 2, these results suggest that if a miscibility gap exists, it is restricted to a relatively narrow composition range between about 10 and 30 mole % AlSb.

Casting.—Data for Ingot PC-1, which was progressively cast from a melt containing 75 mole % GaSb at a rate of ¼ in./hr, are typical of results obtained for ingots cast at relatively high linear crystallization rates (i.e., ¼ to 1¼ in./hr). Results of the x-ray analysis (Table II) show that two crystalline phases were present in the ingot. The minor[3] phase was very similar to pure GaSb and

[3] Major and minor are arbitrary designations used to show qualitatively the extent to which each exists.

Table II. X-ray analysis of cast ingots

Sample	Progression, %*	Phase†	Lattice constant, a_o, Å	Mole % AlSb (by Vegard's law)
Progressively cast, ¼ in./hr; melt 75 mole % GaSb, 25 mole % AlSb				
PC-1-1	5	Major	6.1260 ± 0.0005	75
		Minor	6.0970 ± 0.0005	
PC-1-2	16	Major	6.1250 ± 0.0005	72
		Minor	6.0966 ± 0.0005	
PC-1-3	29	Major	6.1201 ± 0.0003	60
		Minor	6.0965 ± 0.0005	
PC-1-4	32-42	(Annealed)	6.114 ± 0.001	45
PC-1-5	55	Major	6.1077 ± 0.0003	29
		Minor	6.0962 ± 0.0005	
PC-1-6	76	(Single)	0.0963 ± 0.0003	
Progressively cast, 0.05 in./hr; melt 50 mole % GaSb, 50 mole % AlSb				
PC-2-1	20		6.1327 ± 0.0003	92
Zone cast, 0.05 in./hr; charge 50 mole % GaSb, 50 mole % AlSb				
ZC-1-1	8		6.1310 ± 0.0003	87
ZC-1-2	17		6.1288 ± 0.0003	82
ZC-1-3	47		6.1266 ± 0.0003	76
ZC-1-4	64		6.1176 ± 0.0005	54
Zone cast, 0.05 in./hr; first zone 75 mole % GaSb, 25 mole % AlSb; remainder of charge 50 mole % GaSb, 50 mole % AlSb				
ZC-2-1	9		6.1237 ± 0.0003	69
ZC-2-2	33		6.1200 ± 0.0006	60
ZC-2-3	54		6.1201 ± 0.0003	60
ZC-2-4	74		6.1007 ± 0.0006	11

* Fraction of the ingot crystallized in advance of sample location.
† Major and minor are arbitrary designations.

persisted throughout the ingot.[4] The major phase appeared to be a concentrated solid solution of the two compounds, the composition of which varied in a regular manner with progression along the ingot (Fig. 3a). Lattice parameters indicate that near the head (first to freeze) of the ingot this phase contained high concentrations of AlSb, and that the concentration of AlSb present in this solid phase decreased with progression of the solid-liquid interface along the ingot as concentration of AlSb in the melt was lowered. Beyond a point between 55 and 76% progression, where the supply of AlSb in the melt apparently was exhausted, this phase was no longer precipitated. Lattice parameters for this major phase correspond to those for solid solutions containing 75 to 29 mole % AlSb, as calculated by Vegard's law.[5]

While the polyphase nature of the AlSb-rich portion of the ingot suggests a broad miscibility gap, results of a single annealing experiment, which was carried out with a specimen from this progressively cast ingot, indicate that the polyphase material does not represent an equilibrium precipitate. Sample PC-1-4 was ground to a fine powder and was annealed for 96 hr at 650°C in an evacuated ampoule prior to examination. This anneal treatment appeared to have homogenized the polyphase material, converting it to a single-phase powder with a somewhat diffuse x-ray pattern.

Results of metallographic studies agreed with those of the x-ray analysis. In the first portions of

[4] Due to the slow evolution of antimony from the melt during recrystallization, the last portions of the ingots to be frozen were metallic (gallium) and therefore were not analyzed.

[5] Vegard's law has been found to hold for the systems, GaSb-InSb, GaAs-InAs, and InAs-InP [see ref. (6) and (9)] and has been shown at least roughly applicable in this research (see Table IV).

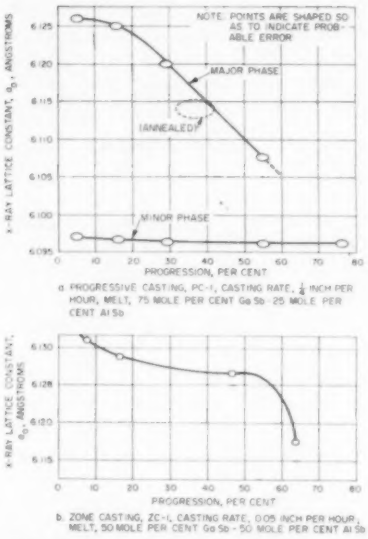
NOTE: POINTS ARE SHAPED SO AS TO INDICATE PROBABLE ERROR
MAJOR PHASE
(ANNEALED)
MINOR PHASE
X-RAY LATTICE CONSTANT, a_o, ANGSTROMS
PROGRESSION, PER CENT
a. PROGRESSIVE CASTING, PC-1, CASTING RATE, ¼ INCH PER HOUR, MELT, 75 MOLE PER CENT GaSb-25 MOLE PER CENT AlSb
b. ZONE CASTING, ZC-1, CASTING RATE, 0.05 INCH PER HOUR; MELT, 50 MOLE PER CENT GaSb-50 MOLE PER CENT AlSb

Fig. 3. Cell size as a function of progression along cast ingots.

ingots cast at relatively high linear crystallization rates (≦¼ in./hr) two distinct phases were present, while only a single GaSb-rich phase was present in the last portions. Knoop hardness values were determined for the two phases by carefully placing the indenter on selected crystallites. Values for the minor phase were consistently low, averaging about 310, which is close to the KHN for pure GaSb. Values for the major phase, however, were significantly higher, ranging up to 348, as would be expected for concentrated solid solutions.

It was possible, by use of a very low rate of crystallization, to prepare single-phase ingots of the solid-solution alloy. This is shown by the results of x-ray diffraction analyses (Table II) of samples from the ingots which were cast at a rate of 0.05 in./hr. Lattice parameters for the single-phase solid solutions thus obtained indicate that concentrations of AlSb present in the solutions ranged from 11 to 92 mole %, assuming Vegard's law to apply throughout the range. Results of metallographic studies also

[6] Note the precipitous drop in cell size between progressions 54 and 74 [illegible] ZC-2. Further note that in these ingots, no cell sizes corresponding to AlSb contents between 11 and 29 mole % have been observed. If, as these results suggest, a miscibility gap exists, Vegard's law should not be expected to hold near the solubility limit.

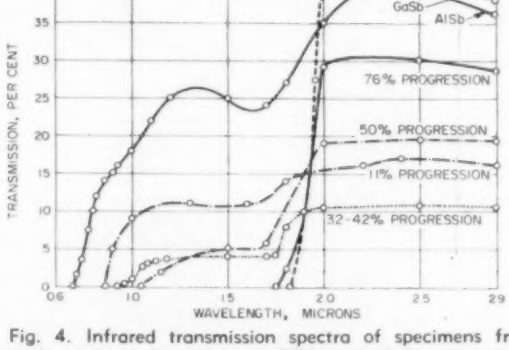

Fig. 4. Infrared transmission spectra of specimens from typical progressively cast ingot PC-1 and of the compounds GaSb and AlSb. Ingot PC-1: Casting rate, ¼ in./ hr; melt, 75 mole % GaSb-25 mole % AlSb.

indicated that these ingots were single phase, solid-solution alloys. Knoop hardness, determined at random locations on a section from the center of Ingot PC-2, progressively cast from a melt containing 50 mole % GaSb was 335 ±7.

The plot of lattice constant vs. progression for Ingot ZC-1 (Fig. 3b), which was prepared by zone casting a charge containing 50 mole % GaSb, follows the relationship expected for a system, or range of compositions, in which the components form solid solutions. Extent of the nearly flat portion of the curve indicates that this technique offers promise as a method for producing sizeable homogeneous specimens of the alloy.

Ingot ZC-2 was formed by zone casting a charge made up of two alloy compositions (an alloy containing 75 mole % GaSb in the first zone length, and an alloy containing 50 mole % GaSb in the remaining length) in an attempt to produce an ingot of more uniform composition. Variation of lattice constants, however, indicates that the estimated location of the solidus, which was used to select the compositions and was based on knowledge of the system at that time, was in error. Composition varied near the head of the ingot, but was again nearly constant over a considerable range of progression in the central regions.

Optical data.—Infrared transmission spectra of specimens from the polyphase Ingot PC-1 are shown in Fig. 4 along with those of the compounds GaSb and AlSb. Energy gap values, summarized in Table III, were computed from these spectra according to the convention described above, which yields gap values generally consistent with other physical parameters for the respective specimens. The spectrum of the specimen taken at 76% progression is seen to be nearly identical with that of GaSb, and shows an absorption edge which corresponds to an energy gap of 0.69 ev. Reading from short to long wave lengths, spectra of the other three specimens each shows a sharp rise in transmission followed by a plateau which is in turn followed by a second sharp rise to peak transmission and then gradual decline to the long wave tail. This is the type of spectrum one might expect for a specimen composed of individual crystallites of two different phases with unequal energy gaps, providing that the crystallites were so disposed that those of one phase do not interfere with transmission through those of the second. (Such disposition of crystallites is quite probable in the polyphase specimens studied.) If such were the case, the threshold of transmission should correspond to that of the second phase.

Applying this interpretation, and normalizing to equal peak transmission for the two phases, energy gaps calculated for specimens at 11, 32, and 50% progression are 1.43 and 0.72 ev, 1.28 and 0.70 ev, and 1.12 and 0.70 ev, respectively. Note that the smaller gap in each case is very nearly equal to that measured for GaSb, as are x-ray lattice constants for the minor phase in each of the specimens from this ingot. It is also possible that manifestation of the absorption band attributed to spin orbit splitting (28), which is present in the spectra of p-type AlSb (and which can also be seen in the spectra of AlSb and of the single phase samples presented here), is responsible for the behavior observed in the vicinity of 1.7μ. However, the plateau and second rise in transmission are very sharply defined, particularly for the samples at 32-42 and 50% progression, whereas gradual changes are characteristic of the absorption due to the spin orbit splitting.

Table III. Optical data for cast ingot*

Sample	Progression along ingot, %	Mole % AlSb (by Vegard's law)	Absorption edge, mμ	Energy gap, electron-volts
PC-1-1a	11	—	865	1.43
PC-1-4	32-42	45	965	1.28
PC-1-4a	50	—	1110	1.12
PC-1-6	76	1	1790	0.69
PC-2-1	20	92	758	1.63
ZC-1-1	9	87	800	1.55
ZC-1-2	16	82	815	1.52
ZC-1-3	31	—	830	1.49
ZC-1-4	53	—	842	1.47
ZC-2-1	9	69	845	1.46
ZC-2-2	33	60	865	1.43
ZC-2-3	54	60	900	1.38
ZC-2-4	74	11	1670	0.74

*Ingot	Casting rate	Charge (mole %)
PC-1	0.25 in./hr	75 GaSb—25 AlSb
PC-2	0.05 in./hr	50 GaSb—50 AlSb
ZC-1	0.05 in./hr	50 GaSb—50 AlSb
ZC-2	0.05 in./hr	75 GaSb—25 AlSb in first zone 50 GaSb—50 AlSb, remainder

Regardless of the phenomena responsible for the 1.7μ absorption, there is little doubt that the spectra show, by the different wave lengths for threshold transmission for the various specimens, the presence of materials with various energy gaps, which decrease from about 1.4 to 0.7 ev with progression along the ingot. It seems clear that these are the energy gaps of solid solutions that increase in GaSb content with progression along the ingot.

Spectra for single phase specimens from the zone cast ingots (Fig. 5 and 6) show well-defined absorption edges, the locations of which indicate that energy gaps for these single phase alloys ranged from 1.55 to 0.74 ev. The relatively small changes in energy gap over rather wide ranges of progression for the zone-cast ingots (Fig. 7), again indicate that this technique offers promise as a method for producing single-phase alloy of uniform composition.

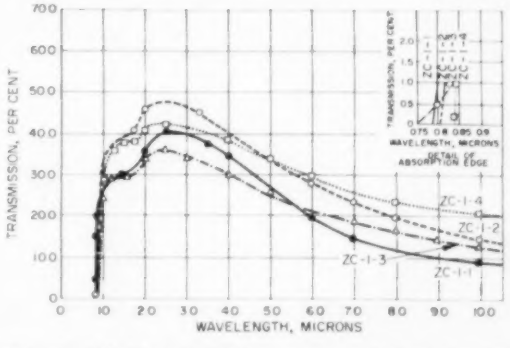

Fig. 5. Infrared-transmission spectra of specimens from zone-cast ingot ZC-1. Casting rate, 0.05 in./hr; charge, 50 mole % GaSb-50 mole % AlSb.

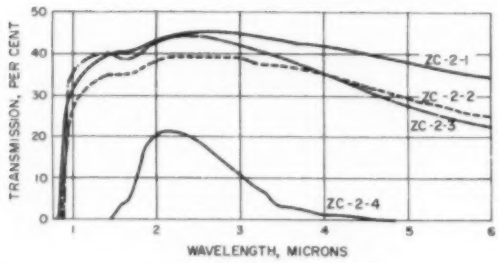

Fig. 6. Infrared transmission spectra of specimens from zone-cast ingot, ZC2. Casting rate, 0.05 in./hr; charge in first zone, 75 mole % GaSb-25 mole % AlSb; remainder of charge, 50 mole % GaSb-50 mole % AlSb.

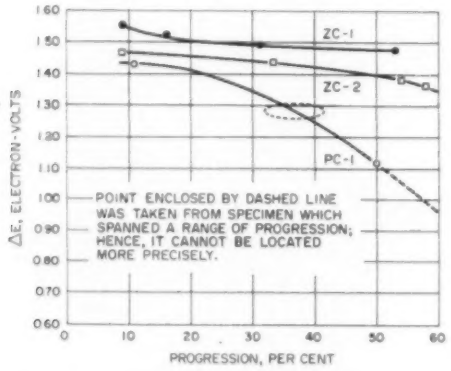
ΔE, ELECTRON-VOLTS
PROGRESSION, PER CENT
ZC-1
ZC-2
PC-1
POINT ENCLOSED BY DASHED LINE WAS TAKEN FROM SPECIMEN WHICH SPANNED A RANGE OF PROGRESSION; HENCE, IT CANNOT BE LOCATED MORE PRECISELY.

Fig. 7. Optical energy gap vs. progression for cast ingots. ZC-1: Zone cast at 0.05 in./hr; charge, 50 mole % GaSb-50 mole % AlSb. ZC-2: Zone cast at 0.05 in./hr; charge, 75 mole % GaSb-25 mole % AlSb in first zone, 50 mole % GaSb-50 mole % AlSb in remainder. PC-1: Progressively cast at ¼ in./hr; charge, 75 mole % GaSb-25 mole % AlSb.

Electrical data.—Electrical measurements have been made both at room temperature and over a range of temperatures for a number of the alloy specimens, but to date, these studies have not progressed far enough to permit the drawing of accurate conclusions. Data for single-phase specimens from Ingot ZC-2, which are presented in Table IV, show a regular variation of resistivity with composition. Figures 8 and 9 show variation of resistivity, Hall coefficient, and mobility as a function of temperature for Sample ZC-2-2. The curves appear to be typical of those generally obtained in the extrinsic region for an impure, high energy gap semiconductor. Mobility for the alloy (Fig. 9) appears to exhibit an approximate $T^{-3/2}$ temperature dependence above 700°K, suggesting that lattice scattering predominates here.

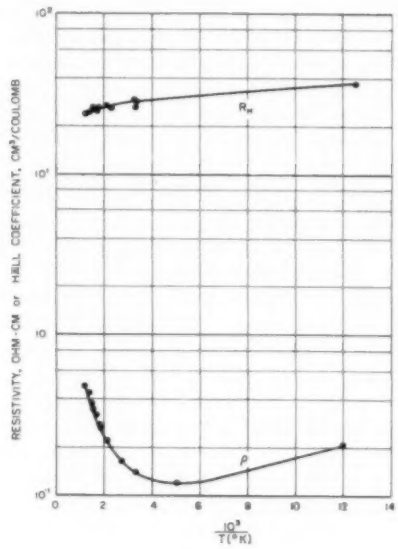

Fig. 8. Hall coefficient and resistivity vs. temperature for single-phase GaSb-AlSb alloy specimen ZC-2-2 (40 mole % GaSb-60 mole % AlSb by Vegard's law).

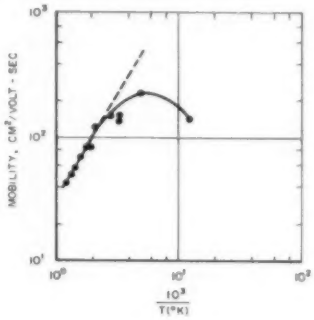

Fig. 9. Mobility as a function of reciprocal temperature for single-phase GaSb-AlSb alloy (40 mole % GaSb-60 mole % AlSb by Vegard's law).

Correlation of Data

More comprehensive analysis was made of material present in zone cast Ingot ZC-2 than of any other material treated in this study. Results of chemical, x-ray, optical, and electrical analyses for four single-phase specimens from this ingot have been summarized in Table IV. The chemical anal-

Table IV. Analysis of zone cast ingot, ZC2*

Sample	Progression along ingot, %	Chemical	X-ray		Optical	Electrical			
		Mole %, GaSb	Lattice constant, a_o (Å)	Mole % GaSb (by Vegard's law)	Energy gap, ΔE (ev)	Hall coefficient, R_H (cm^3/coulomb)	Resistivity, ρ (ohm-cm)	Mobility, μ (cm^2/volt-sec)	Density of carriers, n_p (cm^{-3})
ZC2-1	9	26 ± 4	6.1237 ± 0.0003	31 ± 1	1.46	+58	0.22	264	1.3×10^{17}
ZC2-2	33	38 ± 2	6.1200 ± 0.0006	40 ± 2	1.43	+29	0.11	264	2.6×10^{17}
ZC2-3	54	45 ± 3	6.1201 ± 0.0003	40 ± 1	1.38	+20	0.075	264	3.7×10^{17}
ZC2-4	75	96 ± 3	6.1007 ± 0.0006	89 ± 2	0.74	+5	0.014	357	1.5×10^{18}

* Casting rate, 0.05 in./hr; charge, 75 mole % GaSb—25 mole % AlSb in first zone, 50 mole % GaSb—50 mole % AlSb in remainder.

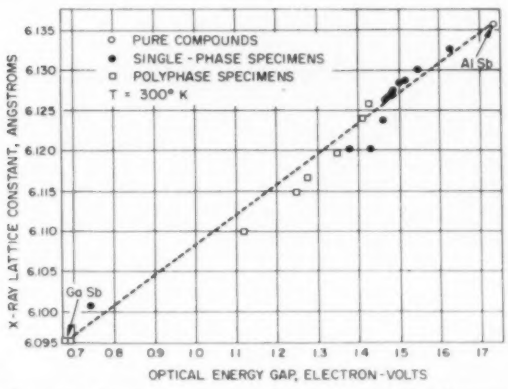

Fig. 10. Energy gap vs. cell size for solid solutions of GaSb-AlSb.

yses were run on very small samples and therefore must be assigned rather wide error limits. Nevertheless, the results constitute direct evidence that concentrated solid solution alloy was obtained. Compositions determined by chemical and x-ray analyses agree reasonably well, differing by only about 2 mole % (beyond stated limits of error) at maximum, thus confirming the applicability of Vegard's law in this system, at least for rough composition determination. The increase in carrier concentration with progression along the ingot probably results from the segregation of an impurity (or impurities) during recrystallization, but could also rise from loss of antimony.

Figures 3 and 7 show variation in lattice constant and energy gap with progression along typical ingots. These two sets of data were combined by eliminating the common variable, percentage progression, where this could accurately be done (i.e., where both parameters had been determined for a single specimen, or in regions of regular variation for the parameters). The combined data have been plotted in Fig. 10. Although there is some scattering of the points, an approximately linear relationship between energy gap and cell size is indicated.

Summary

Ingots of GaSb-AlSb alloy were crystallized from melts (cast) under various conditions. Results of x-ray and metallographic studies, hardness tests, optical transmission studies, and chemical analyses of alloy specimens indicate that:

1. Solid solution prevails in the system, with possible exception of a narrow composition range between 10 and 30 mole % AlSb, which was not investigated.

2. Bulk specimens of single phase, solid solution alloy can be prepared by use of low linear rates of crystallization (0.05 in./hr).

3. At higher linear rates of crystallization (¼ to 1¼ in./hr), two intermingled solid phases are characteristically obtained.

4. The zone casting technique offers promise as a method for producing single phase alloy of uniform composition.

5. An approximately linear relationship exists between lattice parameter and composition of the single phase GaSb-AlSb alloys.

6. An approximately linear relationship exists between lattice parameter and energy gap of the single phase GaSb-AlSb alloys.

Acknowledgment

This work was supported by Union Switch and Signal, Division of Westinghouse Air Brake Company. The authors are also indebted to A. E. Austin for the x-ray work, R. D. Bucheit, who made the metallographic studies, C. D. Smith and R. W. Koch for assistance with optical studies, and J. W. Moody, who made the electrical measurements.

Manuscript received Aug. 11, 1959. This paper was prepared for presentation at the Chicago Meeting, May 1-5, 1960.

Any discussion of this paper will appear in a Discussion Section to be published in the December 1960 JOURNAL.

REFERENCES

1. W. Koster and B. Thoma, *Z. Metallkunde*, **46**, 293 (1955).
2. C. Kolm, S. A. Kulin, and B. L. Averbach, *Phys. Rev.*, **108**, 965 (1957).
3. N. A. Goryunova and N. N. Fedorova, *J. Tech. Phys. (U.S.S.R.)*, **24**, 1339 (1955).
4. J. C. Woolley, B. A. Smith, and D. G. Lees, *Proc. Phys. Soc. (London)*, **B69**, 1339 (1956).
5. J. C. Woolley and B. A. Smith, *ibid.*, **72**, 214 (1958).
6. I. G. Greenfield and R. L. Smith, *Trans. Am. Inst. Mining Met. Engrs.*, **203**, 351 (1955).
7. C. Shih and E. A. Peretti, *J. Am. Chem. Soc.*, **74**, 608 (1953).
8. J. S. Blakemore, *Can. J. Phys.*, **35**, 91 (1957).
9. O. G. Folberth, *Z. Naturforsch.*, **10a**, 502 (1955).
10. W. G. Pfann, *J. Metals*, **4**, 747 (1952).
11. J. B. Nelson and D. P. Riley, *Proc. Phys. Soc. (London)*, **57**, 160 (1945).
12. R. W. Koch, J. F. Miller, and H. L. Goering, "Band Separations of a Number of Semiconducting Compounds From Optical Data," paper presented before The Electrochemical Society, May 5, 1954.
13. R. F. Blunt, W. R. Hosler, and H. P. R. Frederikse, *Phys. Rev.*, **96**, 576 (1954).
14. R. F. Blunt, H. P. R. Frederikse, J. H. Becker, and W. R. Hosler, *ibid.*, **96**, 578 (1954).
15. R. K. Willardson, A. C. Beer, and A. E. Middleton, *This Journal*, **101**, 354 (1954).
16. L. Pauling, *J. Am. Chem. Soc.*, **69**, 542 (1947).
17. H. Leifer and W. Dunlap, *Phys. Rev.*, **95**, 51 (1954).
18. R. G. Breckenridge, R. F. Blunt, W. R. Hosler, H. P. R. Frederikse, J. H. Becker, and W. Oshinsky, *Physica*, **20**, 1073 (1954).
19. V. Roberts and J. E. Quarrington, *J. Electronics*, **1**, 152 (1955).
20. F. Oswald and R. Schade, *Z. Naturforsch.*, **9a**, 611 (1954).
21. H. J. Hrostowski and M. Tannenbaum, *Physica*, **20**, 1065 (1954).
22. R. F. Blunt, H. P. R. Frederikse, and J. H. Becker, *Phys. Rev.*, **94**, 1431 (1954).
23. J. H. Frye and W. Hume-Rothery, *Proc. Roy. Soc.*, **A181**, 1 (1942).
24. J. H. Frye and J. W. Camm, *Trans. Am. Inst. Mining Met. Engrs.*, **152**, 75:83 (1943).
25. W. Guertler and A. Bergmann, *Z. Metallkunde*, **25**, 81 (1933).
26. H. Stohr and W. Klemm, *Z. anorg. u. allgem. Chem.*, **241**, 314 (1939).
27. U. S. Pat. No. 2,710,253, R. K. Willardson, H. L. Goering, and A. E. Middleton to Battelle Development Corporation.
28. R. Braunstein, "Intervalence Band Transitions in GaAs," paper presented before International Conference on Semiconductors, August 18, 1958, Rochester, New York. See also R. Braunstein, *Phys. Rev.*, **111**, 480 (1958).

The Diffused Shot-melting Technique for Making Germanium and Silicon p-n Junction Devices

I. A. Lesk

Semiconductor Products Department, General Electric Company, Syracuse, New York

ABSTRACT

The diffused shot-melting technique involves the melting and resolidifying of a piece (conveniently obtained in the form of shot) of semiconductor on a wafer of the same material (having essentially the same melting point) to form a single crystal boundary region, and the subsequent diffusion of impurities across the interface. Shot-melting may be done so quickly that the interface coincides with the original surface of the wafer. Impurity contents of the shot and wafer may be chosen so that a variety of p-n junction devices results after diffusion, and several junctions may be made on the same wafer by this process to form more complex structures. Although lifetime and resistivity changes generally occur, they can often be minimized by subsequent treatment such as alloy gettering or annealing. Simplicity and flexibility of diffused shot-melting have made it a convenient laboratory technique for making many semiconductor devices.

It is often necessary in the study and design of solid state structures to make a fairly large number of devices having different impurity concentrations and geometries in order to test theories and ideas as they are generated. For greatest versatility, the processes used should be simple and flexible. Although many excellent device fabrication techniques already exist and are used in manufacturing, development, and research, diffused shot-melting has some unique advantages that make its application particularly inviting in some cases.

Shot Melting

The shot melting technique involves the melting and resolidifying of a piece [conveniently obtained in the form of shot (1)] of semiconductor on a wafer of the same material (having essentially the same melting point) to form a single crystal boundary region. Melting of the wafer is prevented by providing a large vertical thermal gradient. Figure 1 illustrates this process, the example chosen being a p-type region on an n-type base. In Fig. 1(a), the shot is placed on top of the n-type wafer. The shot is generally polycrystalline, containing an impurity concentration up to 1% or so. When the heat source, located above the semiconductor pieces, is turned on, the shot starts to melt from the top. The liquid surface contour forms a section of a sphere, so that by the time the shot is all molten it has only a very small area of contact with the n-type pellet, Fig. 1(b). The pellet will not start to melt at this point because of the large vertical temperature gradient, provided by placing the heater above the work and by resting the n-type wafer on a large thermal capacity support. The shot is completely melted because heat is entering it from the top, and very little heat is leaving the bottom by conduction due to the small area of contact with the wafer. This condition lasts but a very short period of time (of the order of a second), following which the molten sphere suddenly spreads at an extremely rapid rate and immediately freezes back part way into a pyramidal shape, Fig. 1(c). At this time the heat source may be removed so the structure freezes the rest of the way, Fig. 1(d). If the heat source were not turned off, the pyramid and then the wafer would subsequently melt.

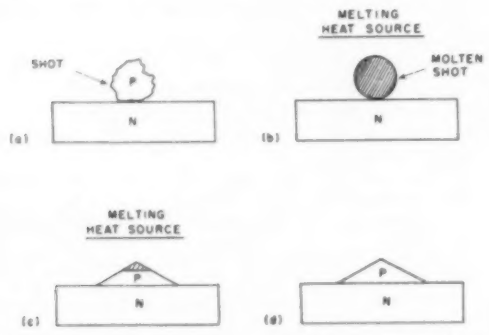

Fig. 1. Steps in the shot-melt process. (a) Shot (p-type) placed on wafer (n-type); (b) heat source turned on, shot just finished melting; (c) heat source unchanged, shot suddenly spreads on wafer and partly refreezes; and (d) heat source turned off, remaining part of shot frozen.

The shot-melt process would be of limited general use in semiconductor device technology were it not for the following two properties.

1. The p-type semiconductor region that forms adjacent to the n-type pellet is single crystal growing epitaxially on the pellet. After a short distance (of the order of a mil) it becomes polycrystalline. However, a single crystal region this thick is more than adequate for most devices. Figure 2 is a photomicrograph of a silicon shot-melt structure section, showing the p-n junction, the n-type pellet, and the grown p-type single crystal region which ends in polycrystalline p-type silicon. The pattern brought

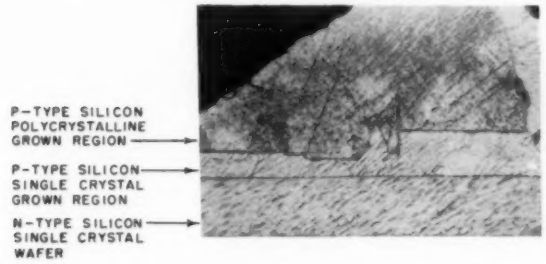
P-TYPE SILICON POLYCRYSTALLINE GROWN REGION
P-TYPE SILICON SINGLE CRYSTAL GROWN REGION
N-TYPE SILICON SINGLE CRYSTAL WAFER

Fig. 2. Photomicrograph of silicon shot-melt p-n junction structure showing single crystal grown region. X190.

out in the single regions by the etch (10% sodium hydroxide, 15% sodium nitrite in water at about 100°C) shows that they have the same orientation.

2. If a very large thermal gradient is maintained, the boundary between pellet and shot-melt regions will coincide very closely with the original surface of the pellet. That is, the penetration of the molten shot into the pellet surface is exceedingly small. Figure 3 is a photomicrograph of a germanium pellet with shot melt regions on both sides (pnp structure) showing that the planes of the p-n junctions are flat and coincide closely with the original surfaces of the pellet. As sometimes occurs with large shot-melt regions, two small voids may be seen in the bottom (p-type) grown region.

The following explanation is proposed to account for the lack of penetration of the molten region into the pellet surface. When the shot first becomes entirely molten, it does not make intimate contact with the pellet. Surface oxide on the pellet may be at least partially responsible for this, since silicon appears to remain at this stage longer than germanium. When intimate contact between the molten and solid semiconductor regions is established at the point of contact between the sphere and plane, lateral wetting is greatly enhanced, and the area of intimate contact quickly increases. As each new incremental area of contact forms, thermal flow to the cooler substrate quickly freezes a small volume of the molten material onto the substrate. As spreading proceeds, the heat content of the shot becomes depleted, so the already deposited regions get thicker. Hence, crystal growth takes place radially as well as upward, the final diameter of the pyramid being determined by the heat content of the molten sphere as well as the temperature, thermal capacity and surface condition of the pellet. If larger shot are used, the spreading will proceed until limited by the edges of the pellet (c. f. bottom region, Fig. 3).

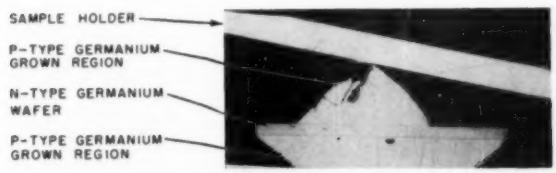

Fig. 3. Photomicrograph of germanium double shot-melt p-n-p junction structure showing how original surface of n-type wafer is preserved. X40.

Diffused Shot-Melting

Because of the short heat cycle during shot melting, little diffusion of the common donor and acceptor impurities takes place even though the temperature is high. Hence, an abrupt boundary exists between the two regions. If graded junctions are required, a diffusion cycle (most conveniently done in a separate furnace) may be subsequently used. When a diffusion cycle follows shot-melting, the complete process will be referred to as diffused shot-melting.

The shot may be made to contain two (or more) impurities. If the ratios of majority to minority impurity concentrations and diffusion coefficients are chosen in the right ranges, then the minority impurity will diffuse ahead and become the majority impurity in a narrow region of the pellet adjacent to the shot-pellet interface. Figure 4 illustrates this process to make a germanium pnp transistor structure.

The impurity concentrations in the grown shot region adjacent to the pellet may be calculated from those in the (uniformly doped) molten shot by taking into account their distribution coefficients. However, since the growth rate is variable, so will be the distribution coefficients (2, 3). The impurity concentration in the shot melt region probably is that governed by the equilibrium distribution coefficient, in a thin plane adjacent to the pellet, and increases with distance into the pyramid because the growth rate increased with distance into the pyramid. For diffused bases, the impurity concentration is critically dependent on that in the source region in a layer approximately as thick as the diffused base itself. For very thin diffused bases, therefore, a first approximation (4) is to assume diffusion from a region of high uniform impurity concentration (determined by the equilibrium distribution coefficients) into a region of low uniform impurity concentration (that of the original pellet). In practice, this approximation has worked well.

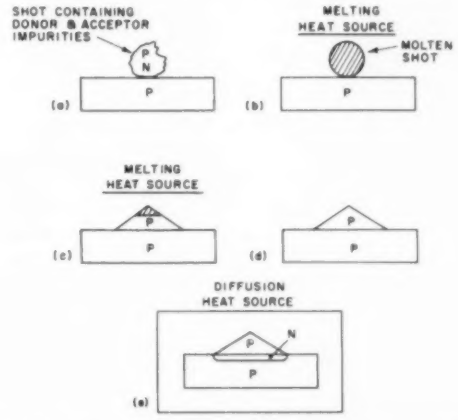

Fig. 4. Steps in the diffused shot-melt process. (a) Shot (containing donor and acceptor impurities) placed on wafer (p-type); (b), (c), (d) same as in Fig. 1; and (e) structure heated, n-type layer formed in wafer by diffusion.

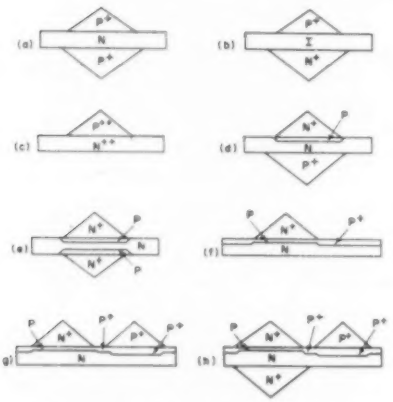

Fig. 5. Some example of shot-melt and diffused shot-melt structures. (a) pnp transistor; (b) pin diode; (c) tunnel diode; (d) pnpn switch; (e) npnpn symmetrical switch; (f) npn transistor; (g) npn transistor with 2 shot-melt contacts; and (h) npn transistor with 3 shot-melt contacts.

Application to Some Semiconductor Devices

Some examples of shot-melt and diffused shot-melt devices, all of which have been made and tested, are shown in Fig. 5. Figure 5(a) illustrates a pnp transistor made by melting shot on either side of a wafer. A similar structure, made to yield a pin diode, is shown in Fig. 5(b). A shot melt structure in which both p-type and n-type regions are degenerate, Fig. 5(c), has a tunnel diode characteristic. This requires a p-n barrier width of at most a few hundred angstroms, giving proof of the abrupt nature of the impurity transition at the boundary between shot and wafer. Figure 5(d) illustrates a pnpn switch, made by diffused shot-melting with double doped shot on one side of the wafer, singly doped shot on the other. This may be extended somewhat to make a symmetrical npnpn switch, as shown in Fig. 5(e).

Surface diffusion can be done at the same time as the bulk diffusion. A structure made in this way is depicted in Fig. 5(f), in which the surface diffused layer is left on only the top side of the wafer. The surface concentration of the vapor diffused layer must be less than that in the shot if a p-n junction is not to form over the surface of the pyramid. In Fig. 5(g) a singly doped p-type shot is placed beside the doubly doped shot (left), and the device diffused in an atmosphere containing an acceptor impurity. The result is a transistor structure, the left pyramid serving as the emitter, the right one as the base. This device is made somewhat more complex in Fig. 5(h), where an n-type impurity doped shot, to serve as a collector contact (bottom) is made before (or after) the diffusion cycle. In this figure, the surface diffused layer is removed from all wafer surfaces except the top one.

Devices made by the diffused shot-melting technique often did not have electrical characteristics as good as those made by other techniques. This is because there is a severe lifetime degradation during the shot-melt cycle, junction size is hard to control, lateral junction spacing [i.e., Fig. 5(h)] is not easy to reproduce, and resistivity often changes when the starting value is high. Nevertheless the ease and versatility with which semiconductor p-n junction structures may be made by diffused shot-melting make its use particularly attractive in some cases. The structures have no low melting components to limit fabrication and assembly techniques. Diffusion is from a volume source, so, except in structures where surface diffused layers are also required, no precise atmospheric control during diffusion is needed. Also, some or all of the lifetime and resistivity degradation produced during the shot-melt cycle can be removed by processes such as surface alloy gettering or annealing during or subsequent to the diffusion cycle.

Acknowledgment

The help of Mrs. L. Roehrig and N. E. Collins in fabricating the structures, and of C. V. Bielan and F. A. Carranti in making the metallographic sections and photomicrographs, is greatly appreciated.

Manuscript received Nov. 18, 1959. This paper was prepared for delivery before the Columbus Meeting, Oct. 18-22, 1959.

Any discussion of this paper will appear in a Discussion Section to be published in the December 1960 JOURNAL.

REFERENCES

1. I. A. Lesk, *This Journal*, **103**, 601 (1956).
2. R. N. Hall, *J. Phys. Chem.*, **57**, 836 (1953).
3. J. A. Burton, R. C. Prim, and W. P. Slichter, *J. Chem. Phys.*, **21**, 1987 (1953).
4. I. A. Lesk and R. E. Coffman, *J. Appl. Phys.*, **29**, 1493 (1958).

Polarographic Studies in Acetonitrile and Dimethylformamide

V. Behavior of Aromatic Ketones and Aldehydes

S. Wawzonek and A. Gundersen

Department of Chemistry, State University of Iowa, Iowa City, Iowa

ABSTRACT

Benzophenone, acetophenone, p-methoxyacetophenone, benzaldehyde, and anisaldehyde are reduced stepwise polarographically in anhydrous dimethylformamide. Large-scale electrolytic reduction of benzophenone indicates that the ketyl anion is formed as a stable intermediate since, in the presence of carbon dioxide and ethyl iodide, benzilic acid and diphenylethylcarbinol are formed, respectively. Acetophenone, benzaldehyde, and anisaldehyde form principally pinacols under these conditions. The reduction of p-methoxyacetophenone is complicated by tar formation.

Previous polarographic studies in acetonitrile and dimethylformamide have shown that this method is capable of furnishing evidence for the existence of stable anion-free radicals in the reduction of aromatic hydrocarbons (1, 2) and semiquinone anions in the reduction of quinones(3).

In the present study the polarographic behavior and electrolytic reduction of aromatic ketones and aldehydes has been investigated to determine whether ketyl anions are produced in dimethylformamide.

Experimental

The solutions were studied in a cylindrically shaped cell with a mercury pool anode and fitted with side arms for the anode connection and for admission of nitrogen. All measurements were made in a water thermostat at 25° ± 0.1°.

The current-voltage curves were obtained with a Sargent Model XII polarograph having a current scale calibration of 0.00497 μa/mm at a sensitivity of one.

The dropping mercury electrode was operated at 60 cm pressure and had a drop time of 3.42 sec in dimethylformamide (open circuit). The $m^{2/3}t^{1/6}$ value was 1.96 $mg^{2/3}$ $sec^{1/2}$.

The dimethylformamide was purified in a manner similar to that reported previously (1). The compounds were obtained from stock and purified by crystallization or distillation.

Electrolytic Reductions

The electrolytic reductions of the various carbonyl compounds were carried out at a platinum anode and mercury cathode in a similar manner to that described earlier (1). The area of the cathode was 65 cm^2 and the line voltage was 80 v. Typical procedures are illustrated below. The results are given in Table II.

Benzophenone.—A solution of 5 g of benzophenone and 7.72 g of potassium iodide in 300 ml of dimethylformamide was deoxygenated with nitrogen for 1 hr. Direct current was allowed to pass through the cell for 20 hr and gave a blue solution.

The catholyte and anolyte were poured into 50 ml of 10% acetic acid solution and the solvent was removed under reduced pressure at 100°. Extraction with ether followed by removal of the solvent gave an oil which was soluble in isopropyl alcohol and in hot petroleum ether. Benzopinacol, if present, would be insoluble in these solvents. When the petroleum ether was cooled, 2.8 g of benzohydrol melting at 66°-68° was obtained. A mixture with an authentic sample melted at the same point. The benzophenone which remained in the petroleum ether was determined in some of the experiments as the oxime.

Benzophenone and carbon dioxide.—A solution of dimethylformamide (300 ml) containing potassium iodide (7.72 g) and benzophenone (5 g) was deoxygenated with carbon dioxide for 1 hr. Electrolysis was carried out for 20 hr while a stream of carbon dioxide was passed through the solution. The cathode compartment remained colorless during the electrolysis. Removal of the solvent under reduced pressure gave a residue which was extracted with ether. The ether insoluble portion was found to be water soluble. Upon acidification of the aqueous solution benzilic acid (3.1 g) melting at 149°-152° precipitated. A mixture with an authentic sample melted at the same point.

Benzophenone and ethyl iodide.—A solution of potassium iodide (7.72 g) and benzophenone (20 g) in dimethylformamide (300 ml) was deoxygenated with nitrogen for 1 hr and then electrolyzed for 15 hr. During the electrolysis, oxygen-free ethyl iodide was dropped into the cathode compartment. Removal of the solvent under reduced pressure was followed by extraction with ether. The yellow oil (17.5 ml) obtained was freed of benzophenone by refluxing with hydroxylamine hydrochloride (9 g) and potassium hydroxide (15 g) in ethanol (30 ml) and water (6 ml) for 5 min. The solution was poured into 1*N* potassium hydroxide (200 ml) and extracted with hexane. After concentration and cooling of the hexane solution 3.2 g of diphenylethylcarbinol melting at 93°-95° was recovered. A

mixture with an authentic sample melted at the same point.

Acetophenone.—A solution of dimethylformamide (300 ml) containing 17 g of tetrabutylammonium iodide and 20 g of acetophenone, was deoxygenated with nitrogen for 1 hr and then electrolyzed for 14 hr. The resulting solution was poured into 600 ml of water containing 20 ml of acetic acid. Extraction with ether was followed by concentration to 100 ml. The resulting solution on mixing with 200 ml of hexane, concentrating, and cooling gave 6.0 g of meso-acetophenone pinacol melting at 117°-120°. A mixture with an authentic sample melted at the same point.

Results

The polarographic data obtained for the various aromatic ketones and aldehydes in various solutions are given in Table I. The waves in all cases were well defined. The addition of water shifted both waves to more positive potentials.

The half-wave potentials of the second wave for benzophenone, acetophenone, and benzaldehyde are more negative than those reported by Given (4). Since the addition of water shifts the second wave to more positive potentials, the latter study was probably carried out in dimethylformamide which was not completely anhydrous.

To help formulate electrode reactions and identify intermediate species large-scale electrolytic reductions were carried out with benzophenone, acetophenone, benzaldehyde, *p*-methoxybenzaldehyde, and *p*-methoxyacetophenone in the presence and absence of carbon dioxide. An electrolysis also was performed with benzophenone in the presence of ethyl iodide. Complete analysis of the products from compounds other than benzophenone was prevented by the formation of tars and oils. Results are summarized in Table II.

Table I. Polarographic behavior of aromatic ketones and aldehydes in dimethylformamide containing 0.175M tetrabutylammonium iodide and varying amounts of water

Compound	Conc.[a]	% Water by volume	$E_{1/2}$ (v) vs. Hg pool 1st Wave	$E_{1/2}$ (v) vs. Hg pool 2nd Wave	I_d[b] 1st Wave	I_d[b] 2nd Wave
Benzophenone	2.34	0	−1.21	−1.78	1.32	0.88
		0.99	−1.19	−1.69	1.33[c]	0.88[c]
		4.76	−1.17	−1.62	1.34[c]	0.70[c]
		9.09	−1.14	−1.57	1.39[c]	0.68[c]
Acetophenone	0.985	0	−1.46	−2.15	1.41	0.55
		0.99	−1.42	−2.05	1.35[c]	1.46[c]
		4.76	−1.37	−1.99	1.34[c]	0.98[c]
		9.09	−1.33	−1.96	1.29[c]	0.95[c]
Benzaldehyde	1.93	0	−1.28	−2.17	2.11	1.18
		0.99	−1.24	−2.09	2.10[c]	1.57[c]
		4.76	−1.20	−2.05	2.00[c]	1.49[c]
		9.09	−1.19	−2.02	1.82[c]	1.48[c]
p-Methoxyacetophenone	1.03	0	−1.50	−1.99	1.88[d]	0.81[d]
p-Methoxybenzaldehyde	0.993	0	−1.48		1.86[e]	

[a] Millimoles per liter.
[b] $I_d = i_d/Cm^{2/3}t^{1/6}$.
[c] Corrected for change in concentration of compound.
[d] Capillary with $m^{2/3}t^{1/6}$ of $mg^{2/3}sec^{-1/2}$ and a droptime of 3.60 sec (open circuit) at 45 cm pressure.
[e] Capillary with $m^{2/3}t^{1/6}$ of 1.56 $mg^{2/3}sec^{-1/2}$ and a droptime of 3.91 sec (open circuit) at 50 cm pressure.

Discussion of Results

Examination of the results in Table I indicates that aromatic ketones and aldehydes are reduced stepwise at the dropping mercury electrode in anhydrous dimethylformamide. In contrast to its effect on the waves of hydrocarbons and quinones addition of water caused little change in the first wave, but caused a shift of the second to more positive potentials and an increase of the diffusion current in some examples. The double waves found are similar to those reported in aqueous alkali by Ashworth (5) and would suggest the following general mechanism of reduction for these compounds.

$$R_2C{=}O + e \rightarrow R_2\dot{C}{-}O^- \text{ (1st wave)}$$

$$R_2C{=}O + 2e \rightarrow R_2\ddot{C}{-}O^- \text{ (2nd wave)}$$

Evidence for these electrode reactions is the observation made in the large-scale electrolytic reduction of benzophenone. In solutions in dimethylformamide containing potassium iodide, in which only the first polarographic wave is obtained, a blue coloration is produced. A similar color is reported for the monosodium derivatives of benzophenone in liquid ammonia (6).

The presence of the intermediate ketyl anion for benzophenone was further demonstrated by the electrolysis of benzophenone in the presence of carbon dioxide and ethyl iodide with potassium iodide as a supporting electrolyte; benzilic acid and diphenylethylcarbinol were formed, respectively. If the reduction is carried out in the absence of these reagents or in the presence of water, the blue color is discharged, slowly in the first case, and benzophenone and benzohydrol are obtained. Changing the supporting electrolyte to lithium iodide produced similar results.

Treatment of metal ketyls in hydrocarbon solvents or ether with ethyl bromide and carbon dioxide produces similar products together with benzophenone (7, 8). The reaction with water likewise results in the formation of benzophenone and benzohydrol (9).

The formation of the ketyl anion also has been demonstrated with electron resonance studies by Austen, *et al.* (10) of solutions of benzophenone reduced electrolytically at controlled potentials in dimethylformamide.

Determination of n for the waves of benzophenone using a micro cell (11) with 0.5 ml of a solution of benzophenone ($2 \times 10^{-3} M$) containing tetrabutylammonium iodide as a supporting electrolyte gave values of 1.54 and 1.82 respectively for the two waves. When the electrolysis was limited to the first wave by using potassium iodide as the supporting electrolyte, no appreciable decrease in the concentration of benzophenone occurred. The latter behavior indicates that the ketyl anion formed is reoxidized at the anode to benzophenone.

Table II. Large-scale electrolytic reductions of aromatic ketones and aldehydes in dimethylformamide

Compound	Amperes		Time of electrolysis	Products formed
	Start	Finish		
HCON $(CH_3)_2$—0.155*M* $(C_4H_9)_4NI$ (300 ml)				
5.0 g $(C_6H_5)_2CO$	0.70	0.10	23 (hr)	Benzohydrol (2.7 g)
20 g $C_6H_5COCH_3$	0.60	0.05	14	Acetophenone pinacol (5.1 g)
20 g $C_6H_5COCH_3$ + excess CO_2	0.60	0.05	14	Atrolactic acid (1.0 g)
20 g C_6H_5CHO	0.60	0.05	19	Hydrobenzoin (7.3 g) Benzaldehyde (5 ml)
20 g C_6H_5CHO + CO_2	0.60	0.05	24	Hydrobenzoin (6.1 g)
20 g *p*-$CH_3OC_6H_5COCH_3$	0.60	0.05	27	2, 3-Dianisylbutadiene-1, 3 (traces)
20 g *p*-$CH_3OC_6H_5COCH_3$ + CO_2	0.60	0.05	20	*p*-Methoxyatrolactic acid (traces)
20 g *p*-$CH_3OC_6H_5CHO$	0.45	0.15	20	Hydroanisoin (1.9 g)
20 g *p*-$CH_3OC_6H_5CHO$ + CO_2	0.40	0.10	24	Hydroanisoin (1.3 g)
HCON $(CH_3)_2$—0.155*M* KI (300 ml)				
5.0 g $(C_6H_5)_2CO$	0.50	0.10	20	Benzohydrol (2.8 g)
5.0 g $(C_6H_5)_2CO$ + CO_2	0.60	0.10	20	Benzilic acid (3.1 g)
20 g $(C_6H_5)_2CO$ + 20% H_2O	2.5	1.0	12	Benzohydrol (17.1 g) Benzophenone (1.5 g)
20 g $(C_6H_5)_2CO$ + C_2H_5I	0.70	0.05	15	Diphenylethylcarbinol (3.2 g) Benzophenone (16.6 g)
HCON $(CH_3)_2$—0.155*M* LiI (300 ml)				
20 g $(C_6H_5)_2CO$	0.50	0.05	14	Benzohydrol (2.76 g) Benzophenone (14.75 g)

Logarithmic analysis of the reduction wave for benzophenone in potassium iodide solution showed a slope of 0.051. A similar analysis in the presence of tetrabutylammonium iodide showed a slope of 0.070 for the first wave and a slope of 0.080 for the second. Both waves show some kinetic character and are irreversible.

Since the ketyl anion is stable in dimethylformamide it is possible that the second wave may represent a

$$(C_6H_5)_2\dot{C}—O^- + e \rightarrow (C_6H_5)_2\ddot{C}—O^-$$

direct reduction of this ion to the dianion. The latter would react more readily with the solvent or water than the ketyl anion and give benzohydrol. The smaller diffusion current observed for this wave may be caused by the repulsion of the ketyl anion from the electrode.

The dianion is a much stronger base than the ketyl anion and would react irreversibly with water to form the carbinol anion.

$$(C_6H_5)_2\ddot{C}—O^- + H_2O \rightarrow (C_6H_5)_2\underset{H}{C}—O^- + OH^-$$

Further reaction of the latter with water would be reversible. The second wave therefore should be influenced more by the addition of water and this behavior was observed.

Acetophenone when reduced electrolytically in the presence of carbon dioxide gives only a 4% yield of atrolactic acid. In the absence of carbon dioxide acetophenone pinacol was obtained.

Under similar circumstances, *p*-methoxyacetophenone gave only traces of acidic material and considerable amounts of tar. Distillation of the tar gave a small amount of 2, 3-di-*p*-anisylbutadiene-1, 3. This compound without doubt resulted from the pinacol.

Benzaldehyde on reduction alone gave a 43% yield of hydrobenzoin. In the presence of carbon dioxide the yield of hydrobenzoin was reduced to 30%, but no mandelic acid was formed.

The reduction of anisaldehyde resulted in considerable amounts of tar and a 5% yield of hydroanisoin.

The different behavior observed for the acetophenones and benzaldehydes in these large-scale electrolyses from that of benzophenone is apparently dependent on the stability of the intermediate ketyl anion

$$2R_2\dot{C}—O^- \rightleftarrows R_2C(O^-)—CR_2(O^-)$$

or the extent of its dimerization to the pinacolate anion.

The results obtained with benzophenone would point to a stable ketyl anion since carbonation produces a high yield of benzilic acid. Under the same conditions the ketyl anions from acetophenone and benzaldehyde and their methoxy derivatives are less stable and either dimerize or undergo reactions which form tars.

The actual mechanism for the reaction of the benzophenone ketyl anion with various reagents is still not known. This anion is no doubt a resonance hydrid and

$$(C_6H_5)_2C{-}O^- \leftrightarrow (C_6H_5)_2\underline{C}{-}O\cdot$$

could undergo a direct reaction with the reagents involved.

$$(C_6H_5)_2\underline{C}{-}O^- + CO_2 \rightarrow (C_6H_5)_2C(COO^-){-}O\cdot$$

The resulting product from the reaction with carbon dioxide would take up an electron in the electrolytic reduction and form the benzilate anion.

$$(C_6H_5)_2C(COO^-){-}O\cdot + e \rightarrow (C_6H_5)_2C(COO^-){-}O^-$$

In the same reaction of metal ketyls in hydrocarbon solvents another ketyl anion would furnish the electron necessary.

$$(C_6H_5)_2C(COO^-){-}O\cdot + (C_6H_5)_2\underline{C}{-}O^- \rightarrow$$

$$(C_6H_5)_2C(COO^-){-}O^- + (C_6H_5)_2C{=}O$$

A similar mechanism is implied for the formation of benzohydrol in the electrolytic reduction of benzophenone in dimethylformamide by Austen, *et al.* (10).

Disproportionation of the ketyl anion to benzophenone and the dianion, which could undergo similar reactions, is considered not to be feasible energetically (12).

$$2(C_6H_5)_2C{-}O^- \rightarrow (C_6H_5)_2\underline{C}{-}O + (C_6H_5)_2CO$$

The possibility of the formation of the pinacolate anion followed by its dissociation into benzophenone and its dianion as

$$2(C_6H_5)_2C{-}O^- \rightleftarrows (C_6H_5)_2C(O^-){-}C(O^-)(C_6H_5)_2 \rightleftarrows$$

$$(C_6H_5)_2C{=}O + (C_6H_5)_2\underline{C}{-}O^-$$

proposed by Acree (13) cannot be completely eliminated as a basis for the reactions of the ketyls.

Manuscript received Aug. 12, 1959. This paper was prepared for presentation at the Buffalo Meeting, Oct. 6-10, 1957 and is based on the Ph.D. thesis of A. Gundersen (June 1960). The research was supported by the Office of Ordnance Research under Contract DA-11-022-ORD-1868.

Any discussion of this paper will appear in a Discussion Section to be published in the December 1960 JOURNAL.

REFERENCES

1. S. Wawzonek, E. W. Blaha, R. Berkey, and M. E. Runner, *This Journal*, **102**, 235 (1955).
2. S. Wawzonek and D. Wearring, *J. Am. Chem. Soc.*, **81**, 2067 (1959).
3. S. Wawzonek, R. Berkey, E. W. Blaha, and M. E. Runner, *This Journal*, **103**, 456 (1956).
4. P. H. Given, M. E. Peover, and J. Schoen, *J. Chem. Soc.*, **1958**, 2074.
5. M. Ashworth, *Collection Czechoslov. Chem. Commun.*, **13**, 229 (1948).
6. C. B. Wooster, *J. Am. Chem. Soc.*, **50**, 1388 (1928).
7. W. Schlenk, J. Appenrodt, A. Michael, and A. Thal, *Ber.*, **47**, 473 (1914).
8. C. B. Wooster and W. E. Holland, *J. Am. Chem. Soc.*, **56**, 2438 (1934).
9. W. E. Bachmann, *ibid.*, **55**, 1179 (1933).
10. D. E. G. Austen, P. H. Given, D. J. E. Ingram, and M. E. Peover, *Nature*, **182**, 1784 (1958).
11. G. A. Gilbert and E. K. Rideal, *Trans. Faraday Soc.*, **47**, 396 (1951).
12. N. S. Hush and J. Blackledge, *J. Chem. Phys.*, **23**, 514 (1955).
13. S. F. Acree, *Am. Chem. J.*, **29**, 588 (1903).

Preparation and Refining of Yttrium Metal by Y-Mg Alloy Process

O. N. Carlson, J. A. Haefling, F. A. Schmidt, and F. H. Spedding

Institute for Atomic Research and Department of Chemistry, Iowa State University, Ames, Iowa

ABSTRACT

Yttrium metal was prepared by the reduction of YF_3 with calcium forming a low melting Y-Mg intermediate alloy. Magnesium was removed by sublimation to produce yttrium metal sponge. A method is described for removing oxygen and fluorine from the alloy by extraction with fused yttrium salts. The results of electron beam melting and zone refining are also presented. Some properties of yttrium metal of 99.9% purity obtained by the extraction refining process are discussed.

Recent interest in the possible uses of various rare earth metals as reactor materials led to this investigation of the preparation of high-purity yttrium metal. An acceptable absorption cross section for thermal neutron (1.31 barns), relatively high melting point (1500°-1550°C), resistance to attack by liquid uranium and uranium alloys (1), and its potential as a new alloying element in high-temperature materials are some of the properties that are responsible for the increasing interest in the metallurgy of yttrium.

Thompson (2), Trombe (3), and Daane and Spedding (4) have previously prepared experimental quantities of yttrium metal. The principal objective of this investigation was the preparation of yttrium metal in higher purity and larger quantities for use in the development of fabrication procedures and in the investigation of the properties of yttrium and its alloys.

The basic process described in this paper is the reduction of YF_3 with calcium in the presence of magnesium to form a low melting Y-Mg alloy. The reaction was carried out at 950°C in a refractory metal crucible under an inert gas atmosphere. Anhydrous $CaCl_2$ was added to the charge to flux the high melting CaF_2 produced by the reaction. A refining step in the process consisted of a fused salt extraction in which some of the interstitial impurities were extracted from the molten Y-Mg alloy. The magnesium was sublimed out of the alloy by heating *in vacuo*, yielding a metallic sponge which was subsequently arc melted into a massive yttrium ingot. The resulting yttrium metal was evaluated by spectroscopic and chemical analyses and by metallographic examination. The hardness, fabricability, and other properties of the metal were also determined.

Materials

In the preparation of high-purity yttrium it is essential that all reactants be of the highest possible purity since most of the impurities in these materials end up in the metal product.

It was recognized from the outset that high-purity YF_3, with a minimum of oxide contamination, was a prerequisite if that material were to be used as the starting salt. The details of the preparation of the YF_3 employed in these studies are given in an Ames Laboratory report (5).

A few pounds of YCl_3 were prepared for use in refining experiments. Yttrium metal sponge was converted to the chloride by reacting it with anhydrous HCl gas at 700°C. The crude product was purified by redistillation *in vacuo* at 950°C. The purity of the best YCl_3 and YF_3 that were obtained is estimated as 99.9%.

Anhydrous $CaCl_2$ of analytical grade purity (greater than 99%) was obtained from the J. T. Baker Co. Since this material contained small amounts of water, it was further dehydrated by heating to 450°C in a stainless steel vessel under a dynamic vacuum. When high-purity $CaCl_2$ was required, as in the extraction experiments, the chloride was given an additional treatment by passing anhydrous HCl over the vacuum-dried salt at 500°C.

Commercially pure calcium metal obtained from the New England Lime Company was vacuum redistilled at 900°C as described by Smith, *et al.* (6). Table I gives the analysis of the calcium after distillation.

Magnesium metal was distilled in the same apparatus at a temperature of 850°C. The carbon content was reduced to 0.02 wt % by this procedure, nitrogen to 0.005 wt %, and oxygen to less than 0.01 wt %.

Reduction of YF_3

Yttrium fluoride can be reduced by calcium in the presence of $CaCl_2$ and magnesium metal to form an Y-24 wt % Mg intermediate alloy. The alloy and slag produced in the reaction are both molten at 950°C, thus making it possible to carry out the reduction in a refractory metal crucible under an inert gas atmosphere. Calcium chloride was selected as the fluxing agent since it forms a low melting eutectic with CaF_2. It also decreases the density of the slag which is an important factor if complete separation from the alloy phase is to be achieved. Removal of the magnesium from the alloy and melting of the yttrium sponge are discussed in a later section of this paper.

Table I. Analysis of redistilled calcium metal

Element	Wt %
Magnesium	0.300
Carbon	0.020
Nitrogen	0.005
Aluminum	0.003
Iron	0.003
Manganese	0.002
Nickel	0.002

Apparatus and procedure.—A sketch of the apparatus used in the reduction process is shown in Fig. 1. The temperature of the retort was measured by a thermocouple placed on the exterior wall surface.

Several refractory metals and oxides were tested as crucible materials and tantalum was found to be the most inert. Most of the small-scale, high-purity experiments were carried out in tantalum; however titanium crucibles were used in the large reductions and in the more routine experiments.

The reductions were carried out in the following manner. Massive pieces of magnesium and calcium were transferred to the reduction crucible, and a mixture of YF_3 and $CaCl_2$ was loaded into the charging hopper. A typical charge consisted of 1500 g YF_3, 1350 g $CaCl_2$, 680 g calcium, and 290 g Mg. The unit was evacuated by means of a mechanical pump prior to placing the retort in the gas furnace.

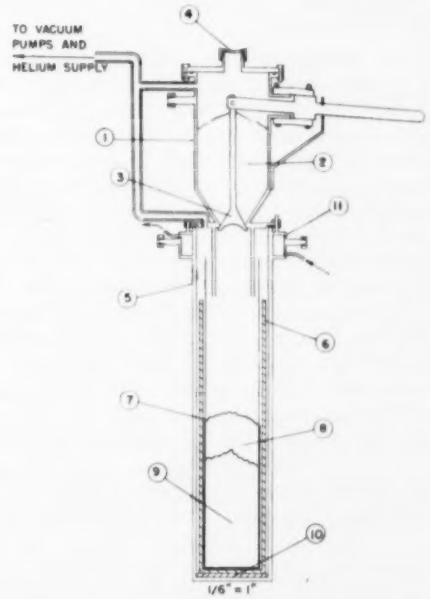

Fig. 1. Schematic drawing of reduction retort and charging hopper; 1, charging hopper; 2, $CaCl_2$ and YF_3; 3, control valve; 4, sight glass; 5, steel retort; 6, Ti or Fe retaining crucible; 7, Ti crucible; 8, Mg; 9, Ca; 10, graphite disk; 11, water jacket.

When the temperature of the retort had reached 800°C, helium gas was admitted and a pressure of 1-5 psi (gauge) was maintained in the system throughout the remainder of the run. When a temperature of approximately 900°C was attained as indicated by a thermocouple immersed in the molten calcium-magnesium phase, the YF_3-$CaCl_2$ mixture was added slowly from the hopper into the heated zone of the reaction crucible. The absence of a sharp temperature rise during the reduction process indicates that the reaction is either endothermic or only slightly exothermic.

At the completion of the run the hot retort was raised from the furnace, placed in a rack, and tilted to a few degrees from the horizontal. By allowing solidification to occur in this position, the slag and alloy could be removed more easily thus avoiding damage to the reduction crucible.

Experimental results.—A comprehensive investigation was made of the effects of reaction conditions, physical state and purity of the ingredients, proportion of the reactants, and handling procedures on the quality and yields of the yttrium metal obtained.

From experiments in which various oxides were added to the reduction charge, it was concluded that any oxides present in the reactants are transferred quantitatively to the Y-Mg phase during the reduction. Comparisons between granular and massive calcium revealed that yttrium prepared from granular calcium contained an average of 0.1 wt % more oxygen than that prepared from massive metal. This differential was observed with calcium on which the grinding and screening operations were carried out in a specially designed dry room. For this reason, the use of freshly distilled calcium and magnesium in massive form is strongly advocated if the oxygen content is to be kept as low as possible.

The composition of the intermediate alloy was set at 24 wt % magnesium, a composition that lies close to the intermediate phase, Y-Mg (7). This alloy possesses the properties of brittleness, low melting point, and relatively high density that are essential to the success of this process. The proper proportions of the other reactants were determined experimentally. A 10 wt % excess of calcium reductant gives a metal recovery of greater than 99% of theoretical; a smaller excess results in some decrease in yield. The critical slag composition was also determined by adjusting the YF_3-$CaCl_2$ ratio in the charge. A slag composition of 52 wt % $CaCl_2$ gave best slag-metal separations and highest metal yields.

Tests showed that the alloy picks up significant amounts of oxygen after a brief exposure to air saturated with water vapor but not from oxygen of the air. Therefore the crushing and transferring of the alloy were handled in a dry box filled with helium.

In spite of these precautions the oxygen content of the best yttrium prepared by this method was in the range of 0.1-0.2 wt %. This is shown along with other analytical data in Table II. The values represented are averages from a large number of reductions made in titanium crucibles. Statistical treatment of these data indicate that the standard deviation for the larger values reported is ± 0.01% or less.

Table II. Major impurities in yttrium metal prepared by the calcium reduction of yttrium fluoride

Impurity	Wt %	Impurity	Wt %
Oxygen	0.170	Nitrogen	0.015
Titanium	0.150	Silicon	<0.015
Fluorine	0.080	Copper	0.004
Nickel	0.035	Magnesium	0.003
Iron	0.030	Calcium	0.001
Carbon	0.020	Total rare earths	<0.050

Magnesium Removal and Arc Melting

The volatile components of the alloy must be removed almost completely before the resulting sponge can be arc melted. At the same time care must be exercised to avoid melting and spattering during the initial stages of the magnesium and calcium removal. As a first step the alloy was crushed into pieces approximately ½ in. in diameter in a jaw crusher enclosed in the dry box.

The sublimation was carried out in a 6-in. diameter stainless steel retort equipped with a condenser. The alloy was placed in a titanium vessel inside the vertical retort. The system was evacuated to a pressure of 10^{-4} mm Hg at the outset, and this pressure was maintained throughout the run. The retort and its contents were heated to 900°C in an electric furnace, held at this point for 4 hr, and then increased to 950°C and held for a period of 20 hr. The magnesium vapors were collected on the condenser which was cooled by a flow of air. The yttrium obtained in this manner was a bright, porous sponge containing approximately 0.01 wt % magnesium and calcium.

The yttrium sponge was consolidated into ingot form by arc melting. The sponge was compacted into electrodes, and these were generally arc melted into 1-lb evaluation ingots in an inert gas atmosphere. In processing larger amounts of yttrium, the sponge was consummably arc melted twice with the second melting being carried out under a dynamic vacuum. The steps in this melting operation are represented by the three forms of the metal shown in Fig. 2. About 90 lb of metal are shown in each processing step.

Refining of Yttrium

In an effort to remove some of the impurities from yttrium, particularly oxygen and fluorine, several

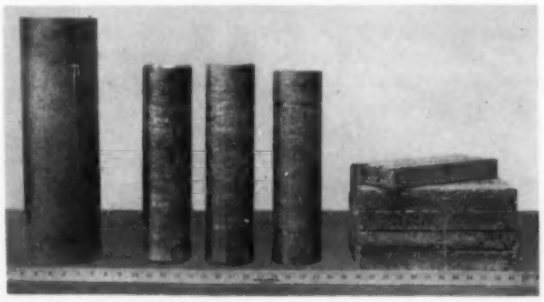

Fig. 2. Six-inch diameter ingot (left); 4-in. diameter ingots (center); and 27 sponge compacts or electrodes.

refining techniques were tried. The more successful methods are discussed in this section.

Refining of Y-Mg alloy with a fused salt.—It was observed that the oxygen content of the Y-Mg alloy was reduced significantly after being in contact with a fused salt containing YF_3 or YCl_3. Several experiments were run in an attempt to gain some understanding of this phenomenon.

The same apparatus that was used in the reduction of YF_3 was employed in these experiments, but with one modification. The charging hopper was replaced by a vacuum head through which the shaft of a stirring rod was inserted. A titanium or tantalum paddle was attached to this shaft and was rotated inside an "O" ring seal. Approximately 0.5 wt % titanium was dissolved by the yttrium alloy when both the reduction and extraction steps were carried out in a titanium crucible with a titanium stirrer. No detectable contamination from the crucible was encountered when a tantalum system was used.

The slag from a regular reduction was removed and the extractant, such as YF_3 and $CaCl_2$, was added to the alloy in the crucible. The alloy and salt phases were brought to the molten state (950°C), the stirrer was lowered to the fused salt-alloy interface and rotated slowly for approximately 30 min to insure adequate mixing during the extraction.

A mixture of YF_3 and $CaCl_2$ was investigated extensively as the extractant salt. Extractions with mixtures of varying composition were run on 1200-g portions of Y-Mg alloy of uniform composition. In one series a fixed quantity of YF_3 was used and the amount of $CaCl_2$ was varied. From this it was observed that the $CaCl_2$ concentration is not critical as long as enough is present to flux the YF_3 properly.

In another series the amount of $CaCl_2$ was held constant and the amount of YF_3 was varied. As is seen from the data in the upper half of Table III, 650 g of fluoride in the extractant produces the maximum purification and increased amounts have no additional effect. Since the alloy contains a sufficient amount of residual calcium to reduce approximately 150 g of YF_3, no decrease in the oxygen content was observed when this amount of fluoride was used in the extractant mixtures.

Further understanding of the extraction process was gained from experiments using two different grades of YF_3 and Y-Mg alloy. The data in Table III show the effect of the oxygen concentration in the alloy and in the YF_3 on the amount of extractant required to produce the maximum decrease in oxygen content. For alloy containing 0.20 wt % oxygen, only 650 g of high-purity YF_3 (0.04 wt % oxygen) was required to decrease the oxygen content of the yttrium to 0.05 wt %, whereas a greater quantity of the lower grade fluoride was required to produce the same purification. For alloy containing 0.5 wt % oxygen, the 650-g quantity of high-purity fluoride did not give metal of maximum purity, although the oxygen content was lowered appreciably. A greater amount of this quality of YF_3 was required to decrease the oxygen content of the alloy from 0.50 to 0.06 wt %.

In an attempt to determine if the form of the oxide influences the distribution of oxygen between the two phases, 0.1 wt % of oxygen was added as MgO, CaO, Y_2O_3, and YOF to successive reductions. As was indicated earlier in this paper, oxygen from all of these compounds is transferred to the alloy phase in the reduction step. The results of this series of experiments indicated that the form of the oxide in the reduction charge does not appear to have any effect on the degree of purification obtained by the fused salt treatment.

Other salt mixtures were investigated as possible extractants of oxygen and fluorine from the Y-Mg alloy. The results of a series of tests using various extractants on alloy initially containing 0.20 wt % oxygen and 0.12 wt % fluorine are summarized in Table IV. The data in the table show that both oxygen and fluorine are extracted by fused YCl_3 and that the fluoride content can be lowered substantially by a contact with $CaCl_2$.

As can be seen from Table IV the purest metal was obtained by extraction with YF_3-$CaCl_2$ followed by a second extraction with YCl_3. This two-stage extraction was performed several times to ascertain the reproducibility of the method. Yttrium metal of the purity shown in Table V was obtained on repeated experiments. The metal prepared in this way was used for metal evaluation, determination of physical constants, and microscopic examination.

The extractant salts are readily recoverable and can be reduced to the metal or used again in refining experiments. The $CaCl_2$ is leached from the salt mixture and anhydrous HF gas is passed over the residual fluoride at 750°C. This results in a quality of YF_3 equivalent to that of the original material. The YCl_3 likewise can be reclaimed by vacuum sublimation.

Table III. Results of experiments using YF_3-$CaCl_2$ extraction mixtures on 1200-g portion of Y-Mg alloy

Oxygen content of* initial alloy, wt %	Wt % O† in YF_3	Grams of YF_3 in extractant mixture	Wt % O in Y† after extrac.
0.20	0.04	1650	0.052
0.20	0.04	1150	0.053
0.20	0.04	650	0.060
0.20	0.04	150	0.210
0.20	0.22	1150	0.063
0.20	0.22	650	0.112
0.50	0.04	1150	0.065
0.50	0.04	650	0.137

* Based on yttrium metal content.
† Spectroscopic values (8).

Table IV. Experiments with various fused salts as extractants for Y-Mg alloy

Extractant salt	Analysis of yttrium after extraction	
	Wt % O	Wt % F
$CaCl_2$	0.170	0.045
YF_3-$CaCl_2$	0.050	0.070
YCl_3	0.060	0.035
Double extraction with YF_3-$CaCl_2$	0.030	0.070
YF_3-$CaCl_2$ followed by YCl_3	0.018	0.007

Table V. Analyses of yttrium metal refined by double extraction method

Impurity	Wt %	Impurity	Wt %
Iron	0.030	Copper	0.004
Nickel	0.020	Nitrogen	0.002
Oxygen	0.015	Calcium	0.001
Silicon	<0.015	Hydrogen	0.001
Tantalum	<0.010	Magnesium	0.001
Carbon	0.009	Titanium	0.001
Fluorine	0.006	Total rare earths	<0.050

Electron beam melting and zone refining.—Several pounds of yttrium sponge containing 0.045 wt % oxygen and 0.060 wt % fluorine were electron-beam melted by the Temescal Metallurgical Corporation. Analysis of the ingot after two melting operations gave 0.045 wt % oxygen and 0.004 wt % fluorine.

An yttrium rod containing 0.052 wt % oxygen and 0.065 wt % fluorine was zone refined at a rate of 6 in./hr. After two zone passes, segments of the bar were again analyzed. The oxygen content showed no significant change, but the fluorine content decreased to 0.002 wt %. No differences were observed in the oxygen or fluorine concentrations at either end of the zone-melted region.

Thus, it appears that fluorine can be removed from yttrium metal by electron beam melting and by zone refining, *in vacuo*, but oxygen is not affected. The major portion of the fluorine is removed as a volatile compound in both methods although the exact species has not been determined.

Properties of Yttrium Metal

Although many of the physical properties of yttrium have been measured previously, a few properties of the higher purity yttrium obtained from this investigation were determined for purposes of comparison. Melting points have been observed from as low as 1450°C to as high as 1550°C for metal of differing purity. Eash (9) reported a value of 1515°C on metal that contained 0.2 wt % oxygen as the major impurity. Since the lattice parameters and melting point of a metal are often sensitive to oxygen content, it appeared desirable to determine these constants for the purer metal. The melting point of 99.9% purity yttrium prepared in this investigation was determined to be 1495° ± 5°C. This determination was made using an optical pyrometer method (10) in which a small hole was drilled into an yttrium rod. The specimen was heated by passing a high current through it, and the temperature within the hole was continuously observed until melting was evident.

Likewise, there are differences in the reported lattice parameters of yttrium. Spedding, Daane, and Hermann (11) reported values of $a = 3.6474$Å and $c = 5.7306$ for the metal that was available to them while parameters of $a = 3.662$Å and $c = 5.752$Å were obtained for the metal prepared in this investigation. The theoretical density of this material was 4.46 g/cc as compared with a measured density of 4.45 g/cc.

Yttrium metal of this quality has a hardness of 35-45 Brinell (500 kg load) and can be worked extensively at room temperature. A specimen was rolled from an original thickness of 0.250 in. to a final thickness of 0.012 in. with no intermediate anneal. This represents a reduction in thickness of greater than 90%. A photograph of the original coupon and of a section of the 18-in. ribbon obtained by cold rolling is shown in Fig. 3. A cylinder, 0.25 in. in diameter before swaging, is shown in the photograph; another cylinder, 0.125 in. diameter after cold swaging, is also shown.

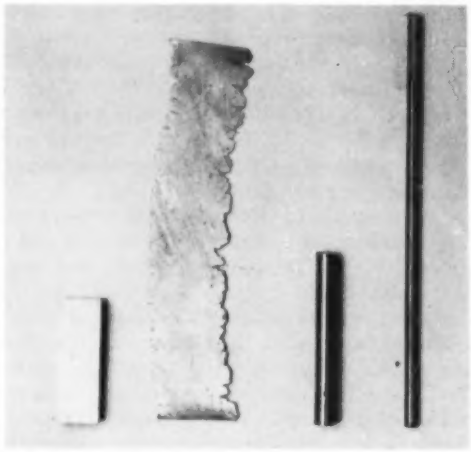

Fig. 3. Yttrium specimen before and after cold rolling to 90% reduction in thickness (left) and before and after swaging (right).

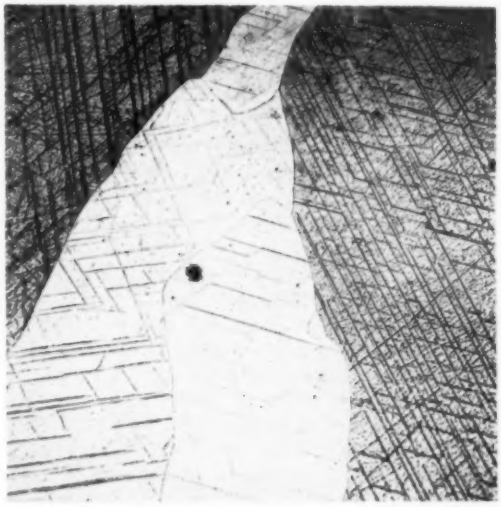

Fig. 4. Grain structure of yttrium metal of 99.9% purity. Etchant: conc. HNO_3. Magnification 250X.

Photomicrographs of yttrium metal of 99.9% purity are shown in Fig. 4 and 5. The coarse grain structure of the arc cast metal can be seen from Fig. 5. The lines that extend across the grains are characteristic of high-purity yttrium. These appear to be deformation bands believed to have been introduced by strains during solidification.

Summary

A process for preparing yttrium metal is described. The basic process consists of the formation of a low-melting intermediate Y-Mg alloy which is subsequently converted to yttrium sponge metal.

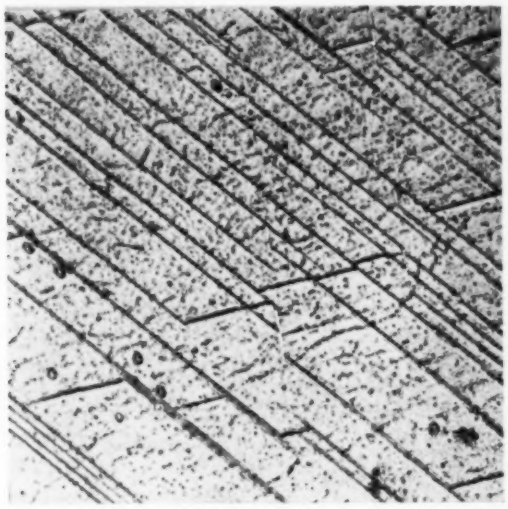

Fig. 5. Enlargement of same area as Fig. 4 showing deformation bands and small inclusions. Magnification 500X.

Several refining procedures are described. One of these involves the extraction of oxygen from the molten Y-Mg alloy by a fused salt containing YF_3 or YCl_3. Fluorine can be removed by an extraction treatment on the alloy or by electron beam melting or zone refining of yttrium metal.

Yttrium metal of 99.9% purity was prepared by methods described in this paper. The melting point, lattice parameters, and hardness were determined on metal of this purity and the cold working characteristics and microstructure were studied.

Acknowledgments

The authors would like to express their gratitude to Dr. V. A. Fassel and members of the spectroscopic group of the Ames Laboratory and to Dr. C. V. Banks and his associates for performing the multitude of chemical analyses. They would like to acknowledge the assistance of C. Moore, I. Jensen, M. Hedberg, R. Griffith, E. Ritland, and M. Thompson in performing these experiments.

Manuscript received Nov. 20, 1959. This paper was prepared for delivery before the Chicago Meeting, May 1-5, 1960. Paper is Contribution No. 815; work was performed in the Ames Laboratory of the U. S. Atomic Energy Commission.

Any discussion of this paper will appear in a Discussion Section to be published in the December 1960 JOURNAL.

REFERENCES

1. R. W. Fisher and C. B. Fullhart, *2nd International Conf. on Peaceful Uses of Atomic Energy*, **7**, 216 (1958).
2. A. P. Thompson, W. B. Holton, and H. C. Kremers, *Trans. Am. Electrochem. Soc.*, **49**, 442 (1926).
3. M. F. Trombe and M. F. Mahn, *Compt. rend.*, **220**, 778 (1945).
4. A. H. Daane and F. H. Spedding, *This Journal*, **100**, 442 (1953).
5. C. V. Banks, O. N. Carlson, A. H. Daane, V. A. Fassel, R. W. Fisher, E. H. Olson, J. E. Powell, and F. H. Spedding, "Studies on the Preparation, Properties and Analysis of High Purity Yttrium Oxide and Yttrium Metal," Report IS-1, p. 13, (July 1959).
6. J. F. Smith, O. N. Carlson, and R. W. Vest, *This Journal*, **103**, 409 (1956).
7. E. D. Gibson aond O. N. Carlson, ASM Preprint No. 146; to be published in *Trans. Am. Soc. Metals*, **52**.
8. C. V. Banks, *et al.*, *op. cit.*, p. 125.
9. D. T. Eash and O. N. Carlson, ASM Preprint No. 142; to be published in *Trans. Am. Soc. Metals*, **52**.
10. H. A. Wilhelm and P. Chiotti, *Trans. Am. Soc. Metals*, **42**, 1295 (1950).
11. F. H. Spedding, A. H. Daane, and K. W. Hermann, *Acta Cryst.*, **9**, 559 (1956).

Manuscripts and Abstracts for Spring 1961 Meeting

Papers are now being solicited for the Spring Meeting of the Society, to be held at the Claypool Hotel in Indianapolis, Ind., April 30, May 1, 2, 3, and 4, 1961. Technical sessions probably will be scheduled on Electric Insulation, Electronics (including Luminescence and Semiconductors), Electrothermics and Metallurgy, Industrial Electrolytics, and Theoretical Electrochemistry.

To be considered for this meeting, triplicate copies of abstracts (*not exceeding 75 words in length*) must be received at Society Headquarters, 1860 Broadway, New York 23, N. Y., *not later than January 2, 1961. Please indicate on abstract for which Division's symposium the paper is to be scheduled and underline the name of the author who will present the paper.* Complete manuscripts should be sent in triplicate to the Managing Editor of the JOURNAL at the same address.

Presentation of a paper at a technical meeting of the Society does not guarantee publication in the JOURNAL. However, all papers so presented become the property of The Electrochemical Society, and may not be published elsewhere, either in whole or in part, unless permission for release is requested of and granted by the Editor. Papers already published elsewhere, or submitted for publication elsewhere, are not acceptable for oral presentation except on invitation by a Divisional program Chairman.

Exchange Current Measurements in KCl-LiCl Eutectic Melt

H. A. Laitinen, R. P. Tischer,[1] and D. K. Roe[2]

Department of Chemistry and Chemical Engineering, University of Illinois, Urbana, Illinois

ABSTRACT

Exchange currents have been measured of some liquid and solid metal electrodes (Cd, Zn, Pb, Bi, Ag, Ni, Pt) and one redox system (V^{2+}/V^{3+}) in a KCl-LiCl eutectic melt at 450°C. Measurements over a hundredfold concentration range permitted calculation of the heterogeneous rate constant and of the transfer coefficient. Two relaxation methods were used: the double pulse method as developed by Gerischer and Krause and the voltage step method as described by Vielstich and Delahay. In cases where both methods were applied independently to the same system the results were in good agreement. The purity of the eutectic melt was improved considerably by filtration and by displacement of heavy metal ion impurities with metallic magnesium. The evaluation of voltage step measurements was revised by allowing for the effect of the finite charging time of the double layer. Agreement was not found with the theory of the double pulse method given by Matsuda, Oka, and Delahay, perhaps because of some additional process, other than diffusion, taking place in a period of time comparable to the duration of the first pulse. On the basis of the reaction of platinum with cadmium at 450°C it is possible to account for the observations made earlier in this laboratory by C. H. Liu and H. C. Gaur on the emf and polarization behavior of cadmium-plated platinum electrodes.

In recent years the increasing importance of fused salts in many fields of science and technology has incited a considerable number of investigations of their properties. Molten salts have found much interest as media for electrochemical processes in connection with their applications in metallurgy, analytical and synthetic chemistry and, more recently, in high-temperature galvanic cells. Relatively few studies, however, have been made of the rates of electrode processes in molten salts, because such electrode processes can be expected to be very fast and their study would therefore require elaborate techniques. The relaxation methods developed recently for the study of fast reactions in aqueous solutions are most suitable for fused salt studies. Doubts have sometimes been expressed as to whether these methods would be able to avoid the interference of diffusion as a rate-determining process, since diffusion in molten salts (1) is often not faster than in aqueous solutions at room temperature. It is possible, however, to distinguish between diffusion-controlled and charge transfer controlled reactions even in fused salts, and diffusion effects can be eliminated under the proper experimental conditions.

The first successful application of a relaxation method to electrode reactions in fused salts was made by Randles and White (2). In a low melting nitrate eutectic the rate of the reaction $Ni^{2+} + 2e^- + Hg = Ni(Hg)$ was evaluated from a-c impedance measurements. Measurements were attempted on several other metal ion-metal amalgam reactions, but they were found to be too rapid for the method.

Laitinen and Osteryoung (3), about the same time, sought to use the same a-c technique with platinum electrodes in the KCl-LiCl eutectic. Direct interpretation of the measurements was not possible because of complicating experimental conditions which caused a very large frequency dispersion of the resistance and capacitance measurements.

Under more amenable experimental conditions, primarily with a melt prepared from dry salts, Laitinen and Gaur (4) were able to make more refined measurements of the same type. Although the frequency dispersion of the measurements on platinum microelectrodes was still present, the data were interpretable by the introduction of a correction for adsorption of the reducible ion (5). The correction was necessary to remove the "inverted" character of the reaction impedance, in which the resistive component is smaller than the capacitative component. While there is no direct evidence that this is a valid correction, the resulting exchange currents for the cadmium and zinc couples appear to have reasonable values, as will be confirmed in this paper.

Hill (6) measured the impedance behavior of silver electrodes using $AgNO_3$ as the solute in a ternary nitrate melt, of silver-plated tungsten electrodes in LiCl-KCl eutectic containing dissolved AgCl, and of tungsten electrodes in Ti(III)—Ti(II) systems in the LiCl-KCl eutectic. In all cases the residual capacity and resistance of the solvent were markedly frequency dependent Many of the faradaic impedance plots were "inverted."

Interpretation of a-c impedance measurements requires the elimination of the double layer capacity. The residual capacity has, in general, been found to be a function of frequency in fused salts. The other relaxation methods, potential step and current step, are made at relatively very short times, which corresponds to high frequencies in the a-c method,

[1] Present address: Gebr. Böhler and Co. AG, Düsseldorf-Oberkassel, Germany.
[2] Present address: Shell Development Co., Emeryville, California.

and should be less ambiguous since the measured resistance and capacitance show less frequency dispersion at high frequencies.

The double pulse method developed by Gerischer and Krause (7) is potentially capable of measuring extremely rapid electrode reactions. The problem of charging the double layer is dealt with directly by the use of two current pulses. The first pulse is as short as possible (1 μsec) and is adjusted in height to just charge the double layer. The second pulse is much smaller and of longer duration. The overvoltage resulting from the second pulse is measured directly with an oscilloscope.

A theoretical analysis of the double pulse method has been given by Matsuda, Oka, and Delahay (8). They show that the concentration change at the electrode surface during the charging pulse cannot always be neglected and that the true reaction resistance can be obtained by extrapolation to zero duration of the first pulse.

The other method used in this investigation is the voltage step method (9). In principle, it is a potential step method, but a reference electrode provided with a Luggin capillary is not used. The voltage applied to the cell is constant, but the potential of the indicator electrode is not constant during the passage of current because of the changing iR drop in the cell. The actual potential can, however, be obtained by subtracting the product of the measurable current and resistance from the known voltage step. The charging current, of course, obscures the oscilloscopic observation of the kinetically controlled current during the initial period of electrolysis, so an extrapolation procedure is used. The method is well suited to fused salt measurements because of the low cell resistance; the charging current duration is thereby shortened. It has the obvious limitation that, with very rapid reactions, diffusion may become the rate-controlling process before the charging is completed. It is possible, however to distinguish between kinetic and diffusion control from the current-time behavior.

Theoretical

Relaxation methods which employ pulse techniques depend on current or voltage measurements at very short times, before diffusion becomes the rate-determining process. During the first moment of electrolysis a large fraction of the current charges the double layer and prevents direct observation of the faradaic process.

In the double pulse method (7) this problem is overcome by charging the double layer with a very short current pulse. The electrolyte resistance is compensated for by a bridge circuit as shown in Fig. 5 in the experimental section. The height of the first pulse is adjusted so that the potential transient, after the charging pulse, starts out with a horizontal tangent, the idea being that the potential for a short moment is constant and therefore the entire current is faradaic because no portion of the current is used for charging. From the potential measured at this moment and from the magnitude of the second pulse measured by the potential drop across the compensating resistor it is then possible to calculate the transfer resistance X, from which the exchange current density is obtained by

$$i_o = \frac{RT}{n\mathbf{F}XA} \qquad [1]$$

where A is the electrode area and the other symbols have their usual significance. One of the limits of this method is encountered with high rates corresponding to very low transfer resistances that are less than 1% of the electrolytic resistance. There are two reasons for this limitation: (a) It is not possible to adjust the compensating resistor for the electrolyte resistance accurately enough by the available procedure. (b) For a ratio of electrolytic resistance to transfer resistance equal to 100, the differential input of the amplifier must be balanced to within 0.1%, even if an accuracy of only 10% is required in measurement of the transfer resistance. This difficulty can be overcome to a certain extent by using lower concentrations. Unfortunately there then arises the other difficulty, mentioned in the original paper by Gerischer and Krause (7) and analyzed quantitatively by Delahay and co-workers (8), that diffusion becomes rate determining after a time comparable to the duration of the charging pulse. Thus the range of concentration that can be investigated successfully with this method becomes smaller and smaller with increasing reaction rate.

In the voltage step method (9) the faradaic current, observed after the charging current has become negligible, is extrapolated back to zero time. The calculation of the exchange current density is immediate from the measured "zero time" current $i_{t=0}$, the known voltage step V and the total resistance of the system R_T. Similar to the above equation

$$i_o = \frac{RT}{n\mathbf{F}A} \frac{i_{t=0}}{(-V - i_{t=0}R_T)} \qquad [2]$$

The sign of V is given by the European convention; when negative, the current is cathodic (positive). Therefore the quantity on the left is always positive, as it should be.

The definition of the exchange current density is

$$i_o = n\mathbf{F}k_s^\circ C_{Ox}^{1-\alpha} C_R^{\alpha} \qquad [3]$$

where k_s° is the standard heterogeneous rate constant at the standard (formal) potential of the couple, C_{Ox} and C_R are the concentrations (in mole cm^{-3}) of the oxidized and reduced forms of the couple and α is the transfer coefficient. From a series of measurements at different concentrations the transfer coefficient is obtained from the slope of a plot of log i_o vs. log C_{Ox} (C_R is constant in the case of a metal/metal ion system using pure metal electrodes). The value of k_s° can then be calculated from Eq. [3]. In the case of a redox system, such as V^{3+}/V^{2+}, it was more convenient experimentally to vary the ratio by oxidizing V^{2+} to V^{3+} with a constant current. The transfer coefficient was calculated by plotting i_o/C_O vs. C_R/C_O, since

$$i_o/C_{Ox} = n\mathbf{F}k_s^\circ (C_R/C_{Ox})^{\alpha} \qquad [4]$$

The current which charges the double layer obeys the relation

$$i_{c_0} = \frac{V}{R_T} \exp\,(-t/R_T C_{dl})$$

where C_{dl} is the differential double layer capacity. In the essential absence of any reducible or oxidizable species, only the charging current will be observed. A semilogarithmic plot of current vs. time has an intercept of V/R_T and a slope of $1/(2.303R_TC_{dl})$. In this way the solution resistances were measured. Also a series of measurements was made over 1.8 v potential range, from which a differential double layer capacity/potential curve was calculated (see Fig. 14).

In the voltage step method, it is assumed that the kinetically controlled current rises instantaneously to a maximum after the application of the voltage step and then decreases linearly with the square root of time until diffusion becomes rate determining. During the charging of the double layer, the potential of the electrode is given by

$$V_t = V[1-\exp(-t/R_TC_{dl})]$$

assuming that the faradaic current is much smaller than the charging current. From this equation it is obvious that the potential is zero at the instant the voltage step is applied. Therefore the kinetic current is not at a maximum, but is zero. During the next several microseconds, the kinetic current should increase as the potential increases and finally reach a maximum when the charging current becomes negligible. Therefore the extrapolated value of the kinetically controlled current at zero time is larger than it should be because the observed current is higher than the current theoretically derived for the condition of infinitely rapid charging of the double layer.

In Fig. 1 is shown the experimental current-time curve of the reduction of V^{3+} to V^{2+}. The charging current is also shown, as measured at the same potential with the same platinum microelectrode. The difference between the two curves is the faradaic current and the figure shows that it corresponds with the general shape described above. In the bottom half of the figure is plotted the current against the square root of time; the linear portion has been extrapolated to zero time. This extrapolation was then transferred to the top graph.

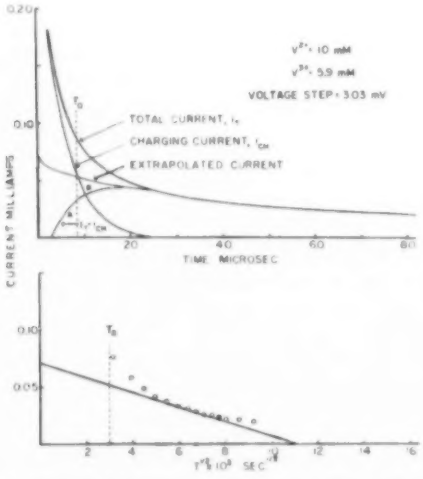

Fig. 1. Current-time curve of V^{3+}/V^{2+} and charging curve

If the charging current were not finite in duration, the faradaic current would have a value at zero time which would be somewhat lower than that shown in the lower graph of Fig. 1. Therefore at one point, which may be called the "effective zero time," the extrapolated faradaic current is equal to the hypothetical current at zero time. This point has been chosen in a way which is only a first approximation, but is nevertheless intuitively satisfying. A vertical line is drawn on the current time graph at such a point, t_o, on the time axis, that the area A under the faradaic current-time curve to the left of the line is equal to the area B between the extrapolated and the observed curves. The current value on the extrapolated line at t_o is then called the "effective zero time" current, i_{t_o}, and is used to calculate the exchange current. The potential across the cell at the same time is equal to the applied voltage, V, minus the product of the total current, i_T, and the total resistance, R_T. The current i_{t_o} is smaller than the extrapolated current at $t = 0$, but the total current, faradaic plus charging, is larger so that the iR correction is larger. Since the exchange current is proportional to the quotient of the current and the corrected voltage step, $(-V - iRT)$, the two effects tend to cancel.

In the treatment of the experimental data, the above method of calculating the exchange current resulted in a significant improvement in the case of the slower reactions. The values for zinc and cadmium, calculated by both methods were within 4% of each other, which is less than the experimental error. However if the circuit resistance was increased, so that the charging time was longer, great deviations in the calculated exchange current resulted unless the modified procedure was applied.

Experimental

Preparation and purification of the KCl-LiCl *eutectic melt.*—Reagent grade KCl and LiCl require extensive drying as well as purification before the resulting eutectic melt is suitable for electrochemical studies. Prolonged vacuum drying and the use of HCl gas during the fusion of the salts has been shown to remove all of the water and reverse the hydrolysis of LiCl (10, 11). Further purification is necessary to remove the heavy metal ion impurities and the decomposition products of what is presumably an organic solvent residue.

The most convenient and expedient method for the removal of heavy metal ions, which are present to the extent of 0.0005% or about 0.4 mM in the molten eutectic (calculated as lead), was found to be simple displacement with a more active metal. Magnesium is ideally suited in this medium because of its very negative standard potential (−2.58 v vs. 1M platinum reference electrode) (12). It is expected that the small concentration of Mg^{2+} will have a negligible effect on the electrode processes of interest here; the most active metal used was zinc, with a standard potential of −1.56 v (12).

The index of melt purity used in this laboratory is the residual current (10), measured with a 26-

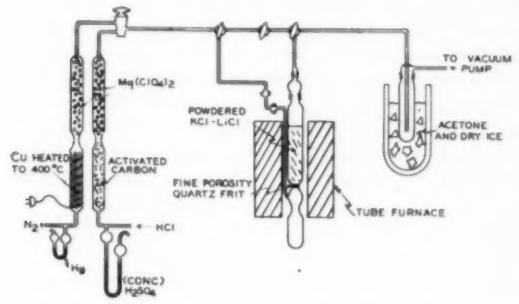

Fig. 2. Apparatus for purifying the melt

gauge platinum microelectrode, ground flat to expose only the cross section of the platinum wire, with an apparent area of 0.13 mm^2. In melts treated with magnesium, the residual current was in the range of 0.08 to 0.4 μa at a potential of −2.0 v vs. a platinum reference electrode. Up to a potential of about −1.5 v, the residual current was anodic by a few hundreths of a microampere. Without treatment with magnesium, the residual current was cathodic over the entire potential range, reaching about 1 to 2 μa at −2.0 v.

Individual batches of the eutectic melt were prepared in the apparatus shown in Fig. 2. Approximately 150 g of KCl-LiCl eutectic mixture, previously powdered in a ball mill, was placed in the vertical Vycor tube. A few tenths of a gram of magnesium turnings or powder was added to the salts. The pressure was reduced to 0.01 mm Hg by a Cenco vacuum pump. After about 12 hr of vacuum drying at room temperature, the furnace was turned on and the temperature was increased slowly over a 36-hr period. Before the temperature increased to the melting point of the eutectic (352°C), the system was vented to dry HCl gas, which had been passed over activated carbon to remove possible hydrocarbon impurities. When the salts were molten, additional HCl was admitted through the small side tube and up through the fine porosity quartz frit. Treatment with HCl for 1 hr is more than enough to drive out the last traces of water. The apparatus was then evacuated with a water aspirator, connected to the system through the dry ice-acetone trap, to remove the HCl gas. Three evacuations, each followed by a nitrogen flush through the quartz frit, removed nearly all of the HCl. Then the molten eutectic was filtered by evacuation below the quartz frit. The ampoule was heated with a gas burner during the filtration. When the process was completed, the tube furnace was raised to expose the constriction in the tube, just below the Vycor-Pyrex graded seal, and the ampoule was sealed off with a torch. When the eutectic mixture is cool, it will not stick to the walls of the ampoule if it is completely dry. "Wetting" of the glass is indicative of the presence of oxide (13).

Fused salt apparatus.—The major part of the apparatus is similar to that previously used in this laboratory (10, 12). The melt was contained in a 6-cm diameter Pyrex tube, about 35 cm long. After thorough cleaning with boiling 70% $HClO_4$, the tube was dried and the ampoule was placed inside. The tube was then heated under vacuum for a time, to remove surface water from the glass. Before the melting point of the eutectic was reached, the system was vented to dry, oxygen-free argon, and the ampoule tip was broken. When the eutectic became molten, the ampoule was raised to allow the melt to drain out and then removed. The cell compartments were then added. In these kinetic studies, simple 20 x 100 mm test tubes were used as cells. The resistance of the cells was reduced somewhat by slightly blowing out the side of the tube, or by sealing in a fritted glass disk. The other electrodes, platinum reference and carbon rod, were contained in the usual fritted glass tubes. The microelectrode was positioned just above the counter electrode in the same compartment. Cell resistances were of the order of 2-3 ohms. Silicone stoppers, because of their superior heat resistance, were used to cover the opening of the cell.

The furnaces were of the vertical tube type and had small windows or peepholes in the side to facilitate the adjustment of the electrodes. Temperature control was provided by proportional or on-off controllers. Short time variations were less than 1°C.

A flowing atmosphere of argon, dried with $Mg(ClO_4)_2$ and deoxygenated over hot copper, was maintained at all times to prevent the entrance of air and moisture.

Electrodes.—Two basic microelectrodes were used in all the kinetic measurements: tungsten sealed in Pyrex or uranium glass and platinum sealed in "soft" glass. Although lead glass (Corning 0120) makes a very good seal with platinum, the lead ions in the immediate vicinity of the seal are reduced when the electrode is used in fused salts at 450°C. This reduction is evidenced by a hump in the polarographic current voltage curve, starting at about −0.9 v vs. a platinum reference electrode. The shape of the hump depends on the polarization rate, but the area under the curve is the same for a given electrode. After a cathodic polarization, the metal-glass seal is black; anodization restores the original appearance of the seal. Several other "soft" glasses were tried, but they either failed to maintain a tight seal with the platinum or were quickly etched by the molten salts. Upon request, the Corning Glass Works kindly prepared a special batch of glass (Corning 010, G-164-EC) which was no longer available. This glass contains no lead oxide, has a very low conductivity and a coefficient of thermal expansion close to that of platinum. Although this glass is slightly etched after several hours in the melt at 450°C, in all other respects it is very satisfactory.

It was found that platinum does not serve as a suitable indicator electrode when coated with a liquid film of low melting metal such as cadmium, zinc, or bismuth. To illustrate the effect, the results of a brief study of the alloying of platinum with cadmium at 450°C will be given. A piece of platinum foil of 1 cm^2 area was plated with 10 mg of Cd from aqueous solution. Upon heating in an evacuated tube for 1 hr at 450°C, the weight of the specimen was unchanged. Upon dissolving the cadmium with

aqueous HCl, a spongy layer of platinum was left on the surface. The total weight of platinum was unchanged; the weight of the spongy layer which was presumed to have been alloyed was determined by carefully scraping it off and weighing it by difference. From the weight of the cadmium and spongy platinum, the composition of the alloy was calculated to be 64 mole % Cd and 36 mole % Pt. This corresponds closely to a compound Cd_2Pt, which has long been known (14) and which has a melting point of 745°C (15). Platinum dissolves readily in liquid Cd at 450°, but with a limited film of Cd, the solid alloy Cd_2Pt is formed and its further diffusion into Pt is very slow. The standard potential of a liquid Cd pool, measured with a tungsten contact, calculated from several series of potential-concentration measurements, differed only 6 mv, in the negative direction, from the value reported by Laitinen and Liu (12). The latter values had been obtained by measurements with a platinum microelectrode soon after plating it during the course of recording a cathodic polarogram. Similarly, the potential of a freshly zinc plated platinum electrode agreed with that of a pure zinc pool. The only potential which was found to be significantly different was that of bismuth, as reported elsewhere in this paper. It is probable that the surface alloy formation of cadmium and zinc may be responsible for the very different results reported (4) from a-c and steady-state current-voltage measurements for the kinetics of the cadmium and zinc couples at plated platinum surfaces.

Tungsten electrodes were prepared from 0.7 to 1 mm diameter rods sealed into Pyrex or uranium glass. The cross-sectional surface was polished to a mirror bright finish with 4/0 emery paper. Prior to use, the surface was cleaned in alkaline hydrogen peroxide, rinsed, and dried. Tungsten was not used as the active electrode material. When a clean tungsten microelectrode was inserted into a pool of liquid cadmium or zinc, a small droplet of the metal would adhere to the surface. This type of microelectrode has many of the advantages of a hanging mercury drop, but the area is not reproducible. Since no evidence of surface contamination with time has been found, the practice was to use the same droplet for a series of measurements at different concentrations. The area was determined by measuring the dimensions of the solidified metal with an ocular micrometer. The geometry of the drop corresponded satisfactorily to a segment of a sphere.

The other liquid metals, i.e., bismuth and lead, used in the kinetic studies would not adhere to a clean tungsten surface. Consequently, bismuth was plated onto the same type of electrode from a concentrated solution of Bi^{3+} in the melt. A layer of about 10^{-3} mm thickness exhibited the same potential as a bismuth pool; the activity of the deposit was therefore unity. Visual inspection showed that the entire surface was covered with bismuth. An alternate method was used to make a lead electrode. The cross section of a tungsten-Pyrex seal was ground out to a small cup and the end of the electrode was bent 180°. The reproducibility of the size of the lead drop in the cup was not satisfactory, and there was a variation of the cell resistance and measured data with changes of the position of the drop in the cup.

Microelectrodes of the metals which are solids at 450°C were made by plating platinum electrodes of the type described with the desired metal from aqueous solutions. The deposit was lightly polished with emery paper and washed with water. The apparent surface area was used in the calculation of the exchange current density.

In the kinetic measurements of the V^{3+}/V^{2+} couple, a platinum ball electrode was used. The end of a 26-gauge platinum wire was heated just to the melting point in a hydrogen-oxygen flame. If the wire was then removed slowly from the flame, a very smooth sphere resulted. This was sealed into Corning G-164-EC glass so that only a hemisphere of platinum was exposed. From differential capacity measurements, with an a-c bridge, at a frequency of 1000 cycles sec^{-1}, in 1M $HClO_4$ solution, it was shown that the roughness factor of this type of electrode is about half the roughness factor of a platinum microelectrode polished with 4/0 emery paper. Comparisons were also made with a piece of platinum foil which had a known roughness factor[3] of 1.12. At a potential of +0.6 v vs. SCE, the capacity/cm^2 (apparent) of the "fire polished" ball was nearly the same as the capacity/cm^2 (true) of the platinum foil.

The low melting metals were added to the test tube compartments as liquids. The cleaned and dried pieces of metal were melted above the compartment in an argon filled Pyrex tube, ending in a small capillary. If any metal oxide was present, it tended to cling to the walls of the tube above the capillary. Electrical contact with the pool counter electrode was made with a tungsten rod sealed in Pyrex; the end of the rod protruded a few millimeters beyond the seal.

Counter electrodes of the metals which are not liquids at 450°C were made from foils of the metal under investigation. A large piece of about 12 cm^2 area was fashioned into a right cylinder. Electrical contact was made with a platinum wire spot welded to the foil.

After the counter-electrode was in the filled cell, the potential was measured against a platinum reference electrode. Even in the most carefully purified melts, the potential corresponded to a low concentration, 0.3 to 0.4 mM, of metal ions. With noble metals, such as platinum and bismuth, the spontaneous concentration was much lower (0.01 to 0.05 mM), as might be expected. If magnesium had not been used in the purification of the melt, the spontaneous concentration was several millimolar. The potential also became more positive with time, indicating an increase in the concentration. It is suspected that silica, leached from the glass, is responsible for the slow oxidation of most of the metals studied.

The concentration of the metal ion was changed by anodizing the counter electrode with a constant current for a known time. From the potential meas-

[3] The roughness factor of a 100-cm^2 area foil was evaluated by the krypton adsorption (B.E.T.) method through the kind cooperation of Professor Norman Hackerman, of the University of Texas.

urements at each concentration, it is possible to calculate the initial concentration. Analysis of the contents of several cells after the experiments confirmed the reliability of this procedure.

Vanadous solutions were prepared by anodizing vanadium metal. It was then necessary to filter the solution into another compartment, because finely divided vanadium metal appeared in the solution. A platinum foil cylinder was placed in the solution to oxidize a fraction of the vanadous ions to the vanadic state with a constant current. The solution was vigorously stirred to avoid concentration polarization. The platinum foil also served as the unpolarizable counter electrode during the kinetic measurements.

Platinum reference electrodes were constructed and used exactly as previously reported (16). The same is true of the carbon rods used as working electrodes for the anodization and cathodization of metals and solutions. The volume of the eutectic in the cells was determined by argentometric titration of the chloride.

Electronic equipment-double pulse method.—A block diagram of the electronic circuit for application of the double pulse is shown in Fig. 3. The Tektronix Oscilloscope 535/S2 was used for triggering the pulses. (The delaying sweep of this scope can be released by a push button, which in turn triggers the main sweep.) The gate from the main sweep was fed into the pulse generators, Tektronix 161 and 163, through a capacitor and a resistor. The relative position of the pulses could be adjusted by the input

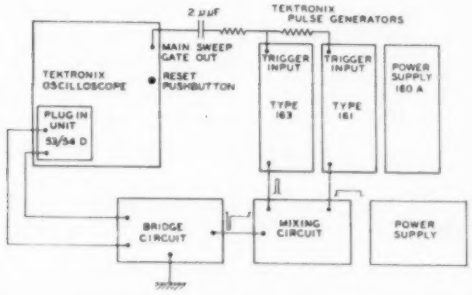

Fig. 3. Block diagram of the electronic circuit for the double pulse method.

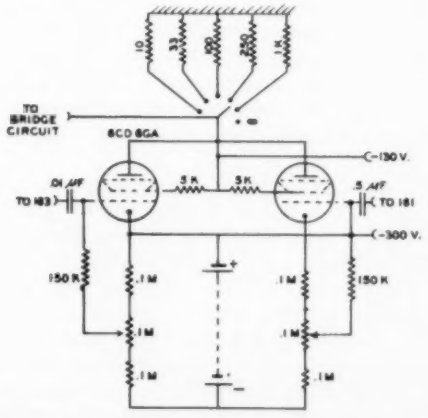

Fig. 4. Circuit for mixing the two pulses

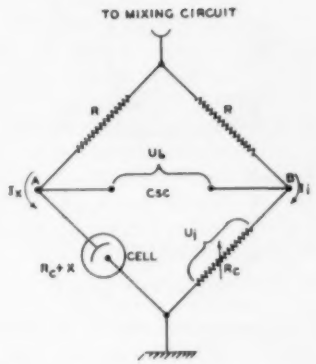

Fig. 5. Bridge circuit for compensating electrolyte resistance.

controls of the generator. The two pulses were mixed in the circuit shown in Fig. 4. The beam power tubes of this circuit are able to pass pulses up to 200 ma. The actual limitation in our measurements was given by the output voltage of the 163 generator which furnished the charging pulse. The grid bias of the beam power tubes was adjusted to a residual current of about 1 μa, which is considered to be negligible. The resistors in the plate circuit were built in for testing purposes. The bridge circuit shown in Fig. 5 was applied as outlined in the introduction. A little slug tuned coil in series with the resistor R_c was used to compensate for the higher inductivity of the cell circuit. In some later experiments two Tektronix 121 preamplifiers were added to improve the frequency response of the system. The rise time was then limited by the pulse generators (0.2 μsec.). The preamplifiers are linear up to an output of 1 v. This limited the current applicable to the cell to

$$\frac{1 \text{ volt}}{\mu(R_c + R_x)}$$

where μ is the amplification of the preamplifiers, R_c is the electrolyte resistance, and R_x is the transfer resistance.

The two pulses used in this method need not be constant current pulses, as has been the usual practice. Using small resistors in the upper branches of the bridge may cause the current to vary somewhat with time, but at the same time improve the frequency response of the equipment. The current I_x, the polarization U_x, and the corresponding transfer resistance X can be calculated from the voltages measured across the bridge U_b and across the compensating resistor U_i with the following formulas:

$$I_x = \frac{U_i R - U_b R_c}{R\ R_x} \cong \frac{U_i}{R_x}$$

$$U_x = \frac{U_b(R + R_c)}{R} \cong U_b$$

$$X = \frac{U_b(R + R_c)R_c}{U_i R - U_b R_c} \cong \frac{U_b R_c}{U_i}$$

The resistors in the upper branches of the bridge are R and the compensating resistor is R_c. The ap-

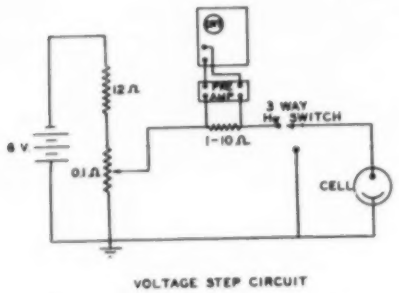

Fig. 6. Circuit for the voltage step method

proximations hold for $R>R_s$. In these measurements U_s was always of the order of magnitude of U_t, or smaller. The above equations, which have been derived for a d-c bridge, should provide a good approximation for the conditions under which the values are measured. From these formulas, an estimate can be made of the necessary value of the resistors in the upper branches of the bridge which will avoid the necessity of corrections in the evaluation. For most of the measurements, resistors R of 10 ohms were used. In checking the effect of the duration of the first pulse, where a constant current is essential, 100-ohm resistors R were substituted without, however, any appreciable difference in results.

Voltage step equipment.—The circuit diagram of the voltage step apparatus is shown in Fig. 6. Its design and function are quite simple. The desired voltage step (usually 2-7 mv) is set by moving the contact on the voltage divider. The exact value was measured to within 0.01 mv with a Student-type potentiometer. The current through the voltage divider was about 0.5 amp, so the resistance across which the voltage step was developed was only 0.005-0.016 ohms. The microelectrode was short-circuited to the counter electrode through the three-way mercury switch. When the switch was moved to the other position, the break occurring before the make, the voltage step was applied between the two electrodes. The current was measured as an iR drop across the precision resistor R_m. The signal was amplified through a video preamplifier (17), modified to operate differentially, and was observed on the screen of a Tektronix 535/S2 oscilloscope equipped with a 53/54 D plug-in preamplifier. The maximum usable sensitivity of the equipment was 0.2 mv/cm and the upper limit of the bandwidth was 0.45 mc. With a 5-ohm measuring resistor, currents could be measured to an estimated $\pm 2\ \mu a$ The accuracy of the electronic equipment was periodically checked with a potentiometer and was always within 1%. Sweep rates of 10 or 20 μsec/cm were generally used.

The current time curves were photographed on 35-mm Kodak Plus-X film. The beam intensity and grid line illumination were adjusted to give only a minimum exposure. The image on the negative was very fine and when enlarged to twice the size of the oscilloscope screen, the lines were less than a millimeter wide. The enlarged curves were traced on graph paper with the aid of a french curve. Current-time points from the traced lines were then plotted as current vs. the square root of time.

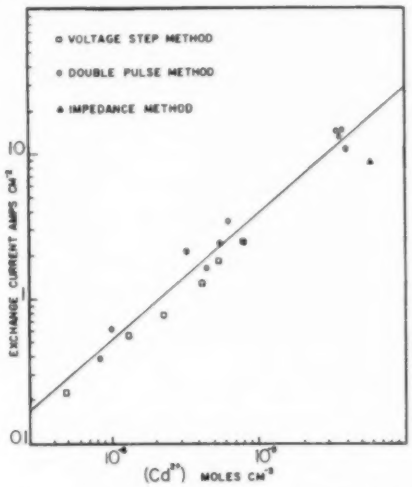

Fig. 7. Exchange currents measured on cadmium

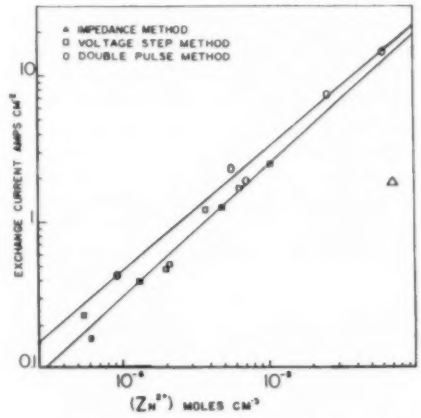

Fig. 8. Exchange currents measured on zinc

Results

Cadmium and zinc.—The cadmium and zinc couples were the first ones studied in this investigation. They were known to be fast reactions, not only from polarographic behavior, but from the a-c impedance measurements (4) described earlier. The earlier impedance measurements were conducted with a polished platinum electrode in melts of a lesser purity. Therefore some difference might be expected between these results and those of Laitinen and Gaur (4).

The exchange currents corresponding to a wide range of Cd^{2+} and Zn^{2+} concentrations are shown graphically in Fig. 7 and 8. On these log-log plots, a linear relation is expected from Eq. [3], with a slope equal to $1-\alpha$. The results of both methods are included on the graphs, as well as the point determined earlier by Laitinen and Gaur. Considering the assumptions that were necessary in the evaluation of the latter experiments and the fact that platinum was used as an electrode, the agreement is surprisingly good.

Each point on the graphs is the average of a series of measurements taken with polarizations between 1 and 10 mv. There was no systematic difference between the results obtained with anodic and cathodic polarizations. The majority of the voltage step measurements were taken in the cathodic direction.

The influence of temperature was investigated in the case of cadmium by measuring the exchange current at 400°, 450°, and 500°C. The activation energy calculated by the Arrhenius equation and was found to be 3 ± 1 kcal mole^{-1}.

Since zinc has a melting point within the range of temperatures investigated, measurements were taken on liquid as well as on solid zinc. Within the limits of accuracy, no difference was observed. This result is similar to the observation of Gerischer and Krause (7) on mercury in a perchloric acid/water eutectic.

Additional experiments were performed with zinc and thallium; no quantitative results can be given for the latter metal because the electrode area was not known. The purpose was to test the influence of the rise time of the double pulse equipment and the extent of the correction obtained when the reaction resistance was extrapolated to zero length of the first pulse. The results for zinc are shown in Fig. 9. Similar behavior was observed with thallium. These results are not in accord with the theory presented by Matsuda, Oka, and Delahay. The dependence of the reaction resistance upon the length of the first pulse was much greater than required by the theory, but still within the over-all limits of accuracy of these measurements (±10%). Calculation of diffusion coefficients from the experimental dependence led to ridiculously low values.

The improvement of the frequency response by using two preamplifiers as mentioned above, enhanced the discrepancies, showing that the poorer rise time of the original equipment was not responsible. Data obtained with and without high rise time equipment differed by 20% when the first pulse was 3 μsec long. But when the values were extrapolated to zero length of the first pulse the results differed by a factor of 2 or more. The shorter the first pulse the bigger was the difference between the two sets of measurements. To explain these results one has to assume some additional process interfering at very short times. The frequency dispersion of the residual capacitance (4) in this melt might be present at these short times. However it does not seem likely that a dispersion which is caused by the establishment of a new steady state on the metal surface with adsorbed ions can occur so rapidly. A quantitative explanation for this effect is still pending and so for the sake of consistency the results listed in Table I are those obtained without taking into account the dependence on the length of the first pulse.

Lead.—With lead, as also with bismuth and thallium, the hanging drop electrode could not be used because the metal did not adhere to the tungsten surface. Double pulse measurements were taken with a lead drop in the cup-type electrode. Results are shown in Fig. 10. The large variation is due to the difficulties encountered with the cup electrode and because of the uncertainty in the surface area measurements. The best results were obtained with a very small drop which did not fill the cup.

Bismuth.—Although the kinetic data for the reaction $Bi^{3+} + 3e^- = Bi(lq)$ lack precision, primarily because of the volatilization of $BiCl_3$ from the melt, there is no doubt that it is the slowest reaction of all those investigated. The transfer coefficient is larger than that of any of the other metal ion-metal couples. Figure 11 illustrates the dependence of the exchange current on the Bi^{3+} concentration as determined by the voltage step method. The "effective zero time" currents were used to calculate the

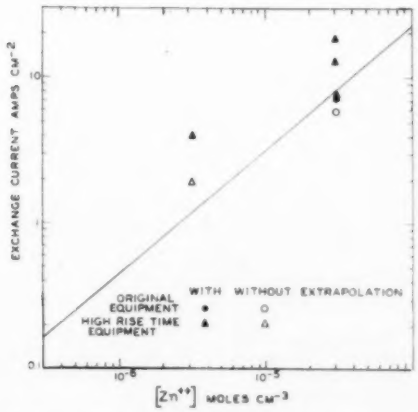

Fig. 9. Exchange currents measured on zinc to test the influence of rise time and extrapolation to zero length of the first pulse.

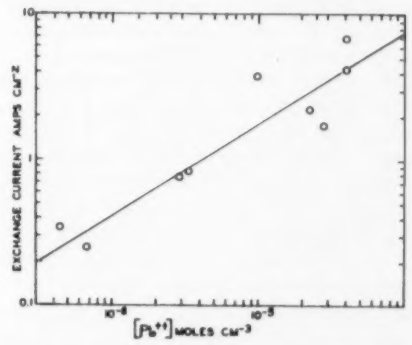

Fig. 10. Exchange currents measured on lead

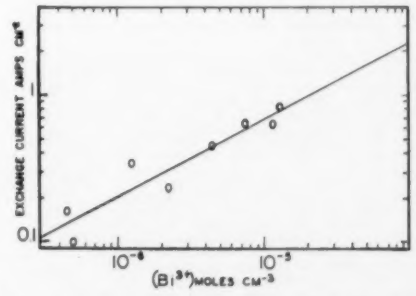

Fig. 11. Exchange currents measured on bismuth

exchange currents according to the method presented in the beginning of the article.

The standard potential of the bismuth couple was calculated from five separate series of measurements of the bismuth potential as a function of concentration. To minimize the error caused by the volatilization of $BiCl_3$, the contents of the compartment were analyzed for bismuth. The average value of E° was -0.640 ± 0.010 v compared to the molar platinum electrode. This is the only case where the potential measured with a tungsten electrode in contact with a metal pool differed appreciably with the potential measured with a plated platinum electrode, as reported by Laitinen and Liu (12). When a platinum electrode was inserted into the same compartment with the tungsten electrode and then plated, the potential corresponded to the one given before, but differed from the potential of the tungsten electrode by nearly 0.1 v. If the platinum electrode was inserted into the bismuth pool, it quickly dissolved. The thermal emf between platinum and tungsten is negligible.

Platinum,[1] *nickel, and silver.*—For solid electrodes there was no difficulty in determining the apparent surface area, which was used in the calculation of the exchange current density. Silver sometimes recrystallized in the melt forming fine whisker-like fibers, causing an increase in exchange current. In such cases, after polishing and cleaning the electrode the measured values were the same as before.

Figure 12 shows the results obtained with these solid metals by the double pulse method without the high rise time preamplifiers. Some of the exchange currents of the silver couple have been calculated by extrapolation to zero length of the first pulse. As can be seen, such points are within the limits of precision of the measurements.

Vanadium(III)-vanadium(II). — This electrode couple is distinctly different from the above examples because both forms of the couple are solvated ions. The exchange current is then a function of two concentrations. The data cannot be compared with the metal ion/metal couples because of the lack of a common reference concentration. The plot of $i_o/(V^{3+})$ vs. $(V^{2+})/(V^{3+})$ shown in Fig. 13 results in a straight line, as expected from Eq. [4].

From measurements at 400°, 450°, and 500°C, the activation energy was found to be 2.8 ±0.4 kcal mole^{-1}; a value which is surprisingly close to that of the cadmium couple.

Evaluation and compilation of the measured data. —Table I contains the kinetic data calculated from the measurements with the two methods. The rate constant k_s" is listed as well as the molar exchange current, "i_o. Since the calculation of the rate constant required an extrapolation of over four orders of magnitude to an imaginary concentration of 1 mole cm^{-3}, no limits of error are given. The molar exchange current, i.e., the exchange current at a concentration of 1 mole liter^{-1}, is considered to be a more suitable measure of the rate of an electrode reaction.

[1] Qualitative observations were made of the anodic behavior of platinum in a melt containing about 0.1 mole liter^{-1} Pt^{++}. At positive polarizations of about 100 mv, the current-voltage curve has an unstable region. The anodic current suddenly drops to less than 100 μa cm^{-2}. A layer of $PtCl_2$ is formed at the electrode surface. The slow dissolution of this layer is now the rate determining process. It was possible to apply cell voltages up to 5 v without much increase in current, because of the ohmic drop in the layer. Some chlorine is evolved, but only at much higher polarizations, due to the iR drop in the layer, than at a carbon surface. The amount of current required for the formation of the layer shows that it is a thick salt layer and not a passive layer. After switching off the current, the cell voltage immediately drops to 1 v and then, within milliseconds to seconds depending on the time of anodization, decreases to its equilibrium value. The quantitative investigation of these phenomena requires the application of an electronic potentiostat because of the unstable region in the current voltage curve. This observation may prove useful in developing a method for electrolytically polishing platinum.

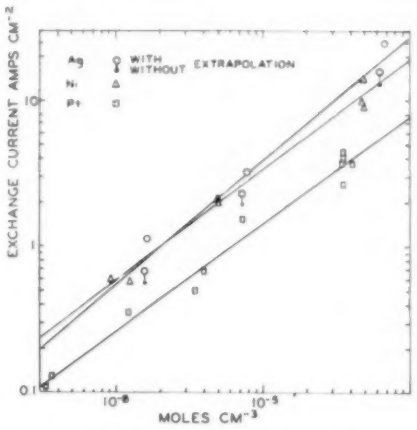

Fig. 12. Exchange currents measured on platinum, silver and nickel.

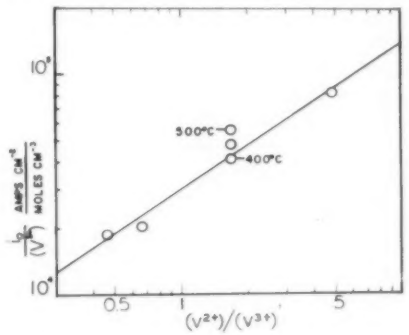

Fig. 13. Exchange currents measured for the V^{2+}/V^{3+} couple

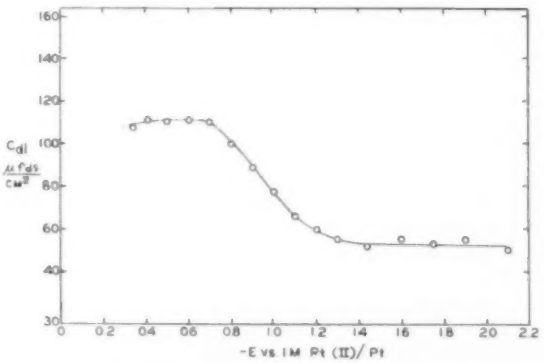

Fig. 14. Differential double layer capacity of platinum in the eutectic as a function of potential.

Discussion

In general, the exchange currents of the electrode reactions in this melt at 450°C are not much

Table I

	Molar exchange current amp cm^{-2}	α	k_s^o, cm sec^{-1}
Both methods			
Cd^{2+}/Cd	210(±50)	0.13(±0.05)	0.4
Double pulse			
Zn^{2+}/Zn	150(±30)	0.16(±0.05)	0.3
Pb^{2+}/Pb	30(±15)	0.38(±0.06)	0.01
Ag^{+}/Ag	190(±50)	0.16(±0.05)	0.65
Ni^{2+}/Ni	110(±20)	0.25(±0.06)	0.1
Pt^{2+}/Pt	40(±10)	0.27(±0.06)	0.03
Voltage step			
Zn^{2+}/Zn	150(±20)	0.10(±0.05)	0.4
Bi^{3+}/Bi	8(±3)	0.5 (±0.1)	0.0009
V^{3+}/V^{2+}	30(±2)	0.67(±0.05)	0.3

higher than those of the fastest reaction so far investigated in aqueous solutions. The transfer coefficient was somewhat lower, except in the case of bismuth, lead, and vanadium(III)/vanadium(II), which were the three slowest reactions found. The obvious similarity in the behavior of several systems with otherwise differing chemical properties suggests a common discharge mechanism which presumably involves the exchange of metal ions between the electrode and chlorocomplex species in solution.

In the previous work on impedance measurements (3, 4) and in the double pulse method employed here, certain features of the observations do not behave in accordance with the simplest reaction model of a one-step charge transfer mechanism involving diffusing species. In particular, the "inverted" capacitance-resistance behavior, which can be caused by specific adsorption of the electroactive species (5), was explained on this basis by Laitinen and Gaur. A similar "inverted" behavior of capacitative and resistive components of impedance can be predicted, at least over a limited frequency range, for a dissociation reaction preceding the charge transfer reaction if the rate of dissociation reaction is less than or comparable to the rate of the charge transfer reaction (18).

It is therefore instructive to consider qualitatively the effects of adsorption and of prior dissociation on the double pulse and voltage step methods. The effect of adsorption of electroactive species would depend on whether the adsorbed layer represents an *additional* reaction path (parallel admittance) as assumed in the treatment of impedance measurements (4, 5) or whether prior adsorption is a step in the main reaction path (series admittance). In the former case, both the double pulse and voltage step methods would respond (for rapid charge transfer to the adsorbed phase) by showing an abnormally large double layer capacity. Indeed, a purely capacitative correction for adsorption was found adequate in several cases of impedance measurements (5), and in any case the resistive component of this correction is very small. For a slow charge transfer reaction to the adsorbed phase, a large time constant would be introduced into the reaction of the adsorbed phase, but in this case the main charge transfer reaction would also be expected to be slow. In the voltage step method the time constant for the charging process was found to be normal even in the presence of an electrode reaction. In the double pulse method, the charging is forced to happen in the short time interval of the first pulse. As has been already mentioned, the detailed behavior of the double pulse method does not comply with the simple charge transfer reaction model.

For prior adsorption as a step in the main reaction (the series admittance model), the effect would be similar to, although not identical with, that of a prior dissociation. All methods of measurement would be affected by the rate of the prior step if its rate were comparable to or slower than the transfer of charge.

Independent proof of the reality of specific adsorption or dissociation is needed before definite conclusions as to reaction mechanism can be reached. The irregularities in the a-c impedance measurements and the unexpectedly large dependence of the measured reaction resistance on the duration of the first pulse in the double pulse indicate, however, that simple charge transfer control does not prevail.

Manuscript received Dec. 9, 1959. This paper was prepared for delivery before the Philadelphia Meeting, May 3-7, 1959.

Any discussion of this paper will appear in a Discussion Section to be published in the December 1960 JOURNAL.

REFERENCES

1. H. A. Laitinen and H. C. Gaur, *Anal. Chim. Acta*, **18**, 1 (1958).
2. J. E. B. Randles and W. White, *Z. Elektrochem.*, **59**, 666 (1955).
3. H. A. Laitinen and R. A. Osteryoung, *This Journal*, **102**, 598 (1955).
4. H. A. Laitinen and H. C. Gaur, *ibid.*, **104**, 730 (1957).
5. H. A. Laitinen and J. E. B. Randles, *Trans. Faraday Soc.*, **51**, 54 (1955).
6. D. L. Hill, G. J. Hills, L. Young, and J. O'M. Bockris, *J. Electroanalytical Chem.*, **1**, 79 (1959).
7. H. Gerischer and M. O. Krause, *Z. phys. Chem. N. F.*, **10**, 264 (1957); **14**, 184 (1958).
8. H. Matsuda, S. Oka, P. Delahay, *J. Am. Chem. Soc.*, **81**, 5077 (1959).
9. W. Vielstich and P. Delahay, *ibid.*, **79**, 1874 (1957).
10. H. A. Laitinen, R. A. Osteryoung, and W. S. Ferguson, *This Journal*, **104**, 516 (1957).
11. W. G. Burkhard and J. D. Corbett, *J. Am. Chem. Soc.*, **79**, 6361 (1957).
12. H. A. Laitinen and C. H. Liu, *ibid.*, **80**, 1015 (1958).
13. H. von Wartenberg, *Z. angew. Chem.*, **69**, 258 (1957); *Z. anorg. u. allgem. Chem.*, **273**, 257 (1953).
14. Strohmeyer, *Schw. J.*, **22**, 376 (1818); W. R. E. Hodkinson, R. Waring, and A. P. H. Desborough, *Chem. N.*, **80**, 185 (1899); A. Pospielow, *Ber. phys. Ges.*, **5**, 346 (1907).
15. K. Rav, *Proc. Iowa Acad. Sci.*, **38**, 166 (1931).
16. H. A. Laitinen and W. S. Ferguson, *Anal. Chem.*, **29**, 4 (1957).
17. Preferred Circuits, Naval Aeronautical Electronic Equipment, NAVAER 16-1-519, p. 26-2, Superintendent of Documents, U.S. Gov't Printing Office, Washington 25, D. C. (1955).
18. Cf. J. E. B. Randles, *Discussions Faraday Soc.*, **1**, 11 (1947); H. Gerischer, *Z. physik Chem.*, **202**, 292, 302 (1953); *Z. Elektrochem.*, **57**, 604 (1953).

A Study of the Oxidation of Hydrogen at Platinized Platinum Electrodes

Thomas C. Franklin and Samuel L. Cooke, Jr.[1]

Chemistry Department, Baylor University, Waco, Texas

ABSTRACT

A coulometric technique using a polarograph was used to study the oxidation of hydrogen at platinized platinum electrodes. The results obtained by this technique are in agreement with results obtained by charging curve and a-c bridge techniques. This technique showed the presence of two forms of hydrogen adsorbed at the surface of the platinum, and it also showed the presence of hydrogen absorbed in the platinum. A study of the effect of pH on the current voltage curves suggested that absorbed hydrogen migrated as a charged species, probably H_2^+.

The oxidation of hydrogen at platinum electrodes has been investigated by a number of workers. Bowden (1) and Butler (2-4) and co-workers studied the process using charging curve techniques. Frumkin and other Russian workers (5-13) followed this with a detailed study of the oxidation of hydrogen on platinum electrodes using similar charging curve techniques. A group of German workers (14-19) have studied the same problem using both alternating current bridge and charging curve techniques.

In Frumkin's work three arrests can be noted in the curves between the potential of the hydrogen electrode and the oxygen region in sulfuric acid solutions. The first two were grouped together as being caused by the process of removing adsorbed hydrogen. The third was attributed, along with another possibility, as being due to the process of removing hydrogen from the interior of the platinum.

Two maxima were obtained in capacitance of the electrode vs. polarizing potential curves plotted from data obtained in the bridge experiments. Eucken and Weblus (14, 15) attributed these effects to the presence of two different forms of adsorbed hydrogen on the surface of the platinum.

In a study of the competition between hydrogen and organic molecules for sites on the platinum electrode (20) the amount of hydrogen was measured by electrooxidation of the hydrogen using a polarograph and by measurement of the number of coulombs used in the oxidation. In conjunction with this study of poisoning, a study was made of the oxidation of hydrogen using this coulometric technique. It was felt that this technique was more rapid than the charging curve experiments of Frumkin and that it did not involve the special equipment needed for the bridge method or the high speed charging curves obtained by workers such as Breiter.

Experimental Materials and Method

The hydrogen electrodes used in this work were made by plating a 1 to 2 cm length of 20-gauge bright platinum wire with platinum black after the manner of Clark (21). A 3% solution of chloroplatinic acid with 0.06% lead acetate present was used as the plating bath. The electrode was washed with distilled water, cleaned of old platinum black with *aqua regia*, checked for surface cleanness by observing the uniformity of hydrogen evolution in 6*N* HCl, and then plated for a prescribed length of time at 2-10 ma. Since no visible evolution of hydrogen occurred at the current densities used, it was presumed that the discharge of platinum was the only significant process occurring. The number of coulombs passed could thus be used as an estimate of the thickness of the platinum black. To obtain a reproducible electrode, the thickness of the platinum black was controlled by the number of coulombs passed (22). Electrodes identical within 1% could be prepared under very carefully controlled conditions.

After plating, the electrodes were washed in a vigorous stream of redistilled water, charged with hydrogen in the electrolyte to be used, and placed in the hydrogen-saturated electrolyte in the apparatus for study. Equilibrium occurred almost immediately as indicated by the cell maintaining a constant potential, which was measured with a L&N K-2 potentiometer.

The apparatus is pictured in Fig. 1. The physical arrangement of the apparatus is shown in the inset.

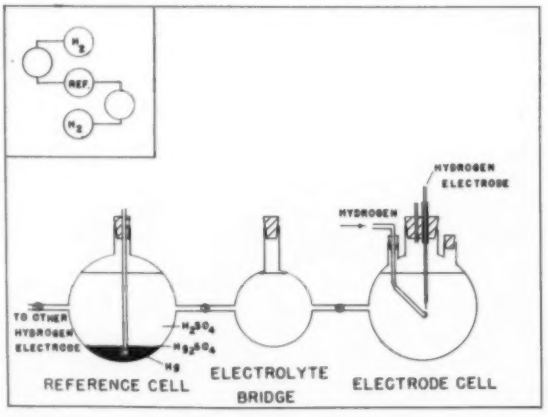

Fig. 1. Apparatus. Inset: physical arrangement

[1] Present address: Interscience, Inc., Richmond, Virginia.

The S-shaped arrangement permitted study of two electrodes with only one reference electrode. The complete apparatus was maintained at 25.0°C. The reference half-cell was Hg, Hg_2SO_4 in sulfuric acid and Hg, HgO, NaOH in basic solutions. The sodium hydroxide and sulfuric acid were of the same concentration as the electrolyte in the hydrogen electrode cell.

A series of runs were made in the pH range between 2*N* sulfuric acid and 2*N* sodium hydroxide. This was done by adding sulfuric acid to sodium hydroxide and *vice versa*. The pH was determined from the hydrogen electrode.

The hydrogen was prepared in a zinc-sulfuric acid Kipp generator and was bubbled through two wash bottles containing electrolyte. In the neutral and basic runs, the gas was first bubbled through strong sodium hydroxide to remove any acid carried over from the generator. Contact between hydrogen and rubber tubing was minimized, and all rubber was digested for two days in hot, concentrated sodium hydroxide and washed with distilled water before use.

In the early phases of the problem an investigation was made of the effect of various purification techniques on the results of the experiments. Several sources of hydrogen were used, including commercial tank hydrogen, Kipp generator hydrogen (using two different sources of zinc and two different sources of sulfuric acid), and electrolytically generated hydrogen. The hydrogen was purified in several different types of trains. Some runs were made in an all-glass apparatus and others were made in which the rubber connections were replaced with Tygon. The apparatus was in all cases soaked for 24 hr or longer, in some cases with distilled water and in others with the solution to be studied. Some experiments were carried out in sulfuric acid solutions that had been pre-electrolyzed overnight according to the procedure of Schuldiner (23). In all of these experiments the results were essentially the same. The presence of a poison decreased the amount of hydrogen at the electrode surface but did not change the general shape of the curves.

Hydrogen was bubbled into the cell for at least twice as long as necessary for potentiometric equilibrium. The cell was then permitted to stand for at least an equal amount of time. Then the hydrogen at the electrode was electrolytically oxidized using a Sargent Model XXI polarograph to record the current-voltage curve for the oxidation. When the cell resistance was greater than 500 ohms it was necessary to insert a compensation circuit. This circuit differed in design but not in principle from that of Nicholson (24). A lathe wound compensating slidewire was placed adjacent to the balancing slidewire of the recorder and an extra contact was constructed on the regular contact mount of the recorder. The current-voltage curves were also current-time curves for the oxidation process, and the area under the curves was proportional to the number of coulombs needed for the oxidation. The compounds used were all of reagent grade. The water was triply distilled.

Data and Results—Sulfuric Acid Solutions

A typical current-voltage curve for the oxidation of the hydrogen present at platinized platinum in 2*N* sulfuric acid is shown in Fig. 2. Three very distinct maxima are observed and are indicated by Roman numerals. A fourth maximum is observed when the voltage is allowed to sweep beyond the region where hydrogen is oxidized. Previous workers (25, 26) have shown the fourth maximum to be due to the formation of a surface oxide of platinum. These maxima are not experimental artifacts as is shown by the fact that they were obtained under a wide

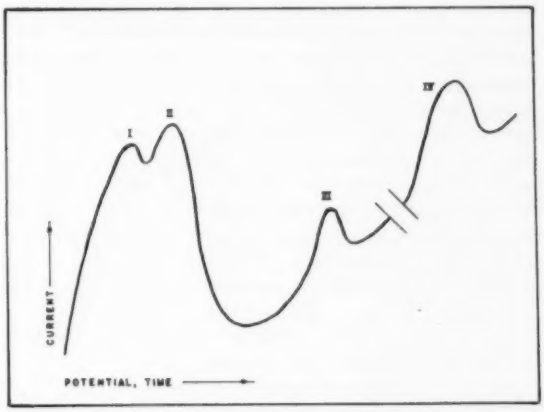

Fig. 2. Typical current-voltage curve for hydrogen oxidation on a platinized platinum anode in 2N sulfuric acid.

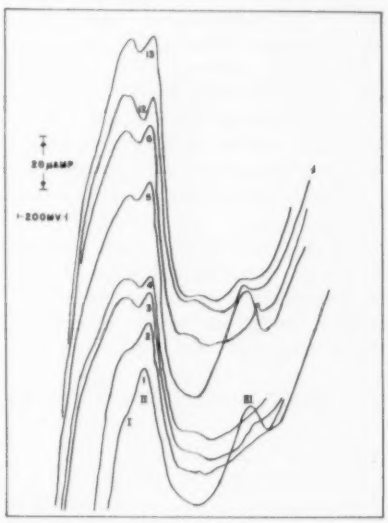

Fig. 3. Effect of oxidations, time, and formation of oxide on the shape of the current-voltage curve.

Number of the Oxidation	Conditions
1	New electrode after hydrogen bubbling.
2	10 min after oxidation No. 1.
3	10 min after oxidation No. 2.
4	10 min after oxidation No. 3.
5	510 min after oxidation No. 4.
6	10 min after oxidation No. 5.
12	10 min after oxidation No. 11, the potential was allowed to sweep through the point of formation of the oxide of platinum.
13	10 min after oxidation No. 12.

Roman numerals denote the maxima. Origin of curves shifted along current axis.

variety of conditions including variations in the voltage sweep rate, the temperature, and the electrode plating conditions. Rotating the electrodes made the curves irregular but did not essentially change the area under the three maxima caused by the oxidation of hydrogen.

Figure 3 shows the effects of (*a*) time since the previous oxidation, (*b*) formation of the first surface oxide of platinum, and (*c*) successive oxidations on the shape of current-voltage curves in sulfuric acid. To prevent the curves from overlapping, the origin is shifted along the current axis. The first and second maxima are observed to develop with successive oxidations and after formation of the oxide. The third maximum is prominent in oxidations No. 1 and 5 and poorly defined in the other oxidations. The third maximum grows slowly as compared to the first two maxima. This is shown by Fig. 4 which represents the relation between area under the third maximum and time since the previous oxidation. The difference in rate of growth of this maximum and of the other two maxima can be appreciated when it is realized that in less than 3 min a similar plot for maxima I or II would go beyond the range of Fig. 4, and equilibrium would be reached in 10 min.

From these data it can be concluded that the first two maxima are a result of the oxidation of two forms of hydrogen adsorbed on the surface of the platinum. This is shown by the fact that the area under these maxima increases with repeated oxidations (Fig. 5) (the expansion and contraction of the crystal lattice on oxidation and then reduction increased the surface area) and by the fact that the area under these maxima decreased following a Freundlich adsorption isotherm in the presence of poisons (20). The third maximum presumably corresponds to the oxidation of hydrogen absorbed in platinum. It is a well-known fact that hydrogen absorbs in metals more slowly than it adsorbs on metals (27).

The above interpretation agrees with the interpretations of the Russian workers (5-13) in that they observed the slow forming absorbed hydrogen. It agrees with the German workers (14-19) in that they distinguished between the two forms of adsorbed hydrogen. Breiter (16-19) observes a third form of surface hydrogen to which this technique is insensitive. However, the interpretation of the two forms of adsorbed hydrogen as hydrogen adsorbed on oxygen, and on platinum (14), might just as well be interpreted as chemically and physically adsorbed hydrogen, respectively.

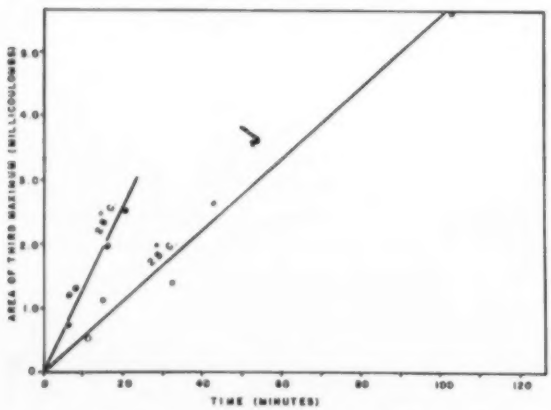

Fig. 4. Effect of time on the area under third maximum in acid solutions.

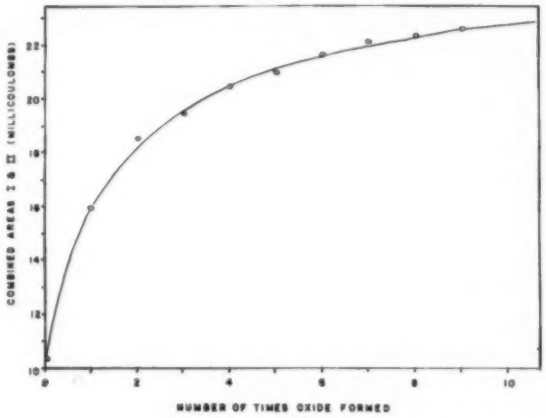

Fig. 5. Effect of oxide formation on combined areas I & II in acid solutions.

Basic and Neutral Solutions

The three maxima were still observed in 2N sodium hydroxide. However, two things made the hydrogen electrode in basic solutions more difficult to study: (*a*) The three maxima are very close together and thus there is a tendency for one or more of them to become ill-defined; (*b*) all three forms of hydrogen were completely replenished in the 10 min normally allowed between oxidations (in acid solutions it took over 3 hr for the absorbed hydrogen to reach equilibrium). Some experiments indicate that this difference in rate was due to poisoning of the electrode by sulfate ion.

Although no quantitative studies, such as those in sulfuric acid, could be made, a qualitative comparison was made of the effects of (*a*) time since the previous oxidation, (*b*) formation of the first oxide of platinum, (*c*) successive oxidations, and (*d*) hydrogen evolution, on the area under the curves in the neighborhood of each maximum in 2*N* sulfuric acid and 2*N* sodium hydroxide. This comparison is shown in Table I.

Table I. Summary of results in acidic and basic solutions

Effect on the area under the curve in the region of each maximum.

Maximum	Successive oxidations	Time since previous oxidation	Oxide formation	Hydrogen evolution
		Basic Solutions		
I(A)	Increase	No effect	Increase	Increase
II(B)	No effect	Increase	No effect	No effect
III(C)	No effect	No effect	Increase	No effect
		Acidic Solutions		
I	Increase	No effect	Increase	Increase
II	No effect	No effect	Increase	No effect
III	No effect	Increase	No effect	No effect

From these results it was concluded that the last two maxima had shifted their relative positions and the I, II, and III maxima in basic solutions correspond in acidic solutions to I, III, and II, respectively. This was further indicated by the fact that if one momentarily generates hydrogen on the electrode in basic solutions and then oxidizes it, one obtains the current-voltage curve shown in Fig. 6 containing only the two peaks I(A) and III(C) corresponding to the two surface forms of hydrogen (I and II in acid solutions). To study further this shift, the behavior of the current-voltage curves was investigated at intermediate *p*H values.

The potentials of the maxima relative to the normal hydrogen electrode are plotted as a function

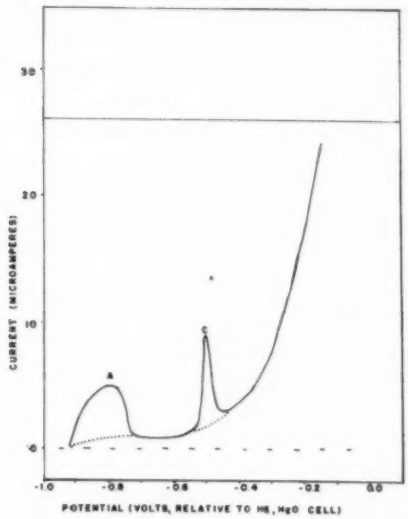

Fig. 6. Current-voltage curve for a hydrogen electrode in basic solution.

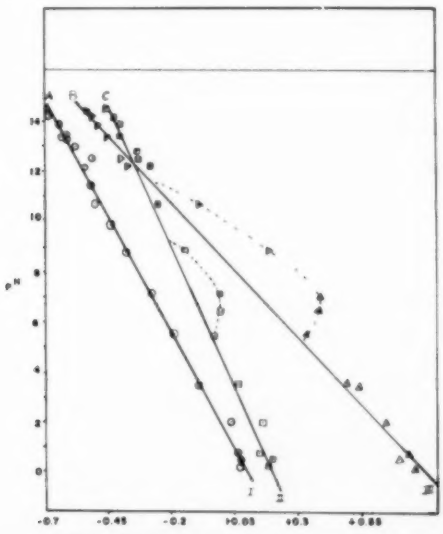

Fig. 7. pH dependence of the potentials of the maxima referred to the normal hydrogen electrode. Circle with dot, maximum I in acid and I(A) in basic solutions; square with dot, maximum II in acid—III(C) in basic solutions; triangle with dot, maximum III in acid—II(B) in basic solutions.

of *p*H in Fig. 7. The data for each maximum are on straight lines, except for a deviation in the *p*H range from 6 to 10. This deviation is attributable to a decrease in the *p*H at the electrode surface in the unbuffered solutions due to the generation of hydrogen ions during the oxidation. There was a definite shift in the relative positions of maxima II and III (acidic) as one goes from acidic to basic solutions. The potentials at which the two surface forms (maxima I and II in acid) are oxidized shift by 0.054 and 0.044 v in the negative direction for each unit rise in *p*H. It is expected that a reversible oxidation producing one hydronium ion for each electron will shift the potential by 0.059 v per *p*H unit. The deviation of these two slopes from the expected value may be due to a voltage drop caused by the resistance of the solution. The effect was more pronounced for the second surface form since the current was much higher. The potential for the maximum corresponding to the oxidation of the absorbed hydrogen (III in acid) shifts by 0.094 v per *p*H unit. This high slope shows that the absorbed hydrogen migrates as a charged species to the surface where it is oxidized. This slope corresponds most nearly to the reaction $H_3^+ = 3\ H^+ + 2e^-$, whose potential should shift by 0.089 v per pH unit. Because of the uncertainty of the resistance correction, the formula of the charged species could be different, but this experiment suggests that absorbed hydrogen must be a charged species. The presence of H_3^+ absorbed in platinum has been indicated by a number of workers (28), and Pearson (29) has concluded that in the absence of water the hydrogen ion prefers to associate with the hydrogen molecule.

Summary

From current-voltage curves for the oxidation of hydrogen at platinized platinum electrodes in aqueous sulfuric acid, it was concluded that three forms of hydrogen are involved. These three forms, in order of ease of electrolytic oxidation, are postulated to be two forms of adsorbed hydrogen and one form of absorbed hydrogen, in agreement with the conclusions of other workers. Hydrogen is absorbed into platinum much more rapidly from sodium hydroxide solutions than from sulfuric acid solutions. The effect of *p*H on the current-voltage curves suggests that absorbed hydrogen is present as a charged species, probably H_3^+.

From these experiments, it can be concluded that the present technique, the use of current-voltage curves (with a constant voltage sweep rate) can be used for a study of the behavior of hydrogen on metal electrodes. This technique is faster than the slow charging curve technique and not as difficult experimentally as the a-c bridge or fast charging curve techniques. In agreement with the work of Frumkin (7, 12) and Eucken and Weblus (14) it showed the presence of two forms of hydrogen adsorbed on the surface of platinum differing in ease of oxidation, and the presence of hydrogen absorbed in the metal.

One of the major disadvantages of this technique is the presence of a residual current that must be subtracted. A residual current is present because of

the oxidation of molecular hydrogen in solution diffusing to the surface. For some reason the absorption of hydrogen in platinum from basic solutions is much more rapid than in acid. The reverse process, the diffusion of hydrogen from the interior of the metal to the surface, causes a high residual current in basic solutions. However, in sulfuric acid solutions especially, one can obtain a measure of the amount of hydrogen present at the electrode surface in the different forms by taking the area under each maximum and subtracting the area due to the residual current.

Acknowledgment

The authors take this opportunity to thank the Research Corporation for the financial assistance they gave to this research.

Manuscript received June 8, 1959.

Any discussion of this paper will appear in a Discussion Section to be published in the December 1960 JOURNAL.

REFERENCES

1. F. P. Bowden, *Proc. Roy. Soc.* (*London*), **125A**, 446 (1929).
2. J. A. V. Butler and G. Armstrong, *ibid.*, **137A**, 604 (1932).
3. G. Armstrong, F. R. Himsworth, and J. A. V. Butler, *ibid.*, **143A**, 89 (1933).
4. J. A. V. Butler and G. Drever, *Trans. Faraday Soc.*, **32**, 427 (1936).
5. A. Slygin and A. Frumkin, *Acta Physicochem, U.R.S.S.*, **3**, 791 (1935).
6. A. Slygin, A. Frumkin, and W. Medwedowsky, *ibid.*, **4**, 911 (1936).
7. A. Frumkin and A. Slygin, *ibid.*, **5**, 819 (1936).
8. B. V. Ershler and M. Proskurnin, *ibid.*, **6**, 195 (1937).
9. B. Ershler, *ibid.*, **7**, 327 (1937).
10. B. Ershler, G. Deborin, and A. Frumkin, *ibid.*, **8**, 565 (1938).
11. A. Slygin and B. Ershler, *ibid.*, **11**, 45 (1939).
12. A. Frumkin and E. E. Aikasyan, *Doklady Akad. Nauk*, **100**, 35 (1955).
13. E. E. Aikasyan and A. I. Fedorova, *ibid.*, **86**, 1137 (1952).
14. A. Eucken and B. Weblus, *Z. Elektrochem.*, **55**, 114 (1951).
15. E. Wicke and B. Weblus, *ibid.*, **56**, 169 (1952).
16. M. Breiter, C. A. Knorr, and R. Meggle, *ibid.*, **59**, 153 (1955).
17. M. Breiter, C. A. Knorr, and W. Volkl, *ibid.*, **59**, 681 (1955).
18. M. Breiter, H. Kammermaier, and C. A. Knorr, *ibid.*, **60**, 37 (1956).
19. M. Becker and M. Breiter, *ibid.*, **60**, 1080 (1956).
20. T. C. Franklin and R. D. Sothern, *J. Phys. Chem.*, **58**, 951 (1954).
21. W. M. Clark, "The Determination of Hydrogen Ions," Williams and Wilkins, Baltimore, Md. (1932).
22. W. M. MacNevin and M. Levitsky, *Anal. Chem.*, **24**, 973 (1952).
23. S. Schuldiner, *This Journal*, **99**, 488 (1952).
24. M. M. Nicholson, *Anal. Chem.*, **27**, 1364 (1955).
25. S. E. S. El Wakkad and S. H. Emara, *J. Chem. Soc.*, **1953**, 461.
26. W. Nestorova and A. Frumkin, *Zhur. Fiz. Kim.*, **26**, 1178 (1952).
27. D. P. Smith, "Hydrogen in Metals," University of Chicago Press, Chicago, Ill. (1948).
28. D. T. Hurd, "An Introduction to the Chemistry of the Hydrides," p. 59, John Wiley & Sons, Inc., New York (1952).
29. R. G. Pearson, *J. Chem. Phys.*, **16**, 502 (1948).

Technical Notes

Charging Curves for Germanium Electrodes

W. W. Harvey, S. Sheff, and H. C. Gatos

Lincoln Laboratory, Massachusetts Institute of Technology, Lexington, Massachusetts

The assertion has been repeatedly made in the literature [e.g., ref. (1-3)] that germanium surfaces in aqueous solution are covered with an oxidic layer. This assertion seems to be based on thermodynamic considerations and on the observation by Turner (4) that, during anodic dissolution, approximately a monolayer of surface oxide or hydroxide is present. However, direct experimental evidence for the existence of an oxidic layer on a germanium electrode not polarized anodically has been lacking. Accordingly, the chemical state of the surface was re-investigated using the method of charging curves, i.e., plots of electrode potential vs. time at constant current density.

Results and Discussion

Figure 1 shows the changing character of the charging curves obtained in 1.0*N* H_2SO_4 on progressive removal of dissolved oxygen [cf. ref. (2, 4)].

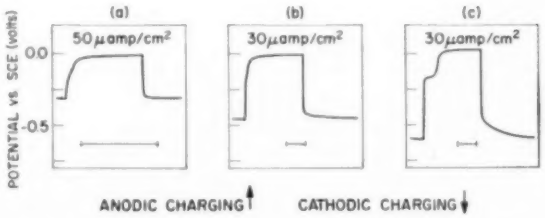

Fig. 1. Changing character of charging curves for germanium on displacing dissolved O_2; horizontal markers represent 10 sec on the abscissa; (a), 1.0N H_2SO_4, as made up; (b) and (c), following N_2 bubbling.

After the concentration of oxygen has been reduced to a low value by prolonged bubbling of purified inert gas, a charging curve such as illustrated in Fig. 2(a) can be obtained. Further removal of oxygen by cathodic reduction results in increased

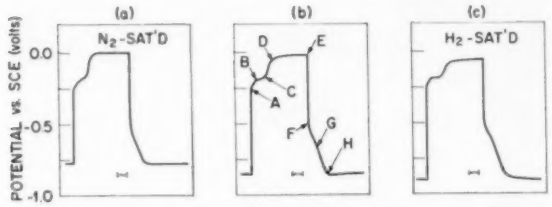

Fig. 2. Charging curves obtained in 0.1N H_2SO_4 after prolonged bubbling of purified N_2; markers represent 150 μcoulomb/cm^2(5 sec) on the abscissa. (a), Initial charging behavior at 30 μa/cm^2; (b), behavior after repeated cycling; (c), same, except solution H_2-satd.

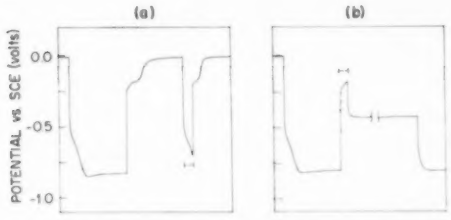

Fig. 3. Examples of charging curve analysis (actual tracings) in 0.1N H_2SO_4; width of markers is equivalent to 150 μcoulomb/cm^2.

polarization during the cathodic step, as shown in Fig. 2(b) and (c). A second consequence is the development of the segment $\overline{BC}$ of the anodic curve. Charging curves similar to those of Fig. 2 but with the cathodic portion extending in a third stage to a more negative potential have also been obtained, particularly at somewhat higher current densities than reported here.

The charging curves have been analyzed in several ways (see below and also Fig. 3); the main features are interpreted as follows: the change in potential along $\overline{AB}$ results from the anodic oxidation of hydrogen atoms chemisorbed during $\overline{GH}$ (by cathodic reduction of hydrogen ions); along the horizontal portion of $\overline{BC}$, hydrogen molecules on the solution side of the interface are oxidized (to hydrogen ions); following this, germanium surface atoms are oxidized. Reversing the current after the final anodic potential has been reached brings about the reduction of the anodically formed surface oxide in the interval $\overline{FG}$.

It is of interest to note that the sequence of processes during charging is different for germanium and platinum, whose charging behavior has been studied most extensively. The first stage of the anodic polarization curve for platinum (5) corresponds to the ionization of cathodically formed hydrogen (6) and consists of an initial horizontal portion (ionization of free hydrogen in the solution), followed by a linear increase of potential (ionization of chemisorbed hydrogen). The second stage for platinum is a rapid increase of potential, corresponding to charging of a double layer. For a polarized germanium electrode, on the other hand, it is evident that an appreciable change in the total semiconductor-electrolyte potential difference must occur before the electric field at the interface has been altered sufficiently to bring about the oxidation of cathodically formed hydrogen or the reduction of anodically formed surface oxide.

In a separate experiment, it was shown that the steady-state anodic reaction in hydrogen-saturated solution is the same (viz., germanium dissolution) as in nitrogen-saturated solution, and so it was established that molecular hydrogen is not oxidized during the anodic dissolution of germanium. In addition, it was shown by chemical tests that metagermanic acid (the product of anodic dissolution) is not reduced to a lower valence state at the germanium cathode.

The charging curves of Fig. 2 and 3 were obtained with hemispherical electrodes (p-type) to insure uniform current distribution at the semiconductor surface. (Similar curves were obtained using disk-shaped n- and p-type electrodes with {111} orientation.) Taking 7.5×10^{14}/cm^2 as the average density of atoms at the real surface and using the value 1.3 as the roughness factor of chemically polished germanium (7,8), it is readily calculated that one electron per surface atom is equivalent to 1.56×10^{-4} coulomb/cm^2. By analyzing spectrochemically for germanium entering the solution during repeated anodic-cathodic charging, it was possible to obtain essential information relevant to the oxidation of germanium surface atoms in the initial stages of the anodic process. Thus, it was found that at 30 μa/cm^2, germanium dissolved is equivalent to 18 sec of the 30-sec anodic stage of Fig. 2(b); i.e., a charge equivalent to 12 sec (3.6×10^{-4} coul/cm^2, or 2.3 electrons per surface Ge atom) at the stated current density is consumed in the oxidation of chemisorbed hydrogen, free hydrogen, and germanium surface atoms. Further, by successively decreasing the cycle duration, it was found that anodic dissolution begins at the inflection in $\overline{CD}$ (i.e., roughly midway between C and D in the figure); however, oxidation of surface atoms is not completed until the steady-state anodic dissolution potential is reached (beyond D). For the specimens employed, the surface coverage by chemisorbed hydrogen during steady-state cathodic charging was equivalent to approximately 0.6 atom layer.

It is evident from the data presented that the anodic formation of surface oxide or hydroxide requires less than two electrons per surface germanium atom. In fact, as indicated by the coulomb equivalent of $\overline{FG}$ [(Fig. 3(a)], not more than one electron per surface atom is required in this process. Time-lapse studies have shown further that in the absence of dissolved oxygen (and other oxidizing substances which attack germanium), chemical species chemisorbed onto, and presumable covalently bonded to germanium as a result of electrolytic processes remain chemisorbed indefinitely.

If a properly prepared germanium surface is polarized cathodically without prior anodic treatment, only the hydrogen reduction portion [beginning at G in Fig. 2(b)] of the charging curve is observed. The same result is obtained if, following a series of charging cycles, the electrode is polarized anodically only to B [see Fig. 3(b)]. These observa-

tions constitute the most direct evidence available at present for the absence of an appreciable oxidic layer on germanium surfaces in nonoxidizing aqueous environments.

Conclusions

It was shown that in dilute H_2SO_4 not more than one electron per germanium surface atom is required during the anodic formation of a surface oxide or hydroxide layer and that the equivalent coverage by chemisorbed hydrogen during cathodic charging is closer to 0.5 than to 1.0. It was further shown that virtually oxide-free germanium surfaces can be obtained in aqueous electrolytes.

Acknowledgment

The authors wish to acknowledge the assistance of Mrs. M. J. Button with some of the experiments.

Manuscript received Jan. 15, 1960. The work reported in this paper was performed by Lincoln Laboratory, a center for research operated by Massachusetts Institute of Technology with the joint support of the U. S. Army, Navy, and Air Force.

Any discussion of this paper will appear in a Discussion Section to be published in the December 1960 JOURNAL.

REFERENCES

1. H. Gerischer, *Bull. soc. chim. Belges*, **67**, 437 (1958).
2. J. Bardeleben, *Z. physik. Chem. (Frankfurt)*, **17**, 39 (1958).
3. J. F. Dewald, "Semiconductors," N. B. Hannay, Editor, p. 727, Reinhold Publishing Corp., New York (1959).
4. D. R. Turner, *This Journal*, **103**, 253 (1956).
5. A. Hickling, *Trans. Faraday Soc.*, **41**, 333 (1945).
6. J. D. Pearson and J. A. V. Butler, *ibid.*, **34**, 1163 (1938).
7. J. T. Law, *J. Phys. Chem.*, **59**, 543 (1955).
8. S. P. Wolsky, *Phys. and Chem. Solids*, **8**, 114 (1959).

A Comparison of Etching and Fracturing Techniques for Studying Twin Structures in Ge, Si, and III-V Intermetallic Compounds

J. W. Faust, Jr. and H. F. John

Research Laboratories, Westinghouse Electric Corporation, Pittsburgh, Pennsylvania

In many cases the detection or location of twins is accomplished most easily by etching. If the etchant is judiciously chosen, one can locate the twin boundary and also determine the orientation of the material on either side of the boundary (1). Three methods of revealing twins by etching and a new method of revealing twins by fracturing are discussed below.

Techniques for Revealing Twins by Etching

1. Preferentially etch a lapped surface. The twin boundary is revealed by the change in the characteristic etch pits as a result of the orientation difference across the boundary. If the orientations of the faces across the twin plane are not equivalent, then a step will also be produced at the boundary as a result of the etch rate being a function of the orientation.

2. Chemically or electrolytically polish a lapped surface. The twin will be revealed as a groove (if the orientations of the faces across the twin plane are equivalent) or as a step (if the orientations are not equivalent).

3. Immerse a mechanically polished surface in a chemical polish or a preferential etch for a very short time. The twin line will be revealed as a groove.

Any of these methods can be applied to the study of twin structures in semiconducting materials; however, difficulties in interpretation can arise if the twins are very closely spaced, and particularly if the etched surface is perpendicular to one of the <211> directions. Billig (2) in his study of twin structures in "dendritic" Ge does not give any details of his experimental technique; however, examination of his photomicrographs indicates that he must have used method 3, i.e., the dendrite cut perpendicular to its length, polished, and etched in a preferential etch. Since his technique reveals not only the twin lamella but also dislocations, a complete analysis of the cross section is impossible in many cases.

Of the three etching techniques, method 3 (employing a chemical polish on a mechanically polished surface) is particularly useful when properly

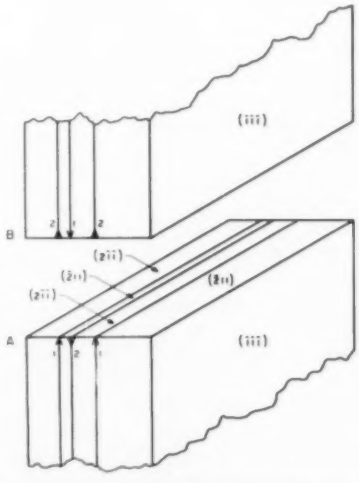

Fig. 1. Diagram of a cut section containing three twin boundaries. The "arrows" on the twin planes are traces of {111} planes.

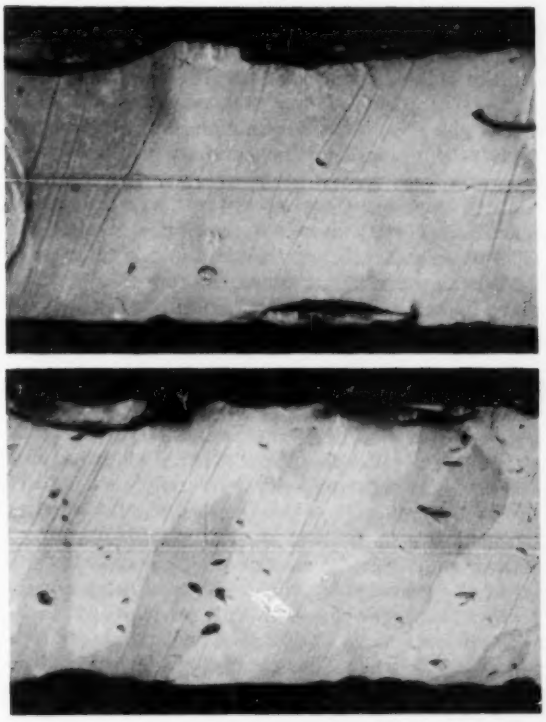

Fig. 2. Side A; Side B. Polished and etched {112} surfaces of germanium containing 3 twin planes. Sides A and B have the crystallographic significance shown in Fig. 1. Magnification 200X before reduction for publication.

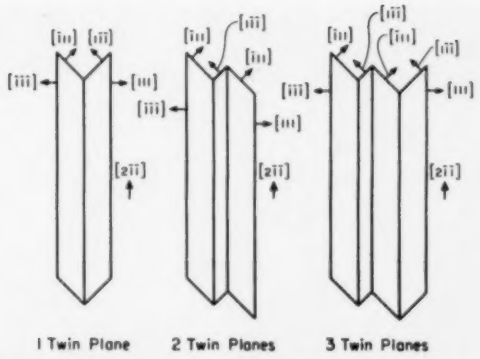

Fig. 3. Diagrams of thin sections fractured at both ends. Indices of twinned segments are referred to parent crystal.

Fig. 4. Photomicrograph of a fractured germanium dendrite showing the 3 twin boundaries. Magnification 500X before reduction for publication.

interpreted; however, our new technique of fracturing thin sections of Ge, Si, or III-V compounds is more rapid and more easily interpreted.

Interpretation of Etch Patterns

As an illustration of the problem involved in interpreting etch patterns obtained according to method 3, let us choose a section of Ge containing three closely spaced twins and cut this section into two pieces, A and B, such that the cut is perpendicular to the <211> directions, as shown in Fig. 1. If sections A and B are mechanically polished and then given a 10-sec CP4 etch,[1] it is found that side A has a definite groove and two faint lines, while side B has two definite grooves and a faint line. In many cases the twins are spaced so close together that one or both of the faint lines will be "lost" in the definite etch groove. Figure 2 shows this apparent etching anomaly for sides A and B. This apparent anomaly is merely the result of the action of the etch on the {111} planes and the effect of the energy of the twin plane on the etch rate. The CP4 is slightly preferential to the {111} planes; however, it is not preferential enough to keep the etch from acting as a chemical polish. Because of the twin boundary energy, the etch attacks more rapidly at the twin boundary starting a groove. If {111} planes converge on the twin plane from the surface, as shown by twin planes marked 2 in Fig. 1, atoms can be removed along these exposed planes also; the result will be a definite groove. If, however, the {111} planes diverge from the surface at a twin boundary, as shown by twin planes marked 1 in Fig. 1, atoms cannot be removed from these unexposed {111} planes, and the result will be a faint groove caused only by the attack of the etch as a result of the energy associated with the twin plane. The number of definite grooves, n, can be found

Fig. 5. Photomicrograph of a fractured germanium dendrite showing 3 twin boundaries, a grain boundary and a single twin boundary at the edge. Magnification 200X before reduction for publication.

[1] Composition, 25 parts HNO_3; 15 parts glacial acetic acid; 15 parts HF; and 0.3 parts bromine.

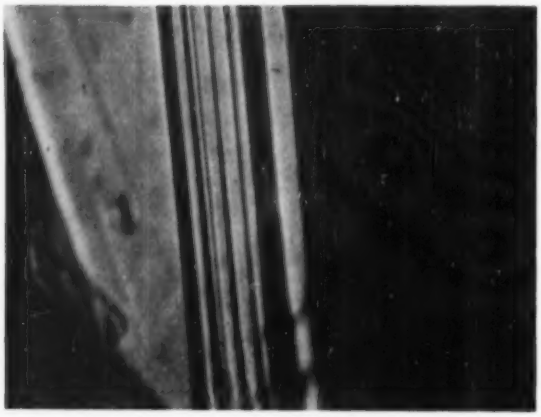

Fig. 6. A fractured germanium dendrite showing 13 twin boundaries. Magnification 1000X before reduction for publication.

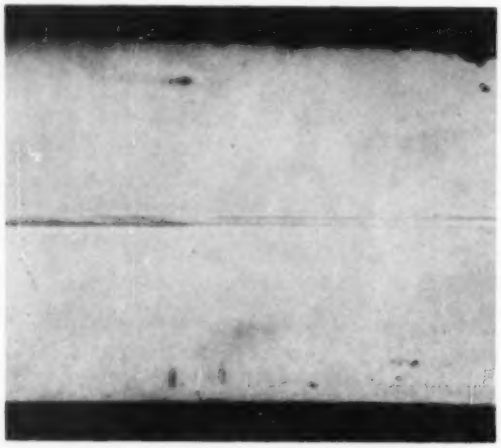

Fig. 7. A fractured germanium dendrite illustrating {112} cleavage: compare uniform focus with Fig. 5. Magnification 200X before reduction for publication.

from the number of twin planes, t, by the following formulas:

For an odd number of twin planes, where A and B have the significance shown in Fig. 1,

$$\text{side A} \quad n = (t-1)/2$$
$$\text{side B} \quad n = (t+1)/2$$

For an even number of twin planes

$$\text{side A or B} \quad n = t/2$$

Interpretation of Fracture Surfaces

The cleavage planes for germanium and silicon are the {111} planes. Upon careful fracturing, these materials break on their cleavage planes. This technique is suitable for use on thin sections cut from grown crystals or on dendritic crystals which grow naturally in the <112> direction. In this technique a line is scribed across the {111} face parallel to the [110] direction to control where the fracturing is to occur; fracturing is accomplished by bending. Each twin plane changes the direction of the {111} cleavage planes as shown in the diagram in Fig. 3; thus each line represents a twin boundary. Figure 4 is a photomicrograph of a fractured Ge dendrite that contained 3 twin boundaries. Electron micrographic examination of such a twinned structure showed no additional twins. The cleavage surfaces show some fracture steps but are, for the most part, excellent. In some cases where the twin lamella ends before reaching the edge of the section, a single twin or grain boundary can extend to the edge; even the grain boundaries are faithfully revealed by this technique, as shown in Fig. 5. This technique has revealed as many as 13 twins in a distance of 20μ as shown in Fig. 6. In a few cases we have observed that cleavage takes place on {112} planes; this is illustrated in Fig. 7 by the fact that the edges of the fracture are in focus with the middle of the Ge section. This method also works well for dendrites of silicon and the III-V intermetallic compounds, although for the latter, the interpretation is somewhat difficult because of the secondary cleavage plane (3).

Acknowledgments

The authors wish to express their thanks to Dr. R. Stickler for the electron microscopic examination.

This work was performed on Contract No. AF33 (600)-39378 BPSN 9-(8-4608)-42019–Wright Air Development Center.

Manuscript received Nov. 19, 1959.

Any discussion of this paper will appear in a Discussion Section to be published in the December 1960 JOURNAL.

REFERENCES

1. J. W. Faust, Jr., I.R.E.-A.I.E.E. Devices Conference, State College, Pa., June 1953 (unpublished); J. W. Faust, Jr., Electrochemical Society, Enlarged Abstracts No. 90, Cincinnati, Ohio, May 1955.
2. E. Billig, *Acta Met.*, **5**, 53 (1957).
3. J. F. DeWalt, *This Journal*, **104**, 244 (1957).

Bonding and Semiconductivity Relationships in Bi_2Te_3 and CdI_2 Type Structures

C. H. L. Goodman

Research Laboratories, The General Electric Company Limited, Wembley, England

It appears of interest to point out a possible relationship between layer structures of Bi_2Te_3 and CdI_2 types.

In a previous paper (1) a simple bonding scheme was put forward for Bi_2Te_3 which satisfactorily accounted for the 28 valence electrons in a manner consistent with the observed semiconductivity of this compound. A related bonding scheme seems possible for the 3-layer CdI_2 structure: I atoms, with the same coordination as the outer Te atoms in

5-layered Bi_2Te_3, would employ p^3 (plus s^2, lone pair) bonding orbitals while the metal atom, with 6-coordination like Bi in Bi_2Te_3, would employ sp^3d^2 hybridized bonding orbitals.[1] The 16 valence electrons of CdI_2 form 2-electron covalent-ionic bonds within the triple I-Cd-I layer structure, I-I inter-layer bonding being of van der Waals' type in agreement with Hartman's calculations (4).

Following (5) this scheme indicates that $A^{II}X_2^{VII}$ and $A^{IV}X_2^{VI}$ compounds with CdI_2 structure (e.g., CdI_2,$ZrSe_2$) should be semiconductors or insulators [in agreement with the findings in ref. (6) and (7) for example] while compounds such as $NiTe_2$ should be metallic [in agreement with the findings in ref. (8)]. Furthermore, ignoring bond-length effects, the greater electronegativity differences for $A^{II}X_2^{VII}$ compared with $A^{IV}X_2^{VI}$ compounds should lead to considerably lower energy gaps for the latter, which, by the same argument, should have higher energy gaps than related $A_2^{V}X_3^{VI}$ compounds with Bi_2Te_3 type structure.

Not all CdI_2 type compounds can be described in this way. Thus Ag_2F requires a scheme with resonating p^3 bonds, (which give rise to Ag-Ag interlayer bonding and accommodate all 9 valence electrons), and, following (5), should also be a semiconductor.

[1] This would appear to require d-orbital contraction; see for example ref. (2). Promotional energies for such bonding orbitals would in any case be much less than those suggested from spectroscopic data for free atoms, as has been pointed out by Wilmshurst (3).

The nature of the bonding in $A^{IV}X_2^{VII}$ compounds such as PbI_2 is less clear. Eighteen valence electrons must be accommodated in closed sub-shells or bonds for the criteria for semiconductivity given in ref. (5) to be satisfied. This might be achieved by p^3d^2 (+lone pair) bonding orbitals for A^{IV} atoms, although coordination symmetry argues somewhat against this view. More detailed bond studies along these lines would appear of interest.

Acknowledgment

It is a pleasure to acknowledge stimulating correspondence with J. Suchet.

Manuscript received Feb. 15, 1960.

Any discussion of this paper will appear in a Discussion Section to be published in the December 1960 JOURNAL.

REFERENCES

1. J. R. Drabble and C. H. L. Goodman, *J. Phys. Chem. Solids*, **5**, 142 (1958).
2. D. P. Craig and E. A. Magnusson, *J. Chem. Soc.*, **1956**, 4895; D. P. Craig, "The Inorganic Chemistry of Sulphur," p. 343, The Chemical Society, London (1958).
3. J. K. Wilmshurst, *J. Chem. Phys.*, **30**, 889 (1959).
4. P. Hartman, *Acta Cryst.*, **11**, 365 (1958).
5. C. H. L. Goodman, *J. Phys. Chem. Solids*, **6**, 305 (1958).
6. E. Putseiko, *Dokl. Akad. Nauk S.S.S.R.*, **67**, 1009 (1949).
7. F. K. McTaggart, *et al.*, *Australian J. Chem.*, **2**, 445 (1958).
8. V. P. Zhuze and A. R. Regel, *Zh. Tekh. Fiz.*, **25**, 978 (1955).

The Adhesion of Vapor-Deposited Molybdenum Coatings

S. T. Wlodek[1] and J. Wulff

Department of Metallurgy, Massachusetts Institute of Technology, Cambridge, Massachusetts

The reduction of molybdenum pentachloride with hydrogen has often been proposed as a method of producing a dense molybdenum coating (1, 2). The exploitation of this process has been advanced recently by a theoretical treatment of the plating kinetics (3) and the development of a technique capable of plating large articles (4) with vapor deposited molybdenum.

The purpose of this note is to report on the factors which control the adhesion of the molybdenum coating, restricting the discussion to the formation of the plate on a metallic base. The most important variables which affected the adherence of the molybdenum plate studied in this investigation were: purity of raw materials, sample preparation, and the chemical composition of the material being coated.

Experimental

The plating technique used in this study was basically the same as that described by Spacil and Wulff (3). High-purity molybdenum pentachloride was prepared by the chlorination of molybdenum powder followed by the redistillation of the resultant product to prepare a fraction free of oxychloride contamination. After purification by passing over copper gauze (500°C), followed by a dry ice trap and a magnesium getter (500°C), hydrogen (36 l/hr) was passed over solid molybdenum pentachloride and saturated with the pentachloride vapor. The degree of saturation was kept constant by adjusting the temperature (100-120°C) of the pentachloride so that the color of the resultant gas mixture compared to an empirically arrived at standard (saturated solution of methyl orange in water diluted 1:400 in alcohol). The H_2-$MoCl_5$ gas mixture was then introduced into the reaction chamber where the plate was deposited on the inside of 0.5-in. diameter, 4.0-in. long tubes of the material to be plated. The reduction conditions in the actual plating chamber were 900°C and a pressure of 2.0 cm Hg. The whole system was constructed of Pyrex or Vycor.

After plating, the relative room temperature adherence of the base metal-molybdenum plate assembly was determined by compressing the sections of the as-plated tubing to 50% of the initial diameter and by completely flattening sections taken parallel to the length axis of the original as-plated tube. As shown in Fig. 1, these tests allowed an empirical characterization of five classes of adhesion; the first representing a bond strength which

[1] Union Carbide Metals Company, Niagara Falls, N. Y.

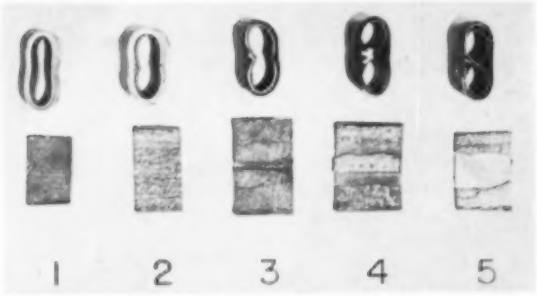

Fig. 1. Typical results of adhesion tests showing examples of the five main classes of adhesion.

exceeded the tensile strength of as-plated molybdenum; the fifth a bond weak enough to result in the complete exfoliation of the coating after testing.

In regard to the role of plating conditions on adherence, the effect of sample preparation and accidental contamination of the pentachloride with oxychlorides were found to be critical. Surfaces cleaned by chemical etching were found preferable to those prepared by mechanical cleaning. The presence of oxychlorides in the plating system, which were subsequently reduced to produce layers of MoO_2 in the plate, destroyed any adherence, even if the oxide films were less than 10^{-4} in. thick. In addition, if an oxide-contaminated molybdenum plate was deposited on iron or nickel, bulging or blistering of the plate would occur often (Fig. 2). Since this structural defect was observed only when MoO_2 was present at an interface highly permeable to hydrogen, the blistering could have been produced by entrapment of steam due to the reduction of the molybdenum oxides by the hydrogen that can diffuse through the nickel or iron base.

The effect of sample composition on the adherence of the as-plated molybdenum was studied by plating specimens of pure iron, 1020 and 1030 plain carbon steel, 18-8 stainless steel, pure copper and nickel, and Inconel. In addition, pure iron, and in some cases low carbon steels, electroplated with nickel, cobalt, copper, chromium, and rhodium were also evaluated. As indicated in Table I, satisfactory as-plated adhesion of the molybdenum plate could not be obtained on pure iron, stainless, low-carbon steel, or on chrome-plated surfaces. Nickel, copper, and Inconel, or any of the iron or steel samples which had been electroplated with nickel, cobalt, copper, or rhodium before vapor plating with molybdenum exhibited excellent as-plated adherence.

Table I. Effect of base material on adherence

Base material	Thickness of molybdenum plate, in. × 10^3	Adhesion rating*
Pure copper	28.0	2
Pure nickel	7.0	1
Inconel	3.0	1
Pure iron	2.0	4
1020 steel	3.0	5
1030 steel	2.0	4
18-8 stainless steel	7.0	3
Chromium (0.001-in.) plated iron	8.0	3
Copper (0.001-in.) plated iron	6.0	1
Cobalt (0.001-in.) plated iron	8.0	1
Nickel (0.002-in.) plated iron	8.0	1
Nickel (0.0008-in.) plated iron**	6.0	1
Rhodium (0.0006-in.) plated iron	8.0	1
Chromized 1020 steel	3.0	5
Nickel plated (0.0003-in.) 1030 steel**	2.0	1

* See Fig. 1 for classification of adhesion ratings.
** Replacement nickel phosphide coating, all other electrolytic.

Metallographic examination of samples of pure iron, 18-8 stainless steel, or chromium-electroplated iron, vapor plated with molybdenum did not indicate that surface oxide films on these materials were responsible for the poor adherence. Since appreciable amounts of iron and especially chromium chlorides were produced during plating experiments on iron- and chromium-rich surfaces, reaction with chlorides must have occurred during the plating of these materials. The degree of reaction was strong enough to remove any oxide films originally present.

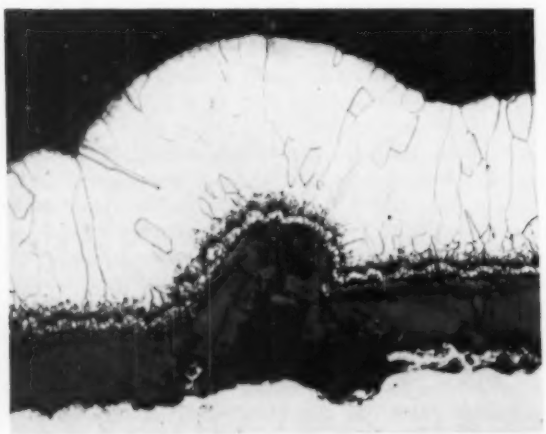

Fig. 2. Vapor deposit of molybdenum (top) on iron (bottom). Note the thick band of MoO_2 and the associated "blister." Etched with alkaline ferricyanide. Magnification 250X before reduction for publication.

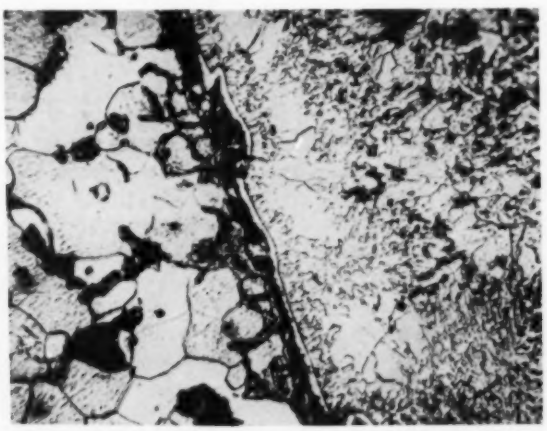

Fig. 3. S.A.E. 1030 steel (left side) coated with molybdenum (right side). Note the thin band of Mo_2C at the interface and Mo_2C inclusions in the plate. Etched with alkaline ferricyanide. Magnification 750X before reduction for publication.

Table II. Hardness and width of the intermetallic phases formed in the interface between molybdenum coating and material on which it is deposited

System	Characteristic adherence	Phase	Hardness* V.P.N. 16-g load	Width,* in. × 10^{-5}
Mo-Cu	1 to 2	immiscible	—	—
Mo-Co	1	Mo_6Co_7	1700	18
		$MoCo_3$	1050	15
Mo-Fe	4	Mo_6Fe_7	750	20
Mo-Ni	1	MoNi	1200	28
		$MoNi_3$	1600	17
Mo-Rh	1	Epsilon	1500	18

* As measured on samples annealed 100 hr at 900°C after plating. Identification of phases after Hansen and Anderko (6).

Evidence of grain-boundary attack of chromium-rich surfaces but not of chromium-free steels was often noted.

Although the carburization (Fig. 3) of the molybdenum plate deposited directly on a steel was believed to be the main reason for the poor adhesion always found with carbon steel specimens, the poor bonding exhibited by stainless steel, pure iron, or chromium-plated specimens was not found to be related to the formation of brittle films of intermetallic compounds at the molybdenum-base metal interface. Indeed, no correlation was found between the hardness (Table II) or width of the intermetallic phases that form on prolonged annealing (100 hr at 900°C) in the iron-molybdenum, nickel-molybdenum, copper-molybdenum, cobalt-molybdenum, or rhodium-molybdenum systems and the as-plated adherence. It should be stressed that these observations were made on specimens whose integrity on metallographic examination was excellent (Fig. 4 and 5).

In addition, the excellent relative bond strength of vapor-deposited molybdenum to pure iron electroplated with nickel, copper, cobalt, or rhodium

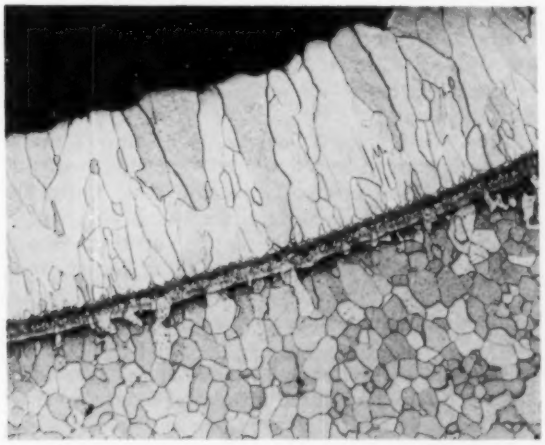

Fig. 4. Pure iron (bottom) plated with molybdenum (top). Note the Mo_6Fe_7 band. Etched with nital and alkaline ferricyanide. Magnification 75X before reduction for publication.

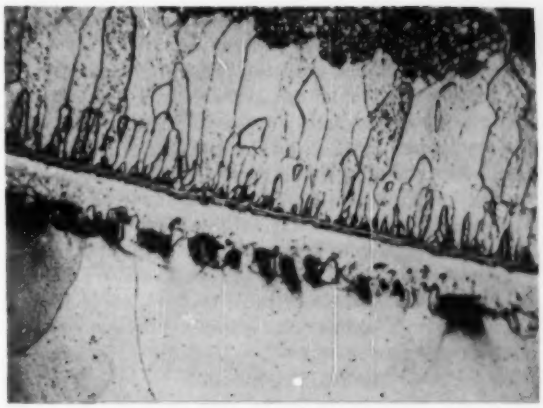

Fig. 5. Rhodium (0.0006 in.) electroplated pure iron (bottom) and vapor plated with molybdenum (top). Note thin gray band of the molybdenum-rhodium epsilon phase. Etched with nital and alkaline ferricyanide. Magnification 200X before reduction for publication.

remained completely unaffected by the 100-hr anneal at 900°C as long as the electroplate was thicker than 0.001 in. The poor bond strength of pure iron to pentachloride molybdenum was not improved by the same anneal.

Discussion

These results indicate that if carburization or oxide contamination of the molybdenum plate is prevented, the nature of the intermetallic phases that form at the molybdenum-base metal interface does not govern the as-plated adherence. In addition, the adherence of the plate after prolonged annealing is also only slightly affected by the growth of brittle intermetallic bands. The only correlation between the adherence of pentachloride molybdenum and the nature of the surface on which it is deposited seems to be a chemical one. In brief, metals such as iron or chromium which form chlorides more readily than molybdenum (5) were always found to be unsatisfactory surfaces for vapor deposition. Conversely, surfaces rich in copper, nickel, cobalt, or rhodium, all of which form less stable chlorides than molybdenum (5), consistently provided an excellent bond to pentachloride reduced molybdenum. Since appreciable amounts of chromic chloride or ferric chloride were always found in the exhaust system following plating experiments on iron- or chromium-rich surfaces, some experimental justification for associating poor adherence with chloride reactivity exists. It is suggested that the formation of chlorides involving the constituents of the metal being plated on, destroys the adherence by contaminating the surface. Also, since this reactivity occurs only with surfaces that form more stable chlorides than molybdenum, a replacement reaction could occur between the molybdenum chloride gas and the constituents of the surface. Since any reduction of the molybdenum chlorides by such elements as iron or chromium will produce a plate of higher chlorine, iron, or chromium content than that obtained by hydrogen reduction, a lower purity material of lower ductility, and thus poorer adherence, could form.

It is not possible to associate the poor adherence of vapor-deposited molybdenum to iron- or chromium-rich surfaces with the presence of oxide films on the steel or chromium surface. Any films of iron oxide present on the sample would be reduced by the hydrogen and chloride plating environment, while the chromic oxide films would be etched off by the chloride attack. The contention that affinity for oxygen does not characterize a strata to which poor adherence is to be expected is borne out by the excellent adherence found in deposits formed on rhodium-plated steels or pure Inconel, surfaces that possess a high affinity for oxygen but good resistance to chloride formation.

From these studies, it is possible to conclude that adherent coatings of molybdenum can be vapor plated onto surfaces which are free of carbon or constituents that form more stable chlorides than molybdenum. The coating system must, of course, be so designed as to eliminate oxygen contamination of the plate. By pre-treating samples containing carbon, iron, or chromium with an electroplate of copper, cobalt, nickel, or rhodium, adherent coatings can be applied to almost any material stable at the plating temperature. In closing, it is possible to suggest that similar criteria may govern the adherence of chromium, tantalum, or tungsten coatings when they are produced by chloride reduction.

Acknowledgment

This research program was supported by the Department of the Army, Boston Ordnance District, Watertown Arsenal.

Manuscript received Nov. 2, 1959.

Any discussion of this paper will appear in a Discussion Section to be published in the December 1960 JOURNAL.

REFERENCES

1. C. F. Powell, I. E. Campbell, and B. W. Gonser, *J. (and Trans.) Electrochem. Soc.*, **93**, 258 (1948).
2. W. J. Childs, J. E. Clive, W. M. Kisner, and J. Wulff, *Trans. A.S.M.* (1950).
3. H. S. Spacil and J. Wulff, Submitted to *Journal of Metals, A.I.M.E.* (1959).
4. P. L. Raymond, *This Journal*, **106**, 444 (1959).
5. L. L. Quill, "The Chemistry and Metallurgy of Miscellaneous Materials-Thermodynamics," McGraw-Hill Book Co., New York (1950).
6. M. Hansen and K. Anderko, "Constitution of Binary Alloys," 2nd ed., McGraw-Hill Book Co., New York (1958).

Brief Communication

Growth of Single Crystal Silicon Overgrowths on Silicon Substrates

Albert Mark

U. S. Army Signal Research and Development Laboratory, Fort Monmouth, New Jersey

A single crystal silicon overgrowth has been produced on a silicon substrate. This phenomenon confirms a fundamental principle for silicon showing that it is possible to have a vapor phase chemical reaction between the solid and vapor of one of its compounds. The silicon monolayers grow by accretion of atoms from the generating medium and assimilate as a single crystal overgrowth to the (100) orientation of the silicon substrate.

The reaction is based on the reduction of silicon tetrachloride by hydrogen, $SiCl_4 + 2H_2 \rightleftharpoons Si + 4HCl$, using a slow growth process. The deposited silicon layer or film has an orderly atomic lattice and continues the internal lattice structure of the substrate crystal without boundary layers at the interfaces. In this respect, the silicon layer is synonymous with and is an extension in three dimensions (growth in volume) of the original substrate surface over its entire periphery.

The deposit growth imitates and assumes the same growth pattern as initially exposed after an acid etch of the substrate face prior to a run. Rosette-like formations found in loosely masked areas continue their geometry in extending out and embracing the limits of their original boundary area. These appear to grow more prominently along their outer boundaries with the internal areas gradually filling in as the growth continues. The mechanical quality of the grown surface therefore is dependent to a great extent on the initial substrate geometrical configuration.

The deposit growth eventually assumes a dense jet black glassy surface which is difficult to distinguish from the original substrate face. Fully developed, this characterizes the ideal mechanical overgrowth surface. If the entire substrate face is loosely masked with a cover crystal, a denser, more uniform quality overgrowth results. This is apparently due to reduced heat losses at the crystal interfaces.

Electron diffraction studies of the overgrowths described were made at Purdue University by H. J. Yearian, Professor of Physics. His summation statement of his report follows: "From these results it may be concluded that all of the regions studied were single crystals of at least fair quality. On those

specimens for which a mask had been used, the deposits were thick enough to insure that the results represent the deposit and not the substrate."

The significance of an overgrowth layer of silicon can best be realized by enumeration of some of the probable electronic applications.

1. Application for fabricating surface devices (silicon deposited and growing out from a surface). —(*a*) An overgrowth of single crystal silicon of an opposite conductivity type to that of the silicon substrate crystal on which it is grown will act as a "surface junction." This implies a diode structure form. (*b*) An overgrowth of single crystal silicon acting as a surface junction can be processed to high or low resistivity values. (*c*) An overgrowth of single crystal silicon can be of the same conductivity type as the silicon substrate forming intrinsic pp^+ or nn^+ regions. (*d*) An overgrowth of single crystal silicon as a wide area film will act as a matrix with its surface containing innumerable junction points through proper masking techniques. (*e*) An overgrowth of a single crystal silicon film with a large area junction structure could be made sensitive to various forms of radiation, for example, for use in solar cells.

2. Multilayered devices.—(*a*) Alternate overgrowths of single crystal silicon films on parent or foreign substrates, each with its own discrete resistivity or conductivity type, will alternately act as high resistance I regions, pn and np junctions, and pp^+, nn^+ regions. (*b*) An overgrowth of single crystal silicon can be an active or passive element when used or incorporated into micromodule circuits.

3. Miscellaneous uses.—(*a*) An overgrowth of single crystal silicon allowed to grow to only an extremely thin film will act as a base region permitting the fabrication of very high frequency devices. (*b*) As an overgrowth of single crystal silicon on a foreign substrate with a lattice distance closely matching that of silicon. In this type of device, the substrate, if a metal, would act as the support media and as one pole of an electrical contact.

The perfection and extended use of this process in all its variations will permit the utilization of silicon in presently unexplored device areas thereby broadly increasing its usefulness as a semiconductor material.

Acknowledgment

The author wishes to express his thanks and gratitude to Professor H. J. Yearian and associates of Purdue University for the efforts expended in making the electron diffraction studies and evaluation of the samples.

Manuscript received Jan. 29, 1960.

Any discussion of this paper will appear in a Discussion Section to be published in the December 1960 JOURNAL.

Brief Communications

The JOURNAL accepts short technical reports having unusual importance or timely interest, where speed of publication is a consideration. The communication may summarize results of important research justifying announcement before such time as a more detailed manuscript can be published. Consideration also will be given to reports of significant unfinished research which the author cannot pursue further, but the results of which are of potential use to others. Comments on papers already published in the JOURNAL should be reserved for the Discussion Section published biannually.

Submit communications in triplicate, typewritten double-spaced, to the Editor, Journal of The Electrochemical Society, 1860 Broadway, New York 23, N. Y.

Discussion Section

This Discussion Section includes discussion of papers appearing in the JOURNAL of The Electrochemical Society, Vol. 105, No. 1 (January 1958) and Vol. 106, No. 4, 6, 7, 8, 10, and 11 (April, June, July, August, October, and November 1959). Discussion not available for this issue will appear in the Discussion Section of the December 1960 JOURNAL.

The Anodic Oxidation of Zinc and Zinc-Tin Alloys at Very Low Current Density

S. E. S. El Wakkad,[1] A. M. Shams El Din, and H. Kotb
(pp. 47-51, Vol. 105, No. 1)

(NOTE: The following is Dr. Shams El Din's reply to the discussion by M. Prazák which appeared in the December 1959 Discussion Section, p. 1072. These comments reached the Editorial Office too late to be included in December.)

A. M. Shams El Din: Tin and zinc form a simple eutectic system containing about 8% zinc, so that the electrodeposited alloy containing 20-25% zinc consists of the eutectic plus some free zinc.[2] Because zinc is the more electronegative of the two components, the electrode behavior of the alloy is to a great extent determined by the zinc and not by the tin. Thus, for example, in aerated 3% potassium chloride solution at room temperature, the electrode potential of the alloy vs. the saturated calomel electrode is approximately −1.0 v. The corresponding values of pure tin and pure zinc are −0.45 v and −1.02 v, respectively.[2]

Despite this fact, the tin of the alloy still manifests itself and exerts some of its properties on the general behavior of the alloy. The final behavior of the alloy need not, therefore, be the algebraic sum of its constituents. In the curves given in our original paper and also in the curve accompanying the comments of Dr. Prazák, it is clearly shown that the tin of the alloy oxidizes after the zinc. How much the tin oxide(s) film will affect the behavior of the zinc is difficult to tell, but the main fact is that it does affect it. This is also observed from other corrosion experiments employing techniques such as salt spraying and humidity tests. Thus, for example, salt spraying experiments (20% salt solution) with pure zinc result in the formation of dense white corrosion products which are not observed in the case of the alloy despite its free zinc content.[2] Humidity tests also reveal the superiority of the alloy to the zinc. Apparently, such difference in behavior between the alloy and zinc is to be attributed to the presence of tin.

The interesting finding of Dr. Prazák, that the behavior of the alloy is not the sum of its components, might be due to the fact that after the initial dissolution of the zinc the concentration of the tin at the surface of the alloy becomes higher than the corresponding value in the bulk of the alloy.

The occurrence of two current humps in the polarization curve of zinc in Dr. Prazák's Fig. 1 does not necessarily mean, in our opinion, a building of a new oxide of zinc. If zinc is able to form two oxides, then it should reveal this property also in the galvanostatic curves as do the other metals.[3] The first current hump in Fig. 1 starts at a potential of about −1.2 v which is in good agreement with the potential of the system Zn/ZnO at this *p*H value. A corresponding step is also reported in our paper. The second, smaller, oxidation step starts at about −0.6 v, and a similar step is not observed in our polarization curves. In our opinion, the second step observed in the potentiostatic experiments of Dr. Prazák corresponds to the thickening of the already present oxide film. Simultaneous dissolution in the form of zincate is also to be expected. The constancy of the current associated with this process over an increasing potential range of about 1.8 v suggests a corresponding increase in the resistance of the system electrode/electrolyte. The solution side of the system cannot be the cause of an increase in the resistance, first, because it is a good conductor, and, second, because in the polarization curve of zinc given in Fig. 1 there occur two different constant currents, a fact which reflects the conclusion that the solution side of the system cannot be the cause of resistance increase. The constancy of the current is, therefore, to be ascribed to the increase in the resistance of the oxide film. This can occur through an increase in the thickness of the film and/or the closing of the pores of the oxide. Such processes will have the ultimate result of decreasing the conductivity of the surface film.

Probably, if the effect of variables such as the alkali concentration and the presaturation of the solution with zinc oxide on the limiting current of the second step were to be studied, a clearer insight could be gained concerning the nature of the process(es) taking place at the electrode surface.

Before such understanding of these processes at the surface of both the zinc and the alloy electrodes is achieved, the suggestion of a homogenous passive layer growing on the surface of the nonhomogenous Sn-Zn alloy is to be considered as *ad hoc*.

Other than this point, the interesting observations of Dr. Prazák are in full agreement with ours. Thus, the polarization curve of the alloy shows clearly the oxidation of both the zinc and tin at their respective potentials. The quantities of electricity consumed in the building up of zinc and tin hydroxides on the alloy are less than those for pure zinc and tin alone.

[1] Deceased.

[2] Tin Research Institute, "Tin-Zinc Alloy Plating," Technical Publication, March 1952.

[3] S. E. S. El Wakkad and S. H. Emara, *J. Chem. Soc.*, 1952, 461, *ibid.*, 1953, 3504, 3508; S. E. S. El Wakkad and A. M. Shams El Din, *ibid.*, 1954, 3094, 3098; S. E. S. El Wakkad, A. M. Shams El Din, and J. A. El Sayed, *ibid.*, 1954, 3103; S. E. S. El Wakkad, T. M. Salem, A.M. Shams El Din, and Z. Hanafi, *ibid.*, 1956, 2857.

Controlled Potential Reactions of Cadmium and Silver in Alkaline Solution

G. T. Croft (pp. 278-284, Vol. 106, No. 4)

Indra Sanghi[1]: We have reported some galvanostatic and potentiostatic experiments with zinc[5, 6] and have similar work with cadmium in progress. While the experimental procedure is different from that used by Dr. Croft, some of the basic inferences from the data are very similar. For this reason, I offer the following comments.

In his paper, Dr. Croft has measured currents, at constant overpotential, as a function of time. He found that, after sufficient time had elapsed, current and time were related by an equation of the type $I = F(\phi)\ t^{-1/2}$. From this, he took the oxide to obey the parabolic growth law and interpreted $F(\phi)$ as a function relating the rate of reaction to the overpotential. His basic assumption that the application of the above equation to the currents, *measured after sufficient time*, implies that the oxide grows from the beginning to the end in a parabolic manner is not quite clear, particularly as Charlesby[7] had shown that the rate equation would depend on the time range during which the growth is studied. In fact, he has defined the various thickness ranges in which the logarithmic, the cubic, and the parabolic laws can successively define the oxide layer growth under the same conditions and on the same electrode, the parabolic law taking over when the films have thickened to a definite extent. Moreover, Delahay[8] and Bieri[9] have shown that for the study of the $It^{1/2}$ relationship the first few minutes are very crucial in order to derive any theoretical conclusions as, later on, convection and other effects interfere. Further, Dr. Croft found that currents at equivalent times after application of the same anodic potentials were not generally reproducible. There is then some doubt about the significance of the so-called constancy of $It^{1/2}$ at large values of time.

Our own galvanostatic and potentiostatic studies[10] on Cd, similar to those on Zn,[5, 6] do not lead to a constant I^2t in all cases where the passivation was reached within a few minutes (10 min).

Dr. Croft found that for Cd electrodes $F(\phi)$ has at least one maximum and often two, most probably between 18 and 40 mv overpotential. The significance of this observation is not clear. It is doubtful as to how far these represent actual layer growth. Our potentiostatic measurements reveal that, in KOH concentrations ranging between 1 and 3.5 N, active dissolution occurs during the first 50 mv overpotential. Only when the overpotential is raised beyond 50 mv, a uniform coherent oxide layer starts to thicken, with decrease of current rate. According to our ideas, the predominant layer growth occurs in the current plateau region, clearly revealed by our potentiostatic measurements, at a nearly constant rate over a wide overvoltage range (ca 1400 mv) before oxygen evolution commences. This wide range of study has, perhaps, been overlooked by Dr. Croft.

Essentially, this layer grows as oxide, and only at the oxide/electrolyte interface is it partially converted into $Cd(OH)_2$. The electrode, may, therefore, be pictured as $Cd/CdO/Cd(OH)_2/KOH$ solution.

Dr. Croft's observation that a higher current is required to force the electrode to oxidize at 30 mv than at 97 mv is clearly explained by our potentiostatic measurements which show that in the active dissolution region a higher current is sustainable at a lower overpotential than the smaller currents that can be sustained at high overpotentials in the "pseudo passivation region" of 1400 mv extending from ca -0.7 to $+0.7$ v vs. the Hg/HgO/N KOH half-cell.

For the triangular wave transients, Dr. Croft prepolarized Cd anodically at 1 ma/cm^2 till ϕ rose to 30 mv anodic when the current was turned off and later subjected to triangular waves. Our constant current polarization curves indicate that in 5N KOH (as used by Croft) 1 ma/cm^2 would increase the overpotential by 30 mv in less than a minute; surely it would not suffice to render the electrode truly passive. Moreover, the effect of this very short anodic polarization would be mostly lost during the prolonged period in which the current is turned off and the electrode is allowed to come to the equilibrium potential. Thus, the exact significance of this procedure is not quite clear.

Perhaps it was this factor of observing the Cd surface in the active region and/or after leaving it in the electrolyte on open circuit for sufficient time that was responsible for Croft's observation of only $Cd(OH)_2$ on the electrode surface. On the other hand, x-ray and electron optical observations of Huber and Lake and Casey have clearly shown the presence of CdO.

Similarly, Croft's observation of the change of oxidation rate, from the initial logarithmic rate to a parabolic rate later, may be explained on the basis of Charlesby's theories as indicated above.

Our detailed results are under publication separately.

George T. Croft: Dr. Sanghi is quite correct in the statement that the $F(\phi)t^{-1/2}$ relationship[11] *implies* that the hydroxide grows from the beginning to the end in a parabolic manner. On the other hand, it is clear from Fig. 2 of the discussed paper that the entire growth process is not described by a parabolic law and, in fact, most of the oxide growth does not follow the parabolic law. However, the *current* (rate of growth) does fit a parabolic relation for a time equal to about 70% of the total time of observation.

[1] Central Electro Chemical Research Institute, Karaikudi, India. (Present address: Gannon Dunkerley & Co., Ltd., P. O. Box 1547, Fort, Bombay 1, India.)

[5] I. Sanghi and M. Fleischmann, *Electrochimica Acta*, 1, 161 (1959).

[6] I. Sanghi and W. F. K. Wynne-Jones, *Proc. Indian Acad. Sci.*, 47A, 49 (1958).

[7] A. Charlesby, *Proc. Phys. Soc. (London)*, 66, B317 (1953).

[8] P. Delahay, *Anal. Chem.*, 27, 478 (1955).

[9] B. Bieri, Ph.D. Thesis, Berne University, Berne, Switzerland (1949).

[10] I. Sanghi, *This Journal*, Discussion Section, 106, 532 (1959).

[11] G. T. Croft, *This Journal*, 106, 278 (1959).

During this time, the electrode is in such a state that, if it were suddenly forced to oxidize at a constant current density of about 1 ma/cm^2, the electrode potential would go immediately to the oxygen overpotential for the electrode. An electrode in such a state will, for purposes of this discussion, be considered passive or pseudopassive. It is for electrodes in the passive or pseudopassive state that the parabolic law appears best to fit the data. Fixed and sweeping potential measurements of $F(\phi)$ were made, using electrodes in the passive state.

It would, therefore, be more accurate (and perhaps less confusing) to say that Eq. [1] describes the current for a time greater than t_i where t_i is the time required for passivity to set in.

As regards the influence of convection currents in the electrolyte, we found that the current through the electrode (fixed potential) in the passive state was unchanged if the electrolyte was stirred. If one is studying a reaction whose electrode potential is determined by the concentration in solution of the ion undergoing electron exchange at the electrode-solution interface, the true electrode potential can be observed for only short periods of time because, as the reaction proceeds, local concentration changes cause convection currents which give rise to anomalous results.[12] Evidently, we are not studying a phenomenon related to convection because of the long time involved and the failure to observe convection effects directly.

A controversy exists over the products of the electrochemical reaction of cadmium in alkaline solution. Immediate analysis (by x-ray techniques) of reaction products formed prior to onset of passivity and after passivity sets in shows consistently no signs of CdO. $Cd(OH)_2$ is the only reaction product we detected in our laboratory by x-ray techniques. This result is confirmed by the work of Uno Falk,[13] who made a specific search for CdO in an x-ray diffractometer study of cadmium oxidation and reduction *in situ*. He found only Cd and $Cd(OH)_2$. By weighing experiments, he also verified the reaction as $Cd + 2OH^- \rightarrow Cd(OH)_2 + 2e$. Salkind[14] has also shown that only $Cd(OH)_2$ forms during oxidation of cadmium in alkaline electrolytes.

Oxide Nucleation and the Substructure of Iron

E. A. Gulbransen and K. F. Andrew (pp. 511-515, Vol. 106, No. 6)

J. L. Walter and C. G. Dunn[15]: The authors state that the growth of oxide nuclei may be related to the number and arrangement of dislocations in the underlying metal crystal. They also state that the nucleation centers become ordered along definite crystallographic directions when the iron is annealed in impure hydrogen. They conclude that water vapor in the hydrogen is responsible for ordering of the nucleation sites.

Our studies of grain growth in high-purity iron and silicon iron annealed under slightly oxidizing conditions indicate that the nonrandom oxide patterns correlate with the patterns of thermal etch that exist at the surface of grains of certain orientations.

It is known that iron[16] and silicon iron[17] will thermally etch when annealed in atmospheres containing a small amount of water vapor or oxygen. Thermal etching will not occur if the atmosphere is sufficiently pure. Grains having orientations near (100) and (111) at the gas-metal interface thermally etch to striations. The thermal etch steps become curved when the low index planes (100) and (111) are within 1-2 degrees of the plane of a slightly uneven surface.

Fig. 1. 1000 X before reduction for publication

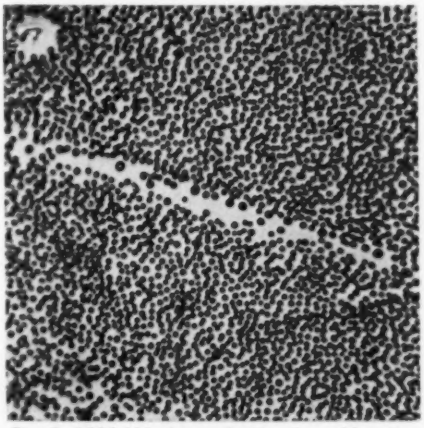

Fig. 2. 1000 X before reduction for publication

The interaction between the thermal etch steps and oxides is clearly seen in Fig. 1 of this discussion. This is a photograph of a sample of high-purity iron annealed for 24 hr at 875°C in tank argon. The oxides formed circular patterns similar to those shown by the authors' Fig. 5. A nearly random distribution of oxides on a grain near (112) is shown in Fig. 2 of this discussion. This was a sample

[12] P. Delahay *Anal. Chem.*, 27, 478 (1955).

[13] Uno Falk, Battery Division Abstract No. 27, Electrochemical Society Meeting, Columbus, Ohio, Oct. 1959.

[14] A. J. Salkind, Battery Division Abstract No. 26, Electrochemical Society Meeting, Columbus, Ohio, Oct. 1959.

[15] Metallurgy and Ceramics Research Dept., Research Lab., General Electric Co., P. O. Box 1088, Schenectady, N. Y.

[16] J. Benard, J. Moreau, and F. Gronlund, *Compt. rend.*, 246, 756 (1958).

[17] C. G. Dunn and J. L. Walter, "On the Thermal Etching of Silicon Iron," Letter to the Editor, *Acta Met.*, In press.

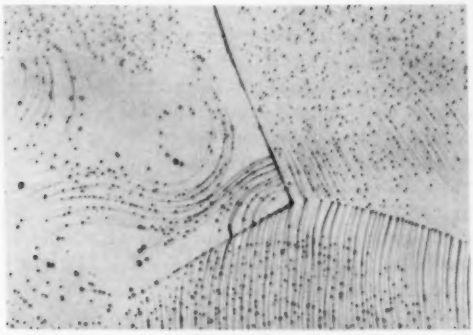

Fig. 3. 500 X

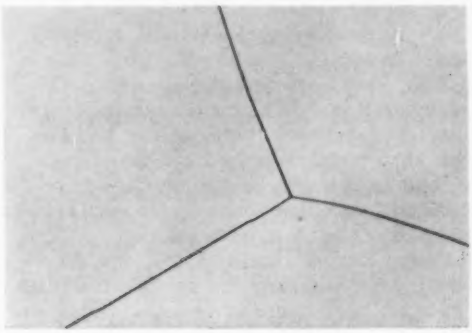

Fig. 4. 500 X

of high-purity silicon iron annealed at 1200°C for ½ hr in tank argon. Grains of this orientation do not show strong thermal etch patterns.

Fig. 3 of this discussion shows a variety of oxide patterns. This sample of high-purity silicon iron was annealed for 1 hr at 1300°C in purified argon. The dew point of the argon was −98°F. All three grains had (100) planes within 3° of the plane of the sample. It can be seen that the oxides, in general, form in rows along the thermal etch steps. Bending of the thermal etch steps at the groove formed by the intersection of the grain boundary with the sample surface is clearly visible. The average number of oxides, measured at the area shown in the photograph, was 9.1 x 10^4/cm^2. After photographing the above area, carbon was added to the sample and it was then electropolished and electroetched in chrome-acetic acid to produce etch pits at dislocation sites. Figure 4 of this discussion shows the same area as is shown in Fig. 3 after the treatment to reveal dislocations. A separate test showed that the amount of carbon added was sufficient to decorate the dislocations introduced by deformation. It is evident that there is no relationship between the oxides at the surface and the dislocations present in the metal since the number of dislocations in the sample was estimated to be approximately 10^4/cm^2.

It is concluded that the pattern of the oxides at the surface of high-purity iron and silicon iron is determined by the nature of the surface discontinuities rather than by the arrangement of dislocations in the underlying metal crystal.

E. A. Gulbransen: The resemblance of thermal etching patterns to oxide nucleation patterns has been pointed out to us by Hoar [18] and by Fraser [19] as early as 1953. We feel that there may be a resemblance between the two phenomena, but we disagree with the conclusions of Walter and Dunn.

Unfortunately, the experiments of Walter and Dunn given here are inconclusive. The spots on their Fig. 3 were assumed to be oxide but were not proven, while the value of 10^4/cm^2 for the number of dislocations in Fig. 4 appear to us to be absurd. Silicon iron is a poor material to use to demonstrate the relationship between dislocations and oxide nuclei. At 1300°C, selective evaporation occurs and a film of silica probably is formed on the surface. Solid phase reactions could occur which would leave residual material on the surface.

Since writing our paper, we now feel even stronger that nucleation centers exist in metals. These centers are involved not only in the formation of initial oxide nuclei but in the formation of oxide whiskers and platelets[20]. These nucleation centers can be oriented by stress, [21] impurities in the metal, and by the nature of the reaction environment.[22] Studies are now being made in our laboratory to elucidate these problems. Whether these nucleation centers can be related to the present concepts of dislocations is problematical at the moment. Most of the present concepts of dislocations have been developed on the basis of mechanical properties and the very complicated phenomena of etch pits.

Rectification by Zircaloy 2 in High-Temperature Water

J. N. Wanklyn and R. Aldred (pp. 529, Vol. 106, No. 6)

P. Cohen[23]: In 1950, the writer experienced the same difficulties reported by the authors, namely electrolytic corrosion of zirconium at 600°F, using 60-cycle current at about 6 v, in heating a zirconium specimen in a heat transfer corrosion test. Failure of the test specimen occurred in 200 hr.

The problem is a general one where electrical heating of zirconium in high-temperature water is required for prolonged periods. In seeking a solution to the problem, the effect of frequency on the electrolytic corrosion of zirconium in NaCl solutions was investigated at room temperature. The corrosion efficiency decreased rapidly and monotonically with increasing frequency, reaching very low values in frequency range 400 to 1000 cycles. Since it could be most readily procured, a 400-cycle 50-kva aircraft type generator was obtained. Coupled with an available 3000-amp 100-kva transformer, the 400-cycle generator was used in subsequent tests of the same type.[24] Actually, 1000-cycle motor generator sets of the size required for this type of work are also available and may be more satisfactory.

[18] T. P. Hoar, Private communication.

[19] M. Fraser, Private communication.

[20] E. A. Gulbransen and T. P. Copan, General Discussion of the Faraday Society on Crystal Imperfections and the Chemical Reactivity of Solids, Kingston, Ont., Sept. 1959.

[21] E. A. Gulbransen and T. P. Copan, "Proceedings of the Symposium on Internal Stresses and Fatigue in Metals," p. 397, Elsevier Publishing Co., New York (1959).

[22] E. A. Gulbransen and T. P. Copan, "Physical Metallurgy of Stress Corrosion Fracture," p. 155, "Metallurgical Society Conferences Vol. 4," Interscience Publishers, Inc., New York (1959).

[23] Atomic Power Dept., Westinghouse Electric Corp., P. O. Box 355, Pittsburgh 30, Pa.

[24] "Out-of-Pile Dynamic Loop Tests of Irradiated Fuel Materials," L. A. Waldman and W. T. Lindsay, Jr., WAPD-PWR-CP-2945, p. 26. Obtainable from Technical Information Service, USAEC.

On an Ion-Exchange Property of Manganese Dioxide

A. Kozawa (pp. 552-556, Vol. 106, No. 7)

Alfons Krause[25]: In his investigation, Kozawa found an exchange between zinc ions and H+ ions on the surface of MnO_2, which he explained as occurring through hydration of the surface; however, not every MnO_2 is suitable for the exchange. It is well known, and also mentioned by Kozawa, that MnO_2 cannot be hydrated when annealed at an excessively high temperature, whereas less annealed samples do add water, in spite of being practically water free. We are dealing here with active and inactive MnO_2, and differences in structure have not been considered by Kozawa in his exchange-scheme. According to this over-simplified scheme, each oxide theoretically should be able to add water, regardless of whether or not this is possible in practice.

In my opinion, these differences can be accounted for by the radical structure[26] which accounts for the active state, i.e., the active sites of a metal oxide. The actual model of the normal structure of MnO_2 is not so important, but rather that only two types of radicals may be found in active MnO_2, namely, R≡Mn- and R≡Mn-O-.[27] The latter is an electron acceptor and a potential anion. It also can be considered as a Lewis acid. The radical R=Mn-, however, is an electron donator and a possible cation. The radicals disappear only by strong annealing due to a "healing" of the MnO_2 lattice, thus making the oxide practically inactive:

$$\underset{\text{(active)}}{R{\equiv}Mn\text{- -O-}Mn{\equiv}R} \rightarrow \underset{\text{(inactive)}}{R{\equiv}Mn\text{-O-}Mn{\equiv}R} \text{ (schematic)}$$

The radical MnO_2 is enabled to add H_2O molecules as expressed in the following equation:

$$R{=}Mn\text{-} + H_2O + \text{-O+}Mn{\equiv}R \rightarrow 2R{\equiv}Mn\text{-OH}$$

The resulting hydroxide reacts further with ammoniacal zinc oxide solution which is, in fact, an exchange of hydrogen for zinc:

$$2\,R{\equiv}Mn\text{-OH} + [Zn(NH_3)_2Cl_2] \rightarrow$$

$$2\,R \equiv Mn\text{-O}\frac{Zn}{2} + 2\,NH_4Cl \qquad [1]$$

For nonradical, i.e., inactive MnO_2, the equations cannot be applied.

The exchange process, incidentally, may be considered in another way, namely that the MnO_2 assumes the function of a chromatographic column. Here, also, the radical structure of MnO_2 is essential as was shown previously for Al_2O_3.[28] Through the action of ammonia, the chromatographic column (MnO_2) assumes a negative charge, whereupon zinc ions can be taken up. This is, in fact, an inhibited coagulation of the chromatographic MnO_2[29]:

$$(R{\equiv}Mn\text{-})_2 + (\text{-O-}Mn{\equiv}R)_2 + [Zn(NH_3)_2Cl_2] + 2H_2O \rightarrow 2\,R{\equiv}Mn\text{-OH} + 2NH_4^+ + 2\,(O\text{-}Mn{\equiv}R)^- + Zn^{++} + 2\,Cl^- \rightarrow Zn(O\text{-}Mn{\equiv}R)_2 + 2\,R{\equiv}Mn\text{-OH} + 2NH_4^+ + 2Cl^- \qquad [2]$$

[25] Institute of Inorganic Chemistry, University of Poznan, Poznan, Poland.

[26] A. Krause and H. Krach, *Ber. deut. chem. Ges.*, 69, 2709 (1936); A. Krause, *Przemysl Chem.*, 28, 267, 558 (1949); A. Krause in J. Alexander's "Colloid Chemistry," Vol. VII, p. 175, New York (1950).

[27] A. Krause, *Z. anorg. u. allgem. Chem.*, 301, 294 (1959).

[28] A. Krause, *Bull. soc. des amis sci. et lettres de Poznan*, Ser. B, XIII, 111 (1956).

Akiya Kozawa: It seems reasonable to assume that the ion-exchange reaction mostly takes place only on the surface of MnO_2, since the ion-exchange reaction attains at a equilibrium in a short time and it is reversible on pH change of the solution (Fig. 9 of the paper). On the surface of MnO_2, there exist unsatisfied chemical bonds which might correspond to "Radicals," R≡M- and R≡M-O- mentioned by Professor Krause. The final surface structure of the MnO_2 with the adsorbed zinc ion, $(R{\equiv}Mn\text{-O})_2Zn$, proposed by Professor Krause [*See* Eq. [1] and [2]; I think there is a mistake in Eq. [1], which should be $2R{\equiv}Mn\text{-OH} + Zn(NH_3)_2Cl_2 \rightarrow (R{\equiv}Mn\text{-O})_2Zn + 2NH_4Cl$], is quite similar to that shown in Fig. 10. Difference between the two mechanisms is as follows: as the surface of MnO_2 before zinc adsorption, he is considering R≡Mn-OH resulting from radicals R≡Mn-O- and R≡Mn- by adding H_2O molecules, and I am considering $R{\equiv}Mn\text{-}OH_2$ by a simple hydration. I do not have experimental results to distinguish between the two. It is, however, well known that metal ions hydrate in aqueous solutions, and so it would be permissible to consider a hydration of manganese ions on the surface of ionic crystal of MnO_2 in an aqueous solution.

Professor Krause considers that the active sites of MnO_2 surface, namely the radical structures, are essential for the ion-exchange adsorption. However Fig. 6 shows that the amount of the ion-exchange (zinc adsorption) is proportional simply to the surface area measured by gas adsorption (B.E.T. method), regardless of those samples, active MnO_2 or inactive MnO_2, which were prepared by annealing the active MnO_2 below 450°C. According to my experimental results, the saturate adsorption of zinc ion in Fig. 8 corresponds nearly to the monolayer coverage, that is, every two manganese atoms on the surface of MnO_2 adsorb one zinc ion as shown in Fig. 10. From these facts only active sites would not be essential, but rather all the surface of MnO_2 may be responsible for this zinc adsorption.

The Significance of the Flade Potential

M. J. Pryor (pp. 557-562, Vol. 106, No. 7)

H. H. Uhlig[30]: Dr. Pryor's model for the passive film on iron introduces another assumed structure additional to structures he quotes assumed previously by others. Unfortunately, for the present state of knowledge in this field, any of these models is not readily proved or disproved. There are only fragments of circumstantial evidence which support one model over the other, but as yet no critical experiment has been performed or offered.

We have come to accept an adsorbed film model of the passive film over all others because it appears to fit in with the greatest number of observations. These observations have been summarized in a previous paper.[30] Among the important lines of evidence are that those metals and alloys (transition group) best able to chemisorb their environment are also those that tend to be passive. Furthermore, the alloying relations leading to optimum catalytic

[29] Corrosion Lab., Dept. of Metallurgy, Massachusetts Institute of Technology, Cambridge 39, Mass.

[30] H. H. Uhlig, *Z. Elektrochem.*, 62, 626 (1958).

properties which depend on chemisorption are similar to those leading to optimum passivity. In addition, the calculated free energy of formation of the chemisorbed passive film on iron is close to the observed value based on measured heat of adsorption.

On the other hand, Dr. Pryor's model suggests that all metals on which semiconducting oxides form should exhibit passive properties. This is not the case. Copper on which a p-type Cu_2O film forms, or zinc on which an n-type ZnO film forms, are not passive in nitric acid or in any aqueous environment in the same sense as are iron and chromium.

The formation of ferric ions on corrosion of passive iron in sulfuric acid is readily explained by local action cells of which the adsorbed passive film represents a large cathodic area in contact with exposed iron at very small pores, in accord with measurements of porosity in the passive film by Vetter.[31] High current densities established at the small anode sites account for corrosion products of valence 3 rather than, 2, an effect which is readily observed during anodic polarization of iron in sulfuric acid employing increasing current densities.

M. J. Pryor: Professor Uhlig's comments are representative of an entirely different view as to the cause of passivity of metals (i.e., adsorption as opposed to three-dimensional film formation). These different views on the nature of passive surfaces must, of necessity, lead to different interpretations of the meaning of the Flade potential. Since these opposed views on the mechanism of passivation are well known, it appears idle to reiterate them in detail at this time.

In order to explain the Flade potential, it previously has been deemed necessary to assume the initial existence of either a two-phase passivating oxide film or an adsorbed passivating layer of some type. Neither concept has received any significant experimental support from structural studies of passive iron surfaces. Accordingly, it appears to be more logical to develop an explanation of the Flade potential based on the breakdown of a crystallographically single-phase passivating γ-Fe_2O_3 film. The present work shows that such a model adequately can explain the Flade potential, provided that a change in defect structure with thickness is assumed. Such changes in defect structure with thickness have been suggested previously for sulfide films on silver.[32]

Professor Uhlig believes that our paper implies that all metals which carry semiconducting oxides should develop passivity as, for instance, by immersion in concentrated nitric acid. Such a hypothesis is nowhere claimed in the article nor is such an implication intended. Instead, we have pointed out that the Flade potential observed on iron can be related well to electrochemical reactions involving protective γ-Fe_2O_3 films having a p-n defect structure. We further have pointed out how such a film structure may develop during the passivation of iron.

In order for a semiconductive surface film to confer passivity to a metal, it is necessary for the film to have either a high electronic resistance, a high ionic resistance, or both. Furthermore, the surface film must be nonporous and compact. If such is not the case, as for instance with copper which forms low-resistance semiconductive films, then passivation in the normal sense will not occur. It is also significant to note that such metals do not normally exhibit a Flade potential.

It appears that one of the advantages of the present model lies in its ability to cover aspects of the Flade potential which have received only cursory attention in the past. For example, most previous investigators have been concerned primarily with measurement of the potential itself. Rather less attention has been directed to the duration of the potential arrest. It is of interest to note that repeated anodic passivation and activation of an iron specimen in sulfuric acid results in a steady and quite spectacular increase in the duration of the Flade potential arrest. This increase in the duration of the potential arrest does not appear to be particularly sensitive to the time for which the specimen is permitted to remain in the active state. Furthermore, differing means of interrupting the polarizing current appear greatly to influence the length of the Flade potential arrest. These observations are difficult to rationalize on the basis of electrochemical reactions unrelated to the defect state of the surface oxide films. They also tend to confirm the general validity of the approach contained in our article.

Peter F. King[33]: Dr. Pryor is to be congratulated for his valuable attempt to explain the Flade potential. His explanation is more satisfying than some of those which have been attempted in the past. The semiconductive oxide approach has some things in its favor, but there are also some shortcomings. One of these is the small amount of reaction necessary to bring about passivity, which is not sufficient to produce an oxide film 50Å thick. It is true that the argument may be made, and may be valid, that the onset of passivity has never been studied on an absolutely clean metal surface and that the small amount of reaction usually measured may, indeed, be only the growth of the excess oxide ion concentration necessary in Dr. Pryor's theory. Even if oxide is not present initially, oxidation of iron and its alloys in passivating media occurs in an apparently logarithmic fashion with time, as shown by the recent work of Brasher[34] and Stern.[35] It is likely that this oxidation results in defect oxides of the type postulated by Dr. Pryor. However, we do not feel that this oxide determines the Flade potential, as it is only the result, not the cause, of passivity.

We contend that the cause of passivity is a layer of chemisorbed oxygen produced on initial immersion of the metal into the passivating medium. One would expect, from (*a*) the approximate equivalence of the Flade potential obtained on iron after anodic passivation with the passivation potential,[36] and (*b*) the equivalence of the thickness of the film

[31] K. Vetter, *Z. Elektrochem.*, **55**, 274 (1951).

[32] F. S. Stone, *Proc. 3rd Int. Congr. Reactivity of Solids, Madrid*, 1956, p. 641.

[33] Metallurgical Lab., Dow Metal Products Co., Midland, Mich.

[34] O. Kubaschewski and D. M. Brasher, *Trans. Faraday Soc.*, **55**, 1200 (1959); D. M. Brasher and D. H. Kingsbury, *ibid.*, **54**, 1214 (1958).

[35] M. Stern, *This Journal*, **106**, 376 (1959).

[36] K. F. Bonhoeffer, *Z. Metallk.*, **44**, 77 (1953).

on passive iron at the Flade potential[37] to the amount of reaction which occurs during the passivation process,[38] that the superior oxide decays first during activation. The result (just before activation occurs) is a film which is almost equivalent to the film formed during the passivation process.[39]

The major argument in favor of the conclusion that chemisorbed oxygen is the cause of passivity in the case of iron and the iron-chromium alloys in aqueous environments, apparently overlooked by Dr. Pryor, is the equivalence of the experimentally observed Flade potential with that calculated, albeit roughly, from the heat of adsorption of oxygen on iron.[40] It is hoped that similar comparisons can be extended to other cases, such as the alloys of iron and chromium, where the Flade potentials have been measured but the heats of adsorption are not yet available.

M. J. Pryor: Dr. King's discussion is appreciated and raises several important points. It is first worth while to point out that the interpretation of the Flade potential advanced by Professor Uhlig and Dr. King[41] and that advanced by the writer have one important feature in common. Both interpretations involve the reduction of oxygen association in some manner with the passive iron surface. The main disagreement centers around the manner in which this oxygen is disposed on the passive surface (i.e., as an adsorbed layer or as part of a nonstoichiometric oxide film) and whether this oxygen per se is responsible for passivity.

Several factors, as pointed out in the reply to Professor Uhlig's discussion, favor the view that the oxygen is associated with a nonstoichiometric oxide film. These include the sensitivity of the length of the Flade potential arrest to the manner in which the passivating potential is interrupted. If, for instance, passivation of iron is achieved anodically in 1.0*N* sulfuric acid at a potential of +0.8 v (hydrogen scale) and the polarizing voltage is interrupted, then a characteristic length of Flade potential arrest may be determined. This duration depends on the time of anodic polarization, the voltage applied, and the specimen history. If the specimen is polarized for the same time at 0.8 v and the polarizing potential is then reduced smoothly and quickly to 0.6 v after which the polarizing voltage is again interrupted, the length of the Flade potential arrest is greatly shortened. In extreme conditions, the arrest may be virtually eliminated. Such an observation fits well with the concept of a p-n layer of γ-Fe_2O_3 in which the distribution of p-type defects is field stabilized. It is also a difficult observation to explain on purely electrochemical grounds unrelated to the defect structure of a three-dimensional surface film.

While the agreement between the calculated "heats of absorption" for the $O \cdot O_2$ layer referred to by Dr. King and the Flade potential[41] is impressive, it should be realized that there is a very broad assumption involved in these calculations. In the absence of supporting data, application of results of Tompkin[42] on chemisorption of dry gaseous oxygen to the rather specialized $O \cdot O_2$ layer, believed by Uhlig and King to exist under passivating conditions, appears to be of uncertain technical validity. Unless this extrapolation can be experimentally justified, it should be realized that the agreement between the calculated heats of adsorption and the Flade potential is speculative in nature.

[37] K. G. Weil, *Z. Elektrochem.*, **59**, 711 (1955).

[38] P. F. King and H. H. Uhlig, *J. Phys. Chem.*

[39] H. H. Uhlig and P. F. King, *This Journal*, **106**, 1076 (1959).

[40] H. H. Uhlig and P. F. King, *This Journal*, **106**, 1 (1959).

[41] H. H. Uhlig and P. F. King, *This Journal*, **106**, 1 (1959).

Surface to Volume Considerations in the Palladium-Hydrogen-Acid System

J. P. Hoare (pp. 640-643, Vol. 106, No. 8)

Gilbert W. Castellan[43] and Robert J. Fallon[44]: We believe that the results obtained in this investigation can be given a simpler interpretation than the one proposed in the article. We have made an extensive investigation [45] of the rate of entrance of hydrogen into palladium in sulfuric acid solution. This investigation shows quite clearly that the rate-determining step is transport of molecular hydrogen through the diffusion layer of aqueous solution at the surface of the metal. The subsequent steps, dissociation at the surface, penetration of the metal skin, and diffusion in the bulk metal, are comparatively fast. We also noticed that the length of the 0.050-v plateau is inversely proportional to the rate of increase of H/Pd with time. We developed the rate equation. It turns out that the rate is a function of area-to-volume ratio, the geometry of the specimen, and the rate constants for the several steps. The author finds that the length of the 0.050-v plateau is a linear function of volume-to-area ratio. This is at best only qualitatively in agreement with the rate equation. There are two important reasons for this: the author used three different geometries, bead, foil, wire; and we believe that he did not give sufficient attention to the stirring in the solution.

Three points in the author's interpretation need further discussion: (*A*) slowness of penetration of the metal skin; (*B*) the irregular "step" type of curve reported for the relative resistance vs. time; (*C*) the "overshoot" of the α-plateau.

(*A*) Skin penetration: If penetration of the metal skin were the slow step, slow compared to transport to the surface, and compared to dissociation, then a layer of H atoms should accumulate on the surface. This surface concentration of H atoms should approach that which is appropriate to the β-alloy and the potential of the electrode should be zero and not 0.050 v.

(*B*) In over 400 experiments on the measurement of relative resistance vs. time, we never observed the step-wise behavior reported by the author. We believe that the reason for this is that in our experiments the cell was small, the wire was a simple loop or helix, the hydrogen flow produced good stirring and established a definite diffusion layer at the wire surface. In the author's experiments the

[42] Quoted by B. Trapnell, "Chemisorption," p. 215, Academic Press Inc., New York (1955).

[43] Dept. of Chemistry, Catholic University of America, Washington, D. C.

[44] Institute of Molecular Physics, University of Maryland, Baltimore, Md.

[45] R. J. Fallon and G. W. Castellan, *J. Phys. Chem.*, **64**, 4 (1960).

cell is long, 19 cm, and the wire is stretched diagonally across the cell. He says that the flow rate of hydrogen was approximately constant but gives no clue as to where the hydrogen was introduced, or how fast or steady the flow rate was. We have not observed the plateau at about $R/R_o = 1.065$ reported by Flanagan and Lewis[46] and by the author; however, in our experiments the rates of absorption were usually much faster and our resistance vs. time curves do show a change in slope in this region. The typical dependence of R/R_o which we observe[45] is quite similar to that reported in Fig. 2 of Flanagan and Lewis.[46]

If the flow rate of the hydrogen is constant as the author claims, and stirs the solution well enough to establish a definite diffusion layer at the metal surface, then we can see no reason for the step type of curve which he observes in the relative resistance vs. time.[45] On the other hand, if the stirring is erratic, such an irregular curve should be observed.

(C) The "supersaturation" or "overshoot" of the α-potential: If, as the α-alloy reaches the saturation limit, the supply of hydrogen is restricted (due to poor stirring), then the hydrogen enters very slowly and the β-phase has a longer time in which to nucleate. The supersaturation which occurs before the β-alloy forms is small and no overshoot is observed. If, on the other hand, an ample supply of H_2 is maintained as the α-limit is reached, the H_2 enters quickly and the supersaturation reaches a noticeable value before the β-phase nucleates. This is exactly analogous to supercooling. If the melt is cooled very slowly, supercooling is less likely to occur; if it is chilled rapidly, it may well supercool. We observe that the overshoot is consistently more pronounced for smaller wires. This supports the above explanation. The author observes the overshoot in the exact circumstances where the stirring is likely to have been very good—the open helix of wire. We do not believe that an extraordinary surface film is responsible for this behavior. Also, we have observed the overshoot too consistently for it to be an accident in preparation.

J. P. Hoare: Although Castellan and Fallon have done very fine work, a few comments may be in order. As one knows, when a palladium sample is immersed in a water solution of sulfuric acid, the surface will be covered with adsorbed water molecules. When molecular hydrogen is bubbled through the solution, some of these molecules will enter the outer Helmholtz plane[47] which is the closest approach of a particle to the surface without being physically adsorbed. Then, the hydrogen will be adsorbed, probably by complexing with the adsorbed water to give hydrogen atoms adsorbed on the surface. These will then be dissolved in the metal. The concentration of particles on the surface will contribute to the magnitude of the potential. Castellan and Fallon suggest that, if the solution of hydrogen by palladium is the slow process, one must have a build-up of adsorbed hydrogen atoms on the surface and a potential of 50 mv would not be observed. This may not be the case since the build-up of hydrogen concentration may take place in the double layer as molecular hydrogen, if such a build-up of hydrogen exists. It may be possible that the H_2 in the double layer will not be adsorbed until certain surface conditions are met which are controlled by the solution process of hydrogen entering the palladium metal.

Castellan worked with very small diameter wires. The reported work by Hoare indicated that the step-wise form of the charging curves was most pronounced on wires of larger diameters. The plateau at $R/R_o = 1.065$ is very short on curves taken from wires of small diameter and might well be missed. A step-wise curve can occur if the resistance is a function of the distortion in the palladium lattice which is a function of the way in which the β-phase nucleates. If the β-phase nucleates by the sudden merging of domains of the β-phase, a series of steps may be reflected in the resistance-time curves. Fedorova and Frumkin[48] have arrived at similar conclusions.

As far as the supersaturation effect is concerned, it has been this author's experience that the overshoot only occurs on electrodes which have been cleaned and activated without additional mechanical stress being applied in the mounting of the electrode. This is the case for Castellan's work. If, however, as was done here, the wire, after being prepared, is wound about a polyethylene form or stretched in mounting, the overshoot on the charging curve is not found. This suggests that a film similar to that proposed in the author's paper has been broken up by the mechanical stress and the palladium surface is exposed. Only if the film is intact, as with Castellan's work, will the overshoot be observed since then the palladium surface will not be exposed until the film has been dissolved. It is the solution process of the film that causes the overshoot in the charging curve.

The Relation of Gas Composition to Current Efficiency in an Aluminum Reduction Cell

T. R. Beck (pp. 710-713, Vol. 106, No. 8)

Jack D. Hamlin[49]: I have read with great interest the development presented by Dr. Beck. Endeavoring to understand fully his development, independent calculations have been made, and a development results which leads to somewhat different conclusions.

Allow me to attempt to make my point by considering the electric current as two components. First, there is that fraction of the total current which is the current that is a part of the electrochemical reaction. The second part of the current is that fraction of the total current which is not taking part in the electrochemical reaction. This part is electronic conduction, or in an analogous way, it is current that is shunted around the electrochemical path.

Now consider only the fraction of the current that takes part in the electrochemical reaction. In

[46] T. B. Flanagan and F. A. Lewis, *Trans. Faraday Soc.*, 55, 1409 (1959).

[47] D. C. Grahame, *Chem. Rev.*, 41, 441 (1947).

[48] A. Fedorova and A. Frumkin, *Zhur. Fiz. Khim. USSR*, To be published.

[49] Development Engineering, Reynolds Metals Co., P. O. Box 191, Sheffield, Ala.

terms of the author's Eq. [1], this amount of current produces 4 moles of aluminum and n moles of carbon dioxide. Subsequentially, $\left[\frac{2x}{3}\right]$ moles of aluminum are reoxidized by reaction with CO_2—from Eq. [2]. A point I wish to emphasize is that if n moles of CO_2 are produced initially then 4 moles of aluminum are also produced initially.

Now consider the fraction of the current that did not take part in the electrochemical reaction. Let us assign a value to this fraction of $\frac{Z}{100}$. We can now ask the question: If all of the current had taken part in the electrochemical reaction, how much aluminum would have been produced initially? The answer is:

$$4 \div \left(1 - \frac{Z}{100}\right), \text{ moles}$$

I, therefore, offer that if n moles of CO_2 actually are produced initially as expressed in Eq. [1] and used in Eq. [6b] then, likewise, 4 moles of aluminum are initially produced and, consequently, Eq. [6a] becomes,

$$\% \text{ CE} = 100\left[\frac{4 - 2/3x}{4}\right]\left[1 - \frac{Z}{100}\right]$$

If x is then solved for in this equation and equated to x as solved for in Eq. [6b], an equation for current efficiency results that is different from that presented in the paper.

$$\% \text{ CE} = \left(\frac{y - n + 6}{3}\right)\left(\tfrac{1}{2}\% \text{ CO}_2 + 50\right)\left(1 - \frac{Z}{100}\right)$$

or

$$\% \text{ CE} = k(\tfrac{1}{2}\% \text{ CO}_2 + 50)$$

Using the data presented by Dr. Beck, the corresponding values of k are as follows:

Anode bake temp, °C	k
959	1.01
1,070	0.98
1,150	0.96

T. R. Beck: I am grateful to Mr. Hamlin for pointing out that my derivation does not properly account for electronic conduction. My assumption that electronic conduction and loss of aluminum or other reduced species to the lining or atmosphere were exactly equivalent was incorrect. I wish to amend my derivation to properly include electronic conduction.

Assume that Z is the per cent loss of equivalent aluminum by the mechanisms presented in the paper: (*a*) escape of sodium from cell; (*d*) formation of sodium and/or aluminum carbide with lining; (*e*) oxidation of aluminum during tapping. Assume Z′ is percentage of current carried by mechanisms: (*b*) direct oxidation of reduced species at anode; (*c*) electronic conduction. In Eq. [4a]:

$$\frac{A}{A + B} = \left(1 - \frac{Z'}{100}\right)$$

$$A = 4$$
$$C = 2/3\,x$$
$$D = 4\,\frac{Z}{100}$$

Eq. [6a] therefore becomes:

$$\% \text{ CE} = 100\left[\frac{4 - (2/3)x - 4\,Z/100}{4}\right]\left(1 - \frac{Z'}{100}\right)$$

Eq. [6c] becomes:

$$\% \text{ CE} = \left[\frac{6 - n + y}{3}\,(50 + \tfrac{1}{2}\% \text{ CO}_2) - Z\right]\left(1 - \frac{Z'}{100}\right) \text{ and}$$

Eq. [10] becomes:

$$\% \text{ CE} = [g(50 + \tfrac{1}{2}\% \text{ CO}_2) - Z]\left(1 - \frac{Z'}{100}\right)$$

Although not necessarily true for all aluminum cells, there are good reasons for believing that electronic conduction was not significant in the 10,000-amp experimental cell. Electronic shunt losses can be divided into several types: 1. losses through faulty insulation exterior to the bath; 2. electronic conduction through the bath; 3. short circuits between anode and cathode by metal splashing; 4. electronic conduction between anode and cathode through accumulated carbon "dust," sloughed from the anodes, floating on the bath surface.

It is certain that there were no significant shunt losses exterior to the bath for the experimental cell, although these have been known to occur in commercial cell lines. The work of Frank and Foster[20] indicates that electronic conduction is not significant through cryolite melts. There were no indications of short circuits by metal splashing in the experimental cell. This, however, can occur in large, high amperage, commercial cells in which large electromagnetic forces acting on the metal pad are developed. It is doubtful that there was significant shunt loss through carbon dust because there was only a small amount in the cell, its conductivity was poor because it was loosely packed, and the carbon lining was insulated from it by a layer of frozen cryolite or "ledge." There was noticeably more "dust" in the cell when using the low-bake temperature anodes. If electronic conduction through the dust were significant, then Z′ would have been larger for the low-bake temperature and the value of k calculated by Mr. Hamlin would be smaller, whereas the reverse was true.

It should be pointed out that error in metering of cell current also would be reflected in the value of Z′, making it either plus or minus. The shunt and ammeter for the experimental cell were calibrated and known to be accurate to $\pm\frac{1}{2}\%$.

Whether direct oxidation of reduced species at the anode occurs is not known, so it is not certain that Z′ was zero. On the other hand, there was considerable direct evidence that Z was not zero. As was stated in the paper, pockets of sodium metal were frequently found condensed in the cell "crust."

[20] W. B. Frank and L. M. Foster, *J. Phys. Chem.* **61**, 1531 (1957).

Metallic sodium was also found in the carbon lining, and it has been observed in linings of commercial cells. It is well known that sodium and/or aluminum carbide is found in used cell linings.

Since there was direct evidence that Z was greater than zero and there was no evidence that Z′ was not zero, I believe that my analysis of the data is correct as it stands.

Influence of Silicon on the High-Temperature Oxidation of Copper and Iron

J. W. Evans and S. K. Chatterji (pp. 860-866, Vol. 106, No. 10)

J. L. Meijering[51]: The authors conclude that the diffusivity of oxygen in Fe is much greater than is commonly supposed. However, their results agree satisfactorily with subscale measurements[52] on iron containing Al, and only the large discrepancy with respect to the measurements of Bramley, *et al.*,[53] is apparent. The latter authors treated their deoxidizing experiments with Fe containing 0.09% oxygen by weight as if the oxygen was homogeneously dissolved, which led to a far too small value of the diffusion coefficient D_o. It now is certain that the solubility c_o is quite small, and then the experiment in footnote 53 can be shown to lead to a value of about 1.5×10^{-11} cm²/sec for c_oD_o at 1000°C,[53] if c_o is expressed as atomic fraction. This is a third of the value deduced from the internal oxidation experiments with Fe containing 1% Al and, in view of the various uncertainties, this must be considered as satisfactory.

For comparison, we roughly calculated c_oD_o from the 998°-run of the authors, using the equation

$$c_oD_o = x\,(x + x_s)\,c_{Si}/t,$$

where x_s is the thickness of the metal layer converted into scale. This equation is valid only for small values of c_{Si}, the atomic fraction of silicon in the alloy. It is readily deduced from section 3 of footnote 54 (see below), if one assumes that each Si atom captures only 2 oxygen atoms in the subscale. This is not certain, and the proportionality of x_s with $\sqrt{t}$ (assumed in deriving the equation) is also not well fulfilled. Nevertheless, the value 3×10^{-11} cm²/sec found from the subscale thickness x and the weight increase after 5 hr at 998°C can be said to be in agreement with the results of footnotes 52 and 53.

J. W. Evans and S. K. Chatterji: We are grateful to Dr. Meijering for pointing out that our results relating to the diffusivity of oxygen in iron confirm his own experiments with aluminum in iron, and those of Bramley, *et al.*, which he has corrected, and sincerely regret not referring to his work.

Although we were aware that the oxygen solubility assumed by Bramley was probably too high (*see* Kitchener, Bockris, Gleiser, and Evans[55]) and, therefore, led to a too low value for the diffusivity, we see that our original remarks did not imply this.

We would like at this time to correct an error in the orignal paper. In the list of References, Ref. 18 should read: J. W. Evans and S. K. Chatterji, *J. Phys. Chem.*, **62**, 1064 (1958).

[51] Philips Research Labs., N. V. Philips' Gloeilampenfabrieken, Eindhoven, The Netherlands.

[52] J. L. Meijering, *Acta Met.*, **3**, 157 (1955).

[53] A. Bramley, F. W. Haywood, A. T. Cooper, and J. T. Watts, *Trans. Faraday Soc.*, **31**, 707 (1935).

[54] J. L. Meijering and M. J. Druyvesteijn, *Philips Research Repts.*, **2**, 81 (1947).

[55] J. A. Kitchener, J. O'M. Bockris, M. Gleiser, and J. W. Evans, *Acta Met.*, **1**, 93 (1953); *Trans Faraday Soc.*, **48**, 995 (1952).

On the Measurement of the Temperatures of Unenclosed Objects by Radiation Methods

A. G. Emslie and H. H. Blau, Jr. (pp. 877-880, Vol. 106, No. 10)

Tibor S. Laszlo[56]: This paper is a valuable contribution to an old and still controversial problem. There is complete agreement on the fact that the dual color pyrometer operates on the assumption that the emissivity does not change with the change in wave length. The controversy begins where the validity of this assumption is considered. There are several reported data on dual color pyrometry with remarkably good accuracy (± ¼% at 1700°K). It is possible that in these cases the experimental conditions were such that the fundamental assumption was valid. The value of the present work lies in the fact that it furnishes information on the magnitude of error when the emissivity does change with wave length.

This writer cannot but completely agree with the authors' conclusion that the emissivity has to be *measured* at the temperature where the optical pyrometer is to be used. The paper quotes an emissivity measurement method (Ref. 5) at high temperatures, using the solar furnace, which was suggested by the writer. In the frame of the paper, however, the procedure appears too difficult to perform. The method, as described briefly in the following, is really rather simple.

For each solar furnace there is a fixed concentration factor, i.e., the ratio between normal incident solar radiation intensity and heat flux at the focal zone. This factor can be determined by the method presented in the reference. Once this factor is known, the emissivity determination consists of a normal incident solar flux measurement using a pyrheliometer and of a simultaneous brightness temperature measurement at the sample in the focal zone using an optical pyrometer. From the incident solar flux, the flux at the focal zone can be calculated and, from this, the black body temperature of the sample. Knowing both the black body and brightness temperature, the emissivity can be calculated.

A. G. Emslie and H. H. Blau, Jr.: A number of methods have been suggested for temperature measurement in imaging furnaces. The method[57] which we have found most suitable involves direct measurement of the spectral reflectance of the hot specimen. Both the absolute temperature of the specimen and the spectral reflectance (and hence spectral emittance) can be determined from measurements of three intensities: the monochromatic intensities emitted and reflected by the hot speci-

[56] Research and Advanced Development Div., Avco Manufacturing Corp., Wilmington, Mass.

[57] H. H. Blau, Jr., "Measurement of Flux Emittance and Related Properties," *Proc. Int. Symposium on High Temperature Technology, Stanford Research Institute, 1960.*

men, and the monochromatic intensity incident on the hot specimen. The measurements can be performed with an optical pyrometer or other suitable instrument. This method requires no assumptions of equality of spectral and total emittance or of absence of conductive and convective heat losses by the sample as would seem to be the case with Laszlo's method.

Herbert W. Newkirk[58] and **B. B. Brenden**[59]: We have the following remarks regarding Emslie and Blau's article.

The basic principle of the two-color pyrometer is that, when the ratio of the radiant intensities from the sample at two wave lengths is determined, the unknown emissivity is eliminated. Eq. [6] assumes at least gray-body conditions, that is, the emissivities at the chosen wave lengths are equal. In general, the gray-body assumption over a wide spectral interval is not valid. However, narrower spectral intervals can usually be found for incandescent solids for which the gray-body assumption is valid. The choice of the wave-length interval will be determined by the amount of radiant energy available and the sensitivity of the ratio to temperature changes.[60] It is considered good practice in two-color pyrometry to make measurements of spectral emissivity for the material in question in order to select the optimum spectral interval.[61]

It is highly unlikely that the ratio of the emissivities for any incandescent solid at the two wave lengths can be greater than 1.2. In the case of tungsten, for example, the ratio of emissivities is 1.1 at 3600°K with $\lambda_1 = 0.47\ \mu$ and $\lambda_2 = 0.65\ \mu$. Thus, the error in the determination of the true temperature using a two-color pyrometer cannot be greater than 2% at this temperature. This accuracy is equal to or considerably better than that attained with conventional pyrometers. Furthermore, two-color pyrometers offer the advantage of providing an electrical output which can be used to drive a recorder, operate control instruments, etc.

Finally, two-color pyrometers are much less affected by smoke, fumes, and emissivity changes during experiments than single-color pyrometers or total radiation pyrometers. Work in this laboratory[62-64] has indicated that the increased accuracy, automation, freedom from emissivity effect, and a temperature limit above 4000°K are features of two-color pyrometers which can be used advantageously in many areas of high temperature research.

[58] RCA Labs., Radio Corp. of America, Princeton, N. J.

[59] General Electric Co., Richland, Wash.

[60] A. I. Dahl and W. E. Hill, "Temperature Measurements—High Temperature Physics," General Electric Co., Schenectady, N. Y., Report No. 58GL6, Jan 24, 1958.

[61] W. E. Hill, "Temperature Measurements—Applications of Two-Color Pyrometry," General Electric Co., Schenectady, N. Y., Report No. 58GL257, Sept. 15, 1958.

[62] B. B. Brenden and H. W. Newkirk, Jr., "Multicolor Pyrometry," General Electric Co., Richland, Wash., HW-56506, Sept. 1, 1958.

[63] B. B. Brenden and H. W. Newkirk, Jr., "A Multicolor Pyrometer," General Electric Co., Richland, Wash., HW-57162 Rev., Nov. 11, 1958.

[64] B. B. Brenden and H. W. Newkirk, Jr., "An Improved Recording Multi-Color Pyrometer," General Electric Co., Richland, Wash., HW-60678, May 27, 1959.

A. G. Emslie and H. H. Blau, Jr.: Experience shows that the two-color pyrometer can be used for accurate temperature measurement in special cases such as those quoted by Newkirk and Brenden. The conclusions given in our paper are nevertheless strictly true and serious errors are often introduced if equal emittance at the two wave lengths is assumed. For example, the ratio of emittances at 0.46 and 0.65 μ is 1.97 for pure copper. This difference would lead to a temperature error of 5% at 1000°K. In fact, gray-body behavior has been observed to be the exception rather than the rule.[65]

The Action of Nickel and Cobalt in Electroluminescent Zinc Sulfide Phosphors

P. Goldberg (pp. 948-954, Vol. 106, No. 11)

W. Lehmann[66]: (*A*) What do you know about the mean particle sizes and the particle size distributions of your samples? We know now that they may have marked influence on the voltage dependence of electroluminescence.

(*B*) If the measurements of the voltage dependence of electroluminescence of your samples had been extended to more decades of the brightness, could not a deviation from either equation [i.e., $n = 0$ and $n = 1$ in $L = AV^n \exp(-b/V^{1/2})$] be expected?

Paul Goldberg: (*A*) It is unlikely that particle size effects or size distribution effects exert any influence (in these experiments) over the changes in voltage dependence of electroluminescence occasioned by the incorporation of nickel or cobalt. All of the specimens in Fig. 4 and 5 of the paper under discussion, including the control, were prepared under identical thermal conditions from separate portions of a single, previously crystallized phosphor. The modifier was incorporated by solid state-diffusion. No data exist as to size or distribution of sizes of the materials in question. It is improbable, however, that the diffusion process, which occurred at 800°C, changed the size or distribution within the family of phosphors. From previous experience with similar preparations, the mean particle size probably lies between 20 and 30 μ. The distribution of sizes is most likely log-normal.

(*B*) It is possible that the voltage dependence of electroluminescence could change were the measurements extended outside the reported range. The burden of the data in Fig. 4 and 5 is to show that phosphors with varying modifier concentrations, when measured in the same range of applied field, exhibit a change in functionality within the group. We have not tested whether this change in functionality occurs in ranges of applied field not covered in the original publication.

[65] G. G. Gubareff, Shao-yen Ko, and P. E. McMall, Jr., Honeywell Research Center Report, GR 2462-R3 (1956).

[66] Lamp Div., Westinghouse Electric Corp., Bloomfield, N. J.

FUTURE MEETINGS OF
The Electrochemical Society

Houston, Texas, October 9, 10, 11, 12, and 13, 1960

Headquarters at the Shamrock Hotel
Sessions probably will be scheduled on
Batteries, Corrosion, Electrodeposition,
Electronics (Semiconductors),
and Electrothermics and Metallurgy

★ ★ ★

Indianapolis, Ind., April 30, May 1, 2, 3, and 4, 1961
Headquarters at the Claypool Hotel
Sessions probably will be scheduled on
Electric Insulation, Electronics (including Luminescence and Semiconductors), Electrothermics and Metallurgy, Industrial Electrolytics, and Theoretical Electrochemistry

★ ★ ★

Detroit, Mich., October 1, 2, 3, 4, and 5, 1961
Headquarters at the Statler Hotel

★ ★ ★

Los Angeles, Calif., May 6, 7, 8, 9, and 10, 1962
Hotel to be announced

★ ★ ★

Boston, Mass., September 16, 17, 18, 19, and 20, 1962
Headquarters at the Statler Hilton Hotel

Papers are now being solicited for the meeting to be held in Indianapolis, Ind., April 30-May 4, 1961. Triplicate copies of each abstract *(not exceeding 75 words in length)* are due at Society Headquarters, 1860 Broadway, New York 23, N. Y., *not later than January 2, 1961* in order to be included in the program. *Please indicate on abstract for which Division's symposium the paper is to be scheduled, and underline the name of the author who will present the paper.* Complete manuscripts should be sent in triplicate to the Managing Editor of the JOURNAL at 1860 Broadway, New York 23, N. Y.

Presentation of a paper at a technical meeting of the Society does not guarantee publication in the JOURNAL. However, all papers so presented become the property of The Electrochemical Society, and may not be published elsewhere, either in whole or in part, unless permission for release is requested of and granted by the Editor. Papers already published elsewhere, or submitted for publication elsewhere, are not acceptable for oral presentation except on invitation by a Divisional program Chairman.

Current Affairs

ECS Division and Section News

Electro-Organic Division

The Nominating Committee of the Electro-Organic Division has submitted the following slate of officers for the next term (fall 1960-1962):

Chairman—M. J. Allen, Ciba Research Labs., 556 Morris Ave., Summit, N. J.

Vice-Chairman—R. A. Day, Jr., Chemistry Dept., Emory University, Atlanta 22, Ga.

Secretary-Treasurer—Edward C. Olson, The Upjohn Co., Kalamazoo, Mich.

G. W. Thiessen, *Chairman*

Indianapolis Section

The Indianapolis Local Section held its fourth technical meeting of the season on Tuesday, April 5, at the Construction League of Indianapolis. It was a joint meeting with the Indianapolis Branch of the American Electroplaters' Society. Dr. Charles L. Faust, of Battelle Memorial Institute, Columbus, Ohio, spoke on "Some Metallurgical Aspects of Coatings for High-Temperature Protection."

Dr. Faust discussed and illustrated conditions of metal surfaces in relation to different preparation procedures and then related these circumstances to performance after electrodeposition, showing that they are often the source of poor behavior which may be attributed to deficiencies in the plating process. After this background information, he outlined the problems faced in metal finishing for oxidation protection at high temperatures and showed how certain specific problems had been solved through use of electroplating techniques. A discussion period concluded the evening's activities.

T. C. O'Nan, *Secretary-Treasurer*

India Section

A business meeting of the India Section was held in March 1960 at the Indian Institute of Science, Bangalore, with Shri J. Balachandra in the Chair. The minutes of the meeting held on July 24, 1959 were confirmed and the Statement of Accounts for 1959 was approved.

The Secretary brought to the notice of the members the substance of the letter received from the Executive Secretary of The Electrochemical Society, regarding the continuance of assistance to India Section members with respect to membership dues. It was decided to communicate the thanks of the Section to the Asia Foundation for the financial assistance regarding the Society dues (1960), and to the President and the Board of Directors of the Society for their help in the matter.

S. Krishnamurthy, *Secretary-Treasurer*

News from India

Indian Science Congress.—The 47th session of the Indian Science Congress was held at Bombay from January 3 to 9, 1960, under the auspices of the University of Bombay. The program covered sectional meetings, symposia, popular and special lectures, visits to institutions and other places, social functions, and an exhibition of scientific equipment. Delegates from many foreign countries participated in the sessions, at which several papers on electrochemistry were presented. The symposia included the following topics: rate processes in physicochemical reactions, recent advances in electroanalytical techniques, instrument industry in the third five-year plan, electronic instruments, alloy steel.

Symposium on Instruments.—A three-day Symposium on Instruments was held during November 1959 at the Technical Development Establishment (Instruments), Dehra Dun, under the auspices of the Research and Development Organization of the Ministry of Defence. The program included the opening address, technical sessions, popular lectures, and an exhibition. It was pointed out that the instrument industry in India is still in its infancy and a great deal of headway has yet to be made. The present estimate of production in the country is of the order of only Rs. 50 lakhs a year, the annual imports amounting to nearly Rs. 10 crores.

Caustic Soda Plant of Dhrangadhra Chemical Works.—The 85-ton-per-day electrolysis plant set up by Dhrangadhra Chemical Works at Sahupuram, Madras State, is the biggest in Southeast Asia, and one of the few of its kind in the world. There are, at present, 42 mercury cells, to be increased to 72, humming with their individual mercury pumps lifting the circulating mercury from the secondary to primary cell. A novel feature of the cell is that the primary cell rests on the secondary. The 50% caustic lye is concentrated to 100% and filled into drums as fused caustic or as flakes. This is accomplished by a cascade-type evaporating system where hot Dowtherm is used as the heating medium which, in turn, is vaporized in oil-fired boilers. The pipelines and all vessels of this section of the plant are of nickel or nickel-lined steel to insure the purity of the final product and to reduce corrosion. The power for the plant is supplied from Periyar through a 110-kv line. The cells get their direct current after the a-c/d-c conversion is made by four contact rectifiers of very high conversion efficiency.

The characteristics of a single cell are: load, 60,000 amp; cathode c.d., 2525 amp/m^2; average operating voltage, 4.1 v; current efficiency, 96/97% on NaOH, and 94/95% on Cl_2; average purity, 99% (Cl_2 plus CO_2) Cl, and 99.8% H_2; average Cl_2 produced, 1.785 tons/day, and NaOH produced as 100%, 2.45 tons/day; approximate dimensions of primary, 16.4 m x 1.7 m; weight of Hg, 2.8 tons.

India Section Publication.—The India Section has released the publication "Symposium on Electrodeposition and Metal Finishing" (188 pages, 1960), which covers the proceedings of the symposium held at Karaikudi in December 1957. There are 36 papers on the theoretical and industrial aspects of the following topics: electroplating, electrorefining, electrowinning, metal powders,

anode phenomena, electropolishing, anodizing, and protective coatings.

The price per copy is: Rs. 2.50 (Members and Associates of the Section); Rs. 10 (others, India); Rs. 15 (others, foreign). Trade discount: 15% single copy, 20% for five copies and above. Orders may be placed with the Editor, *Bulletin of the India Section*, The Electrochemical Society, Indian Institute of Science, Bangalore-12, India.

T. L. Rama Char,
India Correspondent

Ontario-Quebec Section

The third meeting of the 1959-1960 season was held in the Laurentien Hotel, Montreal, on April 8, 1960. Two excellent papers were presented: "Some Impressions of the Japanese Iron and Steel Industry" by Dr. J. H. Walsh, Mines Branch, Dept. of Mines and Technical Surveys, Ottawa, and "Semiconducting Compounds" by Dr. E. Mooser, National Research Council, Ottawa. Mr. T. Hirst, of Sogemines Ltd., Montreal, acted as Technical Chairman.

The following were elected as officers of the Ontario-Quebec Section for the 1960-1961 season:

Honorary Chairman—G. E. Willey, Electro Metallurgical Co., Toronto
Chairman—L. G. Henry, Canadian Industries Ltd., Montreal
Vice-Chairman (Program)—R. A. Ritchie, Electric Reduction Co. of Canada Ltd., Toronto
Vice-Chairman (Membership)—P. G. Walker, Electro Metallurgical Industries Ltd., Ottawa
Secretary-Treasurer—R. A. Campbell, Dept. of Mines and Technical Surveys, Ottawa
Committeemen—Andre Hone, École Polytechnique, Montreal; S. Wagner, RCA Victor Co., Montreal; G. M. Mason, Aluminum Co. of Canada Ltd., Montreal; P. G. Walker, Electro Metallurgical Co., Beauharnois; H. V. Ross, University of Toronto, Toronto; R. C. Jacobson, Ontario Hydro Electric Power Commission, Toronto.

E. R. Landry,
Secretary-Treasurer

New Members

In April 1960, the following were elected to membership in The Electrochemical Society by the Admissions Committee:

By action of the Board of Directors of the Society, all prospective members must include first year's dues with their applications for membership.

Also, please note that, if sponsors sign the application form itself, processing can be expedited considerably.

Active Members

R. B. Allen, U. S. Naval Ordnance Lab.; Mail add: 226 Hillsboro Dr., Silver Spring, Md. (Battery)

W. M. Armstrong, Dept. of Metallurgy, University of British Columbia, Vancouver, B. C., Canada (Corrosion, Electrothermics & Metallurgy, Theoretical Electrochemistry)

Terence Bamford, Sheffield Smelting Co., Ltd., Royds Mill St., Sheffield, England (Industrial Electrolytic)

Beymon Blanchard, U. S. Industrial Chemicals Co., State Rd., Ashtabula, Ohio (Industrial Electrolytic)

Frank Booth, Associated Electrical Industries, Ltd., Ponders End, Enfield, Middlesex, England (Battery)

R. E. Campbell, Bureau of Mines; Mail add: Box 365, Boulder City, Nev. (Electrodeposition)

A. J. Certa, Lansdale Tube Co.; Mail add: 502 Marsha Rd., Norristown, Pa. (Electrodeposition, Electronics)

C. G. Enke, Frick Chemical Lab., Princeton University, Princeton, N. J. (Theoretical Electrochemistry)

J. K. Farrell, Solvay Process Div., Allied Chemical Corp., Box 271 Syracuse, N. Y. (Electro-Organic)

A. V. Fraioli, Faradyne Electronics Corp., 471 Cortlandt St., Belleville, N. J. (Electric Insulation)

Charles Gelman, Gelman Instruments, 106 N. Main St., Chelsea, Mich. (Electronics)

Julius Grossman, Westinghouse Electric Corp., Semiconductor Div.; Mail add: 3813 Oakford Ave., Baltimore 15, Md. (Electronics)

F. L. Howard, Dept. of Metallurgical Research, Kaiser Aluminum & Chemical Corp., Spokane 69, Wash. (Theoretical Electrochemistry)

Hira Lal, Indian Institute of Technology, Bombay 76, India (Theoretical Electrochemistry)

W. D. Loftus, P. R. Mallory & Co., Inc.; Mail add: 11647 Peacock Dr., Indianapolis 26, Ind. (Battery, Electronics)

W. K. McCown, Foster D. Snell, Inc.; Mail add: 1926 Grove St., Ridgewood 37, N. Y. (Battery, Electrodeposition)

J. P. McGowan, Franklin Institute, Library, 20th & Parkway, Philadelphia 3, Pa. (Electrothermics & Metallurgy)

R. M. McLouski, Westinghouse Electric Corp.; Mail add: 205 Baylor Rd., Glen Burnie, Md. (Electronics)

A. M. Moos, Patterson Moos Research Div., Lessona Corp., 90-28 Van Wyck Expressway, Jamaica 18, N. Y. (Battery, Electronics, Theoretical Electrochemistry)

A. K. Nelson, Riverdale Metal Finishers; Mail add: 501 E. 32 St., Chicago 16, Ill. (Electrodeposition)

Nicholas Paraskevopoulos, Picatinny Arsenal, Explosives Research Section; Mail add: 74 Hudson St., Clifton, N. J. (Battery, Theoretical Electrochemistry)

Roelof Reitsema, Metaalinstituut T.N.O.; Mail add: P. O. Box 52, Delft, The Netherlands (Corrosion, Electrodeposition, Electrothermics & Metallurgy, Theoretical Electrochemistry)

J. R. Scholl, Delco-Remy Div., General Motors Corp., Process Dept., Anderson, Ind. (Battery)

L. R. Schulz, Hoffman Electronics Corp.; Mail add: 519 E. Howard St., Pasadena 6, Calif. (Battery, Electronics)

J. J. Thurner, Colgate University; Mail add: 50 Broad St., Hamilton, N. Y. (Electrothermics & Metallurgy)

Rolf Weil, Dept. of Metallurgy, Stevens Institute of Technology, Hoboken, N. J. (Electrodeposition)

R. M. Witucki, Hoffman Science Center; Mail add: 139 Olive Mill Rd., Santa Barbara, Calif. (Electronics)

Associate Members

A. A. Gundersen, State University of Iowa; Mail add: 308 N. Clinton, Iowa City, Iowa (Electro-Organic)

G. F. Hardy, Clevite Transistor Products; Mail add: 56 Whittier Ave., Waltham 54, Mass. (Electronics)

R. C. Lucas, Rheem Semiconductor Co.; Mail add: 677-43rd Ave., San Francisco 21, Calif. (Electronics, Theoretical Electrochemistry)

J. L. Ord, Physics Dept., University of Illinois, Urbana, Ill. (Corrosion)

G. R. Platt, Texas Instruments, Inc.; Mail add: 3438 Knox St., Dallas 5, Texas (Electronics)

D. J. Sharp, P. R. Mallory & Co., Inc., 3029 E. Washington St., Indianap-

olis, Ind. (Electric Insulation, Electronics)

J. P. Wondowski, General Motors Corp., Research Labs.; Mail add: 28182 Los Olas Dr., Warren, Mich. (Battery)

Student Member

R. L. South, Western Reserve University; Mail add: 13304 Forest Hill Ave., Cleveland 12, Ohio (Theoretical Electrochemistry)

Reinstatements to Active Membership

Hal-Curtis Felsher, Claremont Pigment Dispersion Corp.; Mail add: 114 Bounty Lane, Jericho, N. Y. (Electrodeposition, Electro-Organic, Electrothermics & Metallurgy)

S. E. Tobert, Albihns Patentbyra AB; Mail add: Storgatan 15, Sodertalje, Sweden (Battery, Corrosion, Electric Insulation, Electrodeposition, Electronics, Electro-Organic, Electrothermics & Metallurgy, Industrial Electrolytic, Theoretical Electrochemistry)

Reinstatement and Transfer to Active Membership

J. C. Withers, American Machine & Foundry Co.; Mail add: 204 Ashby Place, Fairfax, Va. (Electrodeposition, Electro-Organic, Theoretical Electrochemistry)

Transfer from Associate to Active Membership

W. E. Watts, Reynolds Metals Co., Reduction Research, Box 191, Sheffield, Ala. (Industrial Electrolytic)

Deceased Members

W. G. Allan, Philadelphia, Pa.
A. B. Davis, Whippany, N. J.
Georges Destriau, Paris, France
J. M. Gregory, Ashtabula, Ohio
F. J. Hambly, Buckingham, Que., Canada
Bradley Stoughton, Bethlehem, Pa.

Bradley Stoughton

Bradley Stoughton, a Past President of The Electrochemical Society, and one of its oldest members, died on December 30, 1959. He had been a member of the Society for exactly 50 years. He served as President in 1931, and had been Chairman of the Electrothermics Division in 1922. He was the sixth Richards Memorial Lecturer of the Society; his lecture, entitled "Modern Marvels of Electrometallurgy," was delivered at the New York World's Fair in 1939.

In addition to his service in The Electrochemical Society, Professor Stoughton was active in many other professional engineering societies. He held numerous offices in them, a tribute to his strong leadership, his wise counsel, and the admiration of his colleagues.

The Society of Chemical Industry awarded the Grasselli Medal to Professor Stoughton in 1929. In 1943, the Lehigh Valley Chapter of the American Society for Metals established in his honor the annual Bradley Stoughton Award for outstanding contribution to metallurgy.

Professor Stoughton was born in New York City in 1873. He was characterized by a tremendous amount of energy, enthusiasm, and capacity for work. His health continued to be good and, until the last two or three years, there was little change in his customary vigor. He seemed to thrive on his friendships, on participation in local charities and church work, and on his joy in being of service to others. He counted it a special privilege to keep in touch with many of his former students, and to renew the associations made in many forms of endeavor and wide travel.

Professor Stoughton was a world authority on the metallurgy of iron and steel. During the early part of his life, he was employed in the steel industry, holding positions successively with the Illinois Steel Co., American Steel and Wire Co., and Benjamin Atha and Co. He received patents for a side-blown converter for steel castings and also for a process of oil melting in cupolas. In 1922, he was commissioned by President Harding to make a field study on the feasibility of the eight-hour day in the steel industry, and his report on the results of the study did much to establish that change which has had such a far-reaching influence. His book, "The Metallurgy of Iron and Steel," was the leading textbook on the subject for some 40 years. He was a coauthor of "The Alloys of Iron and Silicon."

Professor Stoughton's career was initiated in the field of education, and to this field he returned at the age of 50. After graduation from Yale in 1893 and from M.I.T. in 1896, he taught for a year at M.I.T. and then for a year at Columbia, where he was assistant to Henry Marion Howe. After his employment in the steel industry, he returned to Columbia and taught for six years in the School of Mines, becoming acting head of the Department of Metallurgy. From the secretaryship of A.I.M.E., he went to Lehigh University to become head of the Metallurgy Department, a position which he held from 1923 until retirement in 1939. From 1936 to 1939, he was also dean of engineering. While at Lehigh, he was coauthor of "Engineering Metallurgy," a textbook which did much to spread the teaching of metallurgy in all branches of engineering. In 1943, Dean Stoughton received the honorary degree of D.Eng. from Lehigh.

Professor Stoughton performed notable service for the Government in the two World Wars. In 1918-1919, he was a member of the National Council of Defense, head of the metallurgical division and later vice-chairman of the engineering division of the National Research Council, and a member of the welding committee of the Emergency Fleet Corporation. In 1941-1945, he was chief of the heat-treating equipment of the tools section of the War Production Board and later acting head of the foundry equipment section. For a time after the war, he was stationed in London as U. S. Government representative of the National Industrial Intelligence Commission.

He is survived by his wife, Merwin Roe Stoughton, and by two sons and two daughters.

Howard Coon Parmelee

H. C. Parmelee, 21st President of The Electrochemical Society, was one of the hardy pioneers who helped found the chemical engineering profession. Few of us today appreciate the important role that electrochemists played in that first formal union of chemistry and engineering. It was at the beginning of this century that the giant turbines at Niagara Falls first made cheap power a reality in America. Electrical engineers, vitally concerned with the success of that development, turned to the electrochemists and electrometallurgists for help in building the great power-consuming industries of the Niagara Frontier. So it was that eminent engineers such as Acheson, Burgess, Becket, Hering, Richards, Sperry, Tesla, Stone, Webster, and Weston joined with Bancroft, Dow, Hall, Sadtler, Whitney, and other outstanding chemists to form the American Electrochemical Society, April 3, 1902. (Ours, too, was the first sapling to splinter from the main trunk of the much older American Chemical Society!)

Almost simultaneously with the founding of our Society, a new journal, *Electrochemical Industry*, was established with Dr. E. F. Roeber as its first editor. Fifteen years later when Dr. Parmelee succeeded him in that post, the maga-

zine was known as *Metallurgical and Chemical Engineering*, having successfully changed its title and content in 1905 to *Electrochemical and Metallurgical Industries*. In 1918 it became *Chemical & Metallurgical Engineering*, adopting its present name, *Chemical Engineering*, in 1946 to serve a profession for which Roeber and Parmelee had laid such a firm foundation.

H. C. Parmelee was born in Omaha on December 4, 1874, and received his formal education at the University of Nebraska, which granted him its B.Sc. and A.M. degrees in 1897 and 1899. In 1917, at the conclusion of his term as president of Colorado School of Mines, he received an honorary doctorate in science from Colorado College. During much of his early career, he was concerned with the mining and metallurgical industries of the West, working in close association with such hardy (and surviving) contemporaries as Milton C. Whitaker and John Van Nostrand Dorr. From 1900 to 1902, he was chief chemist at the Globe smelter of American Smelting and Refining Co. Following three years as a consultant, he edited the *Mining Reporter* until 1906, when he was made editor of *Western Chemist and Metallurgist*. The move to "*Met. & Chem.*" in 1911 was to bring him East in 1917 for the beginning of a long and rewarding association with McGraw-Hill. He became its vice-president and editorial director in 1928 and, for almost 15 years prior to his retirement, he was chief editor of *Engineering & Mining Journal*.

In 1956, the American Institute of Chemical Engineers honored Dr. Parmelee for the important contribution he had made to chemical engineering education. Succeeding the late Dr. Arthur D. Little as chairman of its committee, he put the full authority of the Institute behind an accreditation program that was later to be adopted by the Engineers' Council for Professional Development for the entire engineering profession. Dr. Parmelee was elected and served as secretary of the American Institute of Chemical Engineers from 1927 to 1930.

Howard Parmelee married Eugenia McAusland of Omaha in Washington in 1922, and for many years they made their home in Yonkers, N. Y. Following her death, he moved to Bradenton, Fla., where he lived with his surviving sister, Mrs. Robert T. Hill. There he died on November 17, 1959, within a few days of his 85th birthday. Thus ended a long, fruitful career as a leader of our profession—widely known and respected for his friendliness, courage, and integrity, his even-tempered judgment, and his inspiring confidence in his fellowmen.

Sidney D. Kirkpatrick

Book Reviews

Solid State Physics: Advances in Research and Applications, Vol. 9. Edited by Frederick Seitz and David Turnbull. Published by Academic Press, Inc., New York, 1959. 548 pages, 188 illustrations; $14.50.

Several earlier volumes in this ambitious series have been called to the attention of readers of this JOURNAL. The over-all scheme is to produce authoritative accounts of developments in solid state physics at several different levels, ranging from the narrow, rigorous, or exhaustive treatment of a particular substance, property, or theoretical method to a more relaxed statement of general relationships or principles in a broader area. The series has struck a satisfactory balance on the whole. There are fluctuations, however, and the present seven articles tend toward the specialized. It may be that comparatively few readers of this JOURNAL will consider purchasing this rather expensive book, therefore. On the other hand, its value even in the most modest technical library is undisputed. The book is attractively produced and has extensive author and subject indexes.

D. J. Montgomery reviews "Static Electrification of Solids" in a fresh manner designed to provoke interest in this ancient and poorly understood subject. Technology is now presented with aggravated problems of static electrification because of the high resistivities and large relative velocities common in the processing and use of modern materials, He argues that while "it is a commonplace that the phenomena of static electrification are erratic" and "it is not justifiable to expect values obtained by one experimenter to apply to the findings of another,'" progress can be made simply by careful specification of experimental conditions. An analysis of the net charge transferred between two solids is made into an initial equilibrium charge (when they are in contact) and the fraction retained (when they are separated). The number and nature of the parameters affecting the equilibrium charge may be small. Rather diverse factors (such as gaseous discharge phenomena) may influence the latter. Studies on powders and on liquid-solid interfaces may give useful clues. Montgomery here presents the case, however, for proceeding from a study of solid-solid contacts under idealized conditions.

The discussion of different semiconductor types in this series is extended with W. W. Scanlon's "Polar Semiconductors" article. The substances considered are Pbs, PbSe, and PbTe, which, while bound primarily by ionic forces, have comparatively low electrical resistivities. Nearly half the paper is concerned with the crystal and physical chemical properties of these compounds and associated modifications produced by alloying, by the addition of foreign atoms, and by lattice defects. Electronic band structure, optical and transport properties are then considered. Many of these are not yet well understood.

"Heterogeneities in Solid Solutions" are authoritatively discussed by Andre Guinier, a pioneer in the application of x-ray diffraction techniques to this problem. The fact that sharp diffraction lines are observed from solid solutions shows that the atoms are disposed near the lattice points, no systematic long-range strains being present. The intensity and distribution of the scattering between the sharp maxima gives the information about the degree of disorder of the solution. Here Guinier considers evidence about short-range order in solutions in equilibrium, and evidence on the formation and structure of solute-rich "zones" in nonequilibrium solid solutions. The presentation complements other accounts in the literature nicely.

Two articles on electronic spectra are included. The shorter one, by H. C. Wolf, treats aromatic molecular crystals. It gives experimental details, summarizes present investigations, and compares them to the qualitative theory now available. The longer one, by D. S. McClure, treats molecules and ions in ionic crystals, primarily those ions having unfilled f- or d-shells. A rather full theoretical development is presented as a guide to the interpretation of such spectra and many experimental examples are given. The two articles give 325 literature references!

"Oscillatory Behavior of Magnetic Susceptibility and Electronic Conductivity" is discussed by A. H. Kahn and H. P. R. Frederikse. The properties of charge carriers in solids subjected to very large magnetic fields are strikingly modified. The

theory is now well enough advanced so that the data obtained can be used to reconstruct the electronic energy band structure of a number of solids. Bismuth is the principal example here.

The novel subject "The Interdependence of Solid State Physics and Angular Distribution of Nuclear Radiations" is discussed by E. Heer and T. B. Novey. The angular distribution observed in radiations emitted by nuclei is influenced by the fields present in crystals because nuclei have electric and magnetic moments. The nuclei can then serve as fine-scale probes of these fields, in cases where the application of an external field (as in magnetic resonance studies) is undesirable or where very great sensitivity is required. A major problem is that oriented nuclei are required. Applications to studies of chemical kinetics, for example, can be imagined, but have not yet been made.

R. O. Simmons

Cathodic Protection, by Lindsay M. Applegate. Published by McGraw-Hill Book Co., Inc., New York, 1960. 244 pages, 67 illustrations; $9.00.

This is an amazingly lucid, descriptive treatment of cathodic protection. All phases of cathodic protection are treated and illustrated by means of examples from actual installations. The development of the principles of corrosion and of cathodic protection is in logical sequence at an elementary rather than rigorous level, and therefore makes for easy reading by individuals without benefit of a wide background in electrochemistry. Many solutions to problems of applying cathodic protection in the field are presented as a departure from ideal criteria but which have provided adequate protection where current distribution is nonuniform. The nonuniform current distribution to buried structures is ingeniously illustrated by means of a mechanical analogue of current sheet formed by manipulation of a sheet of rubber. The design of half cells and their reproducibility and polarization characteristics are given adequate treatment for the operator who must use them in the field for potential measurements on corrosion and cathodic protection systems. The design of existing cathodic protection systems, placement of anodes, and interference problems are given considerable space.

This is a valuable "how-to-do-it" text and should be in the corrosion engineer's hands not only for the basic, general information it contains but also as a check list of the many successful cathodic protection installations which the author has illustrated.

W. H. Bruckner

Cathodic Protection, by J. H. Morgan. Published by The Macmillan Co., New York, 1960. 325 pages; $12.00.

The author has painstakingly prepared an outstanding and complete text on the theory and practice of cathodic protection as a means of preventing corrosion of metals. He presents thoroughly a background of corrosion theory as preparation for precise application of cathodic protection.

In discussing the various aspects of the practice of protection, he spares no detail in describing the exact procedures required to overcome field problems and provide an accurately engineered design of the cathodic protection system. The latest advances in development of sacrificial anodes and in permanent anodes are cited, together with operating data of interest to the corrosion engineer. Even the relatively new application of cathodic protection to aluminum structures has been covered, and the results of successful and improper practices have been well illustrated. The measurement of path resistance in the field, calculation, and interpretation of the data for optimum current and anode distribution are discussed, together with the economics of coatings and the distribution system. The book contains a special section on cathodic protection in sea water for ships, piers, ballast tanks, etc., and discussion of the effectiveness of cathodic protection in preventing cavitation damage. There are other chapters on interference problems, instruments, and economics. Reference lists are given at the end of each chapter, and it is noted that "Corrosion" published by NACE had the major share of reference.

W. H. Bruckner

News Items

1960 MAECON

The 12th Annual Mid-America Electronics Conference (MAECON), sponsored by the Kansas City section of the Institute of Radio Engineers, will be presented November 15 and 16, 1960 at the Hotel Muehlebach in Kansas City, Mo.

Papers will be presented on the subjects of semiconductors, microwaves, engineering management, and education, with emphasis on semiconductors. Exhibits of the latest developments in the electronic industry will be on display. The proceedings of the conference will not be published.

Abstracts must be submitted before June 15 to allow ample time for review and selection. Addresses for submission of abstracts are: *Semiconductors*—James Austin, General Papers Chairman, Bendix Aviation Corp., 95th and Troost, Kansas City, Mo., or J. B. Stites (AIEE), AT&T Co., 811 Main, Kansas City, Mo.

Microwaves—C. M. Hyde, Dept. of Electrical Engineering, University of Nebraska, Lincoln, Neb.

Engineering Education and Management—Zvi Prihar, Dept. of Electrical Engineering, University of Wichita, Wichita, Kan.

Additional information can be obtained from Mr. James E. Austin, Papers Chairman, P. O. Box 1159, Kansas City, Mo., or Mr. Donald C. Canning, Publicity Chairman, 17303 Swope Lane, Independence, Mo.

First International Congress on Metallic Corrosion, London, 1961

The First International Congress on Metallic Corrosion, to be held under the auspices of the International Union of Pure and Applied Chemistry, will take place in London on April 10-15, 1961. A Scientific Committee has been set up, under the Chairmanship of Mr. L. Kenworthy (the present Chairman of the Corrosion Group of the Society of Chemical Industry), to organize scientific sessions of the Congress. The scientific program includes four plenary lectures by distinguished corrosion workers from France, Great Britain, U.S.A., and U.S.S.R., with papers expected from laboratories throughout the world.

Preprints will be issued well before the Congress and authors of papers accepted will be invited to introduce their papers briefly for discussion at the meetings. All papers, together with discussions, will subsequently be published in book form as the Proceedings of the First International Congress on Metallic Corrosion: London, 1961.

Further information is available from The Hon. Secretary, First International Congress on Metallic

Corrosion: London, 1961, 14 Belgrave Square, London, S.W. 1, England.

Atomic Weight of Silver Redetermined

The National Bureau of Standards, Washington, D. C., has redetermined the atomic weight of silver by accurately measuring silver's isotopic abundance ratio. The new atomic weight is 107.8731 ± 0.0016 on the chemical scale and 107.9028 ± 0.0011 on the physical scale, where the indicated uncertainties are over-all limits of error, based on 95% confidence limits for the mean, and allowances for effects of known sources of possible systematic error. The atomic weight of silver plays an important part in the determination of such fundamental constants as the faraday, Avogadro's number, and the gas constant. In addition, it is used to establish the atomic weights of many other elements on the chemical scale.

This determination was carried out by W. R. Shields and V. H. Dibeler of the Bureau's mass spectrometry laboratory and D. N. Craig of the electrochemistry laboratory.

References

1. "Absolute Isotopic Abundance Ratio and the Atomic Weight of Silver," W. R. Shields, D. N. Craig, V. H. Dibeler. Submitted for publication.
2. "Improved Value for the Faraday by New Experimental Process," *Tech. News Bull.*, 44, 34 (1960) STR 2447.

Dow Sets Up Fellowship Program to Help Employees Get Ph.D. Degree

A fellowship program which will enable employees to take a leave of absence to obtain the Ph.D. degree has been set up by the Dow Chemical Co. Under the program, the company will make several fellowships available to qualified employees each year. Interested employees may request a fellowship and leave of absence for the final year of work for the degree.

To qualify for a fellowship, the employee must indicate to the company that he has met language requirements for the Ph.D. degree, passed qualifying examinations admitting him as a doctoral candidate, been accepted by a professor for a definite thesis assignment, and has a reasonable expectation of completing his work within one year of leave.

Candidates must have completed two years of Dow service, not including military or other leave, in order to apply. The program will be administered by a Committee on Graduate Assistance.

The amount of the fellowship will be the same as that of other Dow fellowships at the institution of the candidate's choice, and will be administered by the institution according to its policies and practices. If there is no fellowship at that school, an appropriate one will be established within the limits of regular Dow fellowships.

Announcements from Publishers

"Gmelins Handbook of Inorganic Chemistry, Alphabetic Series to the Systematic Subject Index." Published by Verlag Chemie, Gmbh., Weinheim/Bergstr., West Germany, 1959. 109 pages.

This supplements the 1957 Systematic Subject Index in which the terms in the Gmelin classification were listed in the numerical order in which they occur. In the present supplement, the terms are arranged in alphabetical order so that it is now only a moment's work to look up the location of material on any chosen topic. Included are 2500 terms and synonyms, in addition to those already in the Systematic Index. The English index follows the German index.

"Dictionary of Atomic Terminology." Edited by Lore Lettenmeyer. Published by Philosophical Library, Inc., New York, 1959. $10.00.

This is a listing, in alphabetical order, of 1814 English terms used in the literature of atomic reactor physics and engineering, together with their German, French, and Italian equivalents in parallel columns. The main section is followed by separate alphabetical indexes in German, French, and Italian. The book apparently is intended for translators from English to the other three languages who have facility with the ordinary vocabulary.

"Investigation of Silicon Photocells as Converters of Solar Radiation," V. S. Vavilov, G. N. Galkin, and V. M. Malovetskaya, from *Atomnaya Energiya*, June 1958. Soviet technical article translation published by Office of Technical Services, June 1958. Report 59-21000,* 11 pages; 50 cents.

"Soviet Utilization of Solar Energy," May 1958. Soviet technical article translation published by Office of Technical Services. Report 59-21124,* 8 pages; 50 cents.

"Metals Coated with Films of Low Surface Energy as Reference Electrodes for the Measurements of Contact Potential Differences," K. Bewig and W. A. Zisman, U. S. Naval Research Lab., Oct. 1959. Report PB 151994,* 15 pages; 50 cents.

"Thorex Pilot Plant Corrosion Studies: 2. Corrosion of Types 304L, 309SDb, and 347 Stainless Steel during Development and Production-Development Periods," no date. AEC Report ORNL-2844,* 50 pages; $1.50.

"Reduction Cell with Vertical Rotating Mercury Cathode," Jan. 1960. AEC Report Y-1285,* 21 pages; 75 cents.

"Electrorefining of Irradiated Thorium-Uranium Alloy," Jan. 1960. AEC Report NAA-SR-4660,* 18 pages; 75 cents.

"High-Temperature Insulation for Wire (Part 2)," J. N. Harris and J. D. Walton, Georgia Institute of Technology, for Wright Air Development Center, U. S. Air Force, July 1959. Report PB 151944,* 40 pages; $1.25.

"High-Temperature Electrical Insulating Inorganic Coatings on Wire (Part 2)," C. G. Bergeron and others, University of Illinois, for Wright Air Development Center, U. S. Air Force, June 1959. Report PB 151943,* 55 pages; $1.50.

* Order from Office of Technical Services, Business and Defense Services Administration, U. S. Dept. of Commerce, Washington 25, D. C.

Literature from Industry

"Allegheny Ludlum Stainless Steel Tubing." New 34-page booklet gives details on the various sizes, grades, design data, corrosion resistance, and other information valuable to industries interested in both welded and seamless stainless steel tubing.

Copies can be obtained from the Advertising Dept., Allegheny Ludlum Steel Corp., Oliver Bldg., Pittsburgh 22, Pa.

Tungsten Bibliography. A complete bibliography on the element tungsten has been made available.

Said to be the most complete guide to tungsten references available, it includes references appearing in U. S. and foreign publications from 1953 to 1958. Intended for research and development personnel, the book contains 44 pages with 409 references.

To obtain a copy, mail $1.00 with your request to Sylvania Electric Products Inc., Chemical and Metallurgical Div., Towanda, Pa.

Zirconium Facts File. A Fact File in one package is being issued containing technical data, application, and available forms of this unique metal as developed and compiled by manufacturers and fabricators of the metal. Zirconium, a prominent construction material in atomic reactors, has many applications in other industries, and the File contains useful data and sources of supply of zirconium for executives, technical and research personnel engaged in chemical processing, electronics, automotive, aircraft, missiles, and other fields.

Write on company letterhead to the Zirconium Association, 2130 Keith Bldg., Cleveland 15, Ohio.

Holmium Metal and Erbium Metal. Two new data sheets contain information referring to many properties of these rare earth metals, including melting and boiling points, crystal structure, atomic radius, and magnetic movement.

The data sheets can be obtained from Research Chemicals Div., Nuclear Corp. of America, 170 West Providencia St., Burbank, Calif.

Corrosion Resistance Rating Guide has been issued, listing the relative ability of metals, plastics, and synthetic rubbers used in the manufacture of Flo-Ball Valves to resist the corrosive effects of 390 different fluids encountered in industry. An easy-to-read tabulation permits a rapid estimate of the effect of the fluids, alphabetically arranged, on selected materials of construction.

The Guide is available to qualified personnel submitting their requests on company letterhead to Hydromatics, Inc., Livingston, N. J.

"Testing and Evaluating Precious Metal Electroplate," a six-page article, has been reprinted from the February 1960 *American Jewelry Manufacturer*. Thickness measurement, corrosion resistance, tarnishing, oxidation, wear resistance, and hardness measurements are discussed and recommendations are made covering tests to be made and the equipment necessary for these tests.

Reprints are available free of charge from Sel-Rex Corp., Nutley 10, N. J.

New Products

New RCA "Drift Field" Transistors for Use in Industrial and Military Equipment

A comprehensive new family of ten industrial "drift field" transistors specifically designed for application in industrial and military high-frequency communications, instrumentation, control, navigation, and mobile equipment has been announced by the RCA Semiconductor and Materials Division. The new group of germanium p-n-p type transistors has been designated: RCA-2N274, 2N384, 2N1023, 2N1066, 2N1224, 2N1225, 2N1226, 2N1395, 2N1396, and 2N1397.

These types are said to have exceptional stability in equipment designs, assure long-term operating reliability, and be capable of operating up to 50 megacycles and above in radio frequency amplifier service and 125 magacycles and above in oscillator service.

The new transistors feature: maximum junction temperature rating of 100°C; maximum transistor-dissipation rating of 120 mw in free air at 25°C; transistor dissipation rating up to 240 mw with heat sink; maximum collector-to-base voltage rating of —40 v except for the 2N1226 which has a —60 v rating and is intended for those industrial and military applications requiring such a high voltage.

Employment Situations

Positions Wanted

Metallurgist—B.S. degree in mathematics, physics, chemistry. Graduate work in mathematics and spectrographic analysis. Three and one half years' experience in spectrographic, metallographic, physical controls of transistor, die cast, and punch press parts. Desires responsible position in production or research. *Reply to Box 368, c/o The Electrochemical Society, 1860 Broadway, New York 23, N. Y.*

Electrochemical Engineer—12 years' R & D experience in almost all phases of electrochemical processes. Extensive theoretical knowledge with ability in practical application. Combine the above with curiosity, resourcefulness, and creativity. Highly adaptable and capable. Supervisory experience. Desires position of considerable responsibility where experience and abilities will be most valuable. Prefers West Coast location, but will go anywhere. Salary, $11-12,000. *Reply to Box 369, c/o The Electrochemical Society, 1860 Broadway, New York 23, N. Y.*

Positions Available

Research Chemist—Inorganic-Physical Chemical-Electrochemical—For Research Laboratory of a New England supplier of metal finishing processes and compounds.

Interesting projects largely in inorganic chemistry are given both basic and applied approaches. Men with experimental skill and sound training are invited to apply for this challenging position in a medium-sized, well-established and expanding company.

Ph.D. or equivalent research experience required. Metal finishing experience desirable but not a necessity.

Salary commensurate with abilities, liberal insurance and benefit plans, excellent prospects for advancement.

Please apply in detail (résumé of personal data, education, experience, references) to: Research Department, MacDermid Incorporated, Waterbury 20, Connecticut.

Chemists and Chemical Engineers—We need physical, organic, and inorganic chemists and chemical engineers to carry out Engineering and development work in the rapidly growing power sources field. Research & Development center located in Minneapolis near University of Minnesota. Battery experience preferred but not required.

Send résumés to: J. W. Baxter, Employee & Labor Relations, Gould-National Batteries, Inc., E. 1326 First National Bank Bldg., St. Paul 1, Minnesota.

Advertiser's Index

Eagle-Picher Company 132C
General Motors Research Laboratories 128C
Great Lakes Carbon Corp., Electrode Division ..... Cover 2
Lockheed Missiles & Space Division 131C
Stackpole Carbon Company 129C

The Electrochemical Society

Patron Members

Aluminum Co. of Canada, Ltd., Montreal, Que., Canada

International Nickel Co., Inc., New York, N. Y.

Olin Mathieson Chemical Corp., Niagara Falls, N. Y.
- Industrial Chemicals Div., Research and Development Dept.

Union Carbide Corp.
- Divisions:
  - Union Carbide Metals Co., New York, N. Y.
  - National Carbon Co., New York, N. Y.

Westinghouse Electric Corp., Pittsburgh, Pa.

Sustaining Members

Air Reduction Co., Inc., New York, N. Y.

Ajax Electro Metallurgical Corp., Philadelphia, Pa.

Allen-Bradley Co., Milwaukee, Wis.

Allied Chemical & Dye Corp.
- General Chemical Div., Morristown, N. J.
- Solvay Process Div., Syracuse, N. Y. (3 memberships)

Allied Research Products, Inc., Detroit, Mich.

Alloy Steel Products Co., Inc., Linden, N. J.

Aluminum Co. of America, New Kensington, Pa.

American Metal Climax, Inc., New York, N. Y.

American Potash & Chemical Corp., Los Angeles, Calif. (2 memberships)

American Smelting and Refining Co., South Plainfield, N. J.

American Zinc Co. of Illinois, East St. Louis, Ill.

American Zinc, Lead & Smelting Co., St. Louis, Mo.

American Zinc Oxide Co., Columbus, Ohio

M. Ames Chemical Works, Inc., Glens Falls, N. Y.

Auto City Plating Company Foundation, Detroit, Mich.

Basic Inc., Maple Grove, Ohio

Bell Telephone Laboratories, Inc., New York, N. Y. (2 memberships)

Bethlehem Steel Co., Bethlehem, Pa. (2 memberships)

Boeing Airplane Co., Seattle, Wash.

Burgess Battery Co., Freeport, Ill. (4 memberships)

Canadian Industries Ltd., Montreal, Que., Canada

Carborundum Co., Niagara Falls, N. Y.

Catalyst Research Corp., Baltimore, Md.

Chrysler Corp., Detroit, Mich.

Ciba Pharmaceutical Products, Inc., Summit, N. J.

Columbian Carbon Co., New York, N. Y.

Columbia-Southern Chemical Corp., Pittsburgh, Pa.

Consolidated Mining & Smelting Co. of Canada, Ltd., Trail, B. C., Canada (2 memberships)

Continental Can Co., Inc., Chicago, Ill.

Cooper Metallurgical Associates, Cleveland, Ohio

Corning Glass Works, Corning, N. Y.

Diamond Alkali Co., Painesville, Ohio (2 memberships)

Dow Chemical Co., Midland, Mich.

Wilbur B. Driver Co., Newark, N. J. (2 memberships)

E. I. du Pont de Nemours & Co., Inc., Wilmington, Del.

Eagle-Picher Co., Chemical Div., Joplin, Mo.

Eastman Kodak Co., Rochester, N. Y.

Thomas A. Edison Research Laboratory, Div. of McGraw-Edison Co., West Orange, N. J.

Electric Auto-Lite Co., Toledo, Ohio
- C & D Division, Conshohocken, Pa.

Electric Storage Battery Co., Yardley, Pa.

Englehard Industries, Inc., Newark, N. J. (2 memberships)

The Eppley Laboratory, Inc., Newport, R. I. (2 memberships)

Erie Resistor Corp., Erie, Pa.

Exmet Corp., Tuckahoe, N. Y.

Fairchild Semiconductor Corp., Palo Alto, Calif.

Food Machinery & Chemical Corp.
- Becco Chemical Div., Buffalo, N. Y.
- Westvaco Chlor-Alkali Div., South Charleston, W. Va.

Foote Mineral Co., Paoli, Pa.

Ford Motor Co., Dearborn, Mich.

General Electric Co., Schenectady, N. Y.
- Chemistry & Chemical Engineering Component, General Engineering Laboratory
- Chemistry Research Dept.
- General Physics Research Dept.
- Metallurgy & Ceramics Research Dept.

General Instrument Corp., Newark, N. J.

(Sustaining Members cont'd)

General Motors Corp.
Brown-Lipe-Chapin Div., Syracuse, N. Y. (2 memberships)
Guide Lamp Div., Anderson, Ind.
Research Laboratories Div., Detroit, Mich.
General Transistor Corp., Jamaica, N. Y.
Gillette Safety Razor Co., Boston, Mass.
Globe-Union, Inc., Milwaukee, Wis.
Gould-National Batteries, Inc., Minneapolis, Minn.
Grace Electronic Chemicals, Inc., Baltimore, Md.
Great Lakes Carbon Corp., New York, N. Y.
Hanson-Van Winkle-Munning Co., Matawan, N. J. (2 memberships)
Harshaw Chemical Co., Cleveland, Ohio (2 memberships)
Hercules Powder Co., Wilmington, Del.
Hill Cross Co., Inc., New York, N. Y.
Hoffman Electronics Corp., El Monte, Calif.
Hooker Chemical Corp., Niagara Falls, N. Y. (3 memberships)
Hughes Aircraft Co., Culver City, Calif.
International Business Machines Corp., Poughkeepsie, N. Y.
International Minerals & Chemical Corp., Skokie, Ill.
ITT Laboratories, Nutley, N. J.
Jones & Laughlin Steel Corp., Pittsburgh, Pa.
K. W. Battery Co., Skokie, Ill.
Kaiser Aluminum & Chemical Corp.
Div. of Chemical Research, Permanente, Calif.
Div. of Metallurgical Research, Spokane, Wash.
Kennecott Copper Corp., New York, N. Y.
Keokuk Electro-Metals Co., Keokuk, Iowa
Libbey-Owens-Ford Glass Co., Toledo, Ohio
M. & C. Nuclear, Inc., Attleboro, Mass.
Mallinckrodt Chemical Works, St. Louis, Mo.
P. R. Mallory & Co., Indianapolis, Ind.
McGean Chemical Co., Cleveland, Ohio
Merck & Co., Inc., Rahway, N. J.
Metal & Thermit Corp., Detroit, Mich.
Minnesota Mining & Manufacturing Co., St. Paul, Minn.
Monsanto Chemical Co., St. Louis, Mo.
Motorola, Inc., Chicago, Ill.
National Cash Register Co., Dayton, Ohio
National Lead Co., New York, N. Y.
National Research Corp., Cambridge, Mass.
National Steel Corp., Weirton, W. Va.
New York Air Brake Co., Kinney Vacuum Div., Boston, Mass.
Northern Electric Co., Montreal, Que., Canada
Norton Co., Worcester, Mass.
Olin Mathieson Chemical Corp., Niagara Falls, N. Y.
High Energy Fuels Organization (2 memberships)
Peerless Roll Leaf Co., Inc., Union City, N. J.
Pennsalt Chemicals Corp., Philadelphia, Pa.
Phelps Dodge Refining Corp., Maspeth, N. Y.
Philco Corp., Philadelphia, Pa.
Philips Laboratories, Inc., Irvington-on-Hudson, N. Y.
Pittsburgh Metallurgical Co., Inc., Niagara Falls, N. Y.
Poor & Co., Promat Div., Waukegan, Ill.
Potash Co. of America, Carlsbad, N. Mex.
Radio Corp. of America
Tube Div., Harrison, N. J.
RCA Victor Record Div., Indianapolis, Ind.
Ray-O-Vac Co., Madison, Wis.
Raytheon Manufacturing Co., Waltham, Mass.
Reynolds Metals Co., Richmond, Va. (2 memberships)
Rheem Semiconductor Corp., Mountain View, Calif.
Schering Corporation, Bloomfield, N. J.
Shawinigan Chemicals Ltd., Montreal, Que., Canada
Speer Carbon Co.
International Graphite & Electrode Div., St. Marys, Pa. (2 memberships)
Sprague Electric Co., North Adams, Mass.
Stackpole Carbon Co., St. Marys, Pa.
Stauffer Chemical Co., New York, N. Y.
Sumner Chemical Co., Div. of Miles Laboratories, Inc., Elkhart, Ind.
Sylvania Electric Products Inc., Bayside, N. Y. (2 memberships)
Tennessee Products & Chemical Corp., Nashville, Tenn.
Texas Instruments, Inc., Dallas, Texas
Three Point Four Corp., Yonkers, N. Y.
Titanium Metals Corp. of America, Henderson, Nev.
Tung-Sol Electric Inc., Newark, N. J.
Udylite Corp., Detroit, Mich. (4 memberships)
Universal-Cyclops Steel Corp., Bridgeville, Pa.
Upjohn Co., Kalamazoo, Mich.
Victor Chemical Works, Chicago, Ill.
Western Electric Co., Inc., Chicago, Ill.
Wyandotte Chemicals Corp., Wyandotte, Mich.
Yardney Electric Corp., New York, N. Y.